uOttawa

L'Université canadienne
Canada's university

FACULTÉ DES ÉTUDES SUPÉRIEURES ET POSTOCTORALES

uOttawa

L'Université canadienne
Canada's university

FACULTY OF GRADUATE AND POSDOCTORAL STUDIES

Darren John Yip
AUTEUR DE LA THÈSE / AUTHOR OF THESIS

Ph.D. (Microbiology and Immunology)
GRADE / DEGREE

Department of Biochemistry, Microbiology and Immunology
FACULTÉ, ÉCOLE, DÉPARTEMENT / FACULTY, SCHOOL, DEPARTMENT

The Chromatin Remodelling Protein SNF2L Regulates Cell Number in the Developing Brain
TITRE DE LA THÈSE / TITLE OF THESIS

David Picketts
DIRECTEUR (DIRECTRICE) DE LA THÈSE / THESIS SUPERVISOR

CO-DIRECTEUR (CO-DIRECTRICE) DE LA THÈSE / THESIS CO-SUPERVISOR

Alexandre Blais	Rob Bremner (University of Toronto)
Bruce McKay	Valerie Wallace

Gary W. Slater
Le Doyen de la Faculté des études supérieures et postdoctorales / Dean of the Faculty of Graduate and Postdoctoral Studies

The chromatin remodelling protein SNF2L regulates cell number in the developing brain.

Darren John Yip

THESIS
Submitted to the Faculty of Graduate and Postdoctoral Studies in partial fulfilment of the requirements for the degree of

Doctorate of Philosophy
in
Biochemistry, Microbiology and Immunology /
Human and Molecular Genetics

University of Ottawa
Ottawa, Ontario, Canada
17 December, 2009

Your file Votre référence
ISBN: 978-0-494-65580-1
Our file Notre référence
ISBN: 978-0-494-65580-1

Abstract

Mutations in genes encoding chromatin-remodelling proteins, such as the *ATRX* gene, underlie a number of genetic disorders including X-linked mental retardation syndromes; however knowledge of the role of these proteins in CNS development is limited. In *Drosophila*, ISWI is essential for development, the protein functions as the ATP-hydrolysing component in several chromatin-remodelling complexes. The two mammalian ISWI orthologs, *SNF2H* and *SNF2L* are differentially expressed, suggesting that they possess distinct developmental roles. Prevalent expression of SNF2H occurs during neuroprogenitor proliferation while *SNF2L* transcripts are increased in maturing neurons. It is well known that an appropriate balance between neuroprogenitor proliferation and neuronal differentiation during the embryonic stages is critical to regulate the size of the developing neocortex. Here, I have analyzed mice ablated for Snf2l chromatin remodelling activity to determine its role in cortical development. The loss of active Snf2l resulted in a 1.4-fold increase in the ratio between brain weight and body weight. This was accompanied by a concomitant increase in cell number in the cerebral cortical strata ranging from 1.3- to 1.6-fold (in embryonic and adult tissues). This increase did not coincide with an observable change in the frequency of apoptotic events. Pulse-labelling experiments with BrdU resulted in similar proportions of labelled cells within the periventricular zone of embryonic (E15.5) cortices from wildtype and mutant mice. We observed a 3-fold increase in mitotic cells by phospho-histone H3 staining. BrdU birthdating and BrdU/Ki67 double-labelling experiments revealed that there was a 3-fold increase in the number of progenitors that re-entered the cell cycle and a concomitant decrease in cell cycle exit. Gene expression analysis of *Snf2l*-mutants revealed a perturbation in the expression patterns of many genes, including genes encoding neurogenic factors and cell cycle regulators. One such gene identified was *Foxg1*. *Foxg1* is regulated by Snf2l, and limiting Foxg1 mitigated the brain phenotype. Our results suggest loss of Snf2l alters the timing between cell cycle exit and differentiation leading to increased cell numbers in the developing neocortex.

Acknowledgements

Dr David Picketts has lent me a great level of support over the years; I found at times that he had much to offer, scientifically, professionally, but most importantly with a friendship and respect which has pulled me through this 6ish year effort. David you have given me guidance and encouragement; a gift that I will cherish. I also acknowledge the support of my thesis advisory committee, Drs Jonathon Lee, Barbara Vanderhyden and Rashmi Kothary, and though not officially committee members Drs Valerie Wallace and Denis Bulman for having made yourselves available for random questions and advice. You have been essential to my accomplishments.

I must take some time to recognize the friendship of my lab mates, Steve, Tina, Marilyn, Emma, the three M's (Mike, Matt and Maureen), Chelsea and Pam. Dominic, Evelyne, Jasmine, Rebecca, Tiffany, Paul, and yes, even you Dahmane have made coming to work seem a reward rather than a challenge. Whether you are coming into a lab for the first time or even if you have been there for a long time already, you tend to rely greatly on those around you for guidance, support and leadership, Drs Maribeth Lazzaro, Adrian De Maria, Marie (Maz) Manglesdorf, Nathalie Berube and Patrick Scott you were very helpful to me. As the longest (to date) member of the Pickets laboratory, I have seen so many people come and go, you are too numerous to list all but I have benefited greatly from swimming in the great pool of experiences you have provided. Josh and Kelley: a BIG thanks to you guys, for the reading/editing of this my thesis of ACYMS [**acronyms**], run-on sentences, and commas.

I must take time to acknowledge the input and advice I have had from all the friends I have made and fellow graduate students I have met at the OHRI, ORCC and BMI, everyone knows graduate school is hard work but everyone around you makes it fun also.

Finally for my family, Mom, Dad, Kevin, Carolyn and Oma, all the support and free food has been so gracious. For Opa, he gets a special recognition, for him, whose interest in genetics and knowledge of live has combined for some of the strangest and yet well designed thought provoking questions I have ever faced.

Table Contents

Table of Figures

Table of Tables

List of Abbreviations

Ab	Antibody
ACF	ATP-dependant Chromatin assembly and remodelling factor
AP	apical boundary of the ventricular one (also ependymus)
ATP	Adenosine Triphosphate
BAF	BRG1- or hBRM-associated Factors
bHLH	basic Helix-Loop-Helix
bp	base pair
BrdU	5-bromo-2-deoxyuridine
BRG1	Brahma Related Gene 1
BRM	Brahma
CA	Cornu Ammonis
CDK	Cyclin Dependant Kinase
cDNA	complimentary Deoxyribonucleic Acid
Cecr2	Cat Eye Syndrome Chromosome Region Candidate 2
CERF	Cecr2-containing Remodelling Factor
CHD	Chromodomain Helicase DNA binding domain
ChIP	chromatin immunoprecipitation
CHRAC	Chromatin Accessibility Complex
CNS	central nervous system
CP	cortical plate
CpG	Cytosine-phosphodiester-Guanine dinucleotide
DAPI	4', 6-diamidino-2-phenylindole
DG	Dentate Gyrus
DNA	Deoxyribonucleic Acid
DNMT	DNA Methyl Transferase
dNTP	Deoxynucleotide Triphosphates
E	embryonic stage / day (as in E13.5, E15.5....)
empVEC	empty vector control plasmid
Ex6DEL	*Snf2l*, exon 6 deleted
FGF	Fibroblast Growth Factor
FOXG1	Forkhead Homeobox Gene G1
G	gram
G1	Growth 1 phase of the cell cycle
G2	Growth 2 phase of the cell cycle
GAPDH	Glyceraldehyde-3-phosphate dehydrogenase
GE	ganglionic eminence
GFAP	Glial Fibrillary Acidic Protein
GFP	Green Fluorescent Protein
H	Histone
HAT	Histone Acetyltransferase
HC	hippocampus
HDAC	Histone Deacetylase
HET	heterozygous
HRP	Horseradish Peroxidase

IP	Immunoprecipitation
IPC	Intermediate Progenitor Cell
IPL	Intermediate Progenitor Cell Layer
ISWI	Imitation Switch
IZ	intermediate zone
Kb	kilobase
LV	lateral ventricle
M-Phase	Mitosis phase of the cell cycle
MBP	Methyl Binding Protein
mg	miligram
mRNA	Messenger Ribonucleic Acid
MUT	mutant Snf2h expressing plasmid
MZ	marginal zone (also Layer I)
n	sample size
NE	neuroepithilal progenitors
NRSF	Neuron Restrictive Silencing Factor
NURF	Nucleosome Remodelling Factor
OEXP	overexpressing Snf2h plasmid
ORF	open reading frame
P	postnal stage / day (P0.5, first day after birth or P7.5, one week after birth)
PAGE	polycrylamide gel electrophoresis
PBS	phosphate buffered saline
PCR	polymerase chain reaction
PH3	Phosphohistone-H3
PS	pial surface
REST	Repressor Element-1 Silencing Transcription Factor
RNA	Ribonucleic Acid
RT	Reverse Transcriptase
S-phase	DNA synthesis phase of the cell cycle
SANT	SWI3, ADA2, N-CoR and TFIIIB (a DNA binding domain)
SC	stem cell
SEM	standard error of the mean
SNF2L	Sucrose Non-fermenting 2L
SNF2H	Sucrose Non-fermenting 2H
SWI/SNF	Switching / Sucrose Non-Fermenting
SVZ	subventricular zone
Tuj	β III-tubulin, marker of neuronals
UTR	untranslated region
V	volts
VZ	ventricular zone
WT	wildtype

1.0 Introduction.

A fundamental challenge in biology is to understand how genetic information is interpreted in order to guide the formation of specialized regions and tissues within a multicellular organism. During mammalian development, precise tissue-specific patterns of gene expression are established by epigenetic modification in response to intrinsic and extrinsic signals. The term epigenetic modification refers to biochemical processes wherein a cell imposes transcriptional regulation over one or numerous genes without altering the DNA code [1-3]. Therefore, for correct expression, spatially, temporally and quantitatively, a gene requires not only intact coding sequences and functional regulatory elements but also an appropriate chromatin environment [4-7]. Epigenetic modifications of chromatin are thus a major point of regulation in establishing tissue specific patterns of gene expression and as well, cell fate and differentiation, including neuronal development. In this thesis I have studied the regulation of proliferation and differentiation (neurogenesis) in the developing embryonic neocortex and the influence that the chromatin remodelling factor Snf2l has in the regulation of *Foxg1*, a significant contributor to this process.

1.1 Mammalian neurodevelopment.

Neurodevelopment comprises two key processes: **neurulation** (the induction of neuronal specific precursors/tissue and regional association) and **neuron formation** (neuronal subtype specification). Following gastrulation, the mammalian central nervous system originates from a pocket of dorsal ectoderm that forms the neural plate [8]. During

neurulation and in response to growth factors the neural plate proliferates and invaginates, forming the neural tube [8]. The neural plate gives rise to three cell populations; (i) the cells of the inner mass which form the brain and spinal cord, (ii) the neural crest cells which form the autonomic or peripheral nervous system and (iii) cells which eventually form the epidermis of the skin [8]. The formation of the neural tube occurs in an anterior to posterior pattern and forms three primary vesicles: the prosencephalon (forebrain), the mesenchephalon (midbrain) and the rhombencephalon (hindbrain) [8]. The optic vesicles then extend away laterally [8]. The prosencephalon gives rise to two structures, the telenchephalon and diencephalon. The telencephalon (precursor to the forebrain) forms the cerebral hemispheres, which are further subdivided into the left and right cerebral cortex and corresponding ganglionic eminences, and the diencephalon which forms the thalamus, epithalamus and hypothalamus [8, 9]. The mesencephalon becomes the midbrain which includes the brain stem, substantia nigra and basal ganglia [8]. The rhombencephalon or hindbrain then forms the cerebellum and medulla oblongata [8, 10].

1.1.1 Patterning and regionalisation in the developing brain.

Patterning of the CNS occurs along both the dorso/ventral and the anterior/posterior (also called rostral/caudal) axis which are controlled by many organizing signals [8]. These signals, often termed morphogens, belong to the Bone morphogenic protein [BMP], Sonic Hedgehog [Shh], Fibroblast growth factor [Fgf], the Hox, and Wingless-Int protein families [11-13]. The secretion of these molecules occurs in a very spatio-temporal precise pattern, thereby assuring the proper and sequential development and specification of different brain regions. Signaling from these organizational centers induces a gradient of expression of

different transcription factors that specify certain regions or certain cell populations. As an example, the expression of Pax6 which has been shown to play a crucial role in cell proliferation of the developing forebrain is expressed in a posterior (high) to anterior (low) gradient [14]. Later in the developing forebrain Pax6 expression, expressed in a posterior-anterior gradient is limited to the ventricular zone progenitors [15]. *Neurogenin2*, which is a repressed target of Pax6, controls cortical neuron specification, migration and patterning of the forebrain[16, 17]. Neurogenin2 is expressed in an opposing gradient, posterior (low) to anterior (high), effectively inducing differentiation of precursors [18].

1.1.2 Cellular and molecular mechanisms in neuron formation.

Neurons are the key cells of the central nervous system that use biochemical reactions to receive, process and transmit information from external stimuli such as sight, taste, touch and sound. Neurodevelopment is intricately linked to proliferation and differentiation [19]. The point when a cell exits the cell cycle and progresses towards its final cell fate is often referred to as its birthdate. Neuronal fate development is a lengthy and complex process comprising two key stages and several cellular signaling events, both intrinsic and extrinsic [19-22]. The primary stage, **histogenesis**, is a process where undifferentiated pluripotent cells, such as embryonic or adult stem cells (often called neural stem cells [NSC] or neural epithelial cells [NE] in the developing brain) are transformed into a very plastic precursor cell by the irreversible commitment to a neuronal fate [19, 20]. This process does not affect the proliferative capacity of these cells; nevertheless they are designated to be of the neuronal lineage as they express several early neuronal markers and thus are termed neuronal progenitors or neuroblasts [19, 23-25]. Many developmental

pathways have been implicated in neuronal induction and some inducers include the Wnt (*wingless type*), fibroblast growth factor, epidermal growth factor, insulin growth factor, JAK/STAT, MAP kinase signaling pathways and the blockage of the BMP signaling pathway [21, 23, 26, 27]. It is therefore evident that the first indications of neuronal function reside at the precursor level; only later do these committed precursors become postmitotic and differentiate to form neurons or glial cells [19, 21, 24, 28, 29]. The final multi-step progression toward a neuron fate determination is termed **neurogenesis**. During differentiation neurons acquire unique morphological and functional characteristics such as neurite outgrowth, pathfinding, targeting and synaptogenesis (reviewed in [1, 3, 7]). Oligodendrocytes and astrocytes are the two non-neuronal glial cell types that are derived from neuroblasts through a distinct pathway involving the upregulation of *glial fibrillary acidic protein* [*GFAP*] [30]. Glial cells support neurons by producing the myelin sheath-specific proteins and participate in many neuronal activities such as neuron protection and synapse support [30]. Studies have shown that the overexpression of the neurogenic basic helix-loop-helix protein, Ngn1, can dramatically induce neurogenesis but also suppress glial cell formation by inhibiting JAK/STAT3 activation of *GFAP* and instead activating *NeuroD* [29, 31, 32]. Neurogenin1 is thought to be an initiation signal that is active early in the neurogenic pathway and it may represent a "master switch" for neurogenesis [24, 29, 31].

1.1.3 Cell proliferation in the developing brain, mode of cell division.

In the developing embryo, formation of the central nervous system requires a vast amount of cell proliferation, but this has to be well balanced with an opposing time and

region specific process of cell differentiation. Precursor cells have to be produced and specified in exact position and timely sequence in order to acquire their correct neuronal identity, subtype and regionalization. Many sequentially expressed and regional transcription factors play key roles in this process [33]. Initially all the cells in the developing central nervous system are proliferating through the self-renewable symmetric division pattern (Figure 1 a) [34]. Daughter cells of the symmetric mitotic event are both predetermined to become neural stem cells. Over this early developmental period the number of symmetric proliferative divisions tapers off in favour of asymmetric divisions, where one daughter cell leaves the cell cycle while the other remains proliferative, or a third, terminal symmetrical divisions, where both daughter cells exit the cell cycle [34-36]. It had been believed that the orientation of the mitotic cleavage, during cytokinesis, in relation to the apical plane of the VZ is a predictor of division, symmetric versus asymmetric [37, 38]. While the orientation of the plane of cleavage is a means for the identification of symmetry in *Drosophila melanogaster* and *Caenorhabditis elegans*, asymmetric division in higher vertebrates is more correctly associated with the unequal distribution of specific cell fate determinants, see Figure 1 bc [38-41]. Within these distribution-defined asymmetric divisions, which fate determinants go with which daughter cell defines its cell fate. For instance the Numb protein product, an important marker for self renewing neural epithelial cells is always associated with the proliferative daughter cell [42-44]. On the other hand, TIS21 which is an anti-proliferative marker that is always expressed in the cell that is predetermined to exit the cell cycle and differentiate [45].

Figure 1 – Cell division during development of the cerebral cortex.

[A] Throughout neurogenesis cell divisions repopulate the precursor pool. Early in neurogenesis cell divisions are symmetric and thus increase the number of neural progenitors. During the middle stages of neurogenesis more and more asymmetric cell divisions take place, generating one neuron and one precursor cell. Near the end or neurogenesis in the subventricular zone terminal symmetric divisions take place, producing two neurons (picture adapted from Fishell and Kreigstein 2003) [46]. [B] Cell divisions at the ventricular surface can occur at different angles with respect to the apical layer of the ventricular zone. They can be perpendicular (symmetrical orientation) with an equal distribution of cell determinant factors, or perpendicular with an unequal distribution of cell determinant factors. All cell divisions that are parallel to the apical layer (asymmetrical orientation) will have an unequal distribution of cell determinant factors (picture adapted from Wodarz and Hunttner, 2003) [47]. [C] Orientations of cell division are observed by co-staining for the spindle fibre staining γ-tubulin (green), which is concentrated at the centrioles during mitosis, providing a means for determining the orientation of division (white line). All images are arranged in the apical layer orientation down. These nuclei are counter stained for DAPI (blues) and a neuronal specific marker (Tuj; red).

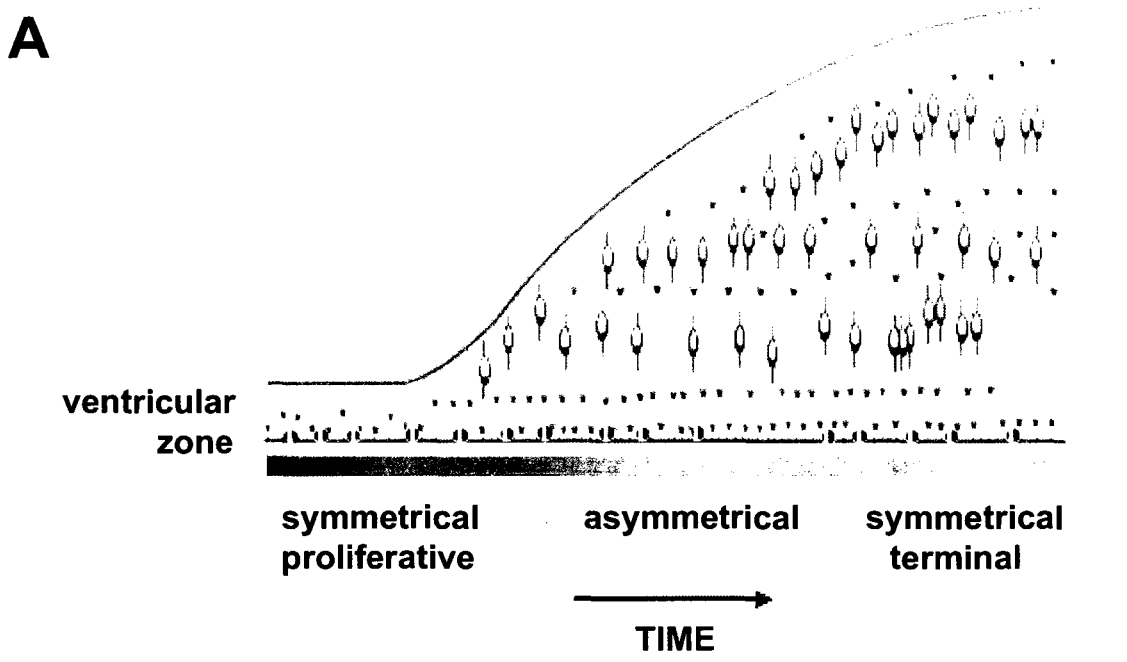
A
ventricular zone
symmetrical proliferative
asymmetrical
symmetrical terminal
TIME

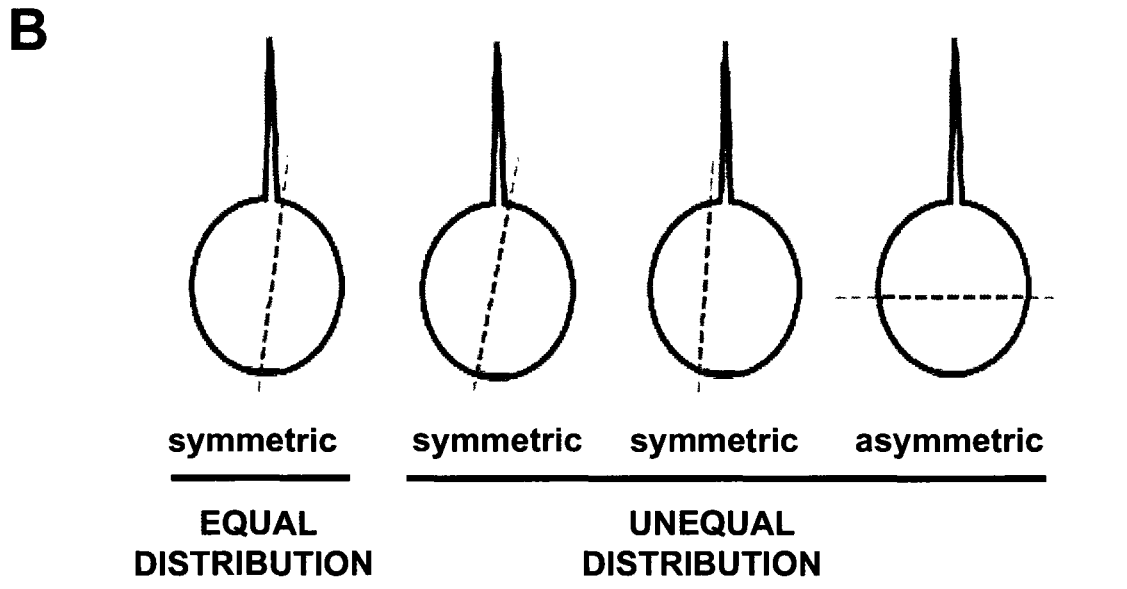
B
symmetric
symmetric
symmetric
asymmetric
EQUAL DISTRIBUTION
UNEQUAL DISTRIBUTION

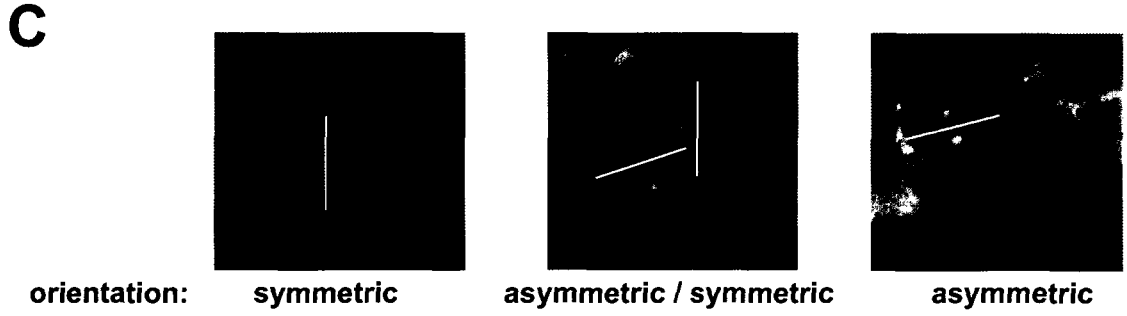
C
orientation:
symmetric
asymmetric / symmetric
asymmetric

1.1.4 Corticogenesis and laminar formation of the mouse neocortex.

The mammalian cerebral cortex comprises six distinct layers (I-VI) of neurons each containing distinct molecular and functional properties [48, 49]. They arise from divisions of the cortical progenitors in the telencephalic ventricular zone, also called the germinal neuroepithelium, a region directly adjacent to the lateral ventricle and migrate out in a radial fashion, see Figure 2 [50, 51]. Recently it was observed that a second population of precursors located in the ganglionic eminence (located ventral to the germinal neuroepithelium) also give rise to neurons which migrate tangentially towards the cortical plate see Figure 2 [52-54]. The six distinct cortical layers are formed between embryonic development days E11-E18 and are persistent into adulthood, see Figure 3 [53, 55]. At E11 the first wave of postmitotic neurons migrates toward the pial surface and forms the preplate [56]. At E13 a second wave is released which migrates through and splits the preplate into Layer I (also called the marginal zone) and the subplate (reviewed in [53]). The earliest born neurons are the Cajal-Retzius cells of layer I, formed during the split of the preplate [57]. The subplate is a transient structure and all cells from this layer will eventually be eliminated by apoptosis before birth [58]. This is then followed by the successive formation of layers V-II, in an inside-out fashion with the outer layers (superficial) migrating through the earlier born deep layers. As nuclei migrate away from the VZ toward the pial surface they no longer undergo DNA synthesis and are therefore no longer participating in mitosis and cell division; this point is the cortical neuron's birthdate [59]. Experiments have shown that neurons from multiple layers are generated from a single progenitor through consecutive asymmetric divisions [59-62]. Moreover, DNA labelling experiments suggest that some cortical progenitors undergo up to 11 rounds of

Figure 2 – Key anatomical structures and direction of neuronal migration in the developing mouse telencephalon.

[A] This thionin stained section of an E15.5 developing mouse embryo telencephalon is labelled for key structures and areas of particular interest. The orange arrows depict the direction of migration of developing neurons from the proliferative regions of the developing telencephalon during neurodevelopment. The radial migrating cells move out from the ventricular zone (VZ) and the tangentially migrating neurons swing out from the ganglionic eminence (GE). [B] A detailed magnification of an E15.5 embryonic cortex stained for DAPI, key regions and structures are labelled. Part A is adapted from Jacobowitz and Abbott (1998) [63].

A

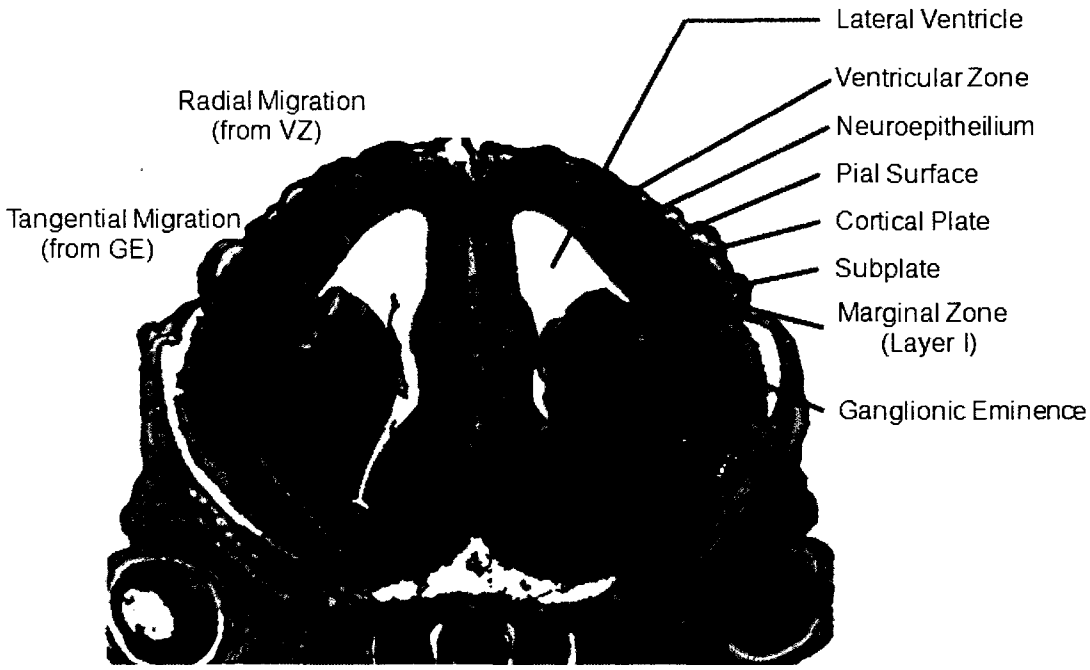

IMAGE FROM Jacobowitz DM and Abbot LC

B

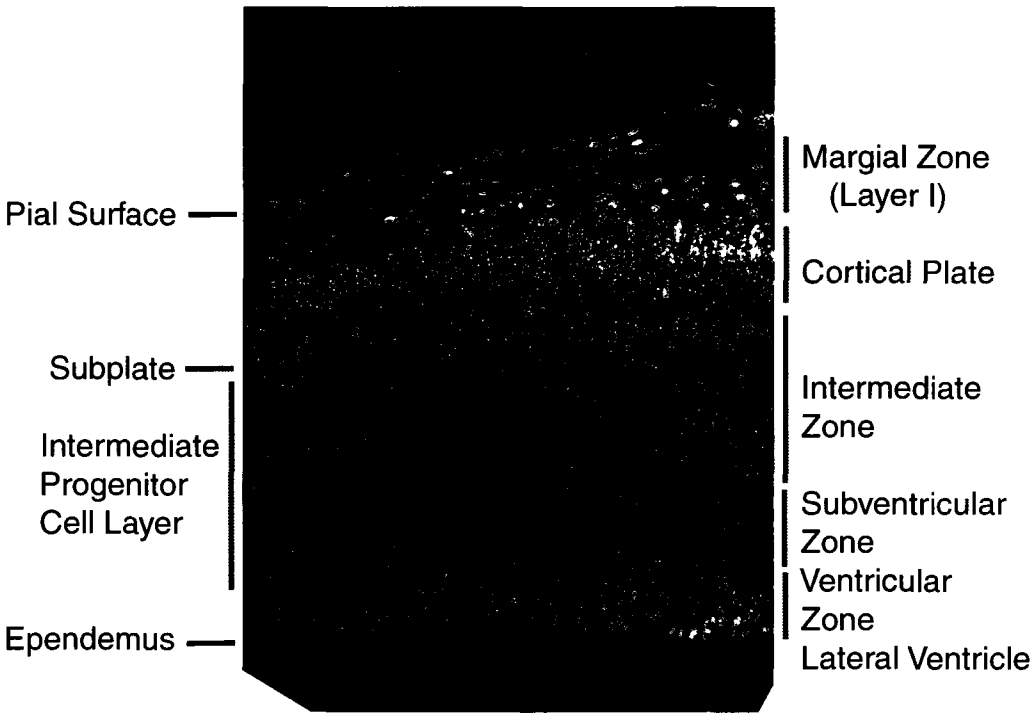

Figure 3 – Key anatomical structures of the adult brain.

Key regions and structures of interest are labelled on 12 μm coronal microsections (approx. Bregma -1.95mm). Sections are stained with [A] Cresyl Violet (NISSL) and [B] DAPI. A magnification of a DAPI stained microsection with the cortical and hippocamal layers demarked.

A

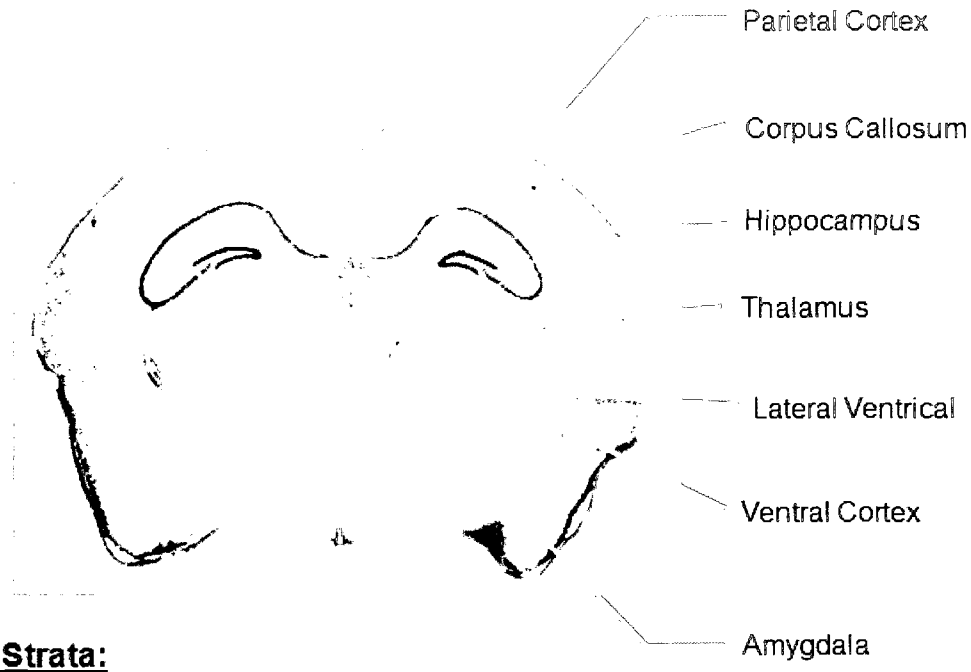
Parietal Cortex
Corpus Callosum
Hippocampus
Thalamus
Lateral Ventrical
Ventral Cortex
Amygdala

B

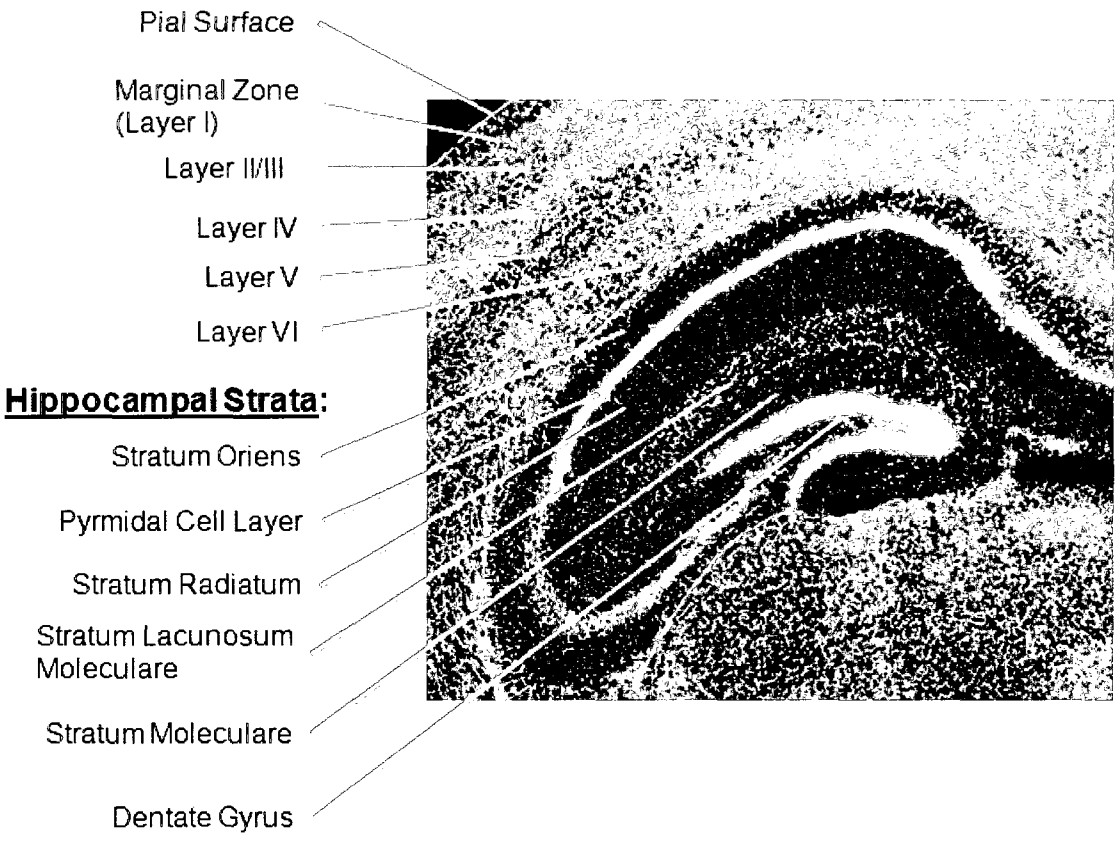
Cortical Strata:
Pial Surface
Marginal Zone (Layer I)
Layer II/III
Layer IV
Layer V
Layer VI
Hippocampal Strata:
Stratum Oriens
Pyrmidal Cell Layer
Stratum Radiatum
Stratum Lacunosum Moleculare
Stratum Moleculare
Dentate Gyrus

division between embryonic development day E10-E17 [34]. Widespread epigenetic cues have been implicated in the sequential generation of different layer and neuronal types [64]. A subset of neural epithelial progenitors, the radial glia, undergo a specialized pattern of migration such that only M-phase nuclei accumulate at or very near to the apical surface of the ventricular zone; this to-and-fro movement, which is correlated to the cell cycle phase, is often referred to as interkinetic nuclear migration [59, 65]. Interkinetic nuclear migration is responsible for the bursts of newly born cells that are the primary basis of the wave of neurons which make the layers of neurons in the cortical plate. Shortly after E10 a second pool of cortical progenitors (basal or intermediate progenitors) leaves the ventricular zone and forms an abventricular or non-apical dividing population at the subventricular zone the intermediate progenitor cell [IPC] layer which overlaps the ventricular and intermediate zones [66, 67]. These cells do not undergo interkinetic nuclear migration and it seems that their main purpose is to amplify neuronal output [68]. Somewhat surprisingly, time-lapse microscopy has identified that these intermediate progenitors produce the majority of neurons between E11-E13 [67]. It is well known that the cortex produces a large excess of neurons; more than 70% of neurons born throughout gestation undergo apoptosis [69, 70]. These newly made neurons have, therefore, to compete for a place in the larger connected networks. Those neurons which are unable to connect to targets are thus surplus and targeted for programmed cell death.

1.2 Chromatin, structure and function.

The genetic identity of an organism is completely contained and encoded on a molecule called deoxyribonucleic acid, or DNA, for short. Within each human cell is

approximately 2 meters of naked DNA (approximately $3x10^9$ base pairs). To put this into perspective, the average size of the nucleus is $1.7x10^{-6}$ meters, or 1.7 μm (http://www.falstad.com/scale/). This suggests that the DNA is compacted/compressed by an approximately ten thousand-fold factor. In order to accomplish this seemingly insurmountable level of compaction, eukaryotic cells make use a hierarchical system of DNA folding. Chromatin, first identified by Walter Fleming in 1882, can be defined as a complex mass of genetic material composed of DNA, proteins and RNA that functions to package DNA molecules into the confines of the nucleus.

1.2.1 Structural overview of chromatin.

The nucleosome is the fundamental and structural unit of chromatin that is comprised of 146 base pairs of DNA (2 nm fibre) wrapped around a **h**istone (H) octamer containing 2 copies of each: H2A, H2B, H3 and H4 proteins [71, 72]. Additional protein subunits such as H1 act as nucleosome linkers [73]. Chromatin has several layers of organizational structure. The linear arrays of nucleosomes that comprise the primary structure of chromatin and which are often described as "beads on a string," or the 11 nm fibre, can be folded upon themselves into higher-order structures through further protein-protein and protein-DNA interactions forming the 30 nm and 300 nm fibres. These in turn are folded upon themselves to form the most condensed, 1.4 μm thick, metaphase chromosome (refer to Figure 4) [74-76]). Chromatin serves as the ultimate repressive structure that must be overcome for many cellular activities such as transcription, DNA replication, recombination and DNA repair [3, 77]. In order for organisms to achieve these

Figure 4 – A Schematic diagram of hierarchical structure of chromatin folding.

Chromatin at its basic structural level is 146 base pairs of DNA wrapped around the nucleosome to form the 11 nm fibre. Long arrays of nucleosomes have the appearance of "beads on a string." This structure is further condensed through a series of protein-protein interactions, forming loops and folds, which further condense the chromatin structure into the most compact metaphase chromosome. This figure is adapted from Lodish et al. 2000 [78].

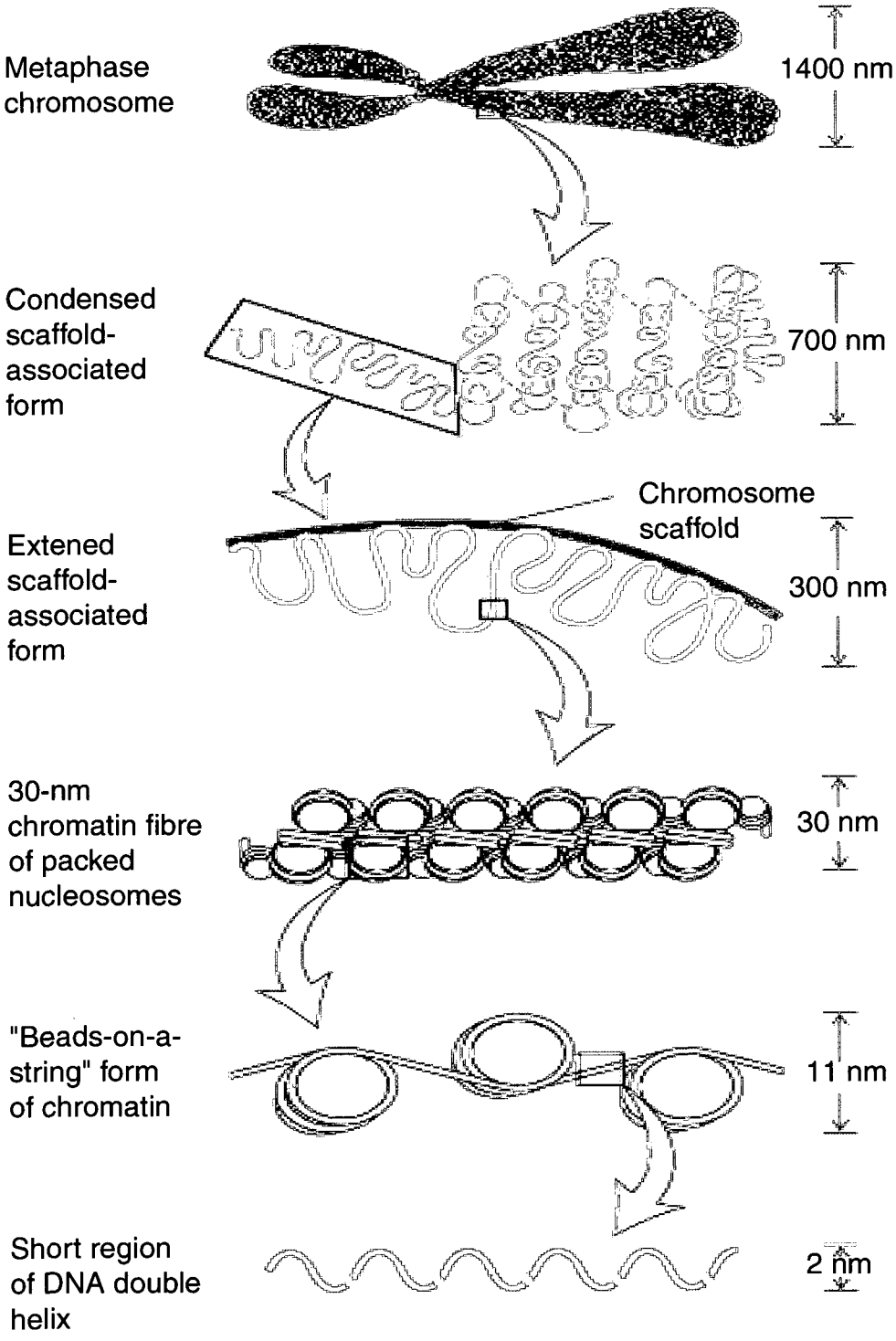
Metaphase chromosome
1400 nm
Condensed scaffold-associated form
700 nm
Chromosome scaffold
Extened scaffold-associated form
300 nm
30-nm chromatin fibre of packed nucleosomes
30 nm
"Beads-on-a-string" form of chromatin
11 nm
Short region of DNA double helix
2 nm

elementary processes they must first overcome the physical barrier that the chromatin presents.

1.3 Chromatin reorganization.

It has been said that the human genome is like a desert, with vast tracks of lifeless space interrupted only by the occasional oasis of activity [79]. In the dynamic regulation of gene expression there are two chromatin states, with varying degrees of compaction. These epigenetic states can be divided into euchromatin (the "oasis", transcriptionally active) and heterochromatin (the "desert", transcriptionally limited). While the biochemical profiles of these expressed and silent loci have been well characterized, little is known about the transition between them. Euchromatin refers to a collection of less condensed regions where the vast majority of actively expressed genes tend to reside [75, 80, 81]. Constitutive heterochromatin is generally low in gene content and tends to be limited to the centromeric and telomeric regions which remains condensed throughout most of the cell cycle [76, 80, 82-84]. However, molecular signalling can result in the stable, yet reversible, formation of a second form of heterochromatin (temporal or facultative heterochromatin); this is a primary means of transcriptional regulation and can occur throughout the genome [85-87]. Both forms of heterochromatin are important for many functions including, but not limited to, nuclear organization, chromosome segregation and gene silencing [4, 5, 79, 81, 83, 88]. The evolutionally conserved mechanisms which shuttle chromatin between euchromatin and facultative heterochromatin are collectively termed epigenetic modifications. There are two strategies in which nucleosome structure is modulated: (1) "passive" histone / DNA modifications which include acetylation,

methylation, and others and (2)"active" chromatin remodelling [89-94]. The coordinated activities of both histone and DNA-modifying enzymes and chromatin remodelling complexes collectively contribute to a heritable regulatory mechanism, the Epigenetic Code; and are involved in a wide variety of cellular functions.

1.3.1 Passive DNA modifications.

The most common form of DNA modification is DNA methylation, a heritable covalent modification which involves the addition of a methyl group to the fifth carbon residue of cytosine bases that are adjacent to guanine residues [CpG dinnucleotides]. CpG [**C**ytosine-**p**hosphodiester-**G**uanine] islands are regions of the genome which contain a relatively high concentration of CpG residues and are very often associated with mammalian promoters [95]. Generally, the presence of 5-methylcytosines on promoters will have the specific effect of silencing gene expression [96, 97]. Indeed, methylation has long been associated with telomeric and centromeric chromatin, the main constituents of constitutive heterochromatin [82, 85]. The methyl-group represses transcription by two basic methods: one by directly interfering with transcription factor binding, and the other, through recruiting methyl binding proteins which are often components of larger multi-protein chromatin remodelling and repressive complexes [97, 98].

CpG methylation is maintained and modified by the catalytic activities of a combination of proteins. The protein product of the *DNMT1* [***DNA methyl transferase gene 1***] gene is responsible for maintenance of methylation status and responsible for heritable re-coding of DNA methylation to daughter strands during DNA replication [99, 100]. While DNMT1 is responsible for continuance of methylation status, DNMT3a and

DNMT3b are the *de novo* methylators of CpG residues and are important for developmental gene repression [97-100].

These methyl-signals are recognized and interpreted by several proteins which contain **m**ethyl-**b**inding **d**omains. These so-called MBD proteins, of which MeCP2 [**M**ethyl **C**pG Binding **P**rotein **2**], is the archetype, bind to and recruit repressive chromatin inducing complexes directly to promoters [101]. These multi-protein complexes, containing **H**istone **Deac**etylases (HDAC) and other chromatin remodelling proteins, initiate chromatin condensation and the formation of facultative heterochromatin and thus cause repression of transcription [102]. The importance of methylation to human disease is highlighted by the Fragile X Syndrome, which is the most common form of familial mental retardation, resulting from increased DNA methylation at an expansion of CGG sequences within the 5' untranslated region of the *FMR1* gene [103, 104]. Furthermore, mutations affecting the function of *MeCP2* are directly linked to the mental retardation disease, RETT Syndrome [105]. Likewise mutations in DNMT3b have been shown to be involved in ICF syndrome [31].

1.3.2 Passive histone modifications.

Histones are highly compact globular proteins, the modification of which is limited, for the most part, to the less-structured histone tail [106]. The tail, located at the N-terminus of the histone comprises 20-40 residues and extends out and away from the core nucleosome, providing sites for various post-translational modifications. There are a variety of reversible modifications: acetylation, methylation, phosphorylation, ubiquitination, ADP-ribosylation, sumoylation, deimination and proline isomerisation

(reviewed in [96]. Many residues have been identified as targets for such modification. These modifications can influence how the core histones interact with the DNA and other proteins, and in turn make up the basis of the "Histone Code" [106]. The "Histone Code" was a term first coined to describe the specific combinations of post-translational modifications to histones which influence gene expression patterns, a language that can be interpreted to govern the chromatin state [107].

The most common histone modification is acetylation, which is typically associated with gene activation [106]. The lysine residues at position 9, 14, 18 and 23 of Histone H3 and the lysine residues at position 5, 8, 12 and 16 of Histone H4 are the most frequently targeted [108]. The acetylation of histone tails is modulated by two classes of proteins called **H**istone **A**cetyl **T**ransferases [HATs] and **H**istone **Deac**etylases [HDACs] [109, 110]. The modification of histones by acetylation has been shown to increase the accessibility of chromatin by *cis*-binding factors through two mechanisms. One, by introducing a strong negative charge to the nucleosome it neutralizes the potential interaction of positive lysine residues to the negative phosphates of the DNA backbone and causes a natural repulsion. As well, the specifically located acetyl-groups act as beacons in the recruitment of activating chromatin remodelling complexes [101, 111]. Acetylation of lysines represents a signal for the switching of facultative heterochromatin into euchromatin for the purpose of gene expression. Methylation, like acetylation is also a talisman of transcriptional status, but unlike acetylation, methylation is often associated not only with repression but also with gene activation [97, 106]. Methylation of histones is a covalent modification commonly occurring on the side-chain nitrogen atoms of lysine, arginine and histidine residues, but only the methylation status of the lysine and arginine residues is associated with the Histone Code [72, 112, 113]. Methylation of lysine

residues at position 9 and 27 of histone H3 and position 3 and 20 of histone H4 are strong indicators of repressed chromatin as are the methylation of arginine residues at position 2, 17 and 26 of histone H3 [113]. However, methylation can occur in three basic forms, mono-, di- and tri-methylation. **P**rotein arginine **M**ethyltransferases [PRMTs] are a group of proteins which transfer methyl groups to the nitrogen side chains of arginine residues [114]. It was first observed that methylation was involved in regulation of transcription when PRMT4 (also called CARM1), a known co-activator associated protein, was shown to have methyltransferase activity [72, 115]. PRMT4 has long been known to promote gene repression [116]. Furthermore, the methylation status of lysine 9 on histone H3 [H3-K9] (mono-, di- and trimethylated) has been linked to the formation and spreading of facultative heterochromatin [72, 106, 117]. Moreover, methylated H3-K9 serves as a beacon for the binding of **H**eterchromatin **P**rotein **1** (HP1) which can oligomerize to form heterchromatin [118].

The third most common post translational modification to histones involved in the Histone Code is histone phosphorylation. Phosphorylation occurs uniquely on the serine and theonine residues of all the major Histones (**H1** at S139, **H2A** at S1 and T120, **H2B** at S14, **H3** at T3, S10, T11, S28 and **H4** at S1) but the most studied is phosphorylation at the serine 10 residue of Histone H3 [H3-S10], which has been intimately associated with induction of transcription by facilitating GCN5-mediated acetylation of H3-K14 [119, 120]. Interestingly, Histone H3 phosphorylation is also involved in proliferation, since phospho-Histone H3 is a well characterized marker of mitotically active cells in G2-M phase, and is used several times in the experiments of this thesis (**Section 3.0**) [121, 122].

Very little is known about the potentially vast number of other histone modifications (ubiquitination, ADP-ribosylation, proline isomerisation and sumoylation),

but what also remains unclear is how the combination of such modifications may have a role in gene regulation. One pointed example of the interplay between methylation and acetylation is their competition for targets. For example acetylated lysine 9 on histone H3 [H3K9Ac] is associated with gene activation and euchromatin, whereas the same target di-methylated [H3K9Me2] is a strong indicator of repressed facultative heterochromatin [102].

1.3.3 Active nucleosome remodelling.

The Epigenetic Code, as represented by "passive" modifications, is really a combination of the DNA methylation status and the Histone Code, but it is "active" nuclear remodelling which brings its regulatory effects to fruition. Chromatin remodelling and histone modifications are complementary processes. While DNA and histone post-translational modifications influence the histone's affinity for DNA, loosening or tightening this interaction, it is the role of chromatin remodelling complexes to reposition, disassemble and assemble the nucleosomes [74, 123]. Chromatin remodelling is an ATP-dependant process performed by an assortment of multi-protein complexes each of which contains an ATPase catalytic subunit (reviewed in [123]. The coordinated activities of histone-modifying enzymes and chromatin remodelling complexes are involved in a wide variety of cellular functions.

1.4 Chromatin remodelling proteins.

Adenosine triphosphate [ATP]-dependant chromatin remodelling proteins comprise the most studied group of chromatin reorganising proteins. These non-histone proteins are

targeted to the molecular beacons of the Epigenetic Code and acting in a collaborative complex with other proteins effect the reorganization of nucleosomes, allowing greater access or restricting access to regulatory sites, such as promoters (refer to Figure 5) [124]. A striking example of this is the *beta-globin* gene cluster. In cells where *beta-globin* is not expressed (brain, skin) the entire region containing the gene cluster is tightly packed into facultative heterochromatin, however in erythroid cells, which do express *beta-globin*, the higher order chromatin structure is not present [125-127]. Another pointed example is chromatin rearrangement by SWI2/SNF2 in the regulation of the yeast *suc2* promoter [128].

Chromatin remodelling is a multiple step process performed by an assortment of multi-unit complexes, each of which contains a protein that has a SWI/SNF (**Swi**tching/ Sucrose **n**on-fermenting)-like ATPase of the SNF2 family [129]. The diverse nature of these ATP-hydrolyzing subunits has led to a classification system based on alternative structural and functional similarities; there are 7 subgroups (refer to Figure 6) [105, 123, 130]. The three most common subgroups are the SWI2, CHD and ISWI groups, with the major distinguishing structural feature being a different protein-protein or protein-DNA interacting domains. They are the bromodomain (which bind to acetylated lysines), chromodomain (which bind to methylated histones) and the SANT domain (**S**WI3, **A**DA2, **N**-CoR and **T**FIIIB, important for DNA binding) [131-135]. In complexes, these proteins collectively act to destabilize or reconstitute nucleosome structure along the DNA template [136-139]. In order to do this they use the energy from ATP hydrolysis to introduce a superhelical torsion into the DNA, which in effect pries it away from the nucleosomes allowing for a change in position or removal of histones [140-143].

Figure 5 – Alterations in chromatin structure; histone modification and chromatin remodelling.

Local alteration in the chromatin structure is directed by "passive" histone modifications and "active" chromatin remodelling. Histone acetylation, mediated by HATs [Histone Acetyl-transferases] and chromatin remodelling complexes render chromatin packaged DNA more accessible to *cis*-DNA binding factors. Transcriptional activation is dependent upon such structural modifications. Adapted from Alberts, B.J. et al., (2002) [144].

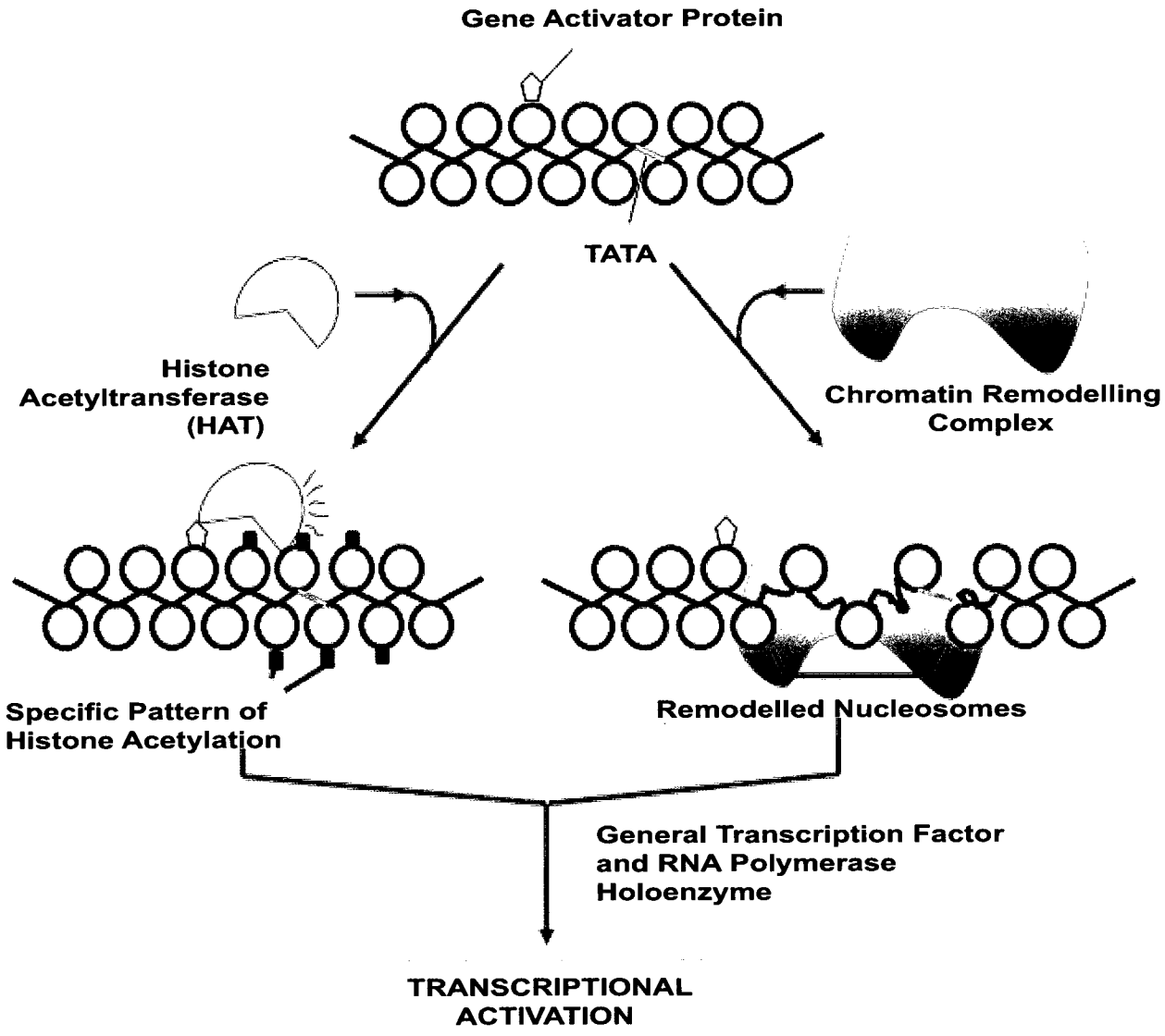
Gene Activator Protein
TATA
Histone
Acetyltransferase
(HAT)
Chromatin Remodelling
Complex
Specific Pattern of
Histone Acetylation
Remodelled Nucleosomes
General Transcription Factor
and RNA Polymerase
Holoenzyme
TRANSCRIPTIONAL
ACTIVATION

Nucleosome remodelling is a term given to describe a set of reactions which increase/decrease nuclease accessibility by altering DNA supercoiling or through invoking octamer relocation in *cis* or in *trans*. They are also involved in the removal/replacement of entire histone subunits. One method of nucleosome relocating is "sliding," where intact nucleosome units are repositioned on adjacent *cis*-DNA [145]. There are two models for nucleosome sliding, one involving a twisting motion of the nucleosome through its connected DNA, the other by creating bulges of DNA in the upstream direction of nucleosome movement (also called the Looping model) [146]. According to the looping model, small lengths of DNA are released from the nucleosome by an ATP-driven enzyme; the propagation of this loop results in the sliding movement of the nucleosome [145]. While the second method of nucleosome relocation, *trans*-displacement, involves the disassembly of histone octomers, it may also occur in the absence of chromatin remodellers [145]. The initiation of both of these chromatin remodelling strategies involves the identification and recruitment of chromatin remodelling complexes to molecular targets such as the histone modification beacons discussed above. These methods of chromatin remodelling typically involve the manipulation of DNA around the nucleosome, but another form of remodelling can occur at the histone subunit. There are many sequence variants within Histones themselves, for example, within the H2A family there is a specific variant called H2AZ (~10% of all H2A)[147]. Nucleosome remodelling complexes can release the nucleosome from the DNA and allow H2AZ to replace H2A. When H2AZ is incorporated into the core group of histones, it has the specific effect of altering nucleosome stability [147].

Figure 6 – Helicase and related Proteins with conserved NTP-binding motifs.

The SNF2-like family of ATPases contains conserved ATP-binding motifs that are present in many DNA and RNA helicases. This diagram, updated from Pazin et al., (1997) [138], shows selected examples of known family members.

Helicases and Related Proteins with Conserved NTP-binding Motifs

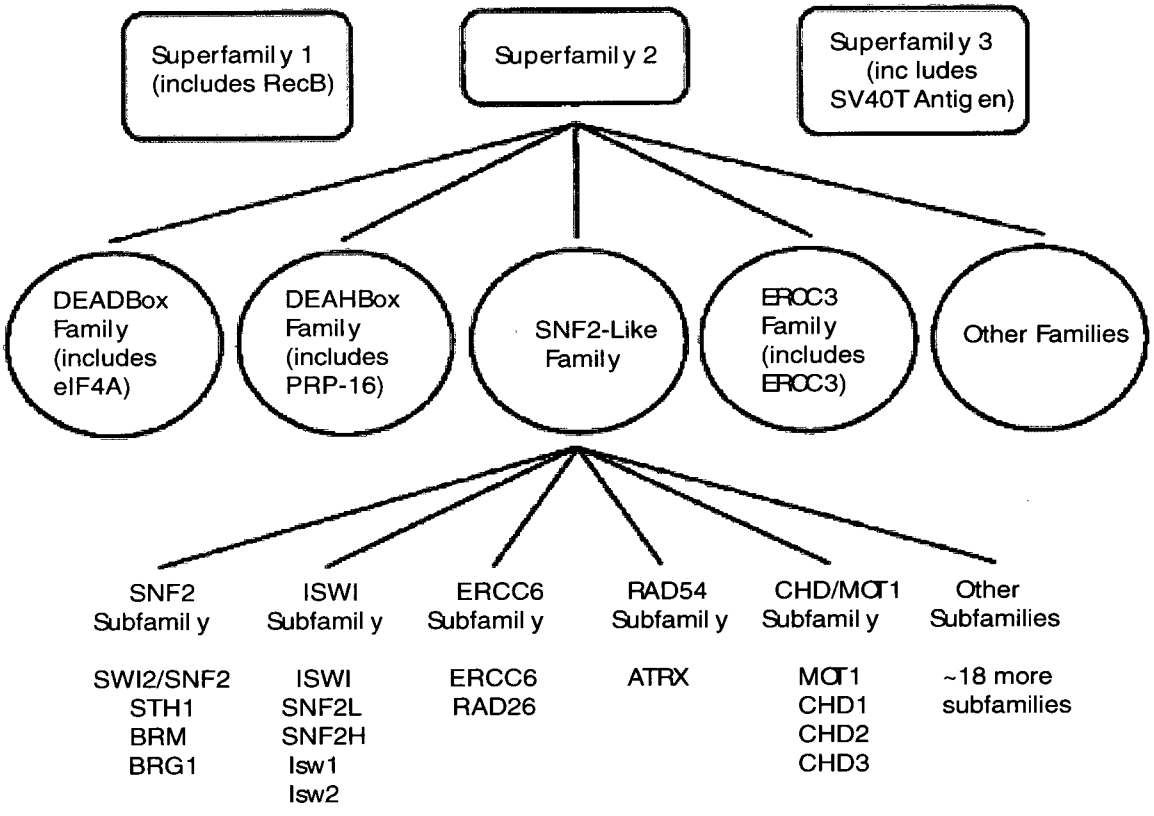

1.4.1 The SWI/SNF family of proteins.

The SWI2/SNF2 ATPase is called such because the *swi2* and the *snf2* genes, though independently isolated, were found to be the same gene. It was first described in yeast in the early 1990's [6, 148]. They represent a class of proteins that are important as enhancers of transcriptional activation in response to molecular cues; however they have also been associated with repression [128, 148-152]. The SWI/SNF complex (~2 MDa), which contains the SWI2/SNF2 ATPases with SNF5/INI1, BAF155, and BAF170 as its core complex, is highly conserved from yeast to humans and has been shown to disrupt nucleosome positioning and increasing accessibility of transacting factors *in vitro* and *in vivo* [153, 154]. In mammals there are two homologs, *Brahma* (*Brm*) and *Brg1* [***Brahma related gene 1***] [154, 155]. Moreover, in *Drosophila,* which only has one of the homologs, Brm, it has been shown to be required for RNA polymerase II association with chromatin, suggesting a role for Brm in transcription [156, 157]. The bromodomain, the discerning structural feature of the SWI2/SNF2 family, has been shown to recognize and bind to acetylated lysines of the N-terminal tail of histone H4 [132, 158, 159]. For a more detailed discussion, the roles of BRG1 and BRM are addressed in section 1.6 Chromatin Remodelling and Development.

1.4.2 The CHD/Mi2 family of proteins.

The presence of a chromodomain, which is a motif that is involved in binding to methylated histone tails, is the defining feature of the CHD [**C**hromodomain-**h**elicase **D**NA binding] ATPases. Mi-2, the most abundant member, has been identified as the ATPase subunit of the NURD complex, which also includes the histone deacetylases HDAC1 and

HDAC2 [160, 161]. The NURD complex reprograms gene expression by removing acetylation and promoting repression [160, 162]. Moreover, Mi-2 is recruited to target promoters by the hunchback protein, which is known to be required for transcriptional repression [163, 164].

1.4.3 The ISWI family of proteins.

The ISWI [**I**mitation **Swi**tch] family is the largest and most diverse family of SNF2-like ATPases and has been shown to bind to the N-terminal tail of Histone H4 through an interaction with nucleosomes at the paired SANT domain [131, 133, 134, 165]. ISWI was first isolated in *Drosophila,* from which three complexes have been identified: NURF [**N**uclear **R**emodelling **F**actor], CHRAC [**C**hromatin **A**ccessibility **C**omplex], and ACF [**A**TP-dependant **C**hromatin assembly and remodelling Factor] [166-168]. These ISWI complexes have been found to be highly conserved from yeast to humans, and an additional 5 novel complexes have been identified in mammals [166, 169]. For a complete list of mammalian ISWI complexes and their functions refer to Table 1. As the ISWI proteins are found in so many complexes with divergent functions, it is assumed that these roles are dependent upon the other complex members. As an example the Nurf301 subunit (BPTF, in mammals) of the NURF complex can interact with the GAGA transcription factor, providing a mechanism of recruitment in the activation of transcription [170]. However, the majority of ISWI complexes do not co-localize with RNA polymerase II, which suggests that transcriptional activation/repression is not its only function [171-174].

Table 1 – The mammalian ISWI complexes and their functions.

This table shows the known mammalian chromatin remodelling complexes which contain either SNF2H or SNF2L. SNF2H complexes (with the exception of NoRC) are often characterized with functional involvement in replication dependant processes whereas CERF and NURF, the two SNF2L complexes are known to be, but not exclusively involved, in transcriptional activation.

COMPLEX	SUBUNITS	FUNCTION	REF
SNF2H-Complexes:			
ACF	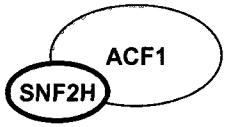	**-chromatin assembly and nucleosome spacing**	[169]
CHRAC	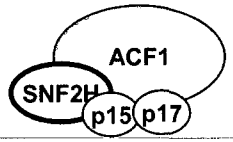	**-chromatin assembly and nucleosome spacing**	[170]
WICH		**-heterochromatin replication and transcriptional regulation**	[188]
RSF		**-chromatin assembly and nucleosome spacing**	[245]
NoRC		**-ribosomal DNA repression**	[185]
SNF2H-Cohesin	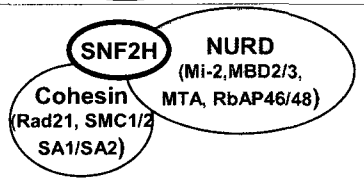	**-sister chromatid cohesion**	[186]
SNF2L-Complexes:			
NURF	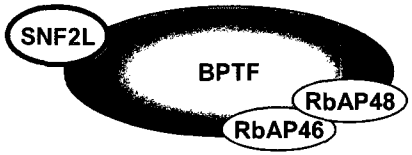	**-transcriptional activation**	[171]
CERF	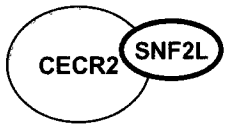	**-transcriptional activation**	[194]

1.5 The mammalian ISWI proteins.

Similar to the SWI/SNF ATPases, Brm and Brg1, there are two mammalian ISWI orthologs, *Snf2h* and *Snf2l;* they are highly similar (approx. 84% identity at the amino acid level) [77, 175-177]. However, *Snf2h* and *Snf2l*, present different expression patterns signifying that they possess distinct developmental roles [77, 175]. There are a total of eight known mammalian ISWI complexes with varied functions. Interestingly, six of these complexes contain, predominantly, SNF2H (ACF, CHRAC, No-RC, SNF2H-Cohesion, WSTF, RSF) while SNF2L is the ATPase component of two complexes (NURF and CERF), see Table 1. Despite their different biochemical properties it has been suggested that SNF2H and SNF2L might be interchangeable. As an example, the **H**uman **Chr**omatin **A**ccessibility **C**omplex [HuCHRAC] contains predominantly SNF2H; however under normal conditions 5% of these complexes contain SNF2L in its place [178].

1.5.1 Characterization of the mammalian ISWI genes.

Located on the X chromosome, the mouse *Snf2l* gene is made up of 24 exons while the human *SNF2L* has an extra 25th exon, designated exon 13, which when incorporated renders an ATPase dead protein [179]. Interestingly, this non-functioning variant is predominant in non-neuronal tissues [179]. The mouse S*nf2l* gene transcript contains a 3195 base pair open reading frame encoding a 1064 amino acid protein [175]. It is also subject to alternative splicing generating multiple isoforms [175, 180]. There are predominant tissue-specific transcripts of approximately 3.7 kb, 4 kb and 5kb in size that are expressed throughout development [175]. The 3.7 kb transcript is exclusively present in the central nervous system [175].

SNF2H is located on chromosome 4q31.1-31.2; it produces a full length transcript that is 3.8 kb and a 1051 aa protein [175]. The central feature of these proteins is the C-terminal SNF2 ATPase/helicase domain (made up from 7 helicase motifs) providing the catalytic core of the protein and the C-terminal paired SANT domain, which define its activity as an ATPase [129, 133]. Refer to Figure 7.

1.5.2 Functional characterization of the mammalian ISWI proteins.

The SWI/SNF and ISWI based complexes have distinct chromatin-remodelling activities [181, 182]. The similarities are that both complexes have an affinity for the N-terminal tail of Histone H4, and both complexes use the hydrolysis of ATP for *in vivo* and *in vitro* activities that can alter the translational position of nucleosomes and allow DNA accessibility. However, ISWI complexes manage DNA accessibility using only the sliding method, while the SWI/SNF complexes utilize both sliding and *trans*-displacement [181, 183]. Once the complex binds to the histone tail target, the energy from hydrolysis of ATP is used to induce a conformation change increasing the torsional stress which results in tearing the DNA away from the nucleosome [143]. It has been shown that while both complexes require ATP, ISWI complexes are stimulated only by nucleosomes, while the SWI/SNF complexes are activated by both nucleosomes and naked DNA [184]. Consistent with this theory, the targeted mutation of the highly conserved ATP binding pocket of the ATPase/Helicase domain not only disconnects the ability to bind ATP, but also creates a functionally null protein lacking the ability to remodel chromatin [169].

Figure 7 – SNF2-like family member structural composition and ISWI subfamily similarity.

[A] Schematic diagrams of the three major identified families of nucleosome remodelling ATPases and their domain structure. Each family is defined by the presence of a distinct ATPase containing signature structural domains and a unique subunit composition. [B] The mammalian ISWI genes *SNF2H* and *SNF2L* (86% identical) contain an ATPase domain near the N-terminus and the paired SANT domains at the C-terminus. Listed, are the percent identities between family members for the ATPase and SANT domains (both domains and intervening sequence combined) as compared with the human *SNF2L* gene. These figures are adapted from [175, 185].

A

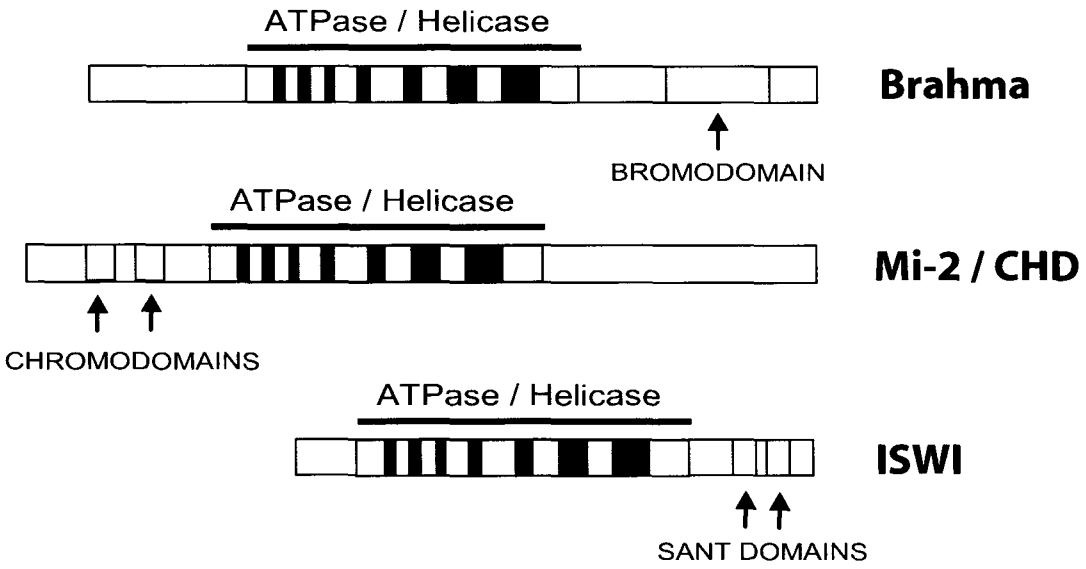

B

Human SNF2L

	ATPase	SANT
Mouse Snf2l	95%	100%
Human SNF2H	87%	87%
Mouse Snf2h	85%	92%
Drosophila ISWI	78%	87%
Yeast ISW1	65%	48%
Yeast ISW2	65%	55%

1.5.3 Expression patterns of the mammalian ISWI proteins.

Initial screens determined that although there are overlapping expression patterns, there are clear underlying differences in expression of *Snf2l* and *Snf2h* in the developing mouse embryo [175]. Both *Snf2l* and *Snf2h* are expressed at low levels throughout the embryo from E9.5-E15.5; *Snf2h* is elevated in the developing neocortex, cerebellum, olfactory epithelium, lungs kidney and gut but gradually decreased into postnatal periods, see Figure 8 [175]. However, *Snf2l* expression is gradually increased postnatally, particularly the 3.7 kb transcript in the brain [175]. One region in the adult mouse where *Snf2h* and *Snf2l* remain highly expressed are the ovary and testes [175]. One major difference between human and mouse *Snf2l* is that while humans express *SNF2L* in all tissues, only the active form (-exon13) is expressed in neurons providing an alternative means of regulation [179]. *Snf2l* is characterized as a brain-enriched transcript with increased expression upon differentiation, suggesting a role in maturing neuronal cell populations and also with strong expression in the reproductive organs [167, 175, 187, 188]. The first isolated mammalian SNF2L protein complex demonstrated that human NURF, like its *Drosophila* counterpart regulated the expression of the neuronal transcription factor *engrailed-1* (*en*-1) and *engrailed-2* (*en*-2) genes [169]. Snf2l was also shown to promote neurogenesis [169, 189]. To this end, it has been revealed that transfection with an ATPase-inactive dominant negative *Snf2l*, leads to the inability of N1E-115 mouse neuroblastoma cells to form neurite extensions [169]. These findings suggest that S*nf2l* becomes particularly active during the differentiation of neurons, revealing the possibility that the protein it encodes may be a positive regulator of

Figure 8 - Expression of *snf2l* and *snf2h* in the adult mouse tissues, the developing embryo and postnatal brain.

This figure, taken from Lazzaro M. B. and Picketts, D. J. (2001) [175], shows the embryonic and postnatal expression profiles of murine *Snf2l* and *Snf2h*. Snf2l expression is limited to the CNS and the reproductive tissues, while Snf2h has a widespread pattern of expression. Northern blot analysis of mouse tissue is depicted. [A] Selected adult mouse tissues, and [B] in the embryonic developing brain (E9.5 and E15.5), and the developing postnatal brain (P1-P24) was analyzed for snf2l transcripts (top panel) and snf2h transcripts (middle panel). Actin was used as an RNA loading control (bottom panel).

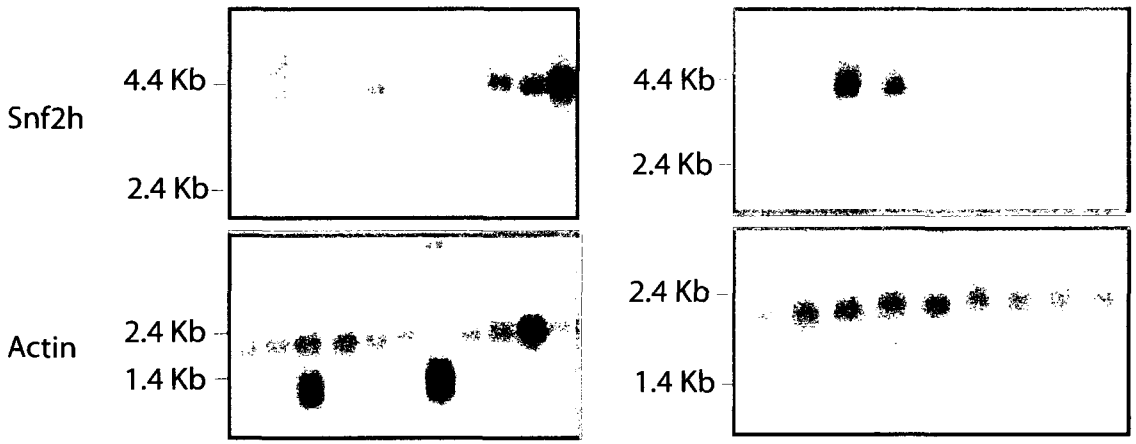
Snf2h
4.4 Kb
2.4 Kb
Actin
2.4 Kb
1.4 Kb
4.4 Kb
2.4 Kb
2.4 Kb
1.4 Kb

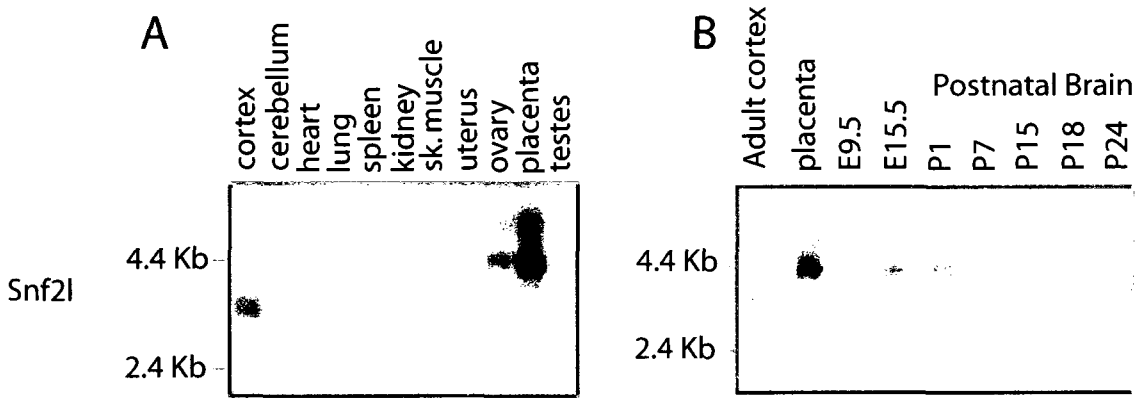
A
cortex
cerebellum
heart
lung
spleen
kidney
sk. muscle
uterus
ovary
placenta
testes
Snf2l
4.4 Kb
2.4 Kb
B
Adult cortex
placenta
Postnatal Brain
E9.5
E15.5
P1
P7
P15
P18
P24
4.4 Kb
2.4 Kb

neurogenesis. A second complex, the **C**ecr2-containing **R**emodelling **F**actor (CERF), has been identified as a heterodimeric complex composed of Snf2l and the transcription factor Cecr2 [**C**at **E**ye Syndrome **C**hromosome **R**egion **C**andidate **2**] [189]. Mice deficient in Cecr2 display exencephaly defects, further signifying a role for Snf2l complexes in neurodevelopment [189]. Recently it was reported that targeted inactivation of *Xenopus* ISWI (xISWI) by microinjection of dominant negative mutant mRNA or antisence morpholino oligonucleotides into fertilized eggs leads to inhibition of gastrulation and neural fold closure [187]. These results suggest a critical role for xISWI in early embryonic development. SNF2L involvement in the regulation of the key neuronal transcription factors *en-1* and *en-2*, and its ability to ectopically induce neuron outgrowth suggests that SNF2L is probably active early in neurogenesis and could represent a key regulator in this process [187]. The two areas of the brain that undergo heightened adult neurogenesis in the mouse are the hippocampus and the cerebellum; these are also areas of high S*nf2l* expression [175]. It is important to note that these regions are vital to learning, memory and motorneural skills, suggesting that Snf2l might be involved in memory encoding and storage [22, 190, 191]. Moreover, due to the location of *SNF2L*, at Xq25-26, and the proximity of several genetically mapped familial cases of mental retardation, the gene has been screened as a possible disease candidate [180]. To date, no mental disorder has been genetically linked to misexpression or mutation of the *Snf2l* gene.

Snf2h has a prevalent expression during neuroprogenitor proliferation [167, 175]. SNF2H complexes have many roles in DNA replication and general chromatin maintenance [167, 175]. Targeted inactivation of Snf2h in mice resulted in peri-implantation lethality due to an inability of ES cells to proliferate [186]. Yet, these results set the stage for a dynamic regulatory mechanism, wherein Snf2h controls proliferation,

and maintains cell growth, while Snf2l promotes cell cycle exit and initiates differentiation into neural tissues and cell types.

1.6 Chromatin remodelling and development.

The modification of chromatin structure between "open" euchromatin and "closed" heterochromatin is a major point of regulation in establishing tissue specific patterns of gene expression that govern developmental processes necessary for proliferation and differentiation [74, 101, 192]. Given the extensive range of cellular functions governed by chromatin remodelling, it has been suggested that these proteins are essential for normal development. Indeed, the targeted inactivation of several chromatin remodelling protein complexes in mice has resulted in early embryonic lethality, including ATRX, Brg1, Snf5 and Snf2h [186, 193-195]. Moreover, null mutations of ISWI in *Drosophila* are lethal, resulting in termination at embryonic-early pupae stages [172]. However, the loss of chromatin remodelling proteins is not always lethal. The most studied chromatin remodelling complex, the SWI/SNF complex, which contains either BRG1 or BRM is linked also to regulation of the cell cycle [196-200]. There is a level of redundancy between these ATPases. *Brg1*, like *Snf2h*, is a predominant ATPase in proliferating cell lines/tissue, and both are vitally important as *Brg1* and *Snf2h* null mutants are embryonically lethal [186, 201]. *Brm* and *Snf2l*, are both expressed predominantly in differentiating cells/tissues and unlike *Brg1*, *Brm* is not a vital gene as the *Brm*-null mouse survives with only a minor developmental phenotype [197, 198]. Similarly, a hypomorphic mutation of *Pasg* (**P**roliferation-**A**ssociated **S**NF2-like **g**ene), which encodes a helicase highly related to *Snf2* and facilitates global DNA methylation, results in growth retardation

and premature aging in mice [202, 203]. The inactivation of several yeast chromatin-remodelling proteins resulted only in a slower growth phenotype [6, 77, 198].

The switch from a proliferative to a differentiated state requires a cell to undergo profound changes in gene expression that are dependent on global chromatin remodelling within the nucleus. An interesting paradigm is the antagonistic interactions of the BAF [**B**RG1- or hBRM-**a**ssociated **F**actors] complexes in mammalian regulation of proliferation and differentiation. Both Brm and Brg1 are known to interact with the "active" hypophosphorylated p105/Rb protein suggesting a role in the control of proliferation [199]. Brg1 interactions with pRb and their association with E2F lead to repression of several genes involved in cell cycle progression, such as *Cyclin A* and *Cyclin E* [197]. Brg1 is required for neurodifferentiation by mediating the transcriptional activities of the proneural bHLH [**b**asic **H**elix-**L**oop-**H**elix] proteins, Neurogenin 3 and Neurod2 [204]. In fact, loss of BRG1 expression is implicated in the transformation of several primary tumour samples and tumour derived cell lines [205-208]. It was also shown that BRG1 is important for animal viability; the protein is stable throughout the cell cycle, and depletion of Brg1 leads to an impediment in cellular differentiation [196, 197, 201, 209]. Brm proteins are phosphorylated, inactivated and degraded during G2/M phase, only to be reactivated and hypophosphorylated in growth arrested cells, suggesting a role for the promotion of differentiation [199, 210]. Moreover it has been shown, *in vitro*, that increasing levels of *Brm* accompany cell cycle withdrawal [199, 211, 212]. Thus, it has been suggested that the Brm-null mouse is viable through compensatory effect of the Brg1 protein, and is about 15% heavier then control littermates, presumably because of enhanced proliferation particularly in the fibroblast population [198, 213].

Similarly, ISWI proteins are implicated in control of cell proliferation and cancer. The human *ISWI* homologue, *SNF2H* which itself is a vital component of the cellular proliferation mechanism [186], is also linked to various forms of cancer, particularly in ovarian and breast carcinomas [188, 214-217]. Even chromatin remodelling proteins of the CHD/Mi-2 class of ATPases are implicated with direct roles in the regulation of cellular proliferation and cancer [218, 219]. Indeed, defective epigenetic regulation has been implicated in a wide range of other genetic disorders including mental retardation and autoimmune disease. Moreover, it has been suggested that gene regulation at the chromatin level plays a significant role in neuroprogenitor cell growth and neuronal differentiation [24, 220].

1.6.1 Chromatin remodelling in the developing brain.

The brain, the most complex organ in the mammalian body, contains the largest diversity of cell types. This complexity is obvious in the adult human brain where there are about 10-20 billion interconnected neurons and about 5-10 times as many glial cells [221]. Collectively, the cells that form the nervous system express 80% of genes in the genome; however, each cell expresses its own distinct collection [222]. The basic need to manage these cascading subsets of genes falls largely to the role of epigenetic and chromatin regulation [192, 223]. Moreover, the necessity to react to external stimuli and thus remember, learn, feel, and make complex decisions, is itself maintained by a high level of plasticity in gene expression [224]. In human terms the brain is the seat of intelligence; it is responsible for thought processes, emotions, controls movement and interpretation of all the senses. All the cells of the nervous system are derivatives of specialized neuronal stem

cells and progenitors [225]. The coordinated function of various regulatory networks (which include cascading signal transduction pathways and many transcription factors) plays key roles in the specification and differentiation of neural identity [225-227]. The correct sequence and order of transcription factor activity is absolutely fundamental for correct neurodevelopment [228]. The most important of these transcription factors are the activators of signal cascades such as the proneural bHLH transcription factors such as Neurogenin-related-1, the earliest proneural gene to be expressed, closely followed by *Neurogenin*1-3, *Neuro*D1, *Neuro*D2, *Math*1, *Mash*1 and others [192, 224, 226, 227, 229]. Recent studies have proposed a link between chromatin remodeling protein complexes and neurogenic regulatory factors [24, 220]. These experiments have implied that gene regulation plays a critical role in cell growth and neuronal differentiation. Furthermore extracellular signaling systems are involved by interfacing with these diverse mechanisms [24, 230]. It was shown that a factor called Geminin was able to interact with Brg1 and prevent activation of the bHLH proneural genes by SWI/SNF. Only after initiation of neuronal differentiation does Geminin get degraded and release this block [231-233]. Several ATPases involved in chromatin remodelling, such as; *Chd-1*, *Atrx*, *Etl-1*, *Brg1*, *Brm*, *Snf2h* and *Snf2l* are expressed in the embryonic mammalian brain [175, 193, 212, 234, 235]. ATRX is an interesting example, as targeted loss of the protein in the developing telencephalon results in a hypocellularity of the developing mouse forebrain and ultimately perinatal lethality [193]. Moreover, mutations in the *ATRX* gene, which encodes ATRX, result in developmental disorders such as ATR-X [**A**lpha-thalassemia, mental **r**etardation, **X**-linked] syndrome [236].

Equally as important as activation, is the spatial and temporal repression of gene expression during neurodevelopment. Often times a repressed gene must remain silenced

for the remainder of the life of the organism, and as such, facultative heterochromatin is an ideal candidate. In non-neuronal lineages, the REST/NRSF [**R**epressor **e**lement-1 **s**ilencing **t**ranscription factor/**n**euron **r**estrictive **s**ilencing **f**actor] triggers epigenetic silencing of neuronal genes [237-239]. Moreover, REST/NRSF must be reduced in order for neuronal differentiation to occur [237, 240]. In non-neuronal cells, the REST/NRSF factors bind to the NRSE [**n**euron-**r**estrictive **s**ilencing **e**lements]) cis-DNA elements [5'TTC AGC ACC NCG GAC AGN GCC [241]] and block transcription through a complex interaction of HDACs, MeCP2, the co-repressor Co-REST and various epigenetic silencing factors, resulting in the recruitment of HP1 and the formation of facultative heterochromatin [242, 243]. There are a predicted 1800 target genes which utilize the REST/NRSF and Co-REST factors for repression. Many of these are of fundamental importance to neuronal differentiation [244]. To summarize, correct development depends both on the activation of key neuronal organizers and the inactivation of unnecessary genes.

1.7 Rationale and specific aims.

Recently much interest has been directed towards the roles that epigenetic regulatory factors have in the control of cell proliferation and differentiation. A detailed understanding of the role these molecules have in the development of the nervous system is important for establishing a functional connection between neurogenic factors, chromatin remodelling and transcriptional regulation during neurogenesis. I **hypothesize** that Snf2l and Snf2h complexes have an active and complimentary role in regulating the switch between proliferation and differentiation in neuronal lineages and are therefore critical for brain development. To gain insight into Snf2l function during mouse brain development

we have developed a conditional gene-targeted *Snf2l* mouse. I have observed an increase in brain size that is the result of hypercellularity. In the forebrain this hypercellularity is consistent through all cortical layers and hippocampal strata. I **hypothesize** that the Snf2l-null mouse remains viable due to compensation of the closely related Snf2h protein and that the hypercellularity is the result of this compensation. I further **hypothesize** that the increase in cell number observed in Snf2l-null mouse cortices is the result of enhanced proliferation of the neuroprogenitor (both neuroepithelial and intermediate progenitors) during embryonic development, due to an inability to exit the cell cycle in a timely fashion. In this thesis I will present a thorough assessment of the properties of these proteins *in vitro* and the characterization of the Snf2l-null mouse within the context of embryonic corticogenesis to determine the role of Snf2l has in development. To address this question I have set the following aims.

AIM 1 – To evaluate the functions of Snf2l and Snf2h during the proliferation / differentiation switch.

AIM 2 – To fully characterize the brain defect of Snf2l deficient mice.

AIM 3 – To determine why there are increased cells in the Snf2l deficient cortex.

AIM 4 – To identify Snf2l target genes, involved in the regulation of neurodevelopment.

Such information will provide significant insight into how chromatin structure and nuclear organization establish heritable patterns of gene expression in the development of the central nervous system. Furthermore, an understanding of the interplay between epigenetics and transcriptional regulation will lead to an increased comprehension of whole organism development.

2.0 Materials and Methods.

2.1 Materials.

2.1.1 Sources of chemicals and reagents.

Agarose, UltraPure Low Melting Point Agarose, dNTPs and 1kb plus DNA molecular ladder were obtained from Invitrogen (Carlsbad CA). All cell culture media (DMEM, EMEM, RPMI, αMEM), Hank's Buffered Saline Solution (HBSS), additives (Penstrep, Antibiotic Antimycotic, non-essential amnio acids and GlutMAX), Trypan Blue, Geneticin [G418] and lipid transfection vehicles (Lipofectamine Reagent and Lipofectamine 2000) were also purchased from Invitrogen. Retinoic acid, nocodazole and cyclohexamide were purchased from Sigma-Aldrich (St. Louis, MO). Fetal Bovine Serum came from multiple sources including PAA Laboratories Inc, (Toronto), Invitrogen, and Cansera (Rexdale, ONT). All cell culture plates, dishes, flasks were purchased from Falcon (Franklin Lake NJ), Corning (Corning, NY) or Nunc (Denmark). Tryptone, yeast extract and bacto agar are from Becton Dickinson and Co. (Franklin Lake NJ). Aprotinin, PMSF (phenylmethanesulphonylfluoride) and NuPAGE 3-8% tris-acetate Gels were purchased from Invitrogen. The Precision Plus Protein Dual Color Standards and Bio-Rad Protein Assay are from Bio-Rad (Hercules CA). 5-bromo-2-deoxyuridine [BrdU] and 4', 6-diamidino-2-phenylindole [DAPI] were obtained from Sigma-Aldrich (St. Loius, MO). ABsolute QPCR SYBER Green Mix used in realtime PCR is from Thermo Scientific (a subsidiary of Fisher Scientific). The Sepharose A and G beads used in immunoprecipitation and chromatin immunoprecipitation experiments were obtained from GE Healthcare (Uppsala, SWE). Kodak Biomax MR-1 Film and ECL Plus, Western

Blotting Detection System are also from GE Healthcare. CL-X Posure Film was obtained from Thermo Fisher Scientific (Waltham, MA). Pasteurized Skim Milk Powder, No Name Brand is from Loblaw's Inc. (Toronto, ON). Complete EDTA Free Proteinase Inhibitors, 5-Bromo-4-chloro-3-indolyl-phosphate [BCIP] and 4-Nitro blue tetrazolium chloride [NBT] are from Roche (Manheim, GER). O.C.T. Compound (Tissue-Tek, Torrence CA) was used as an embedding medium for frozen tissue specimens. All radiolabelled [α-32P]dCTP isotopes (10 μCi/μL) were purchased from Amersham Pharmacia Biotech. Inc. (now GE Healthcare, Baie d'Urfe, QB). All other common laboratory chemicals are from Sigma-Aldrich, Fisher or Invitrogen.

2.1.2 Enzymes.

Restriction endonucleases were purchased from (New England Biolabs, Fermentas (Burlington, ON), Roche, Invitrogen). *Dpn*I was purchased from Stratagene (La Jolla, CA). The Expand Long Template PCR System, Shrimp Alkaline Phosphatse and Rapid Ligase Kit were obtained from Roche. Taq DNA polymerase, Superscript II reverse transcriptase and Superscript III reverse transcriptase, RNase Out, RNase A and DNase I are from Invitrogen. The Quick Exchange Mutagenesis Kit is from Stratagene. DNA Polymerases: T7, SP6 and T3, used in the generation of *in situ* Riboprobes are from New England Biolabs as were Klenow, and T4 DNA Ligase.

2.1.3 Oligonucleotides.

Random Primer mix containing random hexamers was obtained from Invitrogen. Unless otherwise stated, all custom oligonucleotides used in experiments for genotyping, sequencing, semi-quantitative reverse-transcriptase, realtime quantitative reverse-transcriptase and realtime Chromatin Immunoprecipitation were synthesized by Invitrogen Custom Primers (Frederick MD), Gibco BRL Custome Primers (Ottawa ON), Cortec DNA Service Laboratories Inc. (Kingston, ON) or Intergrated DNA Technologies (Toronto ON). The sequences of the oligogucleotides used are listed in Appendix I (pp155).

2.1.4 Antibodies and riboprobes.

Table 2 - Table of Primary Antibodies

NAME	Host-animal and Dilution*	Pretreatment	Supplier	Notes
for Western:				
Snf2L-Nter	Sheep anti-Snf2L (1:500-1700) directed to the n-terminal region	1 hr minimum in Western Block	Affinity Biologicals Inc.	immunogen to recombinant Snf2L N-terminal fusion Protein
Snf2H-Nter	Sheep anti-Snf2H (1:2000-5000) directed to the n-terminal region	1 hr minimum in Western Block	Affinity Biologicals Inc.	immunogen to recombinant Snf2H N-terminal fusion Protein
P38	Rabbit anti-p38 (1:2500)	1hr in Western Block	Santa Cruz Biotechnology (sc-535)	control for cytoplasmic fraction
Histone	Mouse anti-H1/H5 (1ug/mL)	1 hr in Western	Upstate Biotechnology (05-	control for chromatin fraction

H1/H5		Block	629)	
Lamin A/C	Mouse anti-Lamin A/C (1:500)	1 hr in Western Block	Santa Cruz Biotechnology (sc-7291)	control for nuclear matrix fraction
Flag-M5	Mouse anti-FLAG (M5 clone) (1:500-1000)	1 hr in Western Block	Sigma (F4042)	
β-actin	Mouse anti-beta actin (1:1000-500)	1 hr in Western Block	Sigma (A1978)	Loading control
E7 (β-tubulin)	media containing secreted Mouse-anti beta-tubulin (1:250-500)	1hr in Western Block	DSHB	Loading control

for Immunohistochemistry:

SNF2L-Nter	Sheep anti-SNF2L (1:100) directed to the n-terminal region	1 hr 10% FBS, 0.1% Triton X-100, in PBS	Affinity Biologicals Inc.	immunogen to recombinant Snf2L N-terminal fusion protein
SNF2H-Nter	Sheep anti-SNF2H(1:100) directed to the n-terminal region	1 hr 10% FBS, 0.1% Triton X-100, in PBS	Affinity Biologicals Inc.	immunogen to recombinant Snf2h N-terminal fusion Protein
BrdU	Mouse anti-Bromodeoxyuridine (1:100)	10 min boiling in 0.01M Sodium-Citrate buffer 15-30 min 2N HCl, 15 min Tris-Cl pH8.8, 1 hr 10% FBS, 0.1% Triton X-100 in PBS	Becton Dickinson (347580)	S-phase Marker
Ki67	Rabbit anti-Ki67 (1:100)	1 hr1 hr 10% FBS, 0.1% Triton X-100, in PBS	Novocastro	Marker of proliferation
PH3	Rabbit anti-phosphohistone H3 (1:100)	1 hr 10% FBS, 0.1% Triton X-100, in PBS	Upstate (06-570)	Marker of mitosis
β III-tubulin (Tuj)	Mouse anti-beta III tubulin,TUJ (1:400)	1 hr 10% FBS, 0.1% Triton X-100, in PBS	Stemcell Technologies (01409)	early marker of neurodifferentiation

γ-tubulin	mouse anti-gamma tubulin (1:100)	10 min boiling in 0.01M Sodium-Citrate buffer, 1 hr 10% FBS, 0.1% Triton X-100 in PBS	Sigma (T3559)	stains spindle fibres at centrosomes

*All primary antibodies for Western were diluted in Western Block (1xPBS containing 5% Milk)
**All primary antibodies for Immunohistochemistry and in situ hybridization were diluted in Block (Pretreatment)

Table 3 – Table of Secondary Antibodies

NAME	Host-Animal and Dilution	Supplier	Notes
for Western*			
Sheep-HRP	Rabbit anti-Sheep (1:10000)	DAKO Cytomation (P0163)	Immunoglobins (mainly IgG)
Sheep-HRP	Donkey anti-Sheep (1:5000)	Sigma (A3415)	IgG whole molecule
Sheep-HRP	Rabbit anti-Sheep (1:5000)	Bio-Rad (172-1017)	IgG (H+L)
Mouse-HRP	Sheep anti-Mouse (1:2500)	Sigma (A5906)	IgG whole molecule
Mouse-HRP	Donkey anti-Mouse (1:5000)	Jackson Immuno Research Laboratories Inc. (715-035-151)	IgG (H+L)
Rabbit-HRP	Goat anti-Rabbit (1:5000)	Sigma (A8275)	IgG whole molecule
Goat-HRP	Rabbit anti-Goat (1:5000)	Sigma (A5420)	IgG whole molecule
for Immunohistochemistry*			
Rabbit-FITC	Goat anti-Rabbit (1:500)	Jackson Immuno Research Laboratories Inc. (111-095-003)	IgG whole molecule
Mouse-FITC	Goat anti-Mouse (1:1000)	Sigma (F2012)	IgG whole molecule
Sheep-FITC	Donkey anti-Sheep	Jackson Immuno Research	IgG whole

	(1:1000)	Laboratories Inc. (713-095-003)	molecule
Sheep-FITC	Donkey anti-Sheep (1:1000)	Sigma (F7634)	IgG whole molecule
Mouse Alexa 594	Goat anti-Mouse (1:500)	Molecular Probes (A11005)	IgG (H+L)
Mouse Alexa 594	Donkey anti-Mouse (1:500)	Molecular Probes (A21203)	IgG (H+L)
Mouse Alexa 488	Donkey anti-Mouse (1:500)	Molecular Probes (A21202)	IgG (H+L)
Rabbit Alexa 594	Donkey anti-Rabbit (1:500)	Molecular Probes (A21207)	IgG (H+L)
Rabbit Alexa 488	Donkey anti-Rabbit (1:500)	Molecular Probes (A21206)	IgG (H+L)
Sheep Alexa 488	Donkey anti-Sheep (1:500)	Molecular Probes (A11015)	IgG (H+L)
Goat Alexa 488	Donkey anti-Goat (1:500)	Molecular Probes (A11055)	IgG (H+L)

*All secondary antibodies for Western analysis were diluted in Western Block (1xPBS containing 5% Milk)
**All secondary antibodies were diluted in TBLS Buffer (50 mM Tris-Cl (pH 7.4), 145 mM NaCl, 1% BSA, 60 mM L-Lysine and 0.1% sodium azide)

Table 4 – Table of Riboprobes

NAME	Notes	Reference
Cyclin D1	CDK regulator, involved in cell cycle transition	[acquired from V. Wallace, OHRI]
Foxg1	Repressor of p21 and Mash1, involved in intermediate progenitor proliferation	[245]
Gli1	Effector of Shh pathway involved in proliferation and patterning	[246]
Hes5	Marker of proliferation, Negative repressor of Notch	[247]
Id2	Marker of proliferating cells in the ependymal zone (VZ, IZ)	[248]
Pax6	Marker or Neuroepithilial Cells and Neurostemcells	[249]
Tbr-1	Marker of preplate derived neurons (layer I, VI)	[250]

2.1.5 Cell lines.

Cell lines used are listed in Table 2.1.6. All cells were grown at subconfluence under standard growth conditions in a humid atmosphere (Sanyo CO_2 Incubator) with 5% CO_2 at 37.0°C. All cell cultures were preserved in Growth Media containing 10% DMSO and stored at -80°C or in a Liquid Nitrogen Chest (-196°C). Cells were both harvested by trypsinization or manual scrapping into phosphate buffered saline [PBS; 137 mM NaCl, 10 mM Phosphate, 2.7 mM KCl, and a pH of 7.4.] and pelleted by centrifugation at 1000 r.p.m. in a table top centrifuge. Conversely, for immunohistochemistry, cells were grown on poly D-Lysine coated cover slips and transferred to PBS prior to treatment. All cell lines unless otherwise stated were purchased from American Type Culture Collection (ATCC; Manassas, VA).

Table 5 – Cell Lines and Culture Conditions

Cell Line	Description	Culture Conditions
Human Cell Lines;		
SH-SY5Y	Neuroblastoma	Growth media: EMEM/10%FBS Differentiation medium (neurons): EMEM/1%FBS/10μM Retinoic Acid
Hela	epithelial adenocarcinoma	Growth medium: DMEM/10%FBS
Hep G2	hepatocellular carcinoma	Growth medium: EMEM/10%FBS
THP-1	monocytic leukemia	Growth medium: RPMI/10%FBS/0.05 mM 2-mercatoethanol Differentiation medium (macrophages): RPMI/10%FBS/ 100 ng/mL phorbol 12-myristate 13-acetate (PMA)
HEK293T	kidney cell line	Growth medium: Growth media: DMEM/10%FBS

a549	lung carcinoma	Growth medium: EMEM/10%FBS
OVCA429 *	ovarian cancer cell line	Growth medium: DMEM/10%FBS
Mouse Cell Lines;		
NIH/3T3	fibroblast	Growth medium: DMEM/10%FBS
N1E115	neuroblastoma	Growth medium: DMEM/10%FBS Differentiation Medium: DMEM/0.5-1.0%FBS/ 1%DMSO
Rat Cell Lines;		
ROSE 199 *	ovarian epithelial cell line	Growth medium: alphaMEM/10%FBS

* OVCA429 [251] and ROSE199 were the kind gift of Dr. B. Vanderhyden (OHRI/University of Ottawa)

2.2 Methods.

2.2.1 Animal lines.

The University of Ottawa Animal Care Committee, accredited by the Canadian Council on Animal Care, approved all animal studies. Wildtype mice used in these experiments, CD-1 and C57Bl/6 were purchased from Charles River (Boston MA), and 129Sv wildtype mice are from Jax Laboratories (USA). The viable heterozygous Snf2H mouse line, maintained on a C57Bl/6 background are from the laboratory of Dr. A. Skoultchi (Albert Einstein College of Medicine, Bronx, NY)[186]. Foxg1-Cre animals, in a C56Bl/6 background are from Susan K. McConnell (Stanford University, Stanford, CA) [252]. The Gata-1 Cre animals are maintained on a CD-1 background and the Snf2l conditional flox/flox on a Sv129 background.

2.2.1.1 Generation of the Exon 6 Floxed transgenic mice.

Refer to **Appendix II** (pp161) for descriptive figures of the Snf2l gene-targeting strategy. Briefly, A 4.84 kb *Kpn*I/*Xmn*I fragment of genomic DNA spanning exon 6 of the m*Snf2l* gene was isolated from a 129Sv-derived genomic library (RPCI-22, BAC528D21, ResGen, Toronto). This fragment was subcloned into the pUC19 vector (Fermentas), with the *NeoR* gene cassette cloned by *Eco*RI/*Hind*III digest 5' of exon 6. Three LoxP sequences were cloned immediately flanking the *NeoR* expression cassette by *Xmn*I/*Hind*III and *Xmn*I/*Pst*I and a third site 3' of exon 6 by *Hind*III/*Eco*RI to generate the targeting construct. A resulting linear fragment (*Kpn*1/*Sma*I) was used to ultimately generate targeted embryonic stem cells by electroporation and homologous recombination in to J1ES cells[253]. A single positive recombinant clone was identified, out of 316 screened, by Southern blot with probes directed to the targeting construct. Chimeric animals were generated by blastocyst injection, in collaboration with Michael Rudnicki (University of Ottawa, Canada). Two germ line chimeric animals containing the S*nf2L* Exon 6 floxed allele were generated and the line was maintained on the 129Sv background strain. Unexpectedly, it was later determined that exon 6 of the *Snf2l* gene encoded 60 amino acids, comprising 180 base pairs. Deletion of this exon results in an in frame mutation of the *Snf2l* gene but does not affect the general stability of the RNA or derived poly peptide product, however the deletion encompasses a highly conserved component of the ATPase domain including the ATP binding pocket, and has been used in many species for the development of dominant mutant alleles [169]. DNA isolated from non-brain tissue of weanlings was genotyped by PCR in a total volume of 50 μL containing; 1 μL of DNA; 5 μL of 10x PCR buffer (Invitrogen); 0.5 μL of 100 mM dNTPs; 1.5 mM $MgCl_2$; 0.5 μL Taq

polymerase and with 0.5 mM concentration of the primers for the floxed exon 6 of *snf2L* (Floxed Exon 6 Genotyping). *β-actin* was used as a PCR control. Refer to **Appendix I** (pp155) for primer sequences. Standard conditions were used 35 cycles [94°C (30 s), 56°C (30 s), and 72°C (60 s)]. PCR products (10-15 μL) were resolved and visualized by electrophoresis on a 1.5 % agarose gel in TAE buffer (40 mM Tris acetate and 1 mM EDTA) containing 0.5 μg/mL ethidium bromide.

2.2.1.2 Generation of Ex6DEL transgenic mice.

The ubiquitously expressing *Gata- 1 Cre* transgenic line in the CD-1 background was kindly provided by S. Orkin (Howard Hughes Medical Institute, Chevy Chase MD, USA)[254]. Female mice heterozygous for the floxed *Snf2l* allele ($Snf2l^{f/x}$) were bred to males heterozygous for *Gata-1 Cre* to generate the Ex6DEL line ($Snf2l^{-/y}$) and further F1 crosses were used to generate Ex6DEL females ($Snf2l^{-/-}$). Confirmation of exon 6 excision was performed initially by Southern hybridization, and then by PCR. DNA isolated from weanling tail or embryo biopsies was genotyped by PCR with the Ex6DEL Genotyping reaction. In order to determine the sex of embryos a PCR reaction with primers directed towards *Sry* was performed. Refer to **Appendix I** (pp155) for primer sequences. Standard amplification conditions were used with the exception of a 60°C annealing temperature.

2.2.2 Tissue procurement and preparation.

Adult animals were sacrificed by CO_2 asphyxiation followed by cervical dislocation. Brain tissue (cortices) and other organ tissue (whole brains, hearts, testes,

ovaries, and kidneys) were manually dissected and flash frozen for later protein or RNA extraction. Embryos were removed by hysterectomy and transferred into Hank's Buffered Saline Solution [HBSS]. Similarly embryonic cortices were removed by dissection using fine forceps or the entire head was taken and flash frozen.

2.2.2.1 Cryopreservation and cryosectioning.

Adult and P7.5 animals were perfused with 10 mL or 5 mL, respectively, of 4% Paraformaldehyde (PFA) in 0.1M Phosphate Buffer [0.1M Na_2HPO_4, 0.1M NaH_2PO_4] prior to dissection. Following dissection whole embryo heads, dissected brains and other organs were fixed by immersion in 4% PFA overnight, washed several times with sterile PBS, cryopreserved with 30% sucrose (in PBS) for overnight then imbedded and flash frozen in 1:1 [30% sucrose to OCT compound (Tissue-tek, Torrance, Ca)]. All brain tissue and whole embryo heads where cryosectioned in the coronal plane ranging from 10-14μm in thickness using a Leica CM1840 cryostat. Serial sections were collected on SuperFrost / Plus microscope slides (Fisher) and stored at -20°C.

2.2.2.2 *in vivo* BrdU labelling.

For labelling S-phase cells during incorporation experiments bromodeoxyuridine was given (0.3 mL of 0.016 g/mL, 5-bromo-2-deoxyuridine, BrdU in DMEM) by intraperitoneal injection to E15.5 pregnant dams in two consecutive 1.5 hour pulses. Dams were sacrificed 1.5 hours following the final BrdU pulse injection, whole embryo heads were fixed with 4% PFA overnight and cryopreserved, sectioned and processed for BrdU

incorporation. To label proliferating cells in birthdating experiments, BrdU was injected similarly into E13.5 pregnant dams and offspring were harvested 7 days after birth (P7.5), brains were processed in a similar fashion. For cell cycle re-entry experiments BrdU was injected into E12.5 pregnant dams and whole embryo heads where harvested following a 24-hour recovery period. Positive BrdU incorporation was assessed by immunohistochemistry.

2.2.3 General histological staining.

To assess anatomical features, sections encompassing the cortex, hippocampus and cerebellum were treated with cresly violet stain. Frozen slides containing serial brain sections from various embryonic and postnatal time points were thawed and air-dried at room temperature, then sequentially rehydrated for 15 min each in 95%, 80%, 70% and 50% ethanol, and water. Sections were transferred to 0.25% cresyl violet Stain solution (containing 10% acetic acid) for up to 5 minutes. Following several washes slides were dehydrated in the same ethanol washes, but in reverse order, followed by two 5 minute washes in Xylene (Fisher). In a similar fashion slides were stained for H&E (Heamotoxylin (Sigma) for 5 minutes and Eosin (Sigma) for 30 seconds. Slides were then mounted in a minimum amount of Permount resin (Fisher). Phase contrast micrographs were taken with an Axioplan2 Microscope, using the AxioVision 3.1 Software (Carl Zeiss).

2.2.4 Immunohistochemistry.

2.2.4.1 Standard immunohistochemistry.

Frozen slides containing brain sections from embryonic and postnatal animals were air-dried at room temperature. Slides were then fixed in 70% ethanol, rehydrated in PBS and blocked for a minimum of 1 hour in 10% fetal bovine serum and 1% Triton-X 100 in PBS in a humidified chamber. Cover slips containing adherent cells were fixed for 7 minutes in 3:1 ethanol:methanol at -20°C and washed with PBS, were processed for immunohistochemistry. For a complete list of primary antibodies and specific pretreatment see TABLE 2.1.5.1. Some antibodies required an additional antigen retrieval step; microwave treatment in 10 mM sodium citrate was administered prior to the addition of block. To detect BrdU that has been incorporated into the DNA, sections were depurinated by incubation with 2N HCl for 15 min at 37°C, and neutralized with 0.1M Tris-Cl, pH 8.8 containing 0.1% Tween-20 following antigen retrieval. See TABLE 2.1.5.2 for a list of fluorescent secondary antibodies. For all immunohistochemistry experiments nuclei were counter stained with 4'-6-Diamidino-2-phenylindole (DAPI, 1μg/mL, in PBS) following secondary antibody treatment. Slides were rinsed in PBS before being mounted using florescent mounting medium (Dako). Micrographs were taken with an Axio Imager.M1 Microscope and the AxioVs40 version 4.6 software (Carl Zeiss).

2.2.4.2 Identification of apoptotic cells by TUNEL.

To assess apoptosis, sections were treated with Terminal uridine deoxynucleotidyl transferase dUTP Nick End Labelling (TUNEL) using the *in situ* Cell Death Detection Kit, TMR Red (Roche). The Apoptotic Index is the number of cells that are TUNEL+ divided by the total cells (DAPI+).

2.2.4.3 Mitotic Cell Index.

Quantification of mitotic figures in embryonic cortices (E13.5 and E15.5) was assessed by immunohistochemistry for the M-phase marker phosphohistone-H3, or PH3 [119, 120]. The mitotic index represents the proportion of PH3+ cells to the total number of cells in a 120 μm^2 region which encompasses the ventricular and subventricular zone.

2.2.4.4 Cell Cycle Exit / Re-entry.

In order to assess the proportion of cells that exited the cell cycle after one round of division, BrdU pulse-labelled E13.5 cortices were stained for BrdU and Ki67. The proportion of Cell Cycle Exit was calculated as the proportion of $BrdU^+$ and $Ki67^-$ to the number of BrdU-positive. The Cell Cycle Re-entry was calculated as $BrdU^+$ $Ki67^+$ divided by the $BrdU^-$ $Ki67^+$ cells.

2.2.5 *In situ* gene hybridization.

For a complete list of Riboprobes see Table 4, above.

2.2.5.1 *In vitro* transcription.

To generate *in situ* probes, 1 µg of purified linear plasmid was then mixed with 2.5 µL 10x DIG-UTP mix (Roche), 5µl 10x transcription buffer, 1µl RNase OUT (Invitrogen) and 1µl of the appropriate RNA polymerase (T3, SP6 or T7) for 1 hour at 37°C, followed by ethanol precipitation, and then resuspended in water containing 100 mM EDTA, aliquoted and stored at -80°C.

2.2.5.2 Hybridization and visualization.

In situ hybridization is performed as previously described [255]. Briefly, DIG-labelled RNA probes were diluted 1/500 - 1/1500 in hybridization buffer [50% formamide, 10% dextran sulfate, 1 mg/mL yeast RNA, 1x Denhardt's and 1x salt] and denatured for 10-20 minutes at 65°C. Probes were hybridized overnight at 65°C in a humidified box containing 50% formamide. Slides were then washed once for 15 min and twice for 30 minutes with wash buffer solution [50% formamide 1x SSC, 0.1% Tween-20] at 65°C and then washed several times for up to 20 minutes at room temperature with MABT [100 mM maleic acid, 150 mM NaCl, pH 7.5, 0.1% Tween-20]. Hybridized sections were blocked for 1 hour in blocking solution [20% sheep serum (Sigma) and 2% blocking reagent (Boehringer Mannheim) in MABT]. Primary anti-Digoxigenin conjugated to Alkaline-Phosphatase (Roche) diluted to 1/1500 in blocking solution was then incubated in a humidified box overnight at 4°C. The following day, slides were washed in 1x MABT at room temperature followed by two 20 minute equilibrations in pre-staining buffer [100 mM NaCl, 50 mM $MgCl_2$, 100 mM Tris (pH 9.5) and 0.1%-Tween 20]. The color reaction was allowed to develop for 2-8 hours in staining buffer [100 mM NaCl, 50 mM $MgCl_2$, 100 mM Tris (pH 9.5) and 0.1%-Tween 20 ml 4.5 µL/mL 4-Nitro blue tetrazolium chloride (Roche) and 3.5 µL/mL 5-bromo-4chloro-3indolyl-phosphate (Roche)]. Slides were rinsed in PBS and mounted using a 1:1 mixture of PBS and 30% glycerol. Phase contrast images were taken with an Axioplan2 Microscope, using the AxioVision 3.1 Software (Carl Zeiss).

2.2.6 Generation of plasmids.

For proliferation assays, pcDNA (Invitrogen) mammalian expression plasmids containing coding sequences of Flag-tagged *hSnf2L*, both an active ATPase version and the mutated ATPase-dead version were generated. FLAG-*hSnf2H* active ATPase had already been generated [169]. To correct a cloned point mutation that was identified at base 2515 (in all *snf2H* clones) by sequence analysis, we used the QuickChange XL Site-Directed Mutagenesis kit (Stratagene). For a list of mutagenic primers refer to **Appendix I** (p155). To generate an expression vector containing an ATPase dead h*Snf2H* clone, a 1.1 kb *Xho*I/*Spe*I fragment containing a dominant mutation at base 674 was removed by restriction endonuclease digestion from a mutant h*Snf2h* plasmid (the kind gift of Dr. M. Rudnicki, OHRI/University of Ottawa). This fragment was combined with a 2kb *Spe*I/*Not*I fragment from corrected wildtype FLAG-h*Snf2H* coding plasmid (above) and ligated into the pCLneo mammalian expression plasmid (Promega) using the Rapid Ligation kit (Roche).

2.2.7 Bacterial transformations.

Liquid media (SOB, SOC and LB) and Solid media (LB-agar) were prepared as previously described [256]. Ligated plasmids were transformed into *Escherichia coli*. Stabl2 (Invitrogen), Xl-1 Blue, Xl-2 Blue and Xl-10 Gold (all Stratagene) bacterial cells were prepared as described[257]. Briefly, 10-15 colonies that had been grown overnight at 37°C on solid media were inoculated into 250uL of SOB media and grown to an optical density (A_{600nm}) of 0.6 at room temperature with constant agitation in the dark. The cultured cells were then pelleted and resuspended in ice cold TB media [10 mM Pipes, 55 mM $MnCl_2$ and 250 mM KCl] for 10 minutes. Cells were pelleted and resuspended in 20

mL of TB and DMSO (final concentration 7%) and 500uL aliquots were flash frozen and stored at -80°C until use. Transformation was performed as follows: 150uL of competent cells were thawed and incubated with 3-7 μL of the ligation mix on ice for 20 min (only up to 0.1 μg of previously made plasmids was used). The transformant mix was then heat shocked for 45 seconds at 42°C without agitation and quickly transferred back to ice for an additional 2 minutes. One mL of LB broth (with no antibiotics) was then added to the transformant mix and the tube placed in a 37°C shaking incubator for 1 hour. Following incubation 50-150 μL of the mixture was spread onto LB-agar plates containing the appropriate antibiotic (20 μg/μL Ampicilin or 40 μg/μl Kanamycin). Individual colonies representing a single transformed clone were then harvested and grown in 4mL LB antibiotic cultures in a 37°C shaking incubator overnight. All selected bacterial clones were screened by Endonuclease digestion following Plasmid Mini purification by GFX Micro Plasmid Prep kit (GE Healthcare). Large-scale preparations of positive plasmid clones were then performed by Qiagen Maxi Prep (Qiagen). The quantity of isolated DNA was determined using the absorbance at 260 nm in a Beckman Coulter DU 640 spectrophotometer (Fullerton CA) or a Nanodrop Spectrophotometer (Alpha Innotech). The quality of isolated DNA was determined by the ratio of absorbance at 260nm divided by the absorbance at 280 nm [256].

2.2.8 Cell culture techniques.

2.2.8.1 Transfection of mammalian cells.

For transient transfections $1x10^5$ cells (293, NIH/3T3, N1E115, ROSE199 and HeLa) were seeded onto plates overnight. Each dish was transfected with equal molar ratios of plasmids (for example FLAG-*Snf2H* or FLAG-*Snf2L*, wildtype and mutant) using 2 μL of Lipofectamine Reagent or Lipofectamine 2000 in DMEM (without FBS additive). Empty plasmids and wild type cells were used as control treatments. Four hours post-transfection cells were transferred to growth media. Subsequent to a 48-hour recovery period, replicate plates were either harvested or induced to differentiate and then harvested for protein or RNA extraction. In order to establish stable transfected lines, 1000 cells (293T and N1E115) were treated in the same manner as transient transfections except that after the 48-hour post-transfection period, growth media was replaced with selection media (growth media containing 0.8 mg/mL G418) to select for stable integration of plasmids. G418 resistant colonies were isolated and scraped/harvested by pipetting and transplanted to a 24-well dish (single well per colony). Following successive expansion under growth conditions, clones were screened by PCR amplification, RT-PCR amplification or Western blot analysis.

2.2.8.2 Proliferation assays.

Stable 293-T NIH3T3 clones (and "empty" plasmid controls) expressing active or dominant negative forms Snf2H were assessed for proliferation. Cells were seeded at $1x10^5$ cells per 100 mm x 20 mm culture dishes in growth media (in triplicate). The number of viable cells was determined by counting triplicate samples at every 24-hour period for 7 days. All counts were performed using a haemocytometer.

2.2.8.3 Colony forming assay (Soft Agarose).

Culture dishes containing Bottom Agarose [1% agarose (UltraPure Low Melting Point Agarose, Invitrogen] in water were autoclaved and added to 2X DMEM / 20% FBS plus 0.4 mL or Pen Strep and stored at 37°C. The next day $1x10^6$ of cells (wild type, empty vector and active and dominant negative Snf2H stable clones) were harvested and mixed (1:1) with the same ingredients as the Bottom Agarose and quickly overlayed onto the previously made Bottom Agarose plates. Plates were left to solidify for 10 minutes at room temperature then transferred for up to 20 days incubation in 37°C with 0.5% CO_2. Phase contrast images of agarose imbedded colonies were taken with an Axioinvet S100 microscope, using the AxioVision 3.1 Software (Carl Zeiss).

2.2.9 Genomic DNA isolation from mammalian tissues and cells.

Tissue samples were mechanically disrupted by 15-20 seconds pulse with a Tissue Tearor (Biospec Products Inc.) and then pelleted. Genomic DNA was isolated from cells using Tail Lysis Buffer [50 mM Tris-Cl (pH8.0), 10 mM EDTA, 10 mM NaCl, 1% SDS] containing 20ug/mL freshly added Proteinase K. Following 24-48 hours incubation in Tail Lysis Buffer at 56°C, DNA was isolated from protein and cell debris by three phenol:chloroform:isoamyl alcohol (25:24:1) extractions followed by ethanol precipitation. Quality and quantity of purified DNA was assessed in the same manner as plasmid DNA (above)

2.2.10 Semi-quatitative RT-PCR.

RNA was isolated for the generation of cDNA by reverse transcription. RNA from pelleted mammalian cells, or mechanically disrupted mouse tissues, was isolated using guanidium thiocyante buffer [4 M guanidium thiocyanate, 20 mM sodium acetate (pH5.4), 0.5% sarkosyl] and phenol isolation [258] or using Trizol Reagent (Invitrogen). The quantity and quality of purified RNA was assessed similarly to DNA, above. First strand cDNA sysnthesis was performed with 2.5-5 μg of total RNA was reverse transcribed as described, by Yip and Picketts[259]. Complimentary DNA products were used for PCR amplification under standard conditions [0.5-1 μL, cDNA, 1x PCR buffer, 0.2 mM dNTPs, 0.5 mM primers (each) and Taq DNA polymers] for 24-30 cycles of 94°C for 30s, 56-60°C (depending on primer pair) for 30s, 72°C for 1 min, followed by 10 min at 72°C. For a complete list of primers refer to **Appendix I** (pp155). Following PCR amplification, 10-15 μL of the products were resolved on a 0.8-2.0% agarose gel or an 8.0-10.0% TBE-PAGE gel and visualized with ethidium bromide staining. ImageJ was used for densitometry, and image processing (free software available at http://rsbweb.nih.gov/ij/).

2.2.11 Quantative realtime RT-PCR.

RNA for quantitative realtime RT-PCR experiments was isolated using RNeasy Plus Midi kit from Qiagen (Mississauga, ON). Complimentary DNA was synthesized as described above. Quantitative "realtime" PCR was then performed with an Mx 3000 realtime cycler (Stratagene) using the ABsolute QPCR SYBR Green Mix (Thermo

Scientific). PCR conditions were as follows: 10 minutes at 95°C followed by 35-50 cycles of 30 seconds at 95°C, 30 seconds at 60°C and 30 seconds at 72°C. For a complete list of primers used for quantitative realtime PCR refer to **Appendix I** (pp155). Using the standard curve corresponding threshold method of quantification, PCR product formation was monitored and the threshold cycles were determined using the Mx4000 software. All data was normalized to *Gapdh* and *18S* RNA expression levels and calculated using the delta delta CT (ddCt) method defined as fold change = $2^{\wedge -(Ex6DEL(CT)- Wt(CT))}$ http://www.ambion.com/techlib/basics/rtpcr/index.html.

2.2.12 Polysome assay.

$3x10^6$ cells (Hep G2, 293T and SH-SY5Y) cells were treated with 0.1 mg/mL cyclohexamide for 3 minutes at 37°C. Cells were harvested by and washed twice with ice cold PBS containing 0.1 mg/mL cyclohexamide. Cell pellets were resuspended in 1 mL of Lysis Buffer [300 mM NaCl, 15 mM $MgCl_2$, 15 mM Tri-Cl (pH 7.4), 1% Triton X-100 and containing 0.1 mg/mL cyclohexamide and 1 tablet/10 mL Complete RNAse inhibitors Cocktail] at 4°C. The nuclei were pelleted by centrifugation at 1000g for 5 minutes at 4°C and the resulting supernatant (containing polysomes) was further spun for 5 minutes at 10,000 g in a microcentrifuge to remove cell debris. The lysates (supernatant) were layered on a continuous sucrose gradient [10-15% sucrose, 300 mM NaCl, 15 mM $MgCl_2$, and 15 mM Tris-Cl (pH7.4)] and centrifuged for 90 minutes at 39,000 r.p.m. in a SW41-Ti rotor (Beckman). The absorbance across the gradient was read at 245 nm in a Beckman Coulter DU 640 spectrophotometer (Fullerton CA). Fractions were collected every 30 seconds and flash frozen in liquid nitrogen. RNA was recovered from fractions by phenol-chloroform

extraction, ethanol precipitation and purified using the RNeasy micro kit (Qiagen). Total RNA from non-cyclohexamide treated cells was used as a positive control. The resulting fractions were processed for semi-quantitative RT-PCR (above) and separated on an 8% TBE-PAGE gel [8% Acrylamide, 0.5% APS, TEMED, 45 mM Tris-Borate, 1 mM EDTA] by electrophoresis in a Bio-Rad Mini Trans Blot Cell (Bio-Rad) and visualized with ethidum bromide staining.

2.2.13 Protein isolation.

Protein samples were prepared from flash frozen cortices of control, heterozygous or Ex6DEL mice and embryos or cell pellets by manual dissociation followed by lysis in freshly made modified radioimmunoprecipitation assay (RIPA) extract buffer [1% Nonidet P-40, 0.1% Sodium Dodecyl Sulfate, 0.5% sodium deocycholate and one tablet/10 mL of Complete Mini, EDTA-Free Protein inhibitor cocktail (Roche)] [260]. Nuclear protein extracts were generated from nuclei isolated for 15 minutes at room temperature in a Cell Lysis Buffer (10 mM Tris-Cl (pH8.0), 1.5 mM MgCl2, 5.0 mM KCL 0.5 mM DTT, 1.0 mM PMSF, 0.5% NP-40) and centrifuged for 5 minutes at 1000 r.p.m. in a microcentrifuge at 4oC. Isolated nuclei were subjected to DNaseI treatment (100 U/mL DNase I in Cell Lysis Buffer) for 15 minutes on ice, and then centrifuged at 5000 r.p.m. in a microcentrifuge at 4°C. A final resuspension of nuclear proteins was then performed in Nuclear Lysis Buffer (20 mM Tris-Cl (pH8.0), 25% glycerol, 1.5 mM $MgCl_2$, 400 mM KCl, 0.2 mM EDTA and one tablet of Complete Mini, EDTA-Free Protein inhibitor cocktail (Roche) / 10mL. Protein extracts were quantified by Bio-Rad Protein Assay with

spectrophotometric quantification (A_{750nm}) according to manufacturer's instructions (Bio-Rad).

2.2.14 Cell fractionation assay.

Protocols used for the cell fractionation experiments are adapted from previous experiments [260, 261]. Briefly, 1-2x10^8 cells (a549, or HEK 293-T) were trypsinized and the resulting cellular pellet harvested by centrifugation at 5000 g in a microcentrifuge at 4°C, and washed twice in ice cold PBS. The resulting pellet was gently resuspended in CSK Buffer [10 mM PIPES pH6.8, 100 mM NaCl, 300 μM sucrose, 3 mM $MgCl_2$, 1mM EDTA, 0.5% Triton X-100 containing freshly added 1 mM PMSF and 1 mM DTT] and incubated on ice for 5 min. Following a 5000 g centrifugation in a microcentrifuge, the supernatant containing the Cytoplasmic Fraction was collected in 50 μL aliquots and stored at -20°C. The pellets were then resuspended in 200 μL of CSK buffer containing an additional 90 μg/mL DNaseI, and incubated at 37°C for 15 minutes. An additional 60 μL of 1 M $(NH_4)_4SO_4$ was added and the mixture was incubated on ice for 5 minutes. Following a 5000 g centrifugation in a microcentrifuge, the supernatant containing the Chromatin Fraction was collected in 30 μL aliquots and stored at -20°C. The pellet was once again resuspended in 1:1 100 μL CSK buffer: 100 μL 4M NaCl and incubated on ice for 5 minutes. Following a final 5000 g centrifugation in a microcentrifuge, the supernatant containing the Salt Wash Control was collected in 25 μL aliquots and stored at -20°C. The resulting pellet, containing the Nuclear Matrix Fraction was resuspended in 200 μL of 8M Urea Buffer [8M Urea, 100 mM NaH_2PO_4, 10 mM Tris-Cl (pH8.0)], 25 μL aliquots were then stored at -20°C. 20 μL of the cytoplasmic fraction, 12 μL of the chromatin fraction, 10 μL of the nuclear fraction and 10 μL of the salt wash were used for Western analysis

representing 1/20 total volume of the sample. Antibodies against P38 (cytoplasm), Histone H1 (chromatin) and Lamin A/C (nuclear matrix) served as controls for the three fractions.

2.2.15 Western blot analysis.

Protein lysates (25-50 μg) were resolved by SDS-PAGE on 1.0 mm NuPAGE 3-8% Tris-acetate Gels (Invitrogen) or on 8-10% continuous SDS-PAGE gels and then transferred to Hybond-C Extra membrane (Amersham Biosciences) by electroblotting in Tris-Glycine Buffer [50 mM Tris, 40 mM glycine, 1 mM SDS, plus 20% methanol]. For Western blots all antibody dilutions were made in Block Solution containing 5% dehydrated milk in Tris-buffered saline [TBST; 150 mM NaCl, 25 mM Tris-Cl (pH8.0) with 0.5% Tween-20]. For a complete list of primary and secondary antibodies used for Western analysis see **TABLE 2** and **TABLE 3,** above. Antibodies for β-Tubulin and β-actin were used as a protein loading controls. Western blots were typically incubated with primary antibody for 5-16 hours at 4°C, followed 3 times by, 15 minute washes in TBST. Horseradish peroxidase conjugated secondary antibodies were then incubated for 1 hour at room temperature, washed and the signals detected by chemiluminescence reaction with ECL Plus Western Blotting Detection System (GE Healthcare). Relative protein sizes were calculated by the inverse log (mm migration) compared to log migration of Precision Plus Protein Dual Colour Standards (Bio-Rad).

2.2.16 Immunoprecipitation.

Cortices were dissected from E15.5 embryos, as described above. Dissociated tissues were lysed in WCL Buffer [50 mM Tris-Cl (pH7.4), 150 mM NaCl, 1 mM EDTA, 0.5% NP-40, 10% glycerol and 2mM DTT, 1 tablet of proteinase inhibitors was added to 10 mL of buffer] for up to 2 hours on ice, and cell debris was precipitated by centrifugation at 13,000 g in a microcentrifuge at 4°C. Protein concentration was quantified by Bio-Rad Protein Assay (Bio-Rad). For immunoprecipitation, 500-1000 μg of protein extract was corrected to 1 mL with IP Buffer [WCL Buffer containing 0.02% sodium azide and 1% NP-40]. Each sample was pre-cleared with sepharose A or sepharose G beads (blocked for up to 1 hour with 50 mg/mL BSA); 100 μL of the resulting supernatant was kept as an input control. 5 μg Sheep IgG was then added to the supernatant for 3 hours to overnight, with constant rotation at 4°C and pelleted by centrifugation at 2500 r.p.m at 4°C. Beads were washed twice in IP Buffer and 25 μL of Laemlli Buffer [4% SDS, 20% glycerol, 10% 2-mercaptoethanol 0.004% bromophenol Blue and 124 mM Tris-Cl (pH8.0)] was added, samples were then stored at -20°C. Samples were readjusted to 1 mL with IP Buffer and 5 μg of Snf2L antibody was added and incubated for 6 hours at 4°C with rotation, then blocked sepharose A or sepharose G beads were added and incubated further, overnight and harvested as previously described and stored at -20°C. Samples were boiled for 5 minutes, spun down by pulse centrifugation and separated on a 10% PAGE Western Gel. Immunoprecipitated samples were then visualized by Western analysis.

2.2.17 Chromatin immunoprecipitation.

Chromatin Immunoprecipitation (ChIP) was performed as described [262, 263]. Briefly, for *in vivo* ChIP analysis, E15.5 embryonic cortices were dissected and transferred to HBSS then cells were mechanically dissociated by pipetting up and down through fire-polished and medium coated Pasteur-pipettes. The viable cells were then quantified using a 1:1 dilution of trypan blue and a haemocytometer (VWR). 1-2x10^7 viable cells were then fixed by incubation for 1 hour at room temperature in 1% PFA (final concentration), then washed several times in HBSS and the pellet was collected by 5 minutes centrifugation, 2000 r.p.m. in a microcentrifuge at 4°C and stored at -80°C. For *in vitro* ChIP 1x10^7 growth N1E115 or differentiated N1E115 cells that had been fixed in growth media [DMEM plus 10% FBS] containing 1% formaldehyde for 10 minutes at room temperature. The formaldehyde was then "quenched" with the addition of 125 mM glycine for 5 minutes. Fixed cells were then harvested by carefully scraping them from the cell culture dish in ice cold PBS containing Complete Mini, EDTA-Free Protein inhibitor cocktail (Roche). Cell pellets for *in vitro* ChIP analysis were similarly washed and stored. Cell pellets were resuspended in 400 µL of a cell lysis buffer [50 mM Tris-Cl (pH8.0), 10 mM EDTA and 1% SDS] and incubated for 30-60 minutes at room temperature. The resulting suspension was then treated for 5 to 12 x 10 sec sonication pulses using a Vibra Cell (Sonics and Materials Inc.) set at 30-35% amplitude on ice. At this point 5 µL of each sample was separated on a 0.8% agarose gel to assess sonication efficiency. If fragments retained a size larger then 0.8-1.5 kb then additional sonication steps were applied. Cell debris was removed from supernatant by centrifugation at 14000 g in a microcentrifuge for 15 minutes at 4°C. Pre-blocked [0.2 mg/mL sheared salmon sperm DNA and 0.5 mg/mL BSA in Low

Salt Wash Buffer, see below] protein sepharose A or G beads (GE Healthcare) beads were then added in order to pre-clear the supernatant for a minimum of 1hr with rotation at 4°C. At this point, 100 μL of each sample was removed to represent 1/10 volume of the input, and to the remainder of the sample, 5-10 μg of Snf2l, Snf2h, p107 (positive control ChIP) and purified Sheep IgG (mock treatment) was then incubated overnight with rotation at 4°C. Protein A or G beads were then added and incubated for 3-6 hours with at 4°C. Beads were then pelleted by centrifugation at 2000 r.p.m. in a microcentrifuge at 4°C and washed sequentially by rotation at room temperature followed by centrifugation at 2000 rpm with Low Salt Wash Buffer [20 mM Tris-Cl (pH 8.0), 150 mM NaCl, 2 mM EDTA, 1% SDS and 1% Triton X-100], High Salt Wash Buffer [20 mM Tris-Cl (pH 8.0), 500 mM NaCl, 2 mM EDTA, 1% SDS and 1% Triton X-100], Lithium Chloride Wash Buffer [250 mM LiCl, 10 mM Tris-Cl (pH 8.0), 1 mM EDTA, 1% deoxycholate and 1% NP-40], and twice with TE Buffer [10 mM Tris-Cl (pH 8.0), 1mM EDTA]. Enriched chromatin DNA complexes were then eluted from the sepharose beads in Elution Buffer containing 100 mM sodium bicarbonate ($NaHCO_3$) and 1% SDS, and centrifuged. Supernatants were then reverse-crosslinked by incubation for 6 hours at 65°C and RNase treated for 1 hour at 37°C. Following this samples were incubated with Proteinase K (20 μg/mL) for an additional 2 hours at 37°C, cleaned by phenol: chloroform: isoamyl alcohol (25:24:1) followed by ethanol precipitation in the presence of 1 μL glycogen. Samples were then assessed for fold enrichment along the Foxg1 promoter by quantitative realtime PCR as previously described; see 2.2.11 Quantative realtime RT-PCR. For a complete list of primers used in ChIP analysis refer to **Appendix I** (pp155). Fold change was calculated similarly to realtime qRT-PCR analysis using the ddCt method where fold change = $2^{\wedge-(\text{ChIP (dCT)} - \text{Input(dCT)})}$.

2.2.18 Computational and sequence analysis.

Genomic, open reading frames and cDNA sequence analysis, restriction endonuclease sites and some primer design, was performed using DS gene v1.5 software (Accelrys Inc., USA). All sequencing reaction analysis, and contig analysis was performed using Sequencher version 4.1.4 software (Gene Codes Corp., Ann Arbor, MI). Analysis of proximal promoter regions of potential ISWI targets, Snf2H and Snf2L was performed using the UCSC Genome Browser available on the internet (http://genome.ucsc.edu/cgi-bin/hgGateway) and MatInspector release professional 7.7.3 (http://www.genomatix.de/products/MatInspector/)[264]. The bulk of primer design for ChIP and Realtime RT-PCR analysis was performed using the free Primer3 v4.0 software (http://frodo.wi.mit.edu/) [265]. All primer pairs were checked against homologous sequence databases using standard nucleotide-nucleotide Basic Local Alignment Search Tool [BLAST, http://blast.ncbi.nlm.nih.gov/Blast.cgi][266].

2.2.19 Statistics.

For all data sets (with n = number of biological replicates). Error bars in histograms depict the SEM. Group comparisons were made using a minimum of 3 biological replicates and assayed for significance using a two-sample Student's *t*-test with equal variance, where, p-values smaller than 0.05 were considered significant (*). Calculations of the arithmetic average, standard deviation, the standard error of the mean and Student's *t*-test were performed with Microsoft Excel.

3.0 Results.

3.1 Characterization of SNF2L and SNF2H expression and localization in mammalian cells.

3.1.1 Sub-cellular localization of SNF2L and SNF2H to the nuclear matrix in mammalian cells.

The mammalian ISWI homologs, SNF2H and SNF2L share an approximately 84% amino acid identity [175]. To begin to assess the role of these proteins mammalian cells were screened for subcellular localization by immunohistochemistry, using primary antibodies raised against the N-terminus of both proteins. SNF2H localization is highly restricted to the nucleus by indirect immunofluoresence, when compared to DAPI counterstained interphasic NIE-115 cells (Figure 9a, top panel). Snf2l subcellular distribution pattern illustrates concentrated expression within the nucleus and also a diffuse expression throughout the cytoplasm (Figure 9a, bottom panel). The association of SNF2H and SNF2L to chromatin and their similarity to other SNF2 family members suggested that they may also bind to the nuclear matrix. To further characterize the subnuclear distribution, cytoplasmic, chromatin and core nuclear matrix fractions were extracted following high salt treatment from unsynchronized cells and were analysed by Western blot with the SNF2H and SNF2L antibodies (Figure 9b) [267]. SNF2H is restricted to the nuclear matrix fraction (Figure 9b, top panel). SNF2L is concentrated in the nuclear matrix but is detected in low abundance in the chromatin and cytoplasmic fractions as well (Figure 9b, second panel). The efficacy of the fractionation procedure was determined by immunoblot assay with control antibodies specific to p38, a stress-activated protein found

Figure 9 – Expression of mammalian ISWIs in cultured cells.

[A] Detection of endogenous expression of the mammalian ISWI orthologs with antibodies raised against the N-terminus regions of SNF2H (top) and SNF2L (bottom) by immunohistochemistry (green) in NIE115 cells under growth conditions. Snf2h expression is localised exclusively in the nuclei, while Snf2l is distributed throughout the cell with predominant expression in the nuclei and diffuse expression in the cytoplasm. Nuclei are counterstained with DAPI (blue). [B] Mammalian ISWI expression is highly associated with the nuclear matrix. HEK 293-T (shown), HeLa, A549 and N1E115 cells were extracted to obtain the cytoplasmic, chromatin and core nuclear matrix fractions from cultured cells. WASH sample represents a negative control, containing all remaining proteins (2M NaCl). Equivalent amounts of each fraction were separated by SDS-PAGE and analyzed by Western blot with antibodies for SNF2H, SNF2L, p38 (predominant cytoplasmic expression), Histone H1 (chromatin localization) and Lamin A/C (nuclear matrix subnclear localization).

A

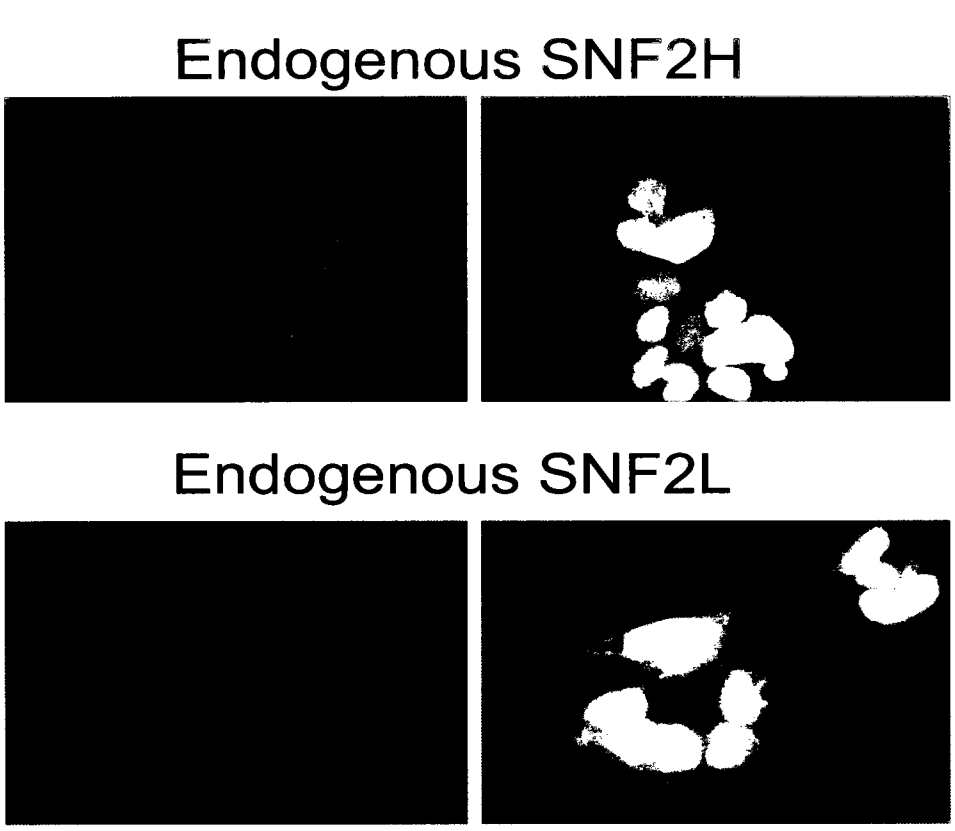
Endogenous SNF2H
Endogenous SNF2L

B

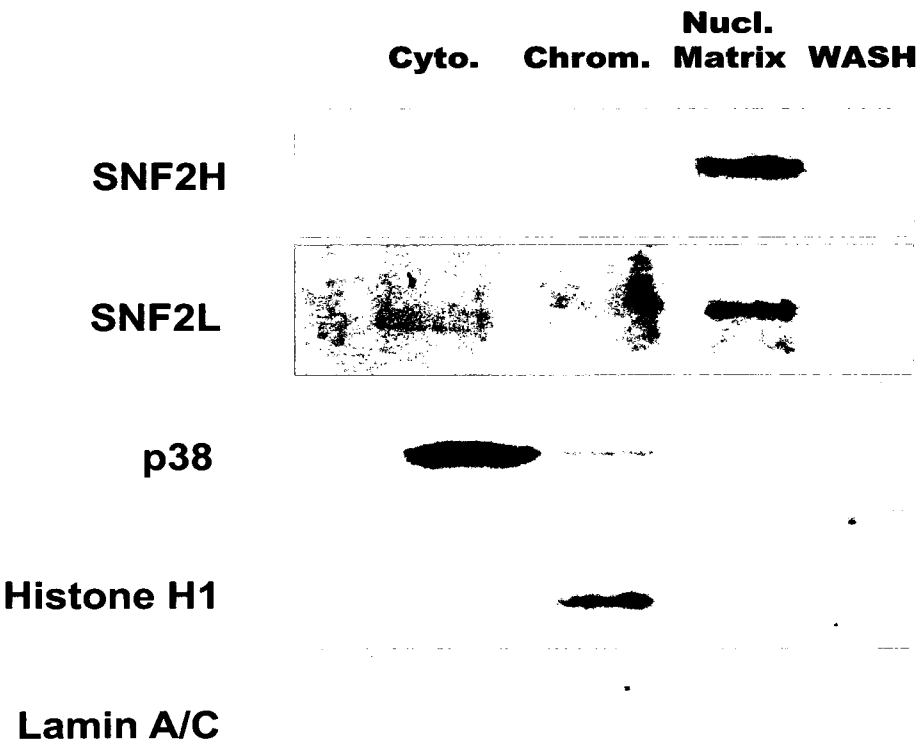
Cyto.
Chrom.
Nucl. Matrix
WASH
SNF2H
SNF2L
p38
Histone H1
Lamin A/C

in the chromatin and the cytoplasm, histone H1/H°, a component of chromatin and Lamin A/C, a core nuclear matrix associated protein [267-270].

3.1.2 Temporal expression of SNF2L and SNF2H during neurogenesis.

It was previously shown that SNF2H and SNF2L are important factors expressed in the developing brain [169, 175]. Initial experiments examining the spatial and temporal expression of *Snf2l* and *Snf2h* indicated that although there are overlapping expression patterns of the two homologs, there were clear variations in specific tissues and cell populations during development. *Snf2h* expression is elevated in proliferating neuroprogenitor populations, such as the external granule cell layer of the cerebellum and neuroepithelial cells of the cortical ventricular zone, and remains relatively low in differentiated neuronal regions [175]. In adult mice *Snf2l* transcripts are restricted to the CNS and reproductive tract. In the brain they were detected by Northern blot analysis and *in situ* hybridization and found to be localized predominantly in the cortex and inner cerebellar layers which suggested a role in maturing neuronal populations [175, 187]. In order to examine the temporal expression of *SNF2L* and *SNF2H* during the functional maturation of neural cells, cDNA was generated from total RNA isolated from the human SH-SY5Y and murine N1E115 neuroblastoma cell lines and transcript levels were measured across a 4 day differentiation time course. During this time course these cells are induced to differentiate morphologically to a neuronal phenotype, wherein they express many of the known neuroregulatory factors [271, 272]. In humans, an alternative *SNF2L* transcript, incorporating exon 13 (+ exon 13) is also expressed, and corresponds to an ATPase dead isoform [179]. Using a primer set which amplifies across exon 13; the levels

of *SNF2L* are increased transiently over the first 48 hours, then return to levels observed prior to differentiation (Figure 10a). In the N1E115 cells where this splice variant is not present, *Snf2l* transcripts are steadily increased over the entire 96 hour time course (Figure 10cd). Densitometric analysis of the scanned images showed that *Snf2l* increases in a 2–Fold above the growth levels (0 hr) during N1E115 differentiation (Figure 10d). Both exon 13 splice variants are identified in polysome fractionation assays, suggesting equal affinity for translation (see **APPENDIX III**, pp162).

3.2 SNF2H promotes proliferation and can confer oncogenic growth characteristics.

The genetic amplification of oncogenes causes cancer. *SNF2H* has been shown to be expressed in proliferating tissues and to be specifically elevated in proliferating neoplastic tissues [175, 216]. Moreover, it was previously shown by Western blot that *SNF2H* has increased expression in high grade malignant ovarian tumours and in established ovarian carcinoma cell lines (hOSE) with drug resistance to cisplatin (**APPENDIX IV**, pp163). In order to determine if SNF2H has specific oncogenic properties, NIH3T3 cell lines that stably expressed either a FLAG epitope-tagged SNF2H or a dominant negative version were established (refer to Figure 11a). The FLAG tag was used to facilitate identification of positive clones by Western blot (not shown), immunohistochemistry and RT-PCR (see Figure 11b). SNF2H expression in interphase cells is nuclear localized, corresponding to the wildtype localization of the protein (Figure 9). An equal number of cells from NIH3T3, empty vector (empVEC) clones, over expressing SNF2H clones (OEXP) and clones expressing the dominant negative version of

Figure 10 – A semi-quantitative expression profile of *Snf2l* and *Snf2h* during a neuronal differentiation time-course.

Complementary DNA was generated from total RNA extracted from SH-SY5Y (A, human) and N1E 115 (C, murine) cell lines during proliferation conditions (0 hours) and at 24, 48, 72 and 96 hours after initiation of differentiation. Expression of *Snf2l* (top panel) and *Snf2h* (middle panel) was assessed at each time-point by RT-PCR analysis. β-*actin* was used as a loading control. [A, C] -RT represents a negative control for genomic contamination; h*SNF2L*, m*Snf2l* and h*SNF2H* plasmid lanes are plasmid constructs containing the cloned Snf2l and Snf2l sequences and serve as positive controls for the PCR reaction. PCR products were separated by TBE-PAGE electrophoresis on an 8.0% gel and visualized by ethidium bromide staining. Digital images of the gels were then analysed for band intensity by densitometry using ImageJ software (ImageJ, U. S. National Institutes of Health, Bethesda, Maryland, USA, http://rsb.info.nih.gov/ij/) and presented as Fold Enrichment over *β-actin* for SH-SY5Y (n=1) [B] and N1E115 (n=1) [D]. The *Snf2l* PCR reaction in A (top panel) amplifies two RNA species *Snf2l* $^{\pm}$ exon 13 (as labelled). There is an increase in *Snf2l* expression during neuronal development and a selective increase in the human only -exon 13 message during neuronal differentiation.

SH-SY5Y

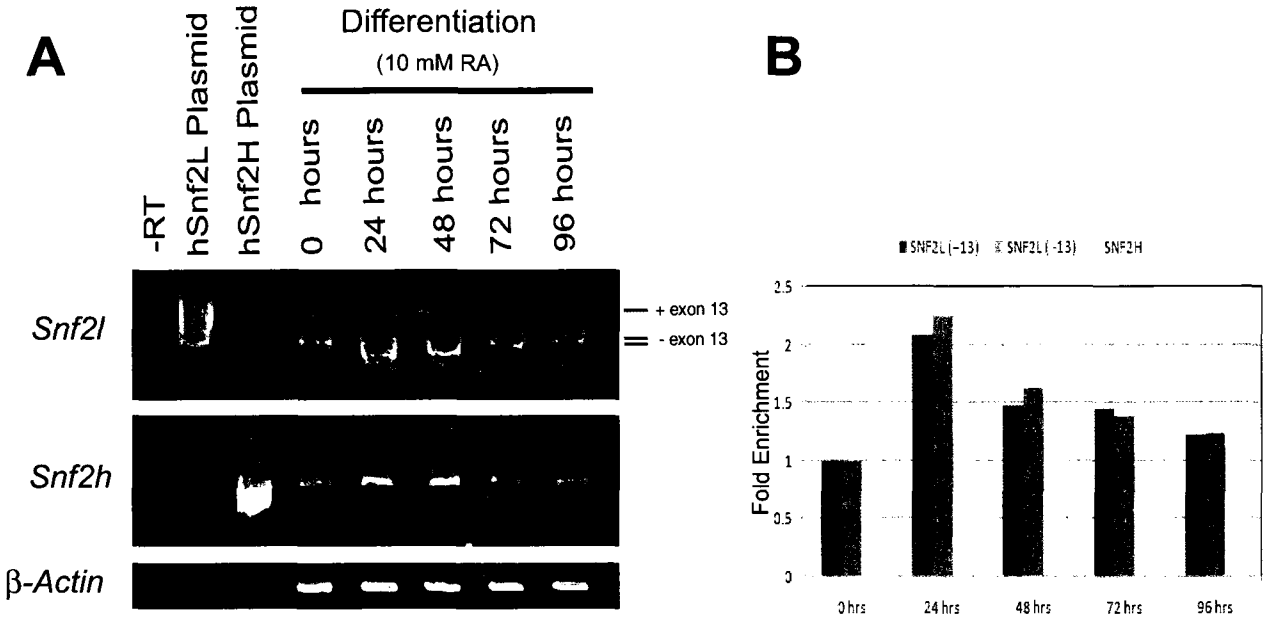

N1E115

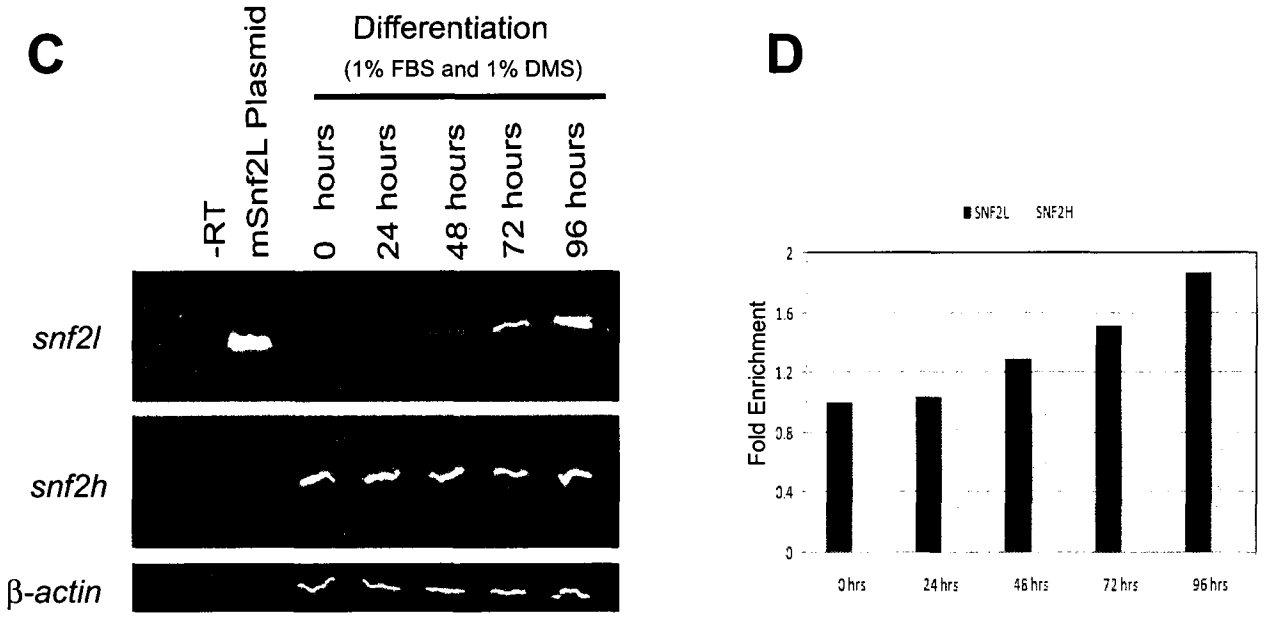

Figure 11 – Over expression of FLAG-*Snf2h* in NIH 3T3 cells results in increased proliferation.

[A] A schematic representation of the Flag-tagged human Snf2h expression vectors (WT *Snf2h*; top, Dominant Negative Mutant *Snf2h* version; bottom). The Flag-tag (green box) was cloned upstream and in frame to the human *SNF2H* cDNA (grey box). Expression is regulated by the constitutively active CMV promoter (black box, with arrow). SV40 regulated expression of *neomycin resistance* gene (*Neo*^{R}; turquoise) provided selection for transfection into NIH 3T3 cells. Ampicillin resistance (peach box) was used for bacterial subcloning and amplification. The ATPase domain of *SNF2H* is highlighted by the red dashed box. [B] Expression of Flag-SNF2H is confirmed by immunohistochemistry with antibodies recognizing Flag (green); nuclei are counterstained with DAPI (blue). Semi-quantitative analysis using Flag directed primers was also employed to confirm expression of Flag-*SNF2H* (right panel). The blank (water) and -RT (no reverse transcriptase) lanes represent negative controls. Flag-SNF2H plasmid is a non-cellular positive control and 293/Flag-SNF2H is a cell line previously shown to overexpress SNF2H. Experimental samples: NIH3T3 (parental cell line), empVEC-17 (empty vector clone; does not contain Flag-*SNF2H*), OEXP-10 (a representative sample of an NIH3T3 clone expressing Flag-*SNF2H* expression cassette) and MUT-29 (a representative sample of a clone expressing the dominant negative mutant version of Flag-*SNF2H* expression cassette). β-*actin* is a positive loading control. [C] Overexpression of Flag-SNF2H increases cellular proliferation in NIH3T3. In triplicate 10000 cells: NIH3T3 (blue), empVEC (red), OEXP (green), and MUT (purple) were plated and maintained under typical growth conditions, viable cells were quantified following 24, 48, 72 and 94-hours. The sample size, biological replicates (each plated in triplicate) is shown, the error bars represent +/- SEM.

A

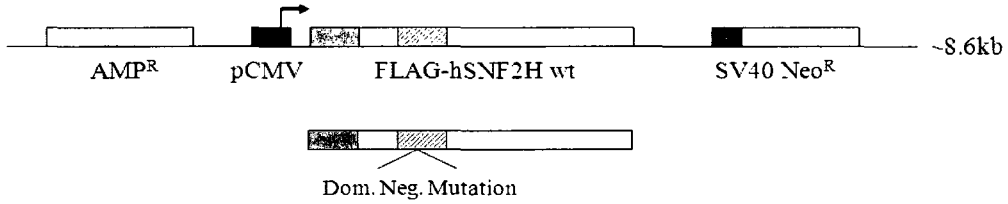
~8.6kb
AMP^R
pCMV
FLAG-hSNF2H wt
SV40 Neo^R
Dom. Neg. Mutation

B

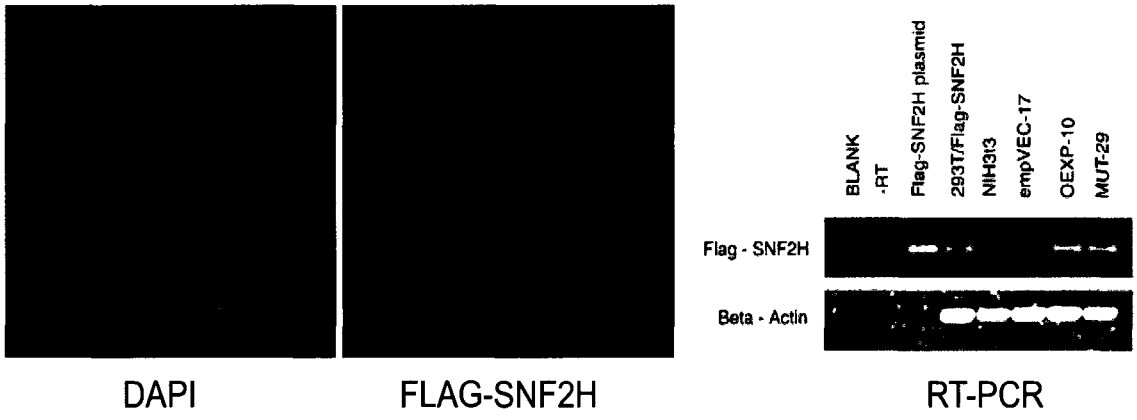
BLANK
-RT
Flag-SNF2H plasmid
293T/Flag-SNF2H
NIH3t3
empVEC-17
OEXP-10
MUT-29
Flag - SNF2H
Beta - Actin
DAPI
FLAG-SNF2H
RT-PCR

C

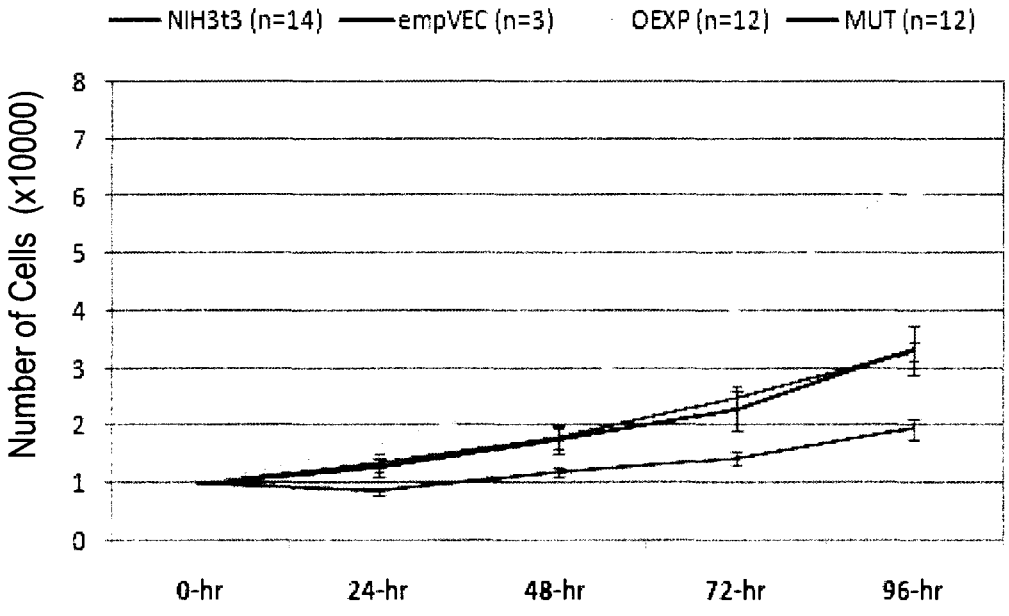
NIH3t3 (n=14)
empVEC (n=3)
OEXP (n=12)
MUT (n=12)
Number of Cells (x10000)
0
1
2
3
4
5
6
7
8
0-hr
24-hr
48-hr
72-hr
96-hr

SNF2H (MUT) were plated and counted after every 24 hours for 4 days (refer to Figure 11c). At the end of the four day period there were approximately twice as many cells in the OEXP clones ($6.43x10^5 \pm 0.38x10^5$, n = 12) compared to the NIH3T3 ($3.30x10^5 \pm 0.15x10^5$, n = 14) (p= 0.007) and empVEC ($3.34x10^5 \pm 0.42x10^5$, n=3) (p= 5.5E-06)controls. Similarly, there were more than three times as many OEXP cells than the dominant negative mutant lines ($1.97x10^5 \pm 0.18x10^5$, n =12) (p= 3.2E-13), suggesting a decrease in proliferation with over expression of the dominant negative form. Moreover, expression of the dominant negative SNF2H conferred an additional 40% reduced growth compared to the controls (p= 4.4E-08).

To further explore the capacity of SNF2H to enhance cell growth, the ability of SNF2H to form foci in a nutrient rich soft agarose culture was measured. This capacity to induce foci formation in culture is considered to be one of the general properties of an oncogene, and has been used to describe the prototypical oncogene, RAS [273]. All treatments (NIH3T3, empVEC, OEXP, and MUT lines) were able to induce colony formation in soft agarose (see Figure 12). However, there were a far greater number of colonies, and colonies of much larger size, produced from OEXP treatments compared to the controls and MUT lines (Figure 12 abcd). The number of colonies (groupings of more than 4 cells) was quantified and presented as % focus formation (number of colonies / total number of cells, see Figure 12 e). There were less colonies formed in the MUT treatments ($0.41\% \pm 0.07\%$, n = 4) compared with the NIH3T3 ($0.91\% \pm 0.13\%$, n = 4)(p= 0.003) and empVEC ($0.81\% \pm 0.15\%$, n = 4) controls. Moreover, the OEXP clones showed a 10-fold increase over controls ($9.06\% \pm 0.51\%$, n = 4)(p= 4.8E-08). These results indicate that SNF2H plays a key role in the regulation of cell proliferation and that the overexpression of this gene may induce cancer.

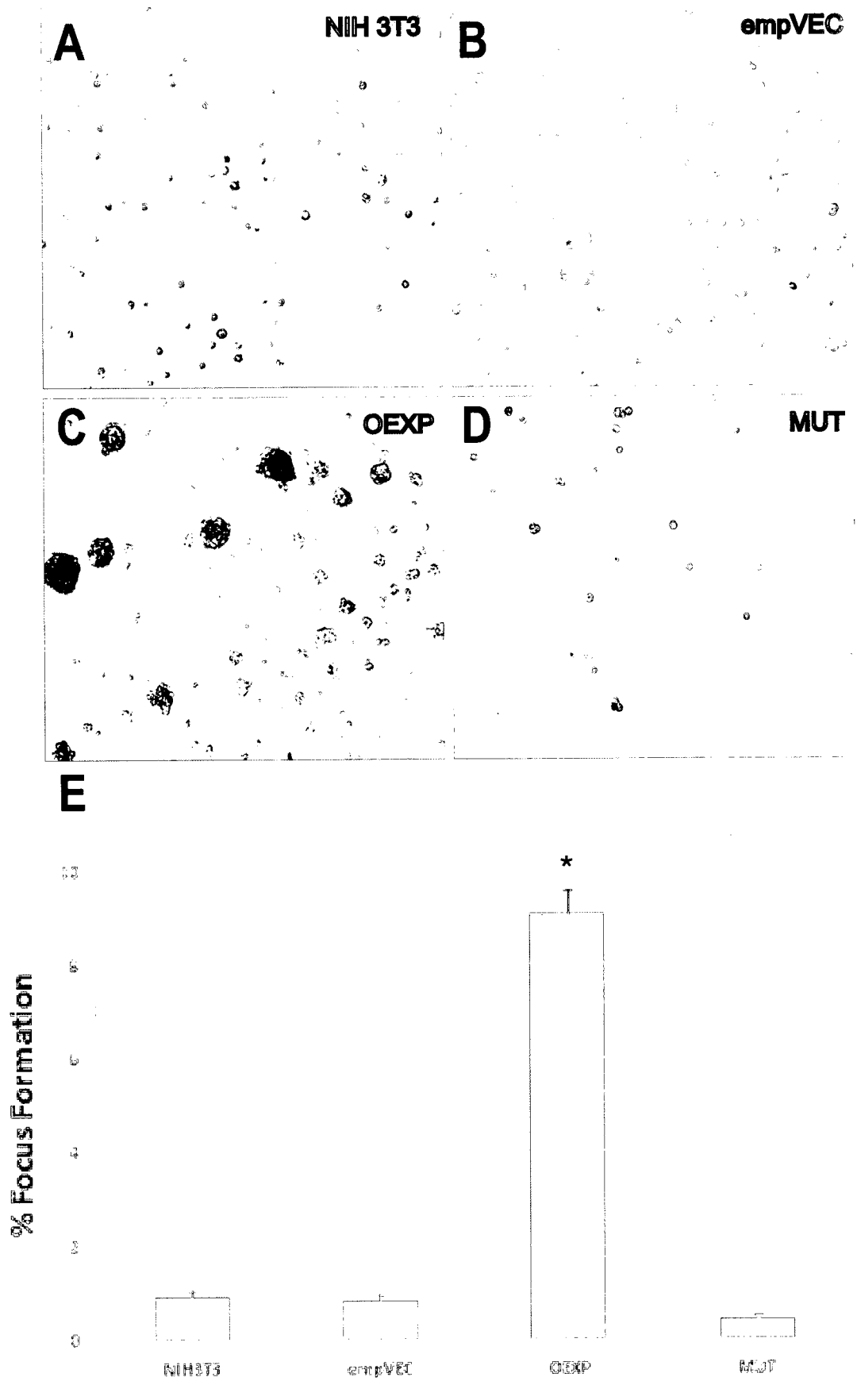
A
NIH 3T3
B
empVEC
C
OEXP
D
MUT
E
% Focus Formation
*
NIH3T3
empVEC
OEXP
MUT

Figure 12 – Over expression of Snf2h increases number and size of foci formation of NIH3T3 clones in soft agar.

Foci formation, a hallmark oncogenic assay, was performed using SNF2H clones. Representative pictures of soft-agar colonies (foci) in [A] NIH3T3, [B] empVEC, [C] OEXP and [D]; MUT are shown. Very large multiple cell colonies are only found in OEXP cultures. [E] Random boxed regions within each micrograph were screened for foci (greater than 4 cells) and divided by the total number of individual cells, representing the % Foci Formation. Each experimental treatment was performed in triplicate for n=4, biological replicates, the error bars represent SEM. (*; $P < 0.050$).

3.3 The generation of the exon 6 deleted gene-targeted Snf2l mice (Ex6DEL).

To investigate the function of *Snf2l* during mouse development the locus was targeted for conditional inactivation by the Cre-LoxP system. For a complete discussion of the cloning and selection of exon 6 targeted transgenic mice please refer to **Appendix II** (pp161). Briefly, a 4.84 kb *Kpn*I/*Xmn*I fragment of genomic DNA spanning the targeted region of the *Snf2l* gene was used to generate the targeting construct and ultimately the generation of *Snf2L* exon 6-floxed mice which contained the neomycin resistance gene, used for ES clone selection (refer to Figure 13a). One recombinant embryonic stem cell clone was generated in J1ES cells and through blastocyst injection used to develop two conditional *Snf2l*-floxed (designated $Snf2l^{f/f}$ females and $Snf2l^{f/y}$ males) animal lines [253].

The early expression of both mammalian *ISWI* genes at embryonic stage E9.5 suggests an important developmental role for both Snf2h and Snf2l [175]. In order to assess the global developmental effects of loss of Snf2l function heterozygous female mice ($Snf2l^{f/x}$, Sv129 background) were crossed to male lines ubiquitously expressing Cre recombinase protein under the control of the *Gata-1* promoter (*Gata-1* $Cre^{+/+}$, CD-1 background [254]). Successful targeting of *Snf2l* ($Snf2l^{-/-}$ females and $Snf2l^{-/y}$ males, here forth referred to as Ex6DEL) was verified by Southern blot and standard PCR. Southern blot analysis (Figure 13b) on genomic DNA isolated from tail, brain and heart from a heterozygous Ex6DEL female, Ex6DEL male and wildtype male mice shows that a shorter fragment always segregates with the Ex6DEL allele. The heterozygous female has both wildtype Snf2l and the Ex6DEL alleles. Likewise, a sample PCR analysis representing a

Figure 13 – Generation and characterization of *snf2l* gene-targeted mice.

[A] A fragment of the m*Snf2l* genomic sequence (wt) was used to engineer a targeting vector containing a floxed neomycin cassette (*NeoR*) within intron 5 and loxP sites (green triangles) flanking exon 6 (yellow box). *Sma*I (S) and *Hind*III (H) sites are shown, and exons are represented by black boxes. A schematic representing the homologous recombinant (hr) with the floxed allele is shown. The orange box represents the relative position of DNA probe used for Southern analysis below, and the blue and red arrow head depict position of primer sets used to PCR and RT-PCR analysis of recombination. [B] Female mice homologous for the floxed *Snfl* allele (*Snf2l* $^{flox/flox}$) were bred to *Gata-1 Cre* male mice to generate the Ex6DEL mice (*Snf2l*$^{+/y}$) and the HET Females (*Snf2l*$^{+/-}$). In further F1 crosses female mice heterozygous for the Ex6DEL allele were bred to male Ex6DEL mice (*Snf2l*$^{-/x}$ and *Snf2l*$^{-/y}$, respectively) to generate WT Males (*Snf2l*$^{X/Y}$) and female Ex6DEL mice (*Snf2l*$^{-/-}$). Confirmation of exon 6 excision by Cre-recombinase is shown by Southern hybridization to DNA extracted from adult tail, brain and heart mouse tissue digested with *Hind*III. Relative position of the probe is shown in [A], orange box. [C] A PCR based screening approach was used to genotype successive litters, generating a 504 bp wildtype (WT)-*Snf2l* band and a 324 bp Ex6DEL band representing the deleted allele. ß-actin is used as a positive PCR control. The relative position of primers used for genotyping is denoted by the blue arrowheads in [A].

A

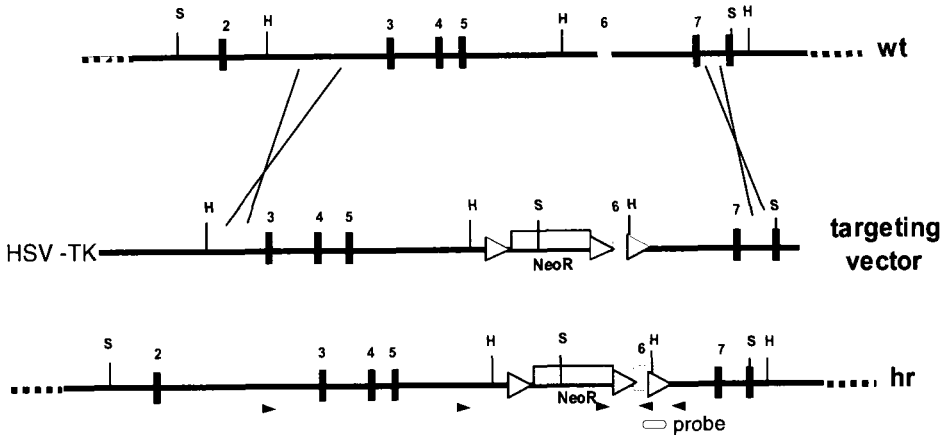
S
2
H
3
4
5
H
6
7
S H
wt
H
3
4
5
H
S
6 H
7
S
HSV -TK
NeoR
targeting vector
S
2
3
4 5
H
S
6 H
7
S H
NeoR
hr
probe

B

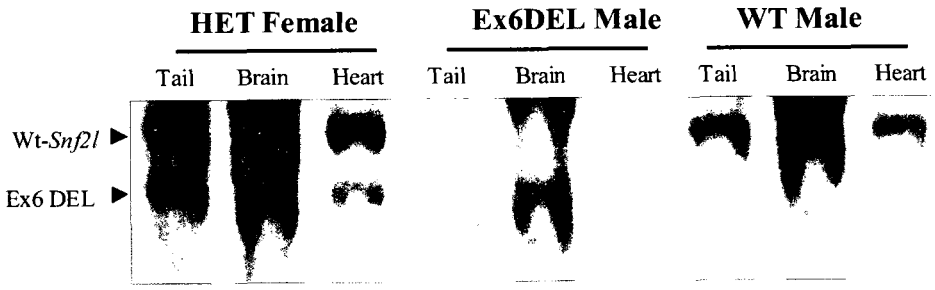
HET Female
Ex6DEL Male
WT Male
Tail
Brain
Heart
Tail
Brain
Heart
Tail
Brain
Heart
Wt-Snf2l
Ex6 DEL

C

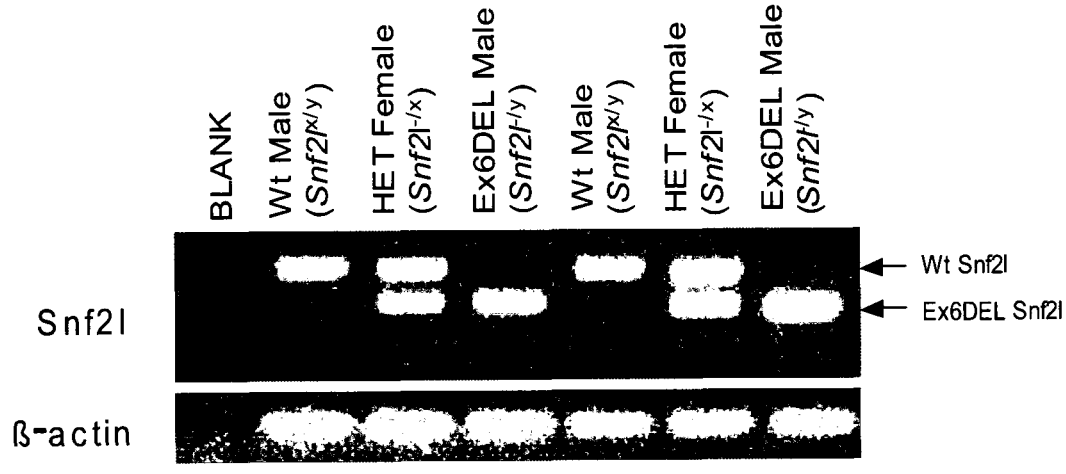
BLANK
Wt Male (Snf2l^x/y)
HET Female (Snf2l^-/x)
Ex6DEL Male (Snf2l^-/y)
Wt Male (Snf2l^x/y)
HET Female (Snf2l^-/x)
Ex6DEL Male (Snf2l^-/y)
Snf2l
ß-actin
Wt Snf2l
Ex6DEL Snf2l

typical genotyping gel (Figure 13 c) shows a similar banding pattern with the shorter band segregating exclusively with the Ex6DEL allele.

A smaller form of the exon 6-deleted *Snf2l* mRNA is stably expressed in homozygous Ex6DEL males and heterozygous females ($Snf2l^{+/x}$) which express both truncated (324 bp) and wildtype (504 bp) transcripts at similar levels (Figure 14a). The deletion of exon 6 (180 bp) does not result in the complete ablation of a protein product. However there is a much more robust signal from extracts prepared from embryonic tissues (Figure 14b), suggesting that Snf2l production is somewhat attenuated in adults. Immunoblot analysis further reveals that the corresponding protein is reduced in size (~125 kDa) when compared to the wt protein product (~133 kDa). The estimated mass of the amino acids encoded by *Snf2l* exon 6 is 6.9 kDa, suggesting that the smaller band represents a stably expressed truncated product from the Ex6DEL allele. Furthermore, Ex6DEL protein production was confirmed by Snf2l immunoprecipitation, wherein the shorter Snf2l product was readily extracted from whole cell lysates (Figure 14c). Taken together these results indicate that loss of exon 6 has little effect on the stability of the mRNA and the Ex6DEL transcript is translated to protein at equivalent levels to wildtype protein.

3.4 Characterization of the Ex6DEL mice.

3.4.1 Increased head size in the Ex6DEL mice.

Snf2l-null mice are viable, born in classic Mendelian ratios and have no overt behavioural phenotypes. However, the Ex6DEL mice have larger heads with no significant

Figure 14 – Expression of the Ex6DEL Snf2l allele in mice.

[A] Reverse transcriptase-PCR analysis of RNA isolated from whole brain, demonstrating the excision of exon 6 from a homozygous Ex6DEL male (*Snf2l*$^{-/y}$), heterozygous Ex6DEL female (*Snf2l*$^{-/x}$) but not the wildtype male littermate (*Snf2l*$^{x/y}$). β-actin is used as a positive RT-PCR control, and HepG2 cells represent a non-*Snf2l* expressing tissue type (liver). The relative position of primer pairs spanning exons 3 to exon 7 is denoted by the red arrowheads in the previous figure (Figure 13a). [B] Western blot analysis of proteins isolated from E15.5 cortices of WT, HET and Ex6DEL animals for Snf2l (top panel) and β-tubulin a loading control (bottom panel) reveals that the exon 6 deleted Snf2l band (~125 kDa) is stably produced and is smaller than the full-length Snf2l (~133 kDa). [C] Whole cell lysates from E15.5 cortices of WT and Ex6DEL animals were used for immunoprecipitation with Snf2l antibodies; immunoprecipatates were analyzed by immunoblotting with Snf2l antibodies to show that the smaller 125 kDa protein is isolated from Ex6DEL tissue, as is the full length Snf2l 133 kDa protein from WT tissue. Sheep IgG represents the pre-immune sample and is a negative control.

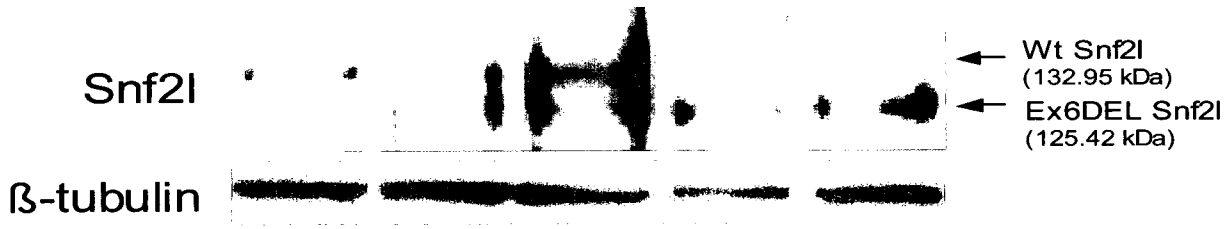
Snf2l
ß-tubulin
Wt Snf2l
(132.95 kDa)
Ex6DEL Snf2l
(125.42 kDa)

C

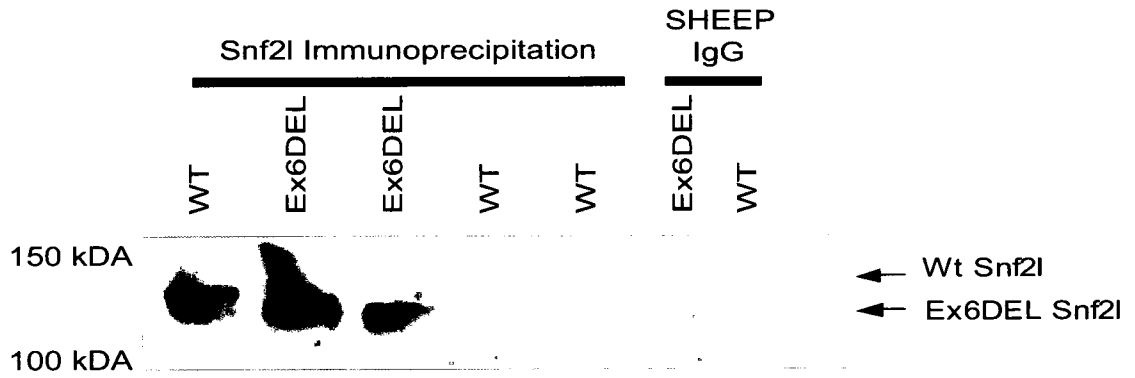
Snf2l Immunoprecipitation
SHEEP IgG
WT
Ex6DEL
Ex6DEL
WT
WT
Ex6DEL
WT
150 kDA
100 kDA
Wt Snf2l
Ex6DEL Snf2l

A
B
ß-actin
Snf2l
Wt Male
(Snf2l x/y)
HET Female
(Snf2l -/x)
HET Female
(Snf2l -/x)
Ex6DEL Male
(Snf2l -/y)
Ex6DEL Female
(Snf2l -/-)
BLANK
-RT Control
HET Female
(Snf2l -/x)
Wt Male
(Snf2l x/y)
Ex6DEL Male
(Snf2l -/y)
HEPG2
(Control)
Ex6DEL Snf2l
Wt Snf2l

difference in body weight (Figure 15a, and data not shown). Upon dissection Ex6DEL brain size and weight was increased (Figure 15a) and brain weight to body weight ratios was enhanced 1.4-fold (males) and 1.5-fold (females) over the sex-matched wildtype and heterozygous mice (Figure 15b). In order to test for other developmental irregularities, mice at 11 weeks of age were sacrificed and the relative size of other organs was assessed (Figure 16 ab). Brains from these Ex6DEL mice had a 1.4-fold increase in brain: body mass ratio, while the kidneys and testes all showed only a meagre increase. The heart, while showing an increasing trend was not statistically significant ($p= 0.0522$). The values obtained for the controls are comparable to values obtained in studies of normal mice [274]. Despite the increase in brain size there was no increase in the propensity toward tumour formation (data not shown).

3.4.2 Global inactivation of Snf2l leads to hypercellularity in the brain.

To determine the cause of the brain phenotype, frozen sections from 3 month old (Figure 17), mice were analyzed with different histochemical stains (Figure 17ab, DAPI, shown). There was an observed increase in cell number within the layers of the Ex6DEL cortices, but no significant disorganization within the cortical lamina in the embryonic and postnatal tissues. The largest difference in cell numbers between adult Ex6DEL mice and wildtype controls lies within the Intermediate Zone (IZ) and Ventricular Zone (VZ) of the cortex, where the difference is 1.8-fold increase to a 1.14 fold increase in layers II/III (Figure 17c). Typically layers II and III are combined because layer II is either very narrow or even indistinguishable as a separate layer in the mouse neocortex [275, 276].

Figure 15 – Ex6DEL mice develop normally with larger brains.

[A] Photographs of the heads and the dissected brains of adult (~23 weeks) male wildtype (WT), Ex6DEL and a Heterozygous (HET) female mouse for comparison of head size and brain morphology. [B] Graphical representation of the brain size as a function of the brain weight to body weight ratio. Red bar represents the mean ratio, compared between sex matched animals. There is a 1.4-fold increase between the male and 1.6-fold increase for female Ex6DEL animals and their sex matched control littermates, heterozygous females are indiscriminate from wildtype controls. (*; $P < 0.050$, the sample size is given in the brackets, error bars represent SEM).

A

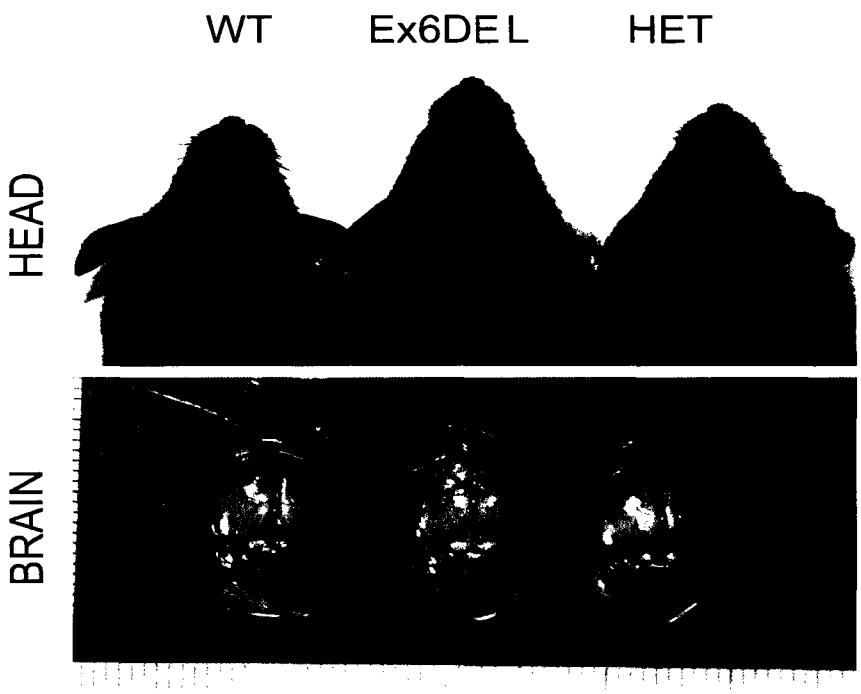
WT
Ex6DEL
HET
HEAD
BRAIN

B

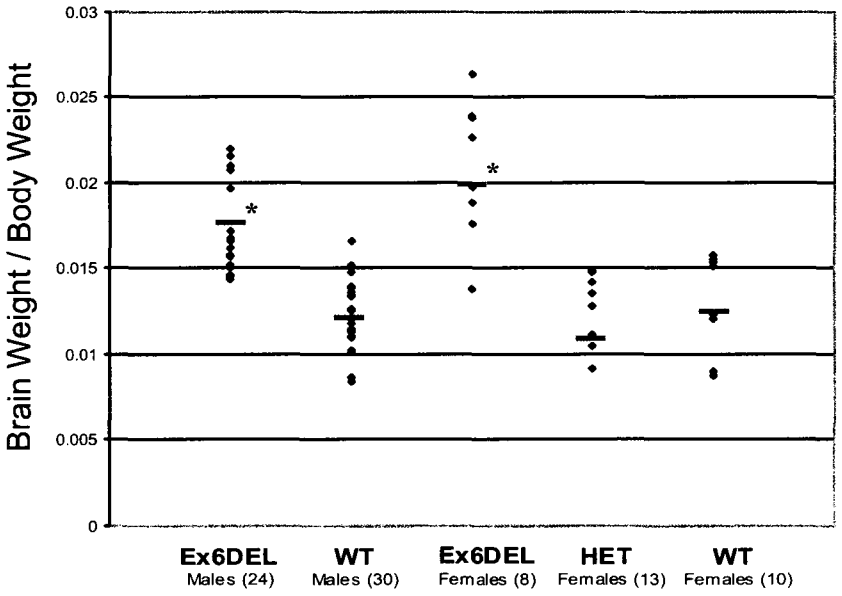
Brain Weight / Body Weight
0.03
0.025
0.02
0.015
0.01
0.005
0
*
*
Ex6DEL Males (24)
WT Males (30)
Ex6DEL Females (8)
HET Females (13)
WT Females (10)

Figure 16 – Ex6DEL mice have marginally larger organs then wildtype littermates.

[A] Photographs of the heads and the dissected organs of adult (~23 weeks) two male wildtype (WT) and an Ex6DEL mouse for comparison of head size and brain morphology. [B] Graphical representation of the Brain, Kidney, Heart and Testes size as a function of organ weight to body weight ratio between 11 week old Ex6DEL (black bars) and WT (gray bars) male animals. All organs show a larger ratio in the Ex6DEL animals except in the heart where the larger trend is observed but it is not statistically significant. (* $P < 0.05$, # $P = 0.0525$; $N = 14$ Ex6DEL and $N = 23$ control animals) Error bars (B, C) represent the SEM. Raw data, including organ and body weights used in this analysis can be found in Appendix IV (pp163).

A

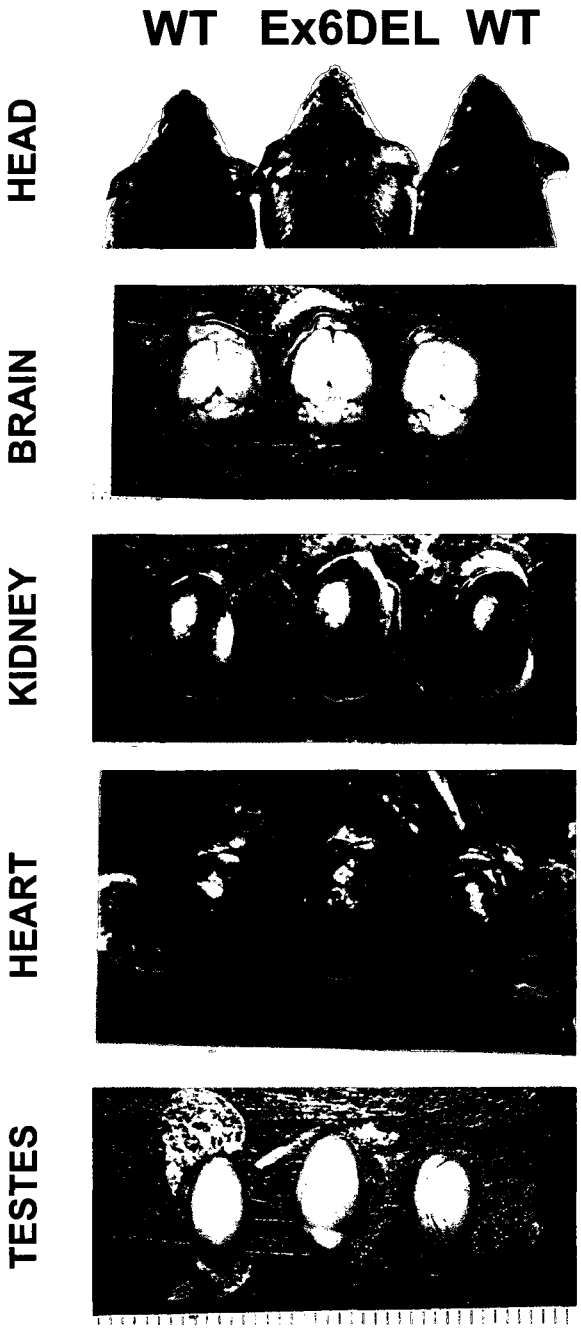
WT Ex6DEL WT
HEAD
BRAIN
KIDNEY
HEART
TESTES

B

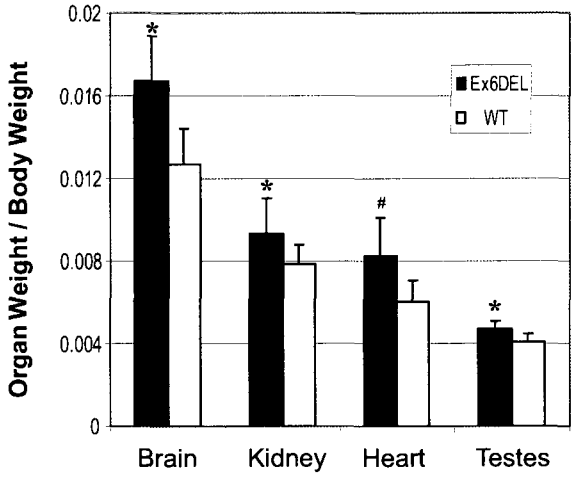
Organ Weight / Body Weight
0.02
0.016
0.012
0.008
0.004
0
Ex6DEL
WT
*
*
#
*
Brain
Kidney
Heart
Testes

Figure 17 – Increased cell numbers observed in the adult Ex6DEL cortex.

[A] A 12 μm coronal section through the cortex of a three month old Ex6DEL mouse stained with DAPI with a section through the laminar cortical layers, highlighted by the white dashed box, is typical of the region (field of view) used for quantifying nuclei. [B] An example of the 160 μm (width) sections used for counting nuclei from wildtype (WT) and Ex6DEL male animals within the distinct cortical layers (II/III-VI), marginal zone (MZ), pial surface (PS), intermediate zone (IZ), ventricular zone (VZ) and the hippocampus (HC). [C] Graphical representation of cell number in the adult brain shows a significant increase in the number of nuclei between the Ex6DEL (black bars) and WT (gray bars) in all cortical layers except in Layer VI. Due to the difficulty in distinguishing layers II and III, they were grouped together (*, P-values < 0.05; $N = 3$) error bars represent SEM.

A

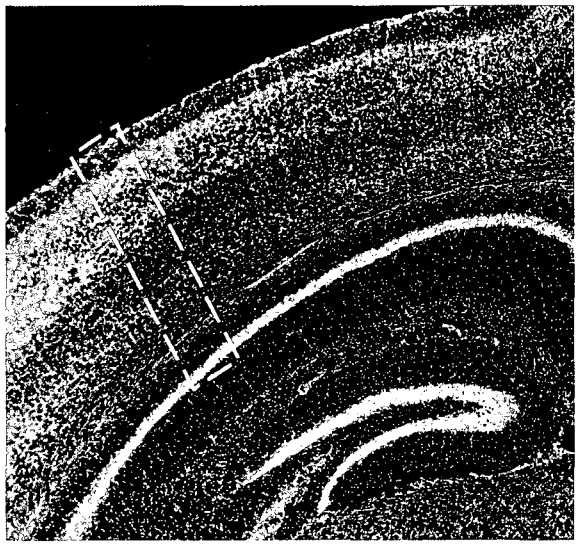

B

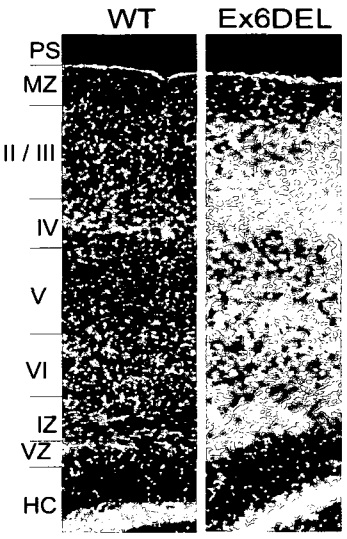
WT
Ex6DEL
PS
MZ
II / III
IV
V
VI
IZ
VZ
HC

C

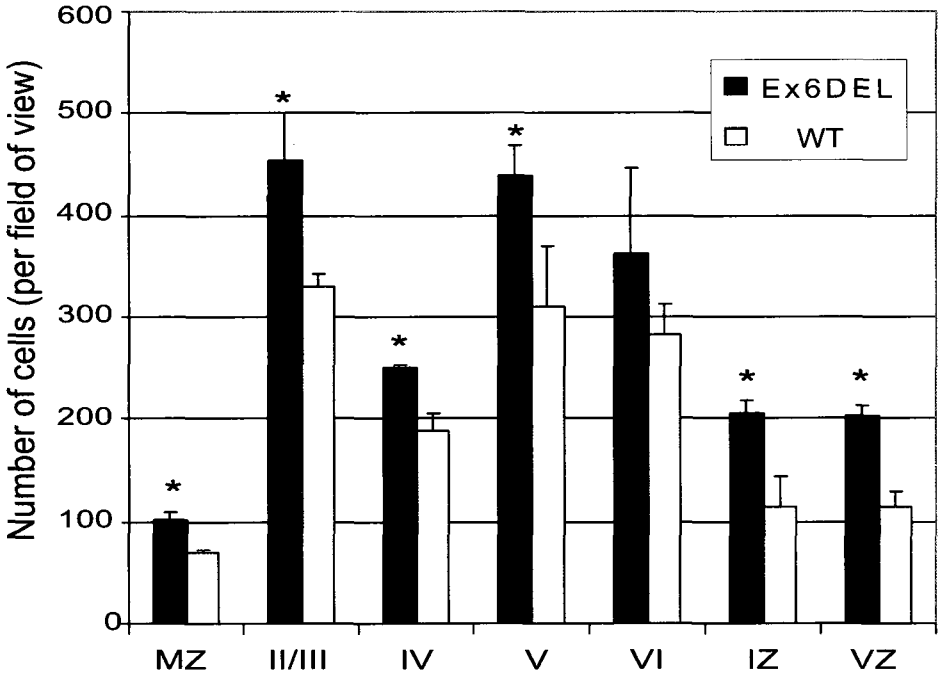
Number of cells (per field of view)
600
500
400
300
200
100
0
Ex6DEL
WT
*
MZ
II/III
IV
V
VI
IZ
VZ

By totalling up the average number of cells in all layers of the section (160 μm) the average for Ex6DEL is 2017.6+/- 86.7 (n = 3), while for wildtype it is 1409.6 +/- 40.7 (n = 3), representing a 1.4-fold increase (p = 0.003). Note that the specific fold-increases for layer VI is 1.28 but that this value is not significant (p = 0.20). In the one-week postnatal animals (P7.5) an increase in cell number was observed for all cortical layers (Figure 18), most notably in layer II/III (1.9-fold) and layer V (1.6-fold, n =4), which are shown at higher magnification (Figure 18b). Similarly by totaling the average number of cells throughout the layers (100 μm) for Ex6DEL is 130.9+/- 4.5 and for 81.9+/-2.6 for wildtype, representing a 1.6-fold increase (p = 4.6E-06). The observations of increased cell numbers and brain weight in postnatal animals is consistent in Ex6DEL mice (*Snf2l*$^{-/y}$ or *Snf2l*$^{-/-}$), female mice heterozygous for *Snf2l* (*Snf2l*$^{-/x}$) appear entirely normal.

3.4.2.1 Hypercellularity in the cortex is the result of a defect during embryonic neurodevelopment.

Due to the similar phenotypes between animals aged 3 month and one week, embryonic time points were also assessed for hypercellular cortices (Figure 19). At embryonic day 15 (E15.5) increases in the Ex6DEL tissue are observed in the MZ, IZ and VZ (1.33-, 1.25- , and 1.34-fold, respectively) (Figure 19 b). Again the total number of cells per section (55 μm) is 483.3+/-19.8 for Ex6DEL and 384.2+/- 24.1for wildtype (1.3-fold, p=0.009, n = 6). By this point only the marginal zone is identifiable, the developing cortical plate (CP) consists only of the layer V and layer VI which are indistinguishable, and the migrating cells that are to become layer IV neurons, in transit [53, 55, 64]. These results suggested the increase in cells observed in the postnatal cortex were the result of a defect which arises during embryonic development.

Figure 18 – Increased cell numbers observed in 1 week old Ex6DEL cortex.

[A] A 10μm DAPI stained coronal sections (100 μm width) from one-week old (P7.5) WT and Ex6DEL mice display increased cellularity throughout the cortical strata (IZ-MZ), intermediate zone (IZ). [B] Sample images of increased magnification from superficial layers II/III and a deep layer (V) are shown. [C] Graphical representation of cell number in the P7.5 brain show a significant increase in the number of nuclei between the Ex6DEL (black bars) and WT (gray bars). In all cortical layers the intermediate zone and ventricular zone regions where not tallied. Due to the difficulty in distinguishing layers II and III they were grouped together (*, P-values < 0.05; $N = 4$) error bars represent SEM.

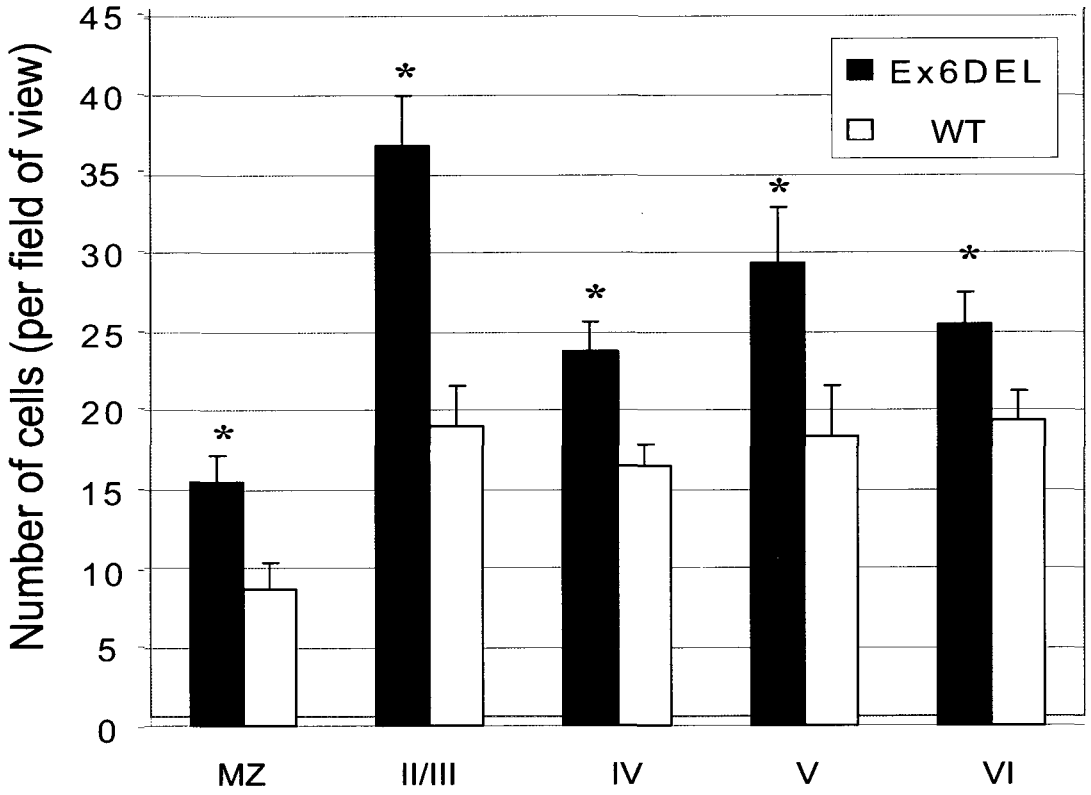
Number of cells (per field of view)
45
40
35
30
25
20
15
10
5
0
Ex6DEL
WT
*
*
*
*
*
MZ
II/III
IV
V
VI

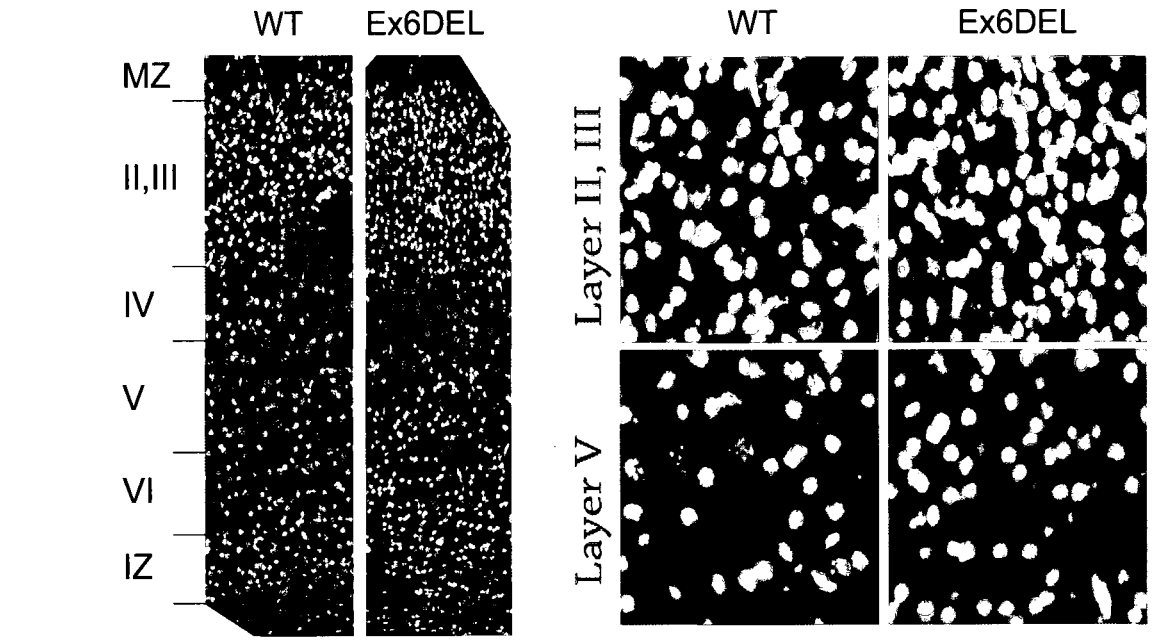
A
WT
Ex6DEL
MZ
II,III
IV
V
VI
IZ
B
WT
Ex6DEL
Layer II, III
Layer V
C

Figure 19 – A trend toward increased cell number is also observed in the E15.5 brain, suggesting that the defect arises during embryonic development.

[A] A 10μm DAPI stained coronal section (55μm width) from WT and Ex6DEL embryonic (E15.5) cortices were also scored for cell number. By this stage in cortical development only the marginal zone (MZ) and deep cortical layers (V and VI) have formed but are indefinable and as such these layers where counted as one region, the cortical plate (CP). IZ (intermediate zone), VZ (ventricular zone). [B] Quantification of cell counts demonstrates the increase observed in the postnatal samples is not recapitulated in the cortical plate of the embryonic tissue, but is observed in the subventricular and intermediate zones (SVZ, IZ) in the number of nuclei between the Ex6DEL (black bars) and WT (gray bars). (*, P-values < 0.05; $N = 6$) error bars represent SEM.

A

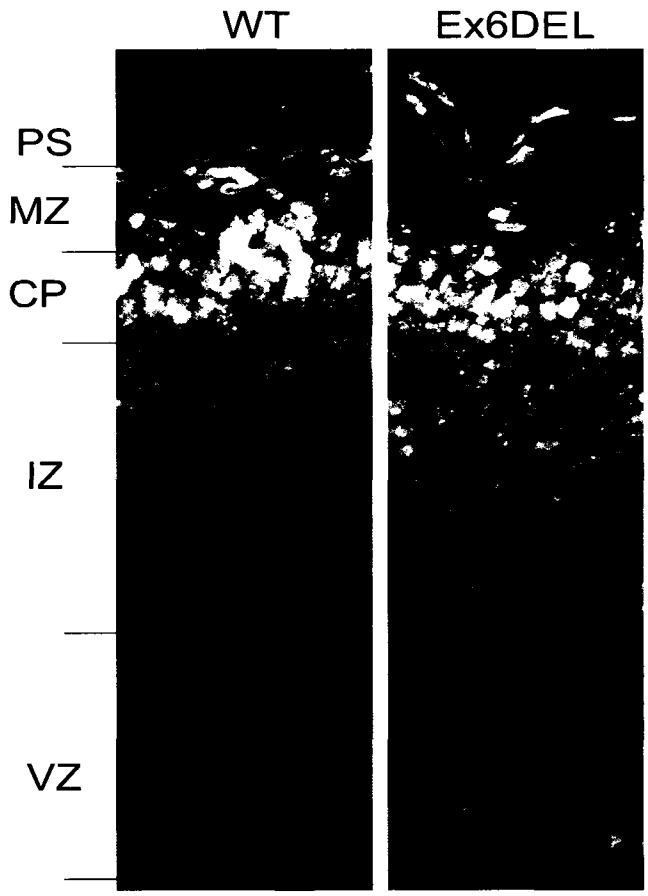
WT
Ex6DEL
PS
MZ
CP
IZ
VZ

B

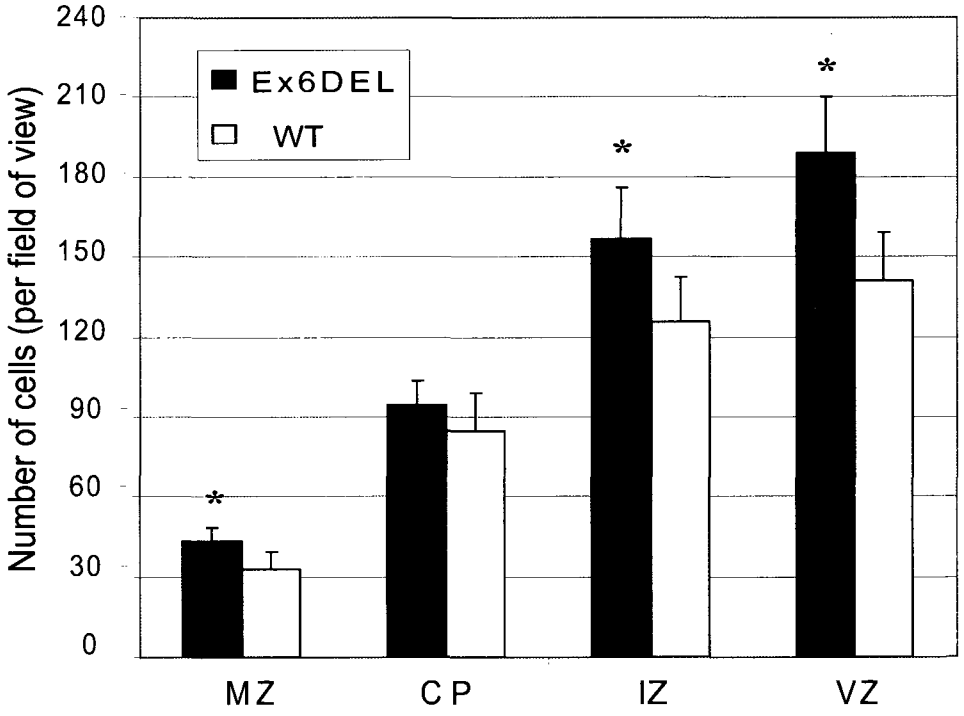
Ex6DEL
WT
Number of cells (per field of view)
240
210
180
150
120
90
60
30
0
*
*
*
MZ
CP
IZ
VZ

3.4.2.2 Hypercellularity is also observed in the hippocampus.

Other regions of the CNS that displayed increased cellularity were also identified. Similar increases were observed in the adult hippocampus (Figure 20). The hippocampus, like the cortex, is a key component of the telencephalon, which in turn is a key constituent of the limbic system that plays major roles in long term memory and spatial navigation [277, 278]. Also similar to the cortex, the hippocampus is made up of stratified layers of distinct neurons (Stratum Moleculare, Stratum Lacumosum Moleculare, Stratum Radiatum, Stratum Pyramidal or *Cornu Ammonis*, and the Stratum Oriens, labelled in Figure 20ab), which migrate radially, from the *Dentate gyrus* (DG). Figure 20ab depicts NISSL substance stained hippocampal sections from a wildtype and Ex6DEL mouse, and inset are magnifications from the Stratum Radiatum. There are significant increases in every layer of the Ex6DEL hippocampus, (Figure 20c). The stratum pyramidal cell layer could not be counted due to the dense cellular nature, however qualitatively there is an increased thickness and darker staining of these regions, particularly in the CA1 and DG of the Ex6DEL tissue (see Figure 20a).

3.5 Regulation of Snf2h in the Ex6DEL Snf2l mutants.

Snf2l and Snf2h are highly similar, approximately 84% at the amino acid level, and they perform similar functions. Reports that Snf2l has been found in Snf2h complexes (specifically, CHRAC and ACF [178]) suggest that these two proteins may, under certain circumstances, functionally replace one another. Furthermore, Brm-null mice are viable through functional compensation by the closely related Brg1 [198]. Perhaps in the absence

Figure 20 – An increased number of cells is also observed in all layers of the adult hippocampus.

Coronal sections (12 μm) through the hippocampus of a three month old wildtype [A] and Ex6DEL [B] mouse stained with cresyl violet (NISSL). The hippocampal strata and the visible *Cornu Ammonis* regions CA1, CA3, and the dentate gyrus (DG) are labelled within panel B. Insets are magnifications from the Stratum Radiatum, showing increased nuclei (number at the bottom right). [C] Graph depicting cell counts from the adult hippocampus shows a significant increase in the number of nuclei between the Ex6DEL (black bars) and WT (gray bars) in all hippocampal strata. (*, P-values < 0.05; # P-value > 0.05; $N = 3$) error bars represent SEM.

A

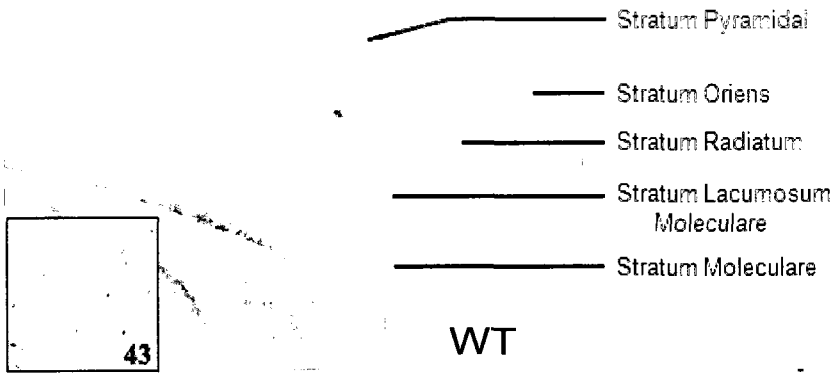
Stratum Pyramidal
Stratum Oriens
Stratum Radiatum
Stratum Lacumosum
Moleculare
Stratum Moleculare
43
WT

B

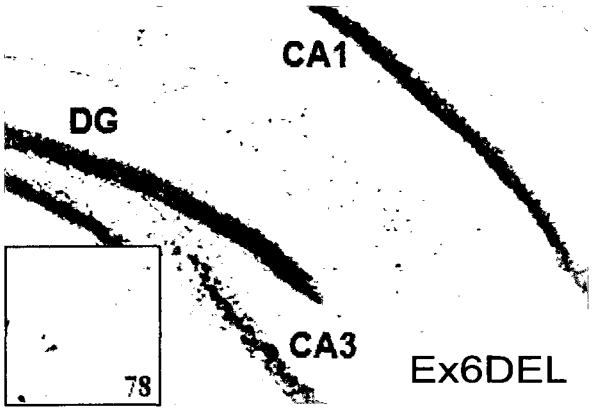
CA1
DG
CA3
78
Ex6DEL

C

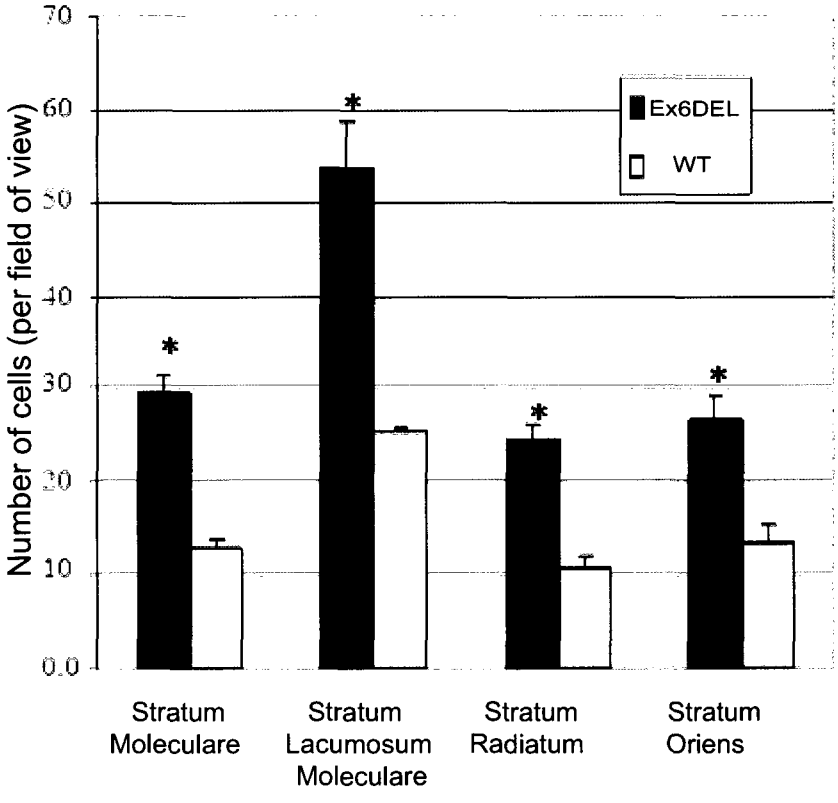
70
60
50
40
30
20
10
0.0
Number of cells (per field of view)
Ex6DEL
WT
*
Stratum Moleculare
Stratum Lacumosum Moleculare
Stratum Radiatum
Stratum Oriens

of a functional Snf2l protein, Snf2h is able to replace it. In order to test if Snf2h levels are enhanced in the Snf2l-functionally null Ex6DEL brain tissue, RT-PCR analysis was performed on E13.5 and E15.5 cortical RNA (Figure 21a). Primers directed to a region of *Snf2l* that span exon 6 (specifically exon 3 to exon 7) were used to amplify the wildtype *Snf2l* or Ex6DEL messages. Similarly, primers specific to *Snf2h* were used to amplify *Snf2h* message. There was no change in the levels of *Snf2h* between wildtype and Ex6DEL tissues. These results were confirmed by Western blotting cortical protein extracts and probing with Snf2l and Snf2h antibodies (refer to Figure 21b). The results do not refute that the Snf2l-null mice are viable through compensation by Snf2h, but show that there is not an upregulation of this protein/transcript in response to the loss of Snf2l.

3.6 Molecular characterization of increased cell number in Snf2l Ex6DEL mice.

The largest difference in cell populations between the Ex6DEL mice and wildtype controls lie within the VZ and IZ (Figure 19). These regions typically contain the bulk of proliferating neuroprogenitors cells and constitute the germinal neuroepithelium, and the IPC (discussed in the Introduction, section 1.1.4). It has been proposed that even the most subtle of changes in the relative production of neuroprogenitor cells can lead to alterations in the neuronal population and thus cortical size [279, 280]. In order to assess imbalances in the progenitor populations, a qualitative analysis of neuroprogenitor and neuronal markers was performed by *in situ* hybridization at two developmental time points. At E15.5, the expression levels of *pax6*, *cyclind1*, *gli1* and *hes5,* are specifically confined to populations of neuroprogenitors, and display a increased level of gene expression in the Ex6DEL animals (Figure 22). The levels of *tbr-1* and *id2*, markers of early born

Figure 21 – Snf2h levels are not affected in Ex6DEL mice.

[A] Complementary DNA was generated from total RNA extracted from E13.5 and E15.5 cortices from both wildtype (WT) and Ex6DEL embryos. Selective expression of *Snf2l* (first panel) and *Snf2h* (second panel) was assessed by RT-PCR analysis. β-*actin* and *Gapdh* bottom panel is a loading control. –RT (without reverse transcriptase) is a negative control for genomic DNA contamination. PCR products were separated by electrophoresis on a 0.8% agarose gel and visualized by ethidium bromide staining. [B] Western blot analysis of proteins isolated from E13.5 and E15.5 cortices of WT and Ex6DEL embryos for Snf2l (top panel) and Snf2h (middle panel). Results indicate that there is no change in Snf2h levels between genotypes. Tubulin is a loading control.

B

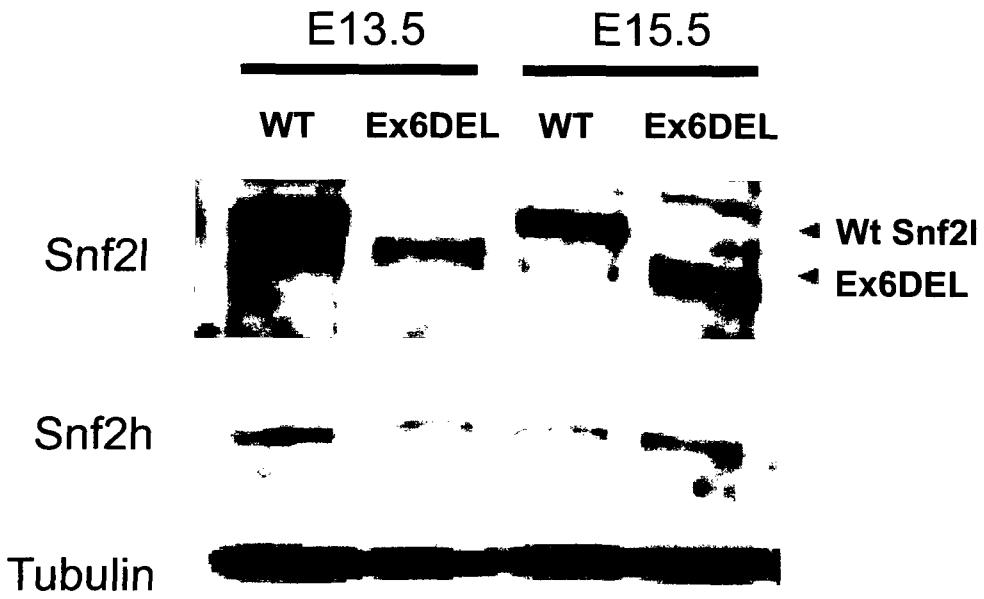
E13.5
E15.5
WT
Ex6DEL
WT
Ex6DEL
Snf2l
Wt Snf2l
Ex6DEL
Snf2h
Tubulin

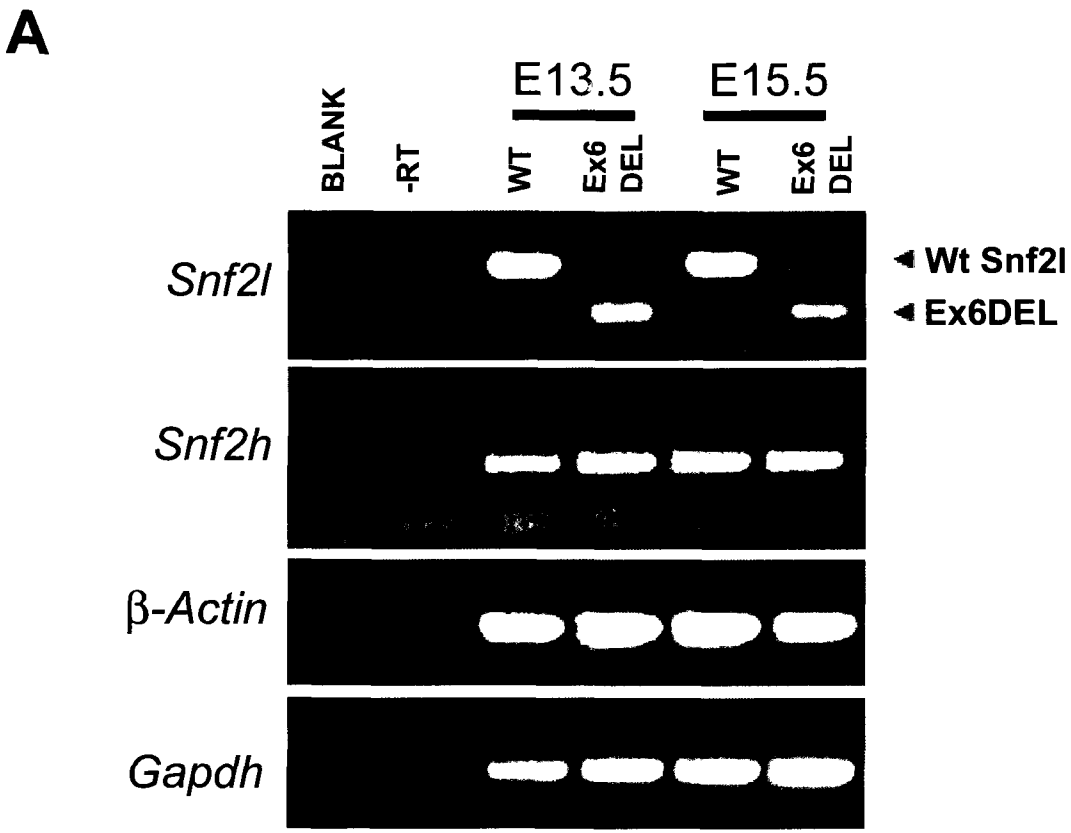
A
E13.5
E15.5
BLANK
-RT
WT
Ex6 DEL
WT
Ex6 DEL
Snf2l
Snf2h
β-Actin
Gapdh
Wt Snf2l
Ex6DEL

Figure 22 – Distribution of neuroprogenitor populations and differentiated neurons in the E15.5 mouse cortex are affected by Snf2l function.

Coronal sections through the E15.5 cortex of WT (left) and Ex6DEL (right) embryos were analysed for expression of neuroprogenitor and neuronal markers. Hybridization of RNA probes for *Pax6* (A,B; n = 5), *Cyclind1* (C,D; n = 5), *Gli*1 (E,F; n = 3) and *Hes5* (G,H; n = 2) show increased expression in the ventricular zone (vz) of the Ex6DEL tissue. Expression of these markers is limited to proliferating populations and are absent in the differentiated neurons of the cortical plate (cp). Likewise, the hybridization patterns of two regulators of differentiation, *Tbr-1* (I,J; n = 5) and *Id2* (K,L; n = 5) suggest an increase in differentiated neurons within the cortical plate (cp) of ex6DEL mice. The lateral ventricle is also labelled (lv).

Markers of Neuroprogenitors

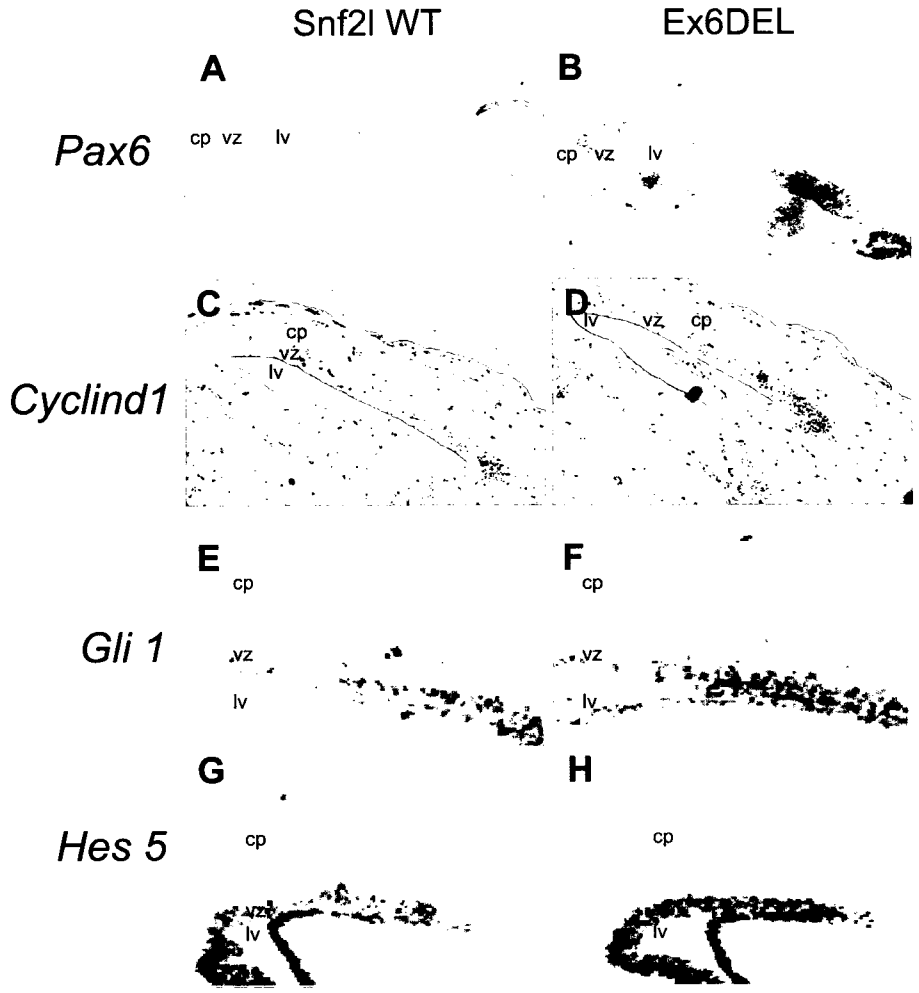

Markers of Differentiated Neurons

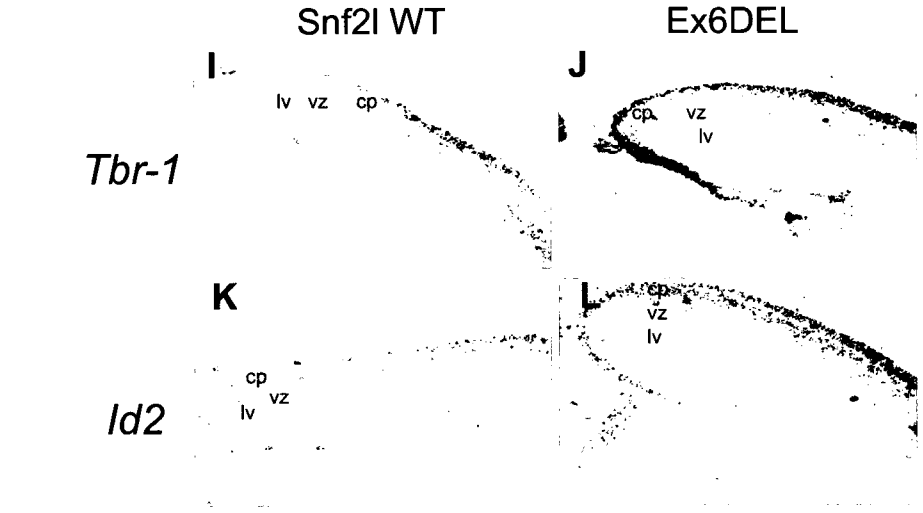

postmitotic neurons of layer VI and of dopaminergic neurons, respectively, also showed increased expression (refer to Figure 22 i-l) [281-283]. Interestingly, at E13.5, *pax6* levels are unchanged while *cyclind1* levels are enhanced (see Figure 23 a-d) in much the same manner as observed in E15.5 tissue. At E13.5, the levels of *tbr-1* and *id2* are marginally increased (Figure 23 e-h) suggesting that the defect in cell proliferation is not as prominent at this earlier timepoint. Moreover, a similar upregulation of *pax6* and *gli1* gene expression was observed in the developing cerebellum (see Figure 24). Development of the cerebellum takes place much later than that of the cortex, initiating near the end of embryogenesis and proceeding into the second week following birth [284]. The proliferative region of the developing cerebellum is the external granular layer (EGL), the outermost layer, and as cells from this region exit the cell cycle and differentiate into neurons they migrate inward to populate the inner granular layer (GL) [284]. The enhanced levels of neuroprogenitor markers (*pax6* and *gli1*) are suggestive of heightened proliferation, as observed in the cortical germinal epithelium.

3.6.1 Size increase and hypercellularity in the neocortex through heightened neuroprogenitor proliferation.

There are three well-documented mechanisms leading to hypercellularity: (1) A decrease or disruption in the apoptosis pathway resulting in increased cell survival [285-287], (2) an increase in ectopic neuronal cell proliferation or the continued generation of daughter cells even beyond terminal differentiation [288], or (3) a delay in cell cycle exit, increase in cell cycle re-entry or a shortening of the cell cycle, all three of which could result in the generation of a larger neuroprogenitor pool.

Figure 23 – Distribution of neuroprogenitor populations and differentiated neurons in the E13.5 mouse cortex are only marginally affected by Snf2l function.

Coronal sections through the E13.5 cortex of WT (A,C,E,G) and Ex6DEL (B,D,F,H) embryos were analysed for expression or neuroprogenitor and neuronal markers. Hybridization of RNA probes for *Pax6* (A,B; n = 3) and *Cyclind1* (C,D; n = 3) show no change in *Pax6* populations and only a marginal increase in *Cyclind1* within the ventricular zone (vz) of the Ex6DEL tissue. Expression of these markers is limited to proliferating populations and are absent in the differentiated neurons of the cortical plate (cp). The lateral ventricle is also labelled (lv). Similarly the hybridization patterns of two markers of differentiated neurons, *Tbr-1* (E,F; n = 3) and *Id2* (G,H; n = 3) are not increased suggesting that differentiated neurons of the cortical plate are not augmented at this time point.

Markers of Neuroprogenitors

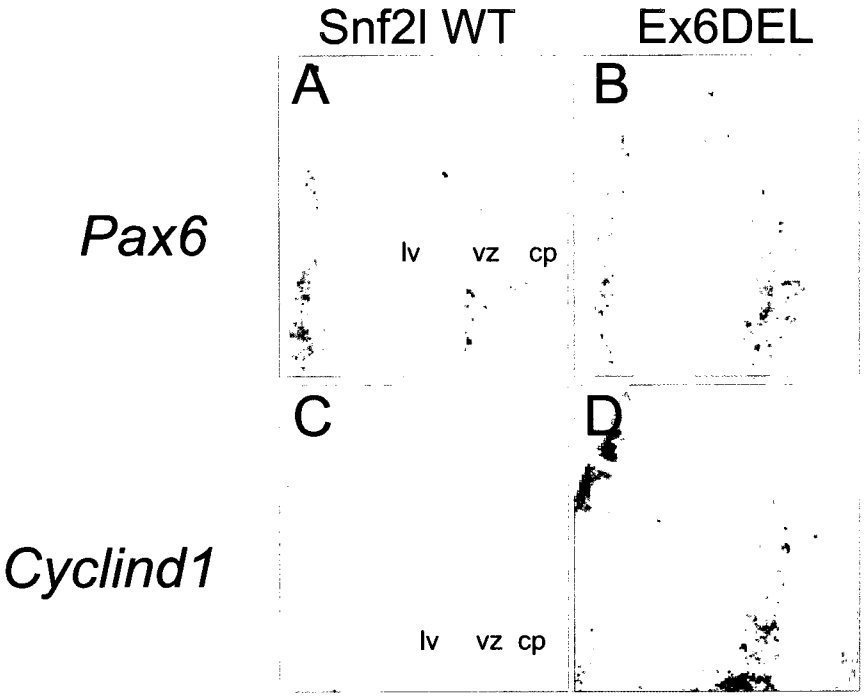

Pax6

Cyclind1

Markers of Differentiated Neurons

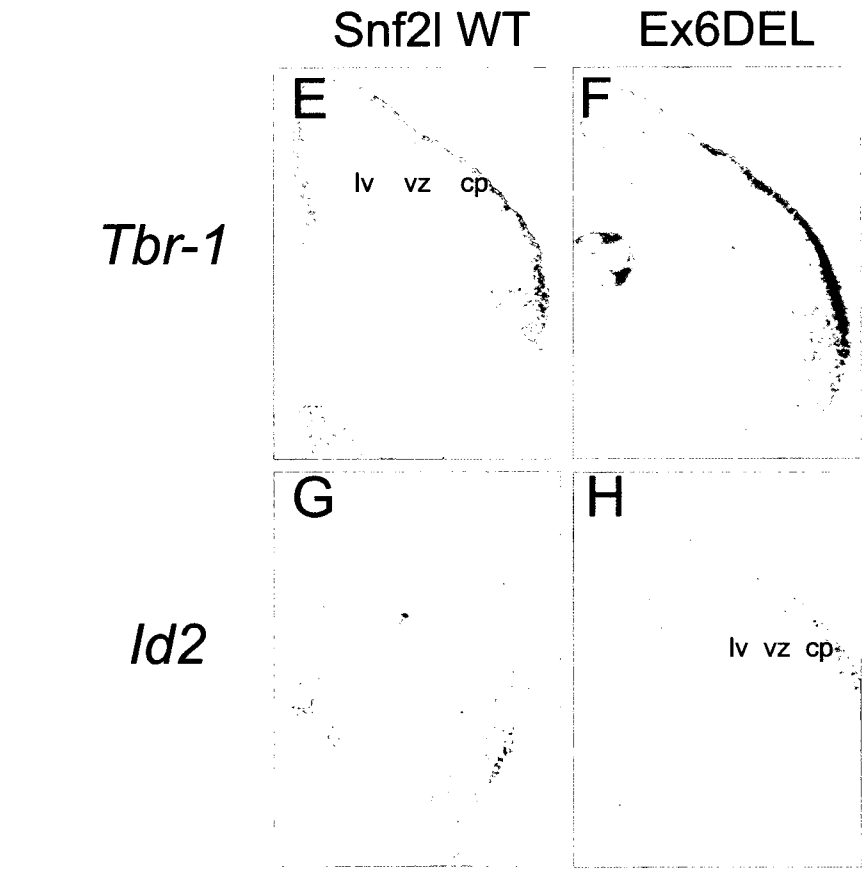

Tbr-1

Id2

Figure 24 – Distribution of neuroprogenitor population in postnatal developing cerebellum is affected by Snf2l function.

Coronal sections through the p7.5 cerebellum of wildtype (WT) and Ex6DEL embryos were analysed for expression of the neuroprogenitor marker *Pax6* and the transcriptional activator *Gli1*. Hybridization of RNA probes for *Pax6* (A,B) and *Gli1* (C,D) show a particular increase in *Pax6* and *Gli1* staining populations in the external granular layer (EGL) of Ex6DEL tissue. Expression of these markers is limited to proliferating populations and are absent in the differentiated neurons of the white matter (WM). Also shown is the Purkinje cell layer (PCL) and internal granular layer (GL).

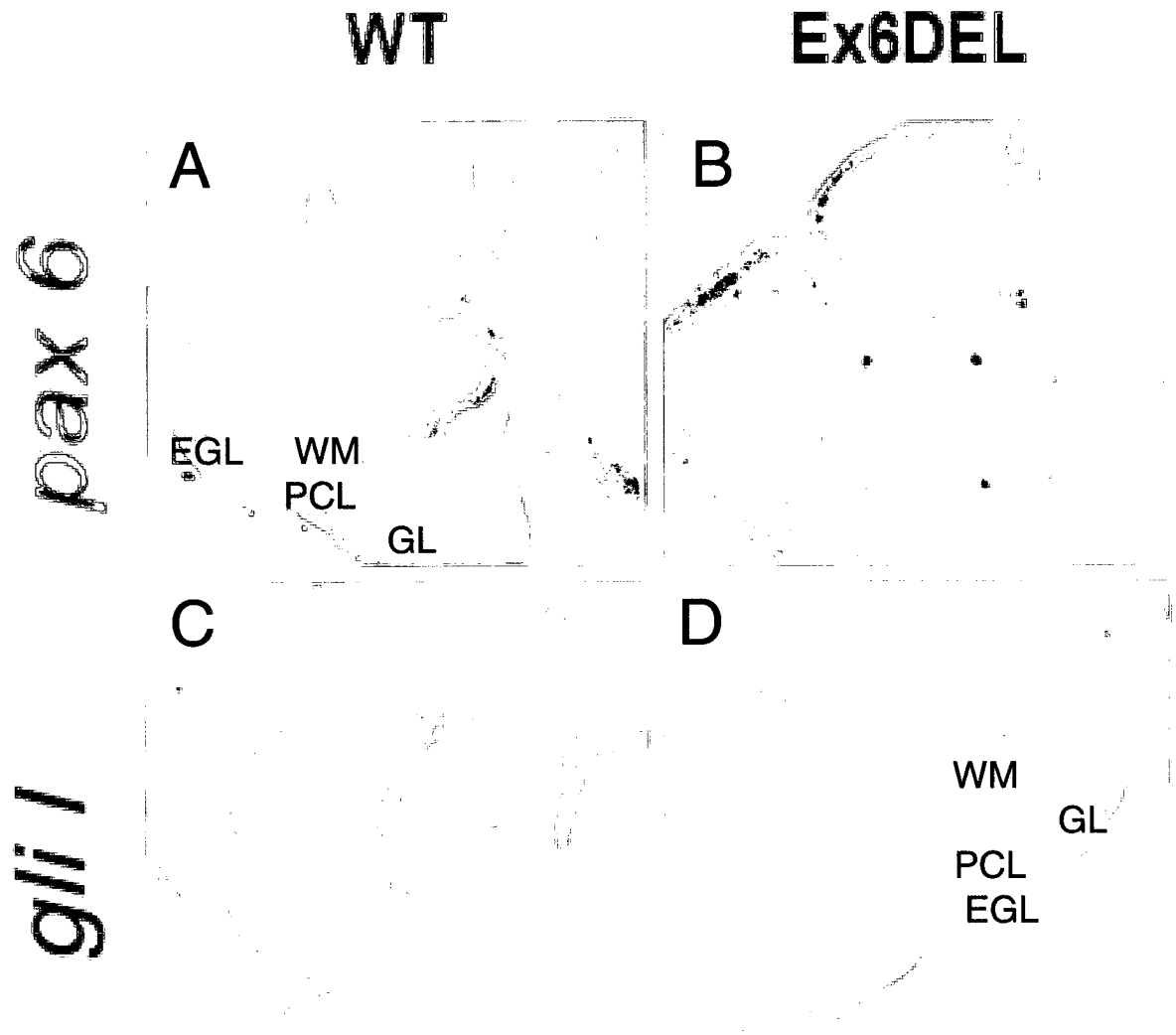
WT
Ex6DEL
A
B
pax 6
EGL
WM
PCL
GL
C
D
gli 1
WM
GL
PCL
EGL

In order to determine if the inactivation of *Snf2l* led to a modification in apoptosis during neurogenesis, cell death was assessed using TUNEL [**T**erminal **D**eoxy**n**ucleotidyl transferase-mediated UTP-nick **E**nd **L**abeling] staining. Positive apoptotic cells were identified by immunohistochemistry and quantified (Figure 25ab). The ratio of TUNEL labelled cells within the developing neocortex revealed that the proportion of cell death was not substantially changed between the wildtype control ($0.048 \pm 0.006/100\ \mu m^2$, n =3) and Ex6DEL ($0.050 \pm 0.002/100\ \mu m^2$, n = 3) animals at E13.5 (Figure 25c). These data suggest that decreased programmed cell death is unlikely for the increased brain size in Ex6DEL mice.

To determine if the inactivation of *Snf2l* led to an increase in ectopic cell division, pregnant females carrying wildtype *Snf2l* and Ex6DEL embryos were injected with bromodeoxyuridine at E15.5 of gestation and harvested three hours later. BrdU incorporation labels cells undergoing DNA synthesis at the time of the BrdU injections. Mutant and control embryos were assayed for BrdU incorporation in the developing neocortex by immunohistochemistry (Figure 26ab). There were few BrdU positive cells in the cortical plate suggesting that the increase in cell number does not arise from ectopic proliferation. The vast majority of BrdU staining lies throughout the intermediate zone (Figure 26ab, bottom panels). Although there was an increase in total BrdU positive cell numbers, the proportion of cells labeled by BrdU compared to total cells (stained with DAPI, not shown) remained consistent with wildtype controls (Ex6DEL 0.37 ± 0.07 and WT 0.28 ± 0.03 per 180 μm^2,respectively; n = 4, Figure 26c).

Figure 25 – Levels of apoptosis in the Ex6DEL embryonic cortex is not affected.

E13.5 cortical sections (coronal, 10μm) co-stained for apoptotic-TUNEL positive (red) and DAPI (blue), [A] Wildtpye, [B] Ex6DEL. Scale bar represents 10 μm. [C] Graph depicting no substantial change in the Apoptotic Index, the proportion of TUNEL positive cells from DAPI per 100 μm^2 (n=3, biological replicates) error bars represent SEM.

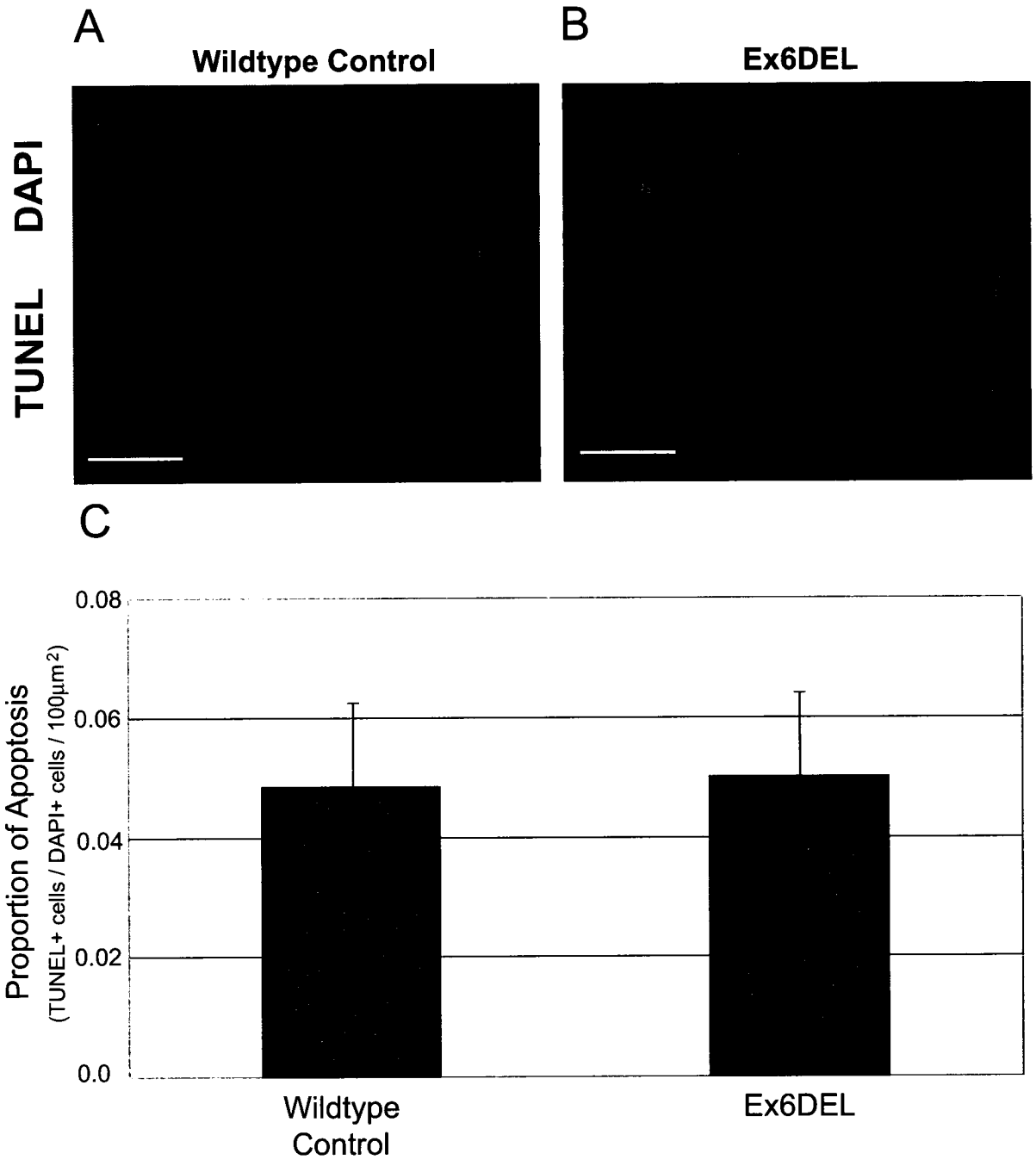
A
Wildtype Control
B
Ex6DEL
DAPI
TUNEL
C
Proportion of Apoptosis
(TUNEL+ cells / DAPI+ cells / 100µm²)
0.08
0.06
0.04
0.02
0.0
Wildtype Control
Ex6DEL

Figure 26 – The BrdU labelling index of newly born cortical cells is not increased.

Immunohistochemistry for BrdU (green) in 3 hour (2x1.5) pulse-labelled E15.5 embryos of [A]wildtype (WT) and [B] Ex6DEL sections (coronal, 12 μm) through the developing neocortex (upper panels). The cortical plate (cp), intermediate zone (iz), ventricular zone (vz) and lateral ventricle (lv) are labelled. The white dashed boxes are representative of the magnified regions (lower panel) depicting BrdU staining in the ventricular and intermediate zones (VZ → IZ), marked by the dashed yellow line, were used for counting the proportion of BrdU labelled cells. White scale bar = 16 μm. [C] Graph depicting of the BrdU labelling index (proportion of BrdU+ cells counterstained with DAPI (not shown), (N = 4), error bars represent SEM.

The larger number of BrdU positive cells in the "proliferative" ventricular zone coupled with the *in situ* gene expression analysis of neuroprogenitor markers suggested that there may be a larger pool of neuroprogenitors. To assess this possibility mitotic cells were quantified. E15.5 brain sections were labeled with an antibody directed against the M-phase marker phospho-Histone 3 [PH3] [119, 120] (see Figure 27ab). The number of PH3 positive cells along the boundary of the lateral ventricle and ventricular zone were quantified as a proportion of the total number of DAPI positive cells (Apical Layer, Figure 27c). There was a 2.7-fold increase in the Ex6DEL tissue (0.548 ± 0.001 vs 0.203 ± 0.002 per 120 μm (width), respectively; n = 3). The number of PH3 positive cells to the number of DAPI cells in the VZ, remained constant at 2.9-fold ($0.118 \pm 7.9\text{x}10^{-5}$ vs 0.040 ± 0.002 per 120 μm^2, respectively; n = 3). These results suggest that while S-phase may not be affected the proportion of mitotic cells is increased. Furthermore, there was an observed increase of mitotic cells along the subplate (not quantified), which forms the boundary between the cortical plate and intermediate zone (Figure 27ab, demarked by the dashed line). This suggested that there was also an in increase and secondary division, observed during cortical genesis in the Ex6DEL mice.

3.6.2 Neuroprogenitor expansion as a result of increased symmetric division during embryonic neocortical development.

The initial observation of hypercellularity in the cortex was evaluated by counting the number of DAPI+ cells on a layer-by-layer basis. In order to further assess how many cortical cells are born at any given time BrdU birthdating experiments were employed.

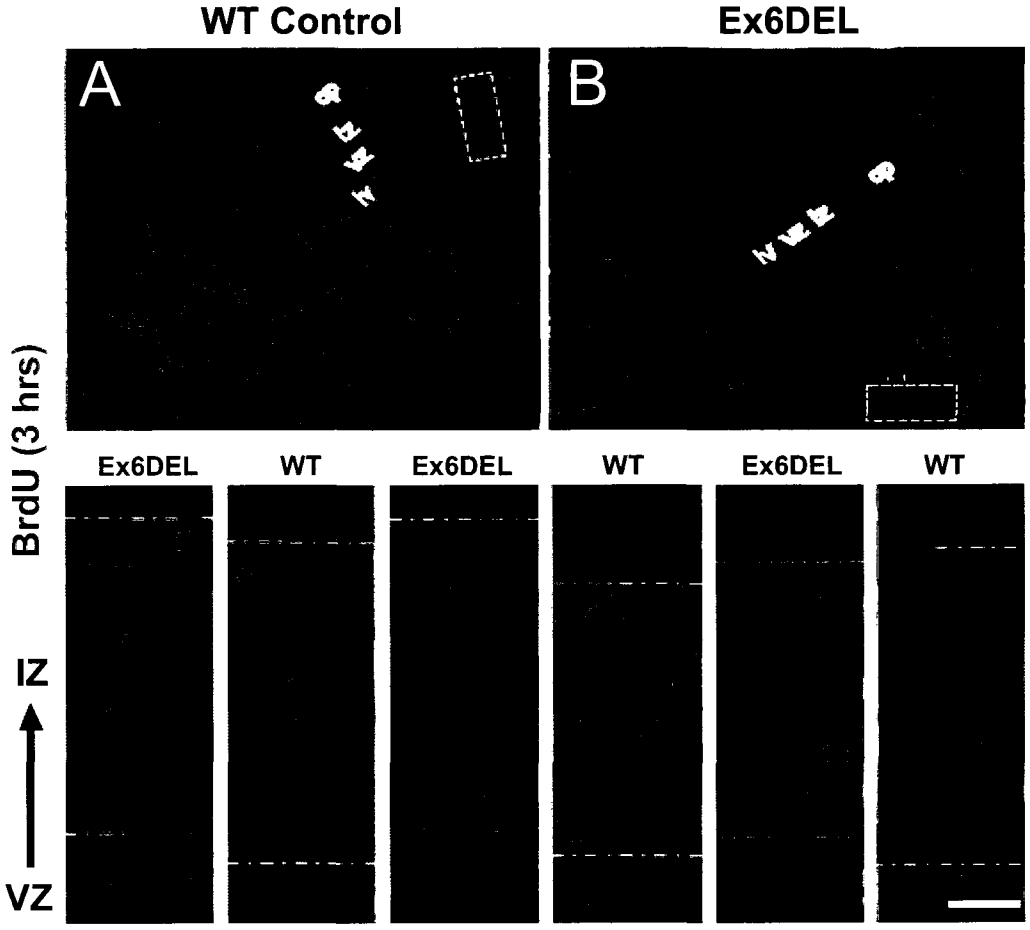
WT Control
Ex6DEL
A
B
BrdU (3 hrs)
Ex6DEL
WT
Ex6DEL
WT
Ex6DEL
WT
IZ
VZ

C

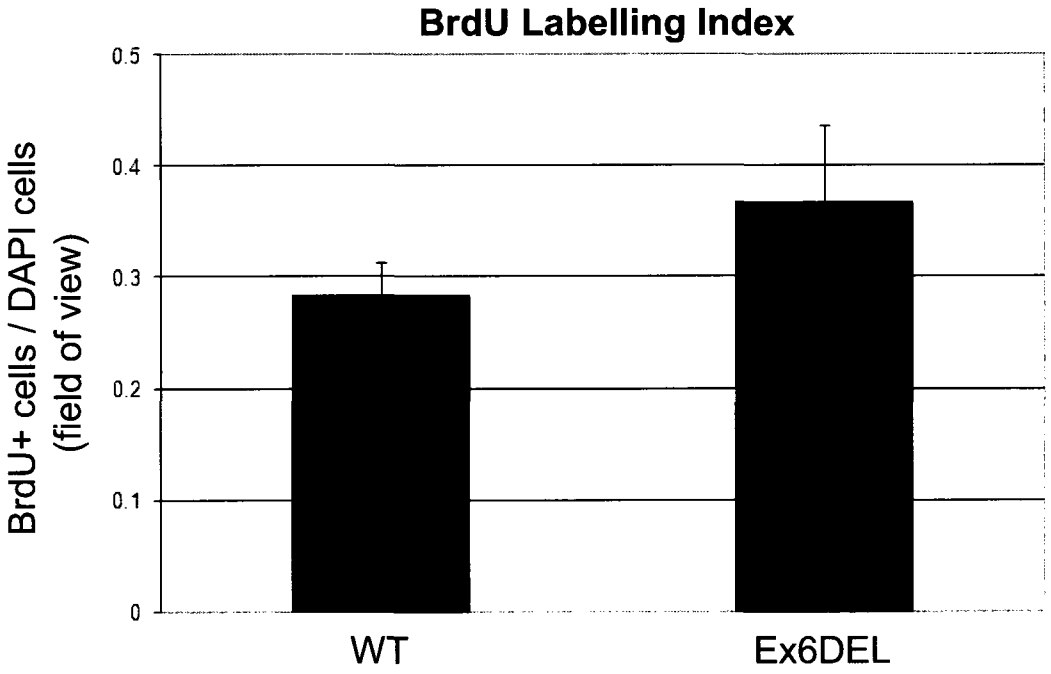
BrdU Labelling Index
BrdU+ cells / DAPI cells
(field of view)
0.5
0.4
0.3
0.2
0.1
0
WT
Ex6DEL

Figure 27 – Hypercellularity in Ex6DEL cortices is the result of heightened proliferation of progenitor cells during neocortical development.

Triple immunofluorescence images of E15.5 embryonic cortex sections (coronal, 10 μm) for the mitotic cell marker Phospho-histone H3 (green) and the early neuronal specific β-III Tubulin (also known as Tuj, red) demonstrate an increase in mitotic cells along the apical boundary of the ventricular zone of wildtype Control [A] and Ex6DEL [B] cortices. Nuclei are counterstained for DAPI (blue). An increase in the number of mitotic cells is also observed at the subplate, a region denoted by the boundary between TUJ positive and TUJ negative stained cells (marked by three dashed lines, incorporating a 30 μm width). Scale bar; 30 μm. [C] and [D] represent magnifications of the 125 μm^2 area used for quantification of cells, denoted by dashed white boxes in A and B. [E] A graph showing the mitotic index (proportion of phospho-histone H3 positive cells to DAPI) within the ventricular zone (125 μm^2) of wildtype control (grey bars) and Ex6DEL (black bars) male animals (*, P-value >0.05; N = 3 biological replicates, error bars represent SEM).

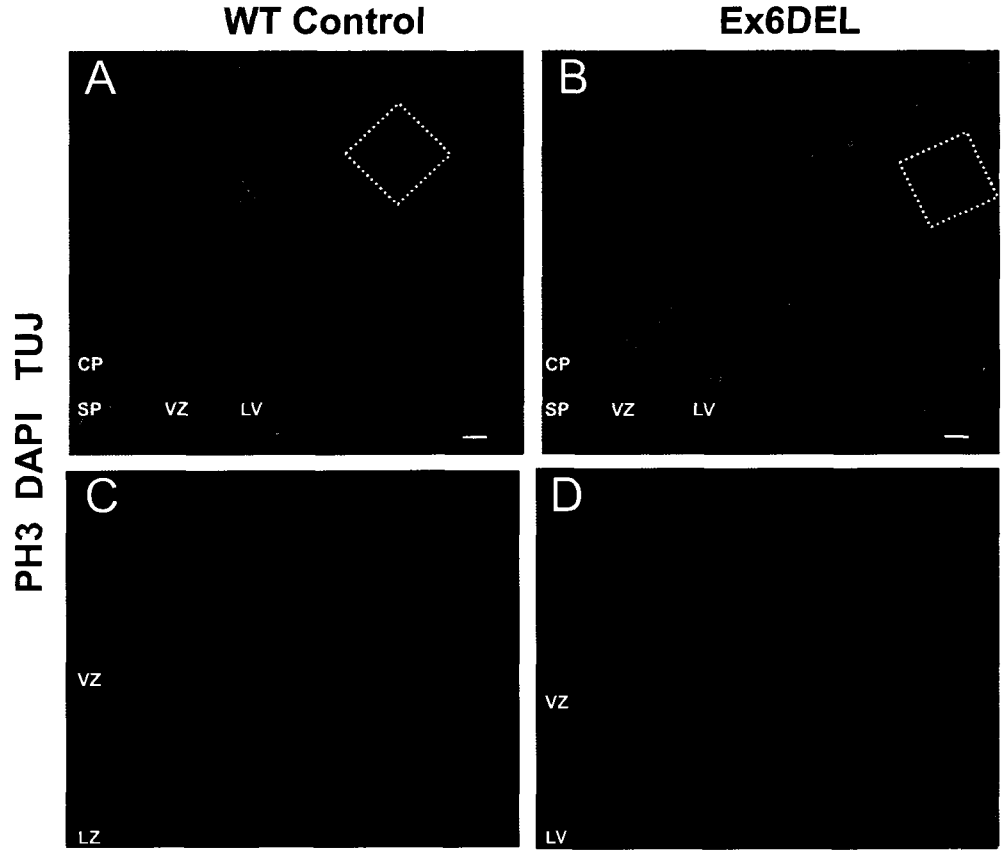
WT Control
Ex6DEL
A
B
C
D
CP
SP
VZ
LV
LZ
PH3 DAPI TUJ

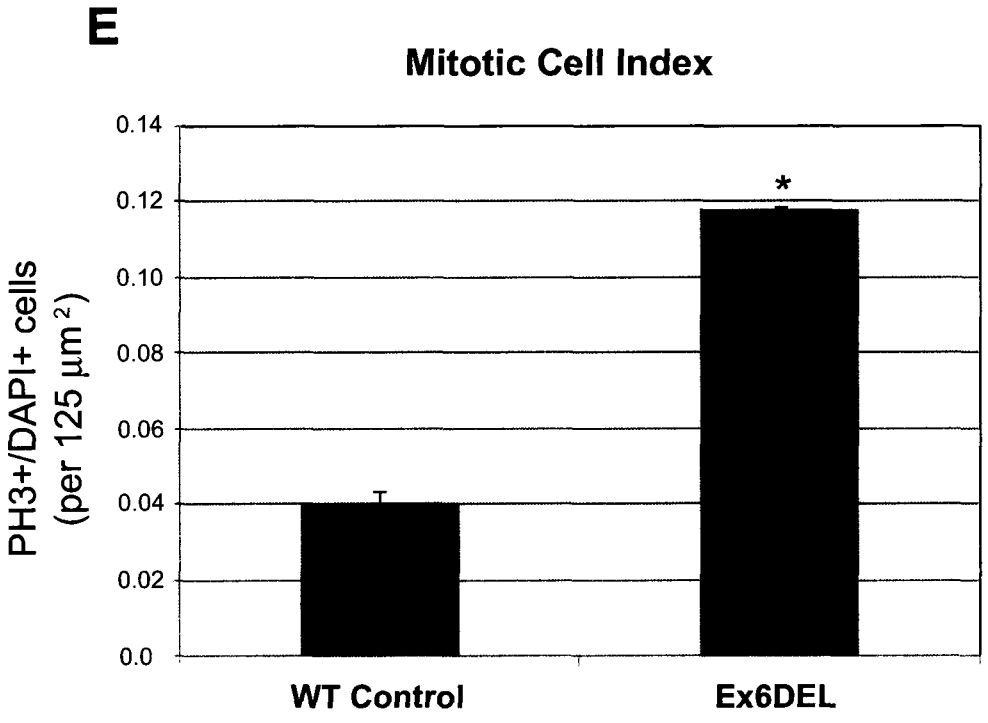
E
Mitotic Cell Index
PH3+/DAPI+ cells
(per 125 µm²)
0.14
0.12
0.10
0.08
0.06
0.04
0.02
0.0
*
WT Control
Ex6DEL

Pregnant females carrying wildtype Snf2l and Ex6DEL embryos were injected with BrdU at E13.5 of gestation. Embryos were allowed to reach full term and pups were harvested at one week of age (P7.5), when the cortical stratification is complete [49, 53, 55]. Ex6DEL mutant and control littermates were assayed for BrdU incorporation in the cortex by immunohistochemistry (Figure 28). A 2-fold increase in the proportion of total BrdU positive cells (green) compared to wildtype littermates was observed. Quantification of fluorescence distinguished two patterns of BrdU staining, densely stained BrdU positive cells (Figure 28cd, yellow arrows), corresponding to cells containing a high amount of BrdU incorporation, and lightly stained or faint BrdU positive cells (Figure 28cd, white arrows) representing those with lower amounts of BrdU. The density of BrdU represents the relative number of divisions since the time of injection at E13.5, where the level of incorporated BrdU is directly proportional to the number of cortical progenitors divisions [43]. We observed a reduced proportion of densely labelled cells in the Ex6DEL cortical layers (0.053 ± 0.007 per 150 μm^2, $n = 3$) compared to the WT (0.126 ± 0.013 per 150 μm^2, $n = 3$), representing a 2.4-fold increase (Figure 28f) and suggesting that fewer cells exited the cell cycle following pulse-labelling. Consistent with this finding there were more faintly labelled cells in the Ex6DEL samples suggesting that many cells labelled during the BrdU pulse underwent additional rounds of proliferation. These additional rounds of proliferation are limited to only a few extra rounds and do not totally dilute the BrdU label and as such a larger proportion (0.396 ± 0.005 per 150 μm^2, $n = 3$) of lightly stained BrdU positive cells where observed in the Ex6DEL tissue compared to the wildtype sample (0.097 ± 0.006 per 150 μm^2, $n = 3$), representing a 4.1-fold increase.

Figure 28 – BrdU birthdating of E13.5 born neurons shows increased proliferation.

Ex6DEL progenitor cells born at embryonic day E13.5 are far more abundant in the superficial cortical strata than are observed in the wildtype cortex (Control). E13.5 pregnant dams were pulse labelled with BrdU, and the resulting pups were sacrificed at postnatal day 7.5. More BrdU labelled cells (green) have migrated into the superficial cortical layers in the Ex6DEL [B] mice than in the controls [A]. DAPI (blue) was used as a counter stain for nuclei. Bottom panels [C, D] are magnified regions depicting the different staining patterns, dense (yellow arrows) and faint (white arrows). lv – lateral ventricle, svz – subventricular zone, iz – intermediate zone, ps – pial surface, and the distinct cortical layers, mz (marginal zone, Layer I) and II-IV. Yellow scale bars: 60 μm. [E] A photograph of a 12 μm coronal brain section at approximately -2.46 mm Bregma from wildtype mouse stained with Cresyl violet depicting the typical region of the lateral cortex used in [A] and for BrdU positive cell quantification (dashed box). [F] A graphical representation of the proportion of BrdU+ staining cells to DAPI in coronal sections (120 μm) of the lateral cortex. There is a higher proportion of BrdU+ cells (total) in the Ex6DEL cortex (black bars) compared to control (gray bars) suggesting an increased proliferation of progenitors at E13.5. An increase in the proportion of Faint stained BrdU+ cells (yellow arrows in C and D) suggests that the Ex6DEL progenitors undergo consecutive rounds of proliferation, thereby diluting the incorporated BrdU. A concomitant decrease in the proportion of Dense BrdU+ cells (white arrows in C and D) is also suggestive of an increase in progenitor proliferation. (* P-value < 0.05; $N = 3$ biological replicates, several sections were assayed).

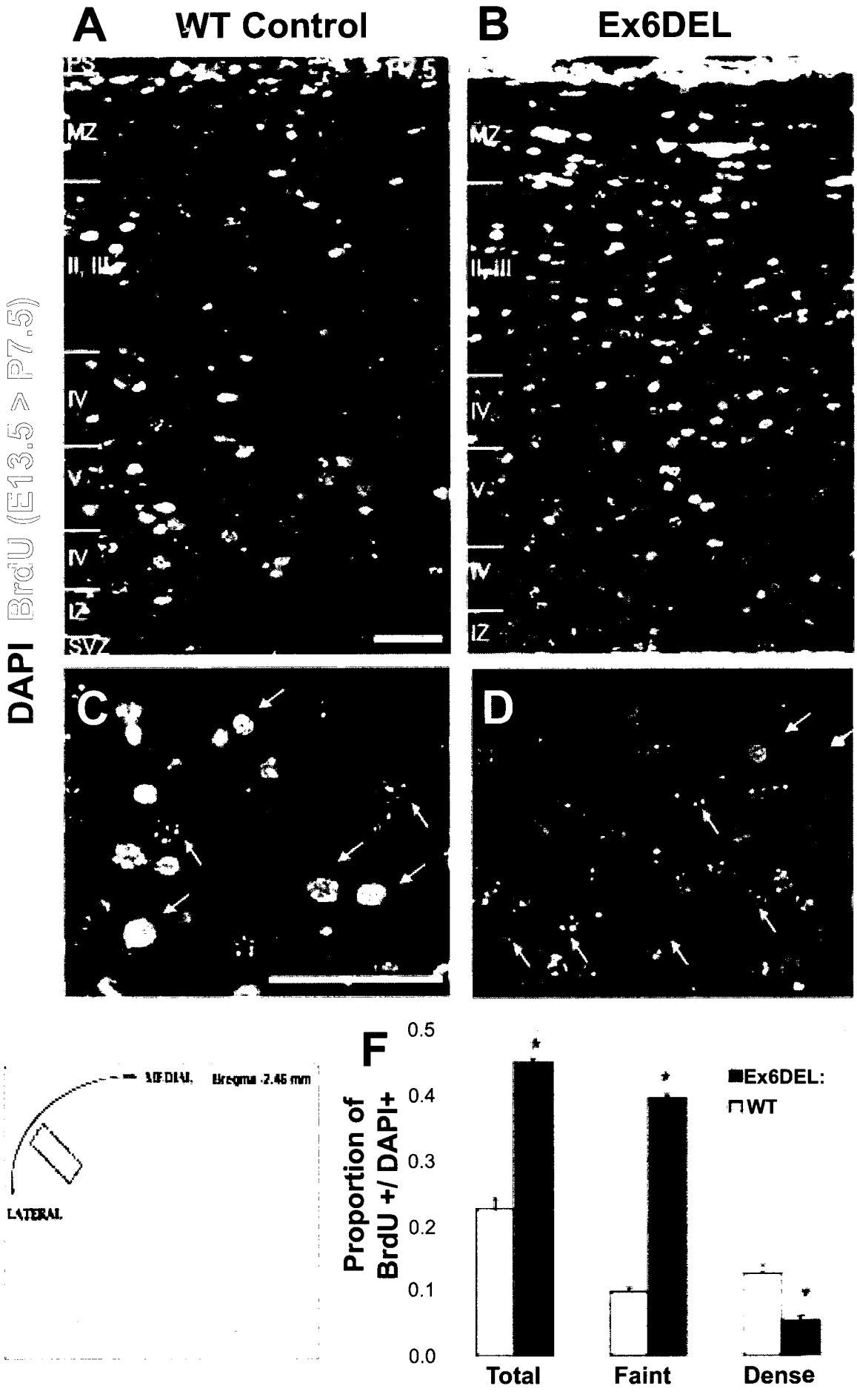
A
WT Control
B
Ex6DEL
DAPI BrdU (E13.5 > P7.5)
PS
P7.5
MZ
II, III
IV
V
IV
IZ
SVZ
C
D
E
Bregma -2.46 mm
LATERAL
F
Proportion of BrdU +/ DAPI+
0.5
0.4
0.3
0.2
0.1
0.0
Ex6DEL:
WT
Total
Faint
Dense

3.6.3 A heightened incidence of cell cycle re-entry results in neuroprogenitor expansion within Ex6DEL cortices.

In order to further assess the potential cell cycle re-entry of Ex6DEL neuroprogenitors the proportion of cells which had exited the cell cycle 24 hours following BrdU labelling was calculated. The E12.5-E13.5 interval was chosen because during normal mouse cortical development there is a well-documented rapid increase in the production of committed neurons; it is the initiation of cortical migration for layer V and layers I and VI are already well formed in the cortical plate [49, 53]. Ex6DEL mutant and control embryo-littermates were assayed for BrdU incorporation in the embryonic developing neocortex. The proportion of cells re-entering the cell cycle can be assessed by co-staining with BrdU (red) and Ki67 (green), a second nuclear marker of proliferation [289] (Figure 29 ab). The cells that have exited the cell cycle (BrdU+ and Ki67-, red), are more numerous in the Ex6DEL cortices compared to wild type mice. However, when expressed as a proportion of total BrdU positive cells a slight decrease in cell cycle withdrawal, or cell cycle exit, in the Ex6DEL cortices was noted (Figure 29 c). The subsets of BrdU-labelled neuroprogenitors that are in cycle are all Ki67+ (green fluorescing), whereas cells re-entering the cell cycle are represented as the BrdU+ and Ki67+ fraction (yellow, depicted by white arrows and arrow heads, Figure 29 ab). Similar to the PH3 stained cells in Figure 27, a higher concentration of double labelled cells in the ependymus (white arrows) and subplate (white arrowheads) regions of Ex6DEL cortices was noted, further signifying a heightened secondary cell cycle re-entry at both mitotic regions. Indeed the proportion of cells that re-entered the cell cycle (BrdU+ and Ki67+ / BrdU+) in the mutant mice displays a 4-fold increase over control littermates (0.334 ± 0.046 vs 0.094 ± 0.008 per 100 μm^2, respectively; n = 3, Figure 29d). These data suggest the root cause of

Figure 29 – Increased cell number in the developing neocortex, resulting from an expansion within the proliferating progenitor pool.

To further analyze the potential increase in progenitor proliferation we assessed the cycling progenitors for the ability to re-enter the cell cycle. E12.5 Wildtype [A] and Ex6DEL [B] embryos were pulse labelled with BrdU to label S-phase cells. At E13.5 frozen cortical sections (10μm) were double labelled for BrdU (red) and a second S-Phase marker Ki67 (green). Cells that have re-entered the cell cycle are positive for both BrdU and Ki67 and appear yellow (white arrows, along the ependymal layer and arrow heads at the subplate). Yellow scale bar = 20 μm. [C] A graphical representation of the relative proportion of cells that exit the cell cycle (BrdU+ Ki67- (red only) / total BrdU+ cells) shows that a there is no difference in the proportion of BrdU+ cells that exit the cell cycle between the control and Ex6DEL animal cortices. [D] However a higher proportion of BrdU+ progenitors choose to re-enter the cell cycle (BrdU+ Ki67+ (yellow) / total BrdU+) representing a 3.5-fold increase. Interestingly in the Ex6DEL cortex there was an increase in BrdU+ Ki67+ double-labelled cells (re-entered) that arise at the subplate (white arrowheads, d) as well at the ependymal layer (white arrows, d) suggesting an accompanying increase in secondary divisions. Sample size, n = 3.

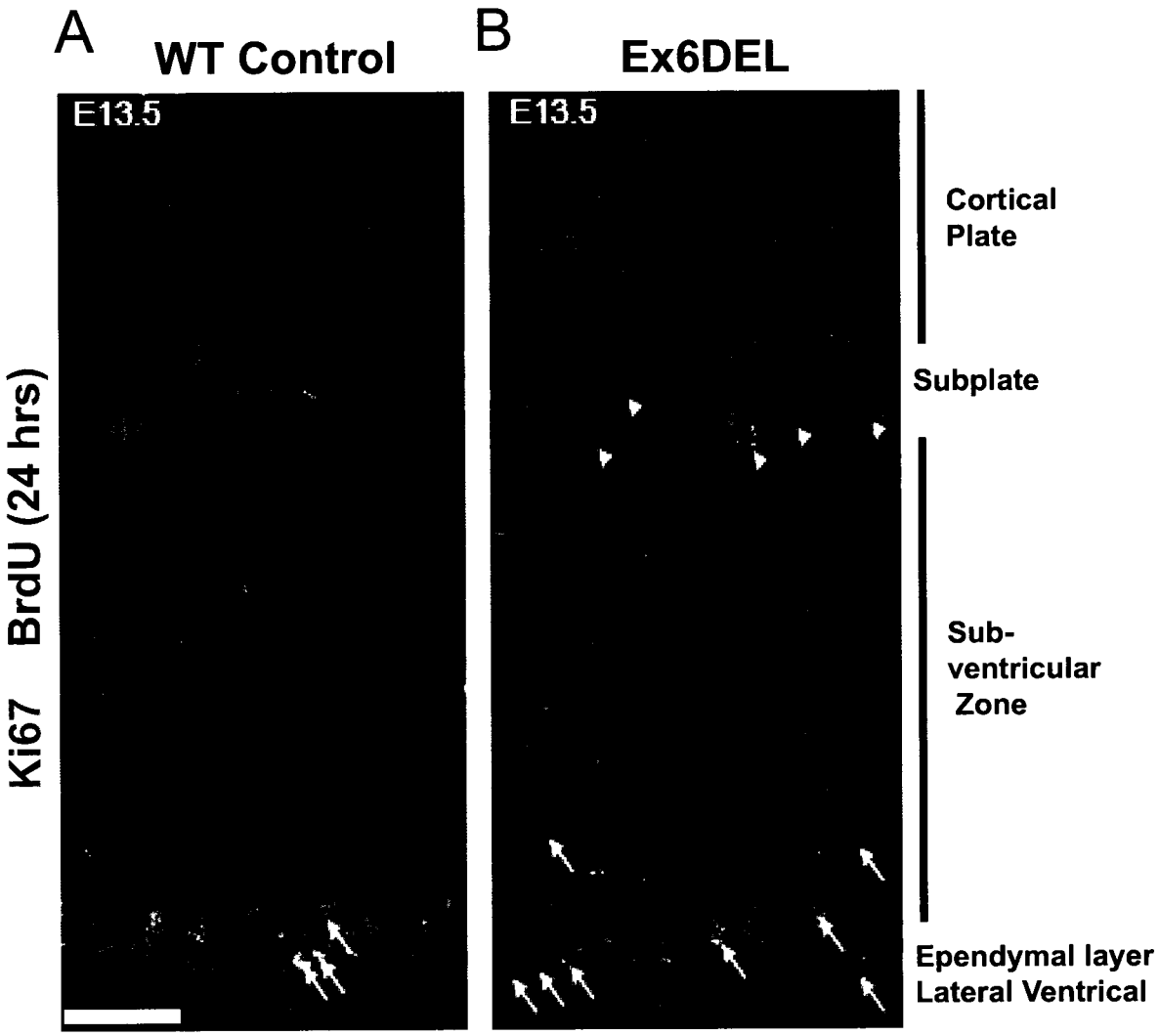
A
WT Control
B
Ex6DEL
E13.5
E13.5
Ki67 BrdU (24 hrs)
Cortical Plate
Subplate
Sub-ventricular Zone
Ependymal layer Lateral Ventrical

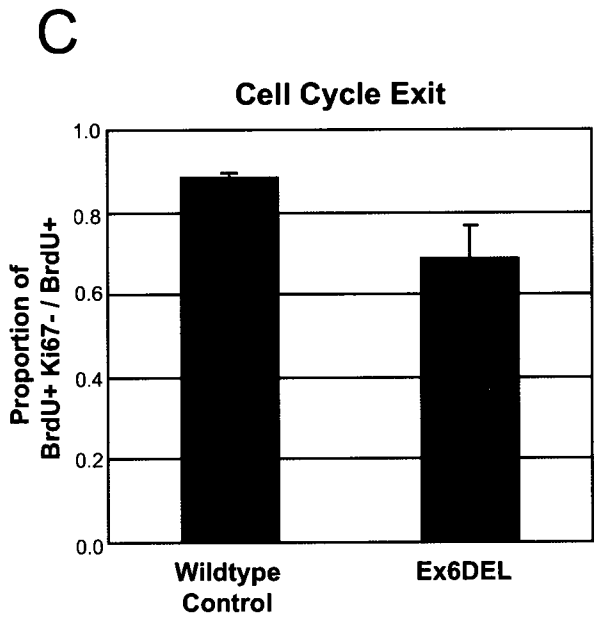
C
Cell Cycle Exit
Proportion of BrdU+ Ki67- / BrdU+
1.0
0.8
0.6
0.4
0.2
0.0
Wildtype Control
Ex6DEL

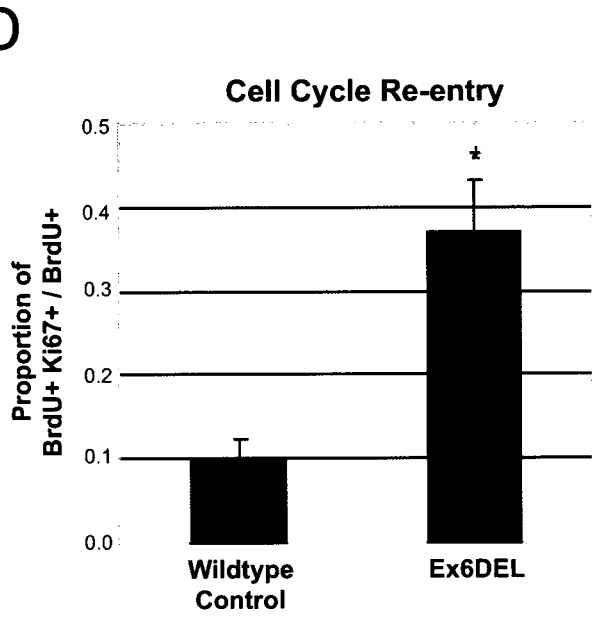
D
Cell Cycle Re-entry
Proportion of BrdU+ Ki67+ / BrdU+
0.5
0.4
0.3
0.2
0.1
0.0
*
Wildtype Control
Ex6DEL

hypercellularity in the developing cortex of the Ex6DEL mice is that a higher proportion of neuroprogenitors in the mutant mice are failing to commit to differentiation and are re-entering the proliferative pool to derive more neuroprogenitors.

3.6.4 Increased symmetric and asymmetric orientation of divisions is observed within the neuroprogenitor pool of Ex6DEL cortices.

The orientation of division can be used as an indicator of the type of division (discussed in Introduction section 1.1.3). γ-tubulin staining can be used to identify the orientation of division. In order to further identify populations of dividing neuroprogenitors, both the ventricular zone (VZ, which contains neuroepithelal, and radial glial progenitors) and the Intermediate Progenitor cell Layer (IPL), which contain intermediate/basal progenitors), were delineated by β-III-tubulin staining (also known as Tuj) in Figure 30ab. The boundary between Tuj positive (red) and negative (blue) cells represents a clear divide between the VZ and IPL, the very edge of the cortical plate representing the uppermost limit of the IPL. γ-tubulin stains the mitotic spindle fibres, these fibres being the key components of the centrioles, are concentrated, and segregate to the poles of the dividing cell at either end across the axis of division. Sections (100 μm, width) through the cortices of Ex6DEL and Wildtype mice were stained for γ-tubulin (green) and positive cells were quantified from within the VZ and IPL (Figure 30 ab). Comparing asymmetric and symmetric oriented cells by the alignment of γ-tubulin positive cells (axis of division) to the lateral apical plane of the ventricular zone, the relative orientation of division can be assessed (examples are shown, Figure 30 ab, magnifications). In both VZ and IPL the number of asymmetric and symmetric divisions was greater in the

Figure 30 – A selective increase in symmetric orientated division of progenitor cells from the subventricular zone and intermediate progenitor layer results in expansion of the proliferative pool.

In order to clearly identify asymmetric mitotic events (yellow arrows) from symmetric divisions (white arrows), E13.5 cortical sections (10 μm) from Wildtype [A] and Ex6DEL [B] cortices were double labelled for γ-tubulin (green), β-III-tubulin (red) and nuclei were counterstained with DAPI (blue). γ-tubulin stains the mitotic spindle fibers which segregate at either pole in dividing M-phase cells making it possible to distinguish the axis of division. Below are magnifications from within the IPL and VZ depicting orientation of division (white line). CP = cortical plate, IPL = intermediate progenitor layer (including the intermediate zone and subplate region), SVZ = subventricular zone. Scale bars = 100 μm. [C] A graphical representation of the relative proportion of asymmetric divisions (divisions along the axis of migration) in 100 μm sections of WT (grey bars) and Ex6DEL (black bars) cortices. There are more asymmetric divisions in the SVZ, but not in the IPL of the Ex6DEL mice. [D] A graphical representation of the relative proportion symmetric divisions (perpendicular to the axis of migration) in 100 μm sections of WT (grey bars) and Ex6DEL (black bars) cortices. There are more symmetric divisions in the SVZ and IPL of the Ex6DEL mice. [E] A graphical representation of the number of nuclei counted in the 100 μm sections of cortical plate of WT (grey bars) and Ex6DEL (black bars) E13.5 embryonic tissue. There are more nuclei in the VZ and of the Ex6DEL mice. (* indicates P-values > 0.05, n=4 biological replicates). Error bars represent SEM.

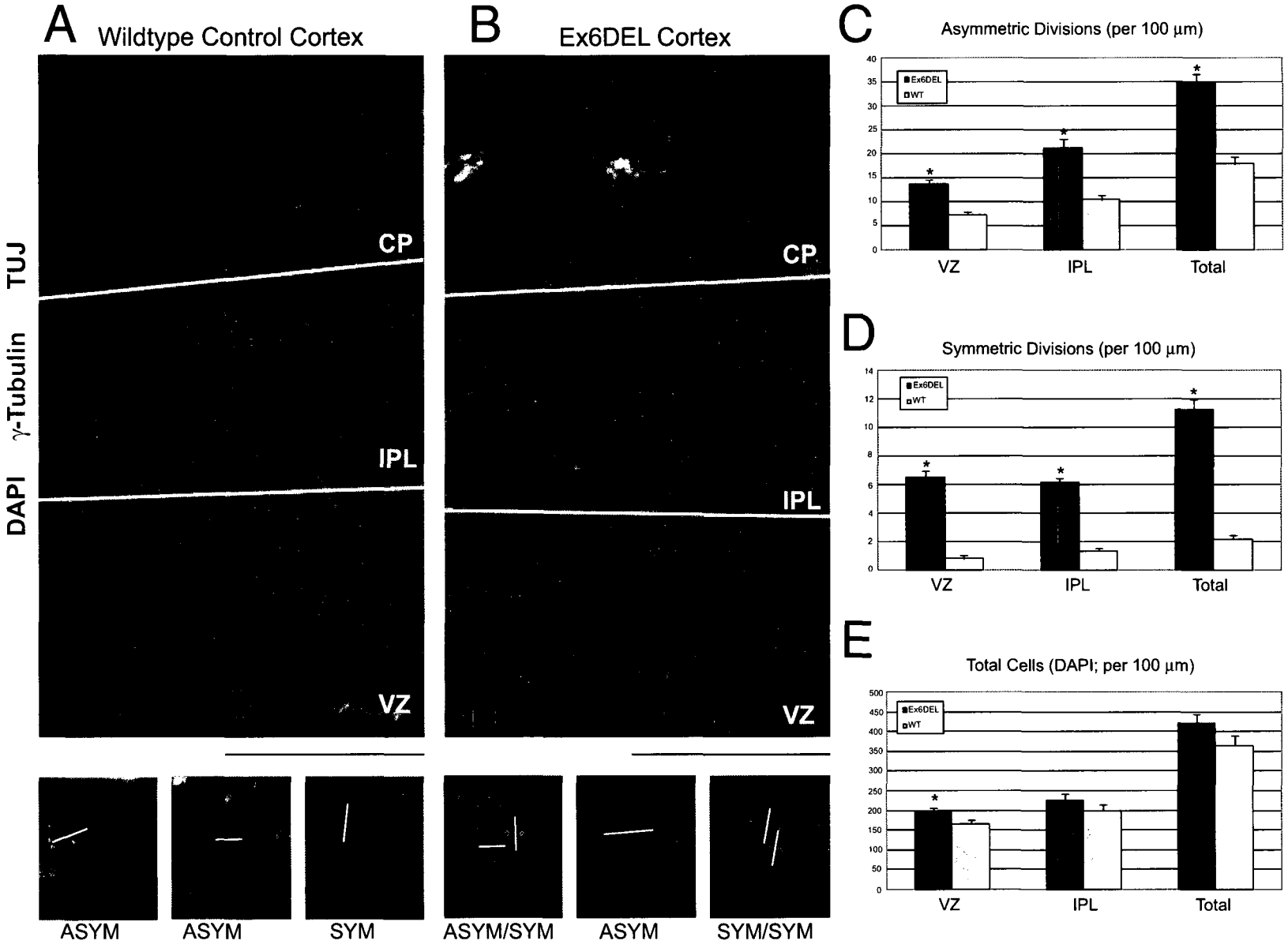
A
Wildtype Control Cortex
B
Ex6DEL Cortex
TUJ
γ-Tubulin
DAPI
CP
IPL
VZ
CP
IPL
VZ
ASYM
ASYM
SYM
ASYM/SYM
ASYM
SYM/SYM
C
Asymmetric Divisions (per 100 μm)
Ex6DEL
WT
VZ
IPL
Total
D
Symmetric Divisions (per 100 μm)
Ex6DEL
WT
VZ
IPL
Total
E
Total Cells (DAPI; per 100 μm)
Ex6DEL
WT
VZ
IPL
Total

Ex6DEL cortices than are observed in the Wildtype tissues. There are 2-fold more asymmetric divisions (perpendicular to the apical plane) and a 4-fold increase in symmetric divisions (parallel to the apical plane) in the Ex6DEL cortices (Figure 30 cd).

3.7 *Foxg1* is a Snf2l target gene.

3.7.1 Potential regulation of neurogenic and cell cycle factors by Snf2l.

To further examine the mechanism underlying the observed cell cycle re-entry phenotype in Ex6DEL mice, a global gene expression analysis was performed. Cortical RNA isolated from E15.5 wildtype and Ex6DEL animals were analysed by microarray (MEEBO - **M**ouse **E**xonic **E**vidence **B**ased **Oligo,** an open-source long (70-mer) oligo set to represent the mouse genome [290]). This analysis demonstrated altered expression (≥2-fold) of 256 genes (183 decreased and 73 increased) including numerous genes encoding neurogenic transcription factors (refer to **APPENDIX VI**, for raw microarray data, pp165). These results suggest that loss of Snf2l alters the neurogenic program perhaps by disrupting the regulation of cell cycle genes and neurogenic factors that affect the timing of differentiation. One of the genes identified by a decrease in expression was $p21^{Cip1}$ (*Cdkn1a*, 2.23-fold decrease, n = 3). In order to further examine cell cycle regulation qRT-PCR was used to analyze the cyclin dependant kinase inhibitors, $p16^{Ink4a}$, $p21^{Cip1}$, $p27^{Kip1}$,

Figure 31 – qRT-PCR analysis of RNA isolated from E15.5 cortices of WT and Ex6DEL mice.

Total RNA was extracted from E15.5 cortical dissections. qRT-PCR was used to analyze the expression of the several targeted genes, including cyclin dependant kinase inhibitors ($p16^{ink4}$, $p21^{cip}$, $p27^{kip1}$, $p57^{kip2}$)and *Cyclinb2* and *Cyclind1* (Cell Cycle Factors) [A]. Results indicate that $p16^{ink4}$, $p21^{cip}$ and $p27^{kip1}$ have decreased expression (fold-change compared to WT) while the $p57^{Kip2}$, *Cyclinb2* and *Cyclind1* were not changed compared to control values (1.0, red line). We also verified microarray data for a selection of misregulated genes (in graph [A] and [B]) confirming an upregulation of *foxg1*. (n=3-4, error bar represent SEM).

A

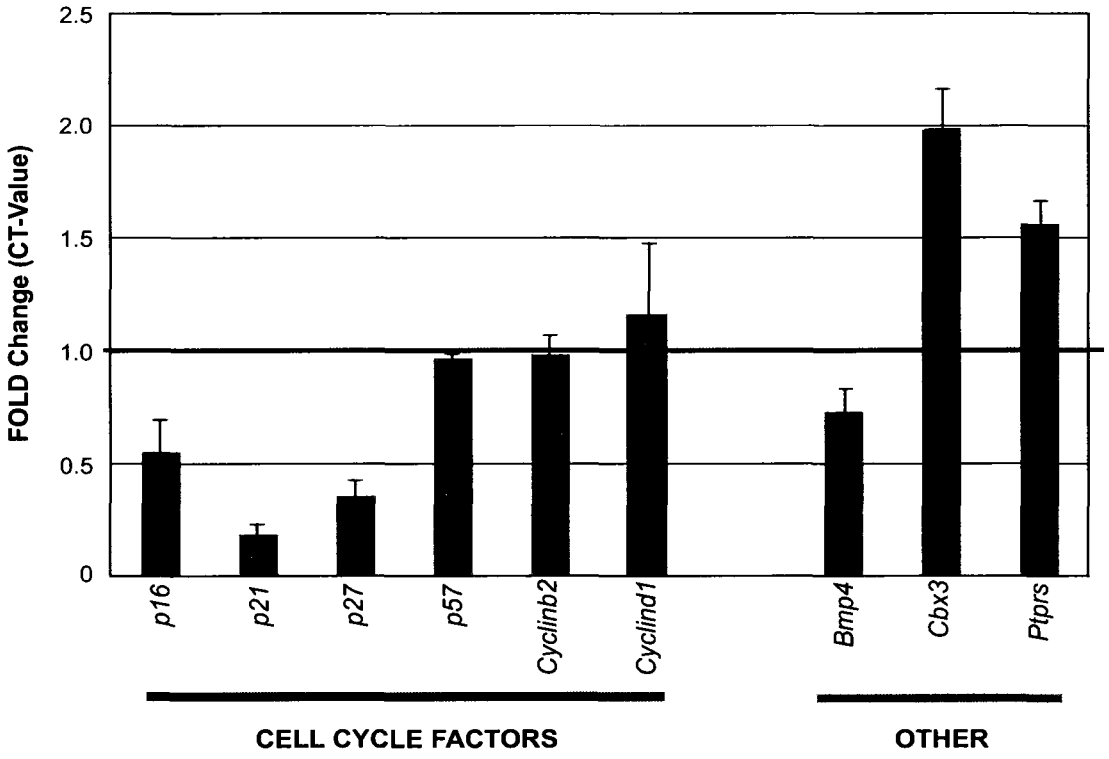
2.5
2.0
1.5
1.0
0.5
0
FOLD Change (CT-Value)
p16
p21
p27
p57
Cyclinb2
Cyclind1
Bmp4
Cbx3
Ptprs
CELL CYCLE FACTORS
OTHER

B

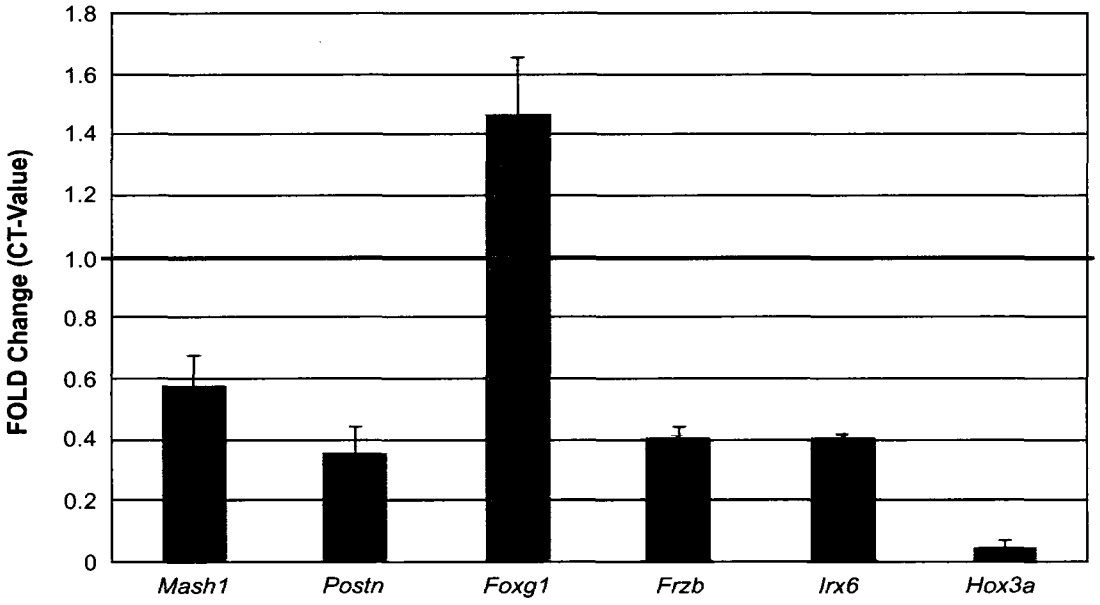
1.8
1.6
1.4
1.2
1.0
0.8
0.6
0.4
0.2
0
FOLD Change (CT-Value)
Mash1
Postn
Foxg1
Frzb
Irx6
Hox3a

and $p57^{Kip2}$. There was a noted decrease in all except for $p57^{Kip2}$, suggesting that some cell cycle regulators are misregulated (Figure 31a).

Several genes from the screen were validated by qRT-PCR, a selection of which is shown in Figure 31 ab. One gene, *Brain factor*-1 / *Foxg*1, a forkhead homeodomain transcription factor was identified as being the most highly upregulated gene by microarray (7.38-fold, **APPENDIX VI**, Table A, pp165), and validated to be 1.4-fold by qRT-PCR (Figure 31 b). *Foxg1 i*s of particular interest as it is expressed in intermediate progenitor cells of the developing forebrain [291]. Moreover, *Foxg1* has been implicated directly in the regulation of neuroprogenitor expansion by negatively regulating expression of $p21^{Cip1}$ and *Mash1*, two genes identified by the gene screen as down regulated in Ex6DEL tissue that are important for differentiation of neurons (Figure 31) [291, 292].

3.7.2 Snf2l binding to proximal *Foxg1* gene.

The *Foxg1* gene is composed of two exons (see Figure 32a), with highly conserved regions 2 kb upstream and 1.5 kb downstream. Chromatin immunoprecipitation (ChIP) was used to analyze the proximal promoter (~500 bp) and the first exon, encompassing the start of the ORF until the ATG start codon (Figure 32a). Using a panel of 5 primer sets, ChIP was performed on wildtype E15.5 cortices. ChIP results indicate binding of Snf2l to two regions of the proximal promoter (Figure 32b).

Figure 32 – Characterization of SNF2l binding to the *foxg1* gene.

[A] A schematic diagram showing *foxg1* gene structure. The gene is comprised of two exons. Location of primer sets used for qPCR following ChIP with Snf2l antibodies is shown. Predicted PCR product length is shown in brackets. The ORF (Black box), 5'UTR (grey box), 3' UTR (blue box), transcriptional start site (arrow) and translational start (ATG) are labelled. The PCR primer pair E, which shows the highest amplification following ChIP is shown in red. [B] A graph showing the relative fold-enrichment of Snf2l binding on the foxg1 gene using cortical samples for WT embryos (n= 4, error bar represent SEM).

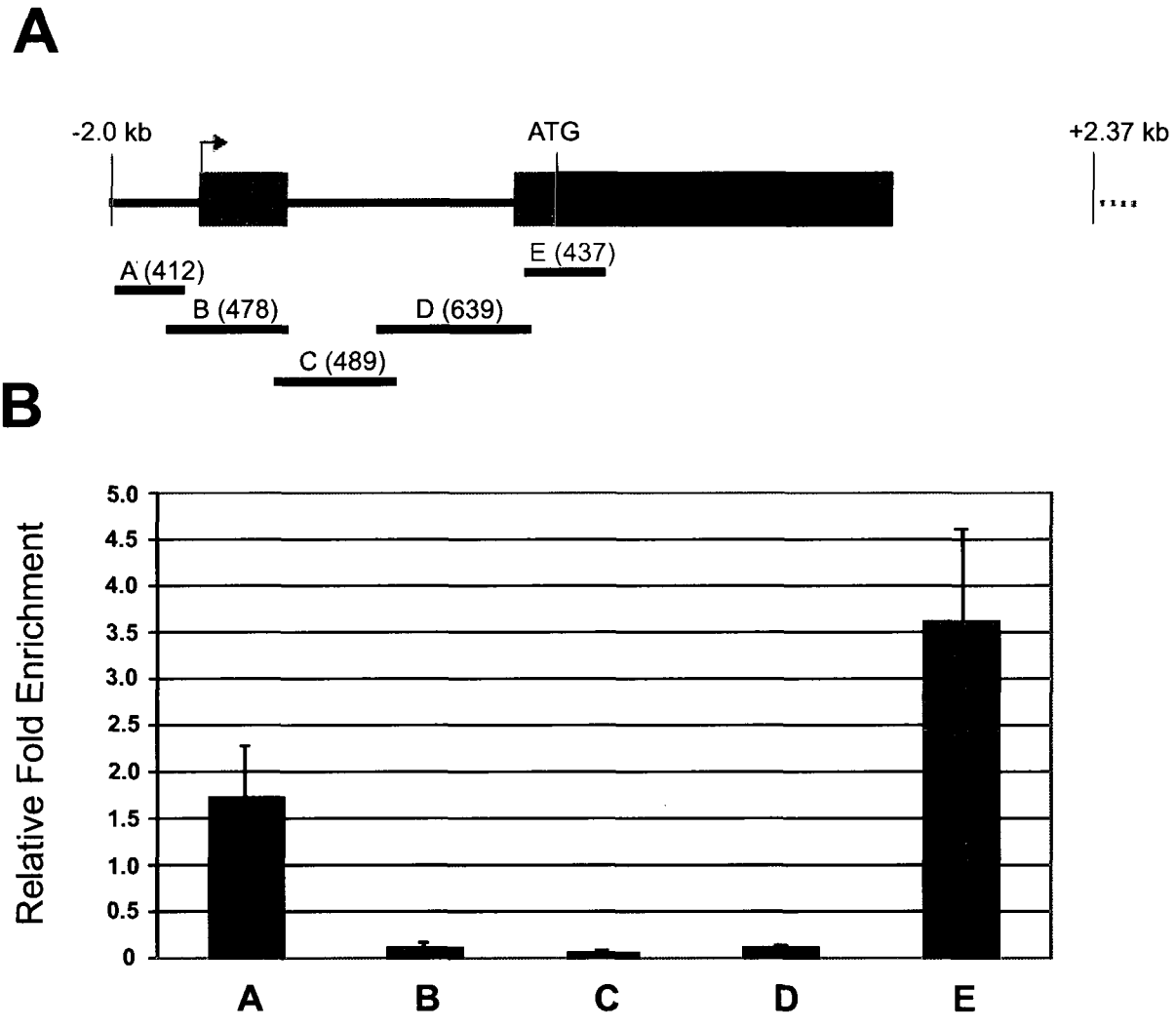
A
-2.0 kb
ATG
+2.37 kb
A (412)
B (478)
C (489)
D (639)
E (437)
B
Relative Fold Enrichment
5.0
4.5
4.0
3.5
3.0
2.5
2.0
1.5
1.0
0.5
0
A
B
C
D
E

Figure 33 – *Foxg1* expression in the developing neocortex

Coronal sections through the E15.5 cortex of *Snf2l* WT (A, B ((rostral cortical sections), C, D (caudal cortical sections)) and Ex6DEL (E, F (rostral cortical sections), G, H (caudal cortical sections)) embryos that are wildtype or heterozygous for *Foxg1* were analysed for expression of *Foxg1* by RNA *in situ* hybridization. Panel I represents a WT mouse sections stained with the Foxg1 antisense probe control. *In situ* analysis shows increased expression (purple) of *foxg1* in Ex6DEL tissue with an expected decrease in the *Foxg1* heterozygous cortices in both Snf2l WT and Ex6DEL cortices. The bottom box shows lack of staining using an antisense probe for hybridization. The red asterisks denote sectioning artefacts which appear densely stained. The lateral ventricle (lv), ventricular zone (vz) and cortical plate (cp) are labelled.

WT Control

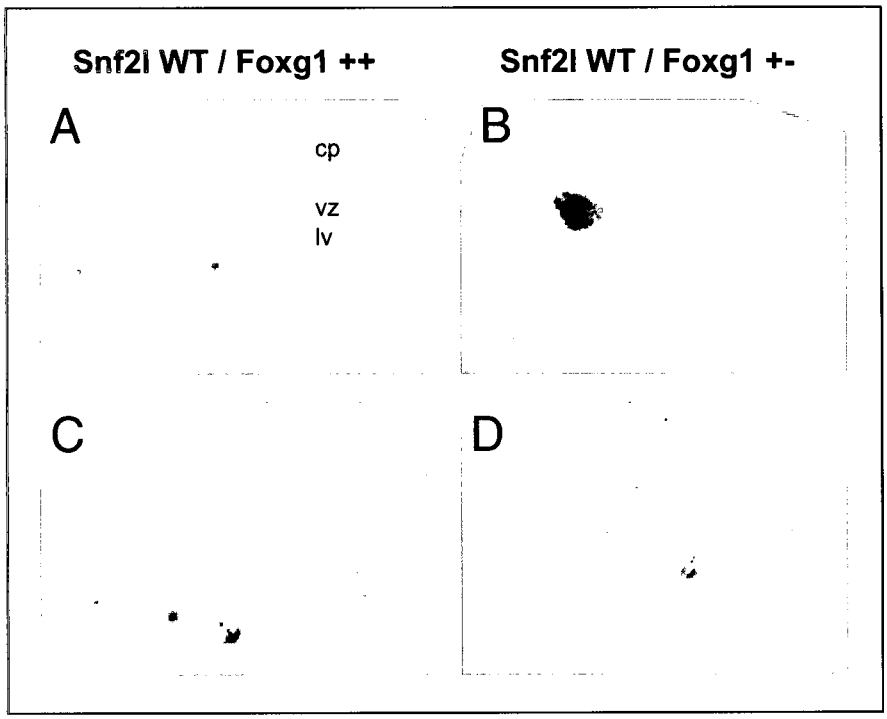

*sectioning artifact

I

foxg1 anitsense (control)

Ex6DEL

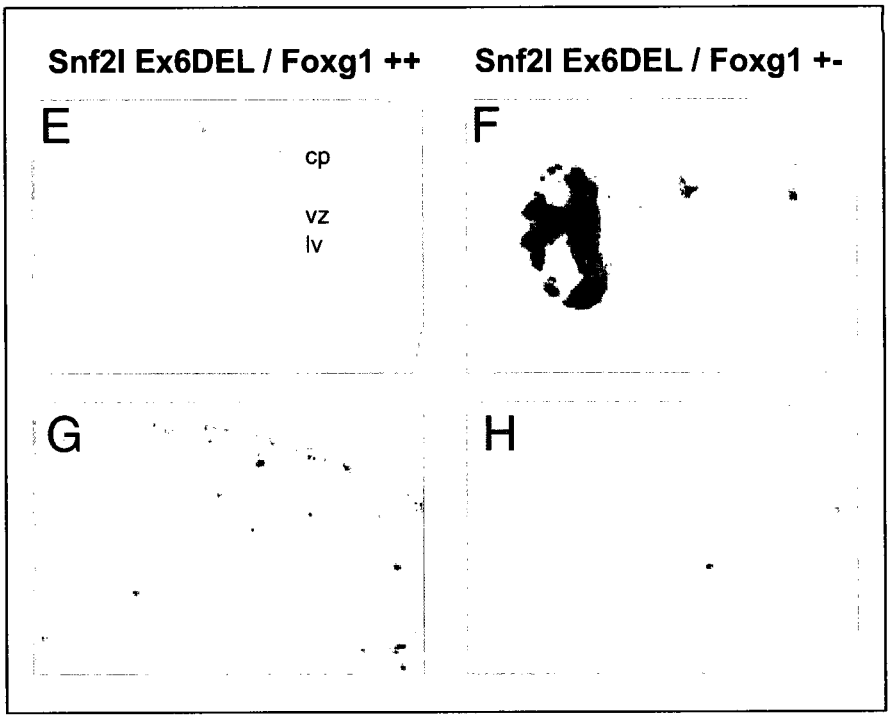

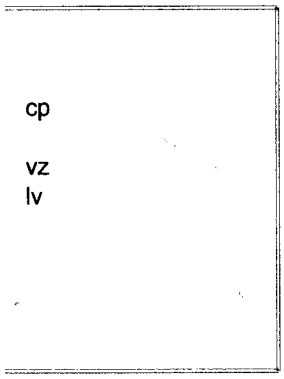

3.7.3 Reduction of Foxg1 message in Ex6DEL mice by gene dosage.

To determine the genetic contribution of *Foxg1* to the Ex6DEL phenotype, we bred a *Foxg1*-null allele onto the Ex6DEL line. Homozygous deletion of *Foxg1* results in embryonic lethality [293], but *Foxg1*$^{+/-}$ animals are viable [252]. Ex6DEL heterozygous females were bred to *Foxg1*$^{+/-}$ males in order to reduce *Foxg1* expression in the developing embryonic cortex. A primary assessment of *Foxg1* gene expression in E15.5 cortex was determined by *in situ* hybridization (Figure 33). As expected *Foxg1* was increased in the Ex6DEL mice over Snf2l wildtype (compare left box to right box). These results also confirmed that the removal of one *Foxg1* allele in the *Foxg1*$^{+/-}$ genotype did reduce transcript levels in both wildtype Snf2l and Ex6DEL backgrounds (compare *Snf2l* WT / *Foxg1*$^{+/+}$ (A,C) to *Snf2l* WT / *Foxg1*$^{+/-}$ (B,D) and *Ex6DEL* / *Foxg1*$^{+/+}$ (E,G) to *Ex6DEL* / *Foxg1*$^{+/-}$ (F,H)).

3.7.4 Rescue of Ex6DEL phenotype by limiting *Foxg1* dosage.

3.7.4.1 Reduced mitosis in Foxg1 heterozygous mice, rescues Ex6DEL mice.

There was a 2.7-fold increase in the proportion of PH3+ stained cells in the Ex6DEL cortex (Figure 27). It was anticipated that reducing Foxg1 dosage would rescue this phenotype to wildtype levels. Sections from *Snf2l* wildtype and *Ex6DEL* mice both wildtype or heterozygous for *Foxg1*, were stained for PH3 (green) and Tuj (red), as previously described, and the number of mitotic cells were quantified (Figure 34 a-d). There was a 3.1-Fold (n = 3) increase in the mitotic cell index in the ventricular zone of

Figure 34 – Animals heterozygous for Foxg1 rescue the observed increase in mitotic index.

Triple immunofluorescence images of E15.5 embryonic cortex sections (coronal, 10 μm) for the mitotic cell marker Phospho-histone H3 (green) and the early neuronal specific β-III Tubulin (also known as Tuj, red) demonstrate a partial rescue in the frequency of mitotic cells along the apical boundary of the ventricular zone of Control and Ex6DEL cortices. Nuclei were counterstained for DAPI (blue). The cortical plate (CP), subplate (SP), ventricular zone (VZ), apical boundary or ependymus (AP) and lateral ventricle (LV) are labelled. An increase in the number of mitotic cells at the subplate, and the ependymal layer is observed in the Ex6DEL cortex but this increase is partially rescued in the Ex6DEL Foxg1$^{+/-}$ animals. For comparison, Snf2l WT/Foxg1$^{+/+}$ [A], Snf2l/WT Foxg1$^{+/-}$ [B], Snf2l Ex6DEL/Foxg1$^{+/+}$ C] and Snf2l Ex6DEL/Foxg1$^{+/-}$ [D] are shown. Yellow scale bars represent 125 μm. [E] Graph showing the rescue of the mitotic index (proportion of phospho-histone H3 positive cells from DAPI) within the ventricular zone (125 μm^2) and [F] along the apical boundary (125 μm) of the ventricular zone and the lateral ventricle of wildtype and Ex6DEL male animals that are wildtype for foxg1 (+/+, black/blue bars) or heterozygous for foxg1 (+/-, grey/purple bars) (*, P-value >0.05; N = 3 biological replicates, error bars represent SEM).

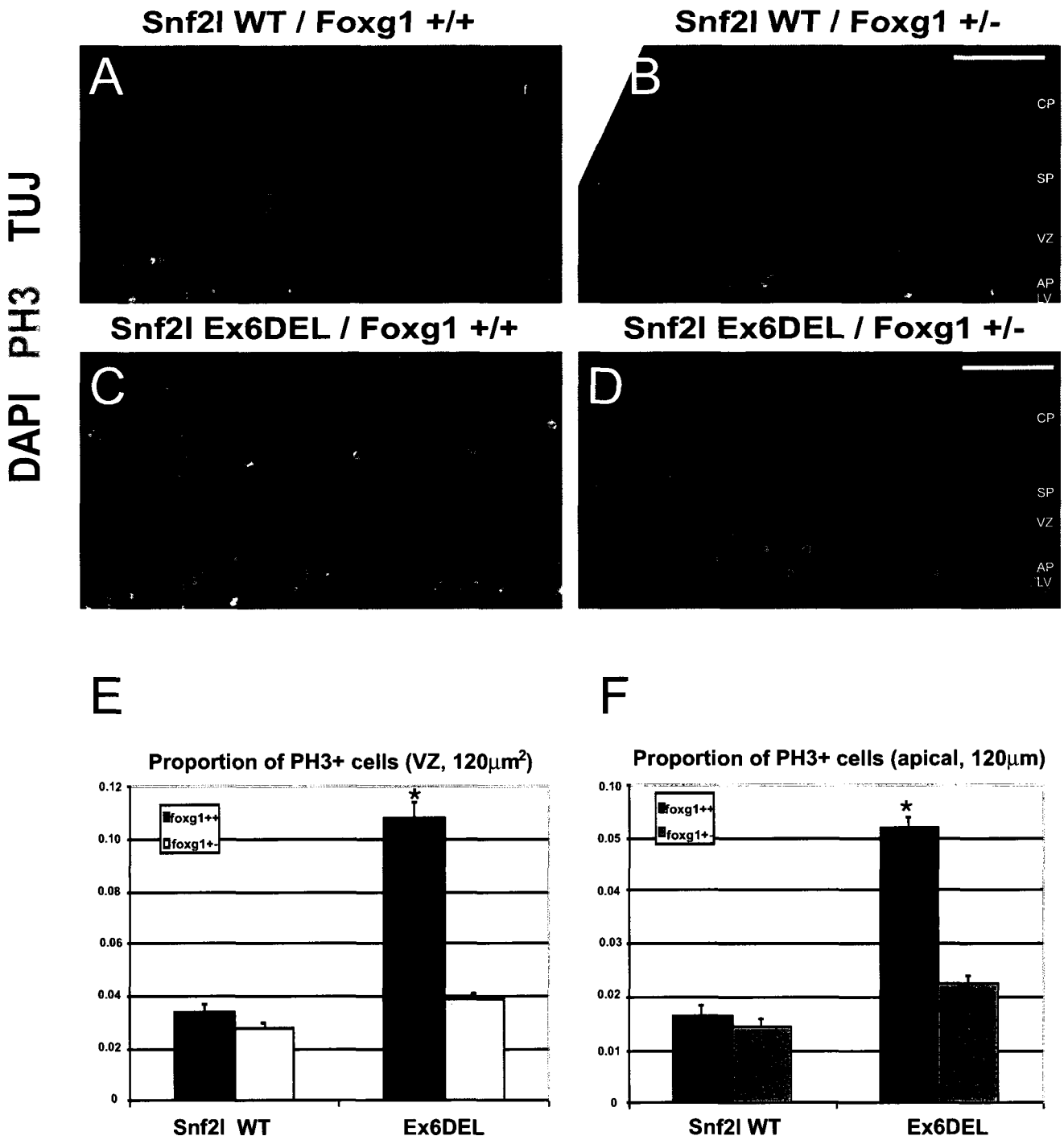
Snf2l WT / Foxg1 +/+
Snf2l WT / Foxg1 +/-
A
B
CP
SP
VZ
AP
LV
DAPI PH3 TUJ
Snf2l Ex6DEL / Foxg1 +/+
Snf2l Ex6DEL / Foxg1 +/-
C
D
CP
SP
VZ
AP
LV
E
Proportion of PH3+ cells (VZ, 120μm²)
foxg1++
foxg1+-
0.12
0.10
0.08
0.06
0.04
0.02
0
*
Snf2l WT
Ex6DEL
F
Proportion of PH3+ cells (apical, 120μm)
foxg1++
foxg1+-
0.10
0.05
0.04
0.03
0.02
0.01
0
*
Snf2l WT
Ex6DEL

Ex6DEL for Foxg1$^{+/+}$ samples (0.337 $\pm$ 0.003 vs. 0.107 $\pm$ 0.006 per 120 μm^2, Figure 34e). Confirming the previous observation where only the apically stained cells were tallied, there was a 3.2-fold increase in the mitotic cell index of apical layer in Ex6DEL mice (0.160 $\pm$ 0.021 vs. 0.520 $\pm$ 0.016 per 120 μm, Figure 34f). There was no change in the mitotic cell index between Snf2l wildtype that were either homozygous or heterozygous for *Foxg*1 in either VZ or Apical layer restricted counts (Figure 34 ef). However in Ex6DEL cortices, limiting *Foxg*1 levels rescued this phenotype (ventricular zone: 0.033 $\pm$ 0.004 vs. 0.039 $\pm$ 0.002 per 120 μm^2, apical layer: 0.166 $\pm$ 0.023 vs. 0.222 $\pm$ 0.002 per 120 μm) (Figure 34 ef). These results suggest that Foxg1 and Snf2l function within the same genetic pathway regulating neuroprogenitor expansion. Furthermore, the increase of mitotic cells along the subplate is also reduced by limiting *Foxg*1 dosage.

3.7.4.2 Reduced divisions in *Foxg1* heterozygous mice confer a partial rescue of symmetric and asymmetric divisions in the cortex of Ex6DEL mice.

Indirect fluorescence for γ-tubulin was again used to analyze the orientation of division in relation to the apical plane of the germinal neuroepithilium for *Snf2l* wildtype and *Ex6DEL* cortices that are either wildtype or heterozygous for *Foxg1* (Figure 35 a-d). As previously shown in Figure 30, the populations of asymmetric and symmetric dividing cells were increased in the ventricular zone (2.4-fold, 4.1-fold, respectively; n = 4, Figure 35 ef) and in the intermediate progenitor layer (2.2-fold, 5.0-fold, respectively; n = 4, Figure 35 ef). Similar to the mitotic cell phenotype the total number of divisions (both asymmetric and symmetric orientations) was rescued to approximately wildtype levels in Ex6DEL mice that are heterozygous for *Foxg1*, while reducing *Foxg1* dosage has no effect

Figure 35 –Animals heterozygous for *Foxg1* confer a reduction in symmetric and asymmetric oriented division of progenitor cells.

E15.5 embryos heterozygous for Foxg1 demonstrate a partial rescue of symmetrically and asymmetrically oriented mitotic divisions in both the ventricular zone (VZ, defined by the boundary between Tuj positive and Tuj negative cells) and intermediate progenitor cell layers (IPL, defined by presence of Tuj, and cytoarchitectural features of the cortical plate (CP)). Triple immunofluorescence images of E15.5 embryonic cortex sections (coronal, 10 μm) for the γ-tubulin (green) and the early neuronal specific (Tuj; red) and nuclei are counterstained for DAPI (blue) for Snf2l WT/Foxg1$^{+/+}$ [A], Snf2l WT/Foxg1$^{+/-}$ [B], Ex6DEL/Foxg1$^{+/+}$ [C] and Ex6DEL/Foxg1$^{+/-}$ [D] are shown (width of images is 100 μm). Quantification of the relative proportion of asymmetric divisions (divisions along the axis of migration) in 100 μm sections cortices from of Snf2l WT Foxg1$^{+/+}$ (XY++; blue bars), Snf2l WT Foxg1$^{+/-}$ (XY+-; purple bars), Ex6DEL Foxg1$^{+/+}$ (-Y++; black bars) and Ex6DEL Foxg1$^{+/-}$ (-Y+-; grey bars). There is a partial rescue in the number of asymmetric divisions [E], symmetric divisions [F] and number of total number of cells [G] (* indicates P-values > 0.05, n=4 biological replicates) Error bars represent SEM.

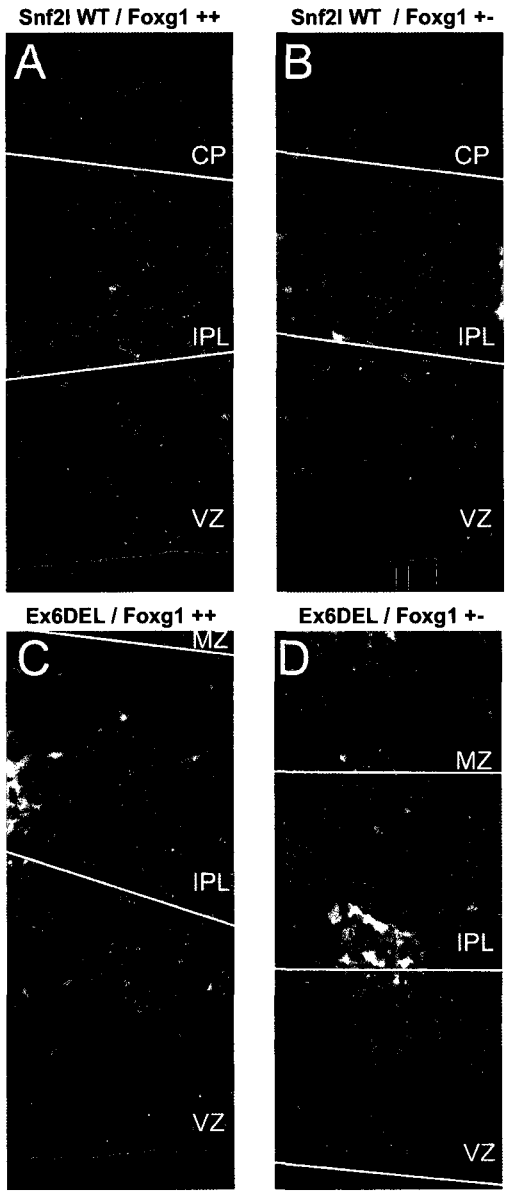
Snf2l WT / Foxg1 ++
A
CP
IPL
VZ
Snf2l WT / Foxg1 +-
B
CP
IPL
VZ
Ex6DEL / Foxg1 ++
C
MZ
IPL
VZ
Ex6DEL / Foxg1 +-
D
MZ
IPL
VZ

E

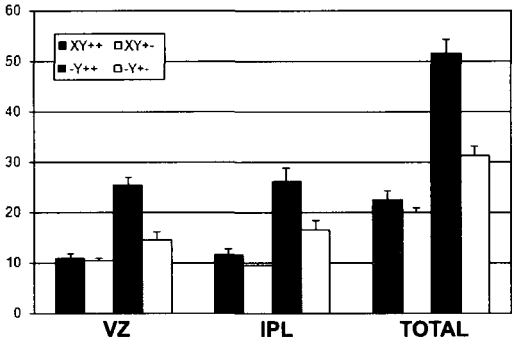
Asymmetric Orientated Divisions (per 100μm)
XY++ XY+-
-Y++ -Y+-
60
50
40
30
20
10
0
VZ
IPL
TOTAL

F

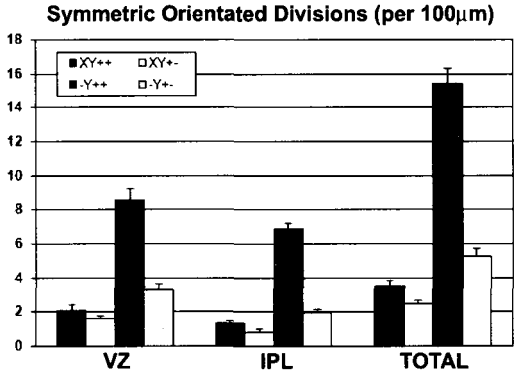
Symmetric Orientated Divisions (per 100μm)
XY++ XY+-
-Y++ -Y+-
18
16
14
12
10
8
6
4
2
0
VZ
IPL
TOTAL

G

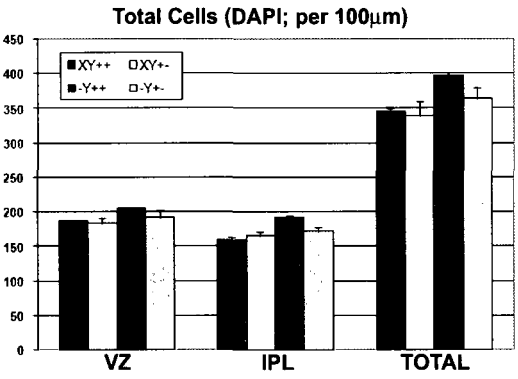
Total Cells (DAPI; per 100μm)
XY++ XY+-
-Y++ -Y+-
450
400
350
300
250
200
150
100
50
0
VZ
IPL
TOTAL

in Snf2l wildtype mice. The total number of cells was also assessed by counting DAPI stained nuclei (Figure 35 g) and no difference between genotypes was observed.

3.7.4.3 Amplification of Tbr-2 intermediate progenitor cells is in Ex6DEL cortices.

Increased proliferation at the subplate (identified by PH3) and within the basal lamina (γ-tubulin positive) suggested that there was an increase in intermediate progenitor cells (IPCs). Intermediate progenitors, as a transiently amplifying population of neuroprogenitors, differ from the neuroepithilial progenitors (NEs) in several ways. Firstly, IPCs are located at basal positions (abventricular) compared to the NEs which divide apically at the ependymal layer [67]. Secondly IPCs expand the neuronal population by increasing symmetric terminal divisions, creating two neurons at each mitotic division, or self-amplify in order to increase population size [36, 67, 294]. However, unlike NE which can divide symmetrically for an unlimited number of divisions, IPCs can only self-renew 1-3 times [68]. IPCs are further distinguished from NE, which express Pax6, by the expression of Tbr-2. Tbr-2 is a factor that directs the conversion of neuroepithilial into Intermediate progenitors and guides neuronal expansion in the developing neocortex [68, 331]. In order to identify IPCs, E15.5 sections from Snf2l wildtype and Ex6DEL mice were stained by antibodies which identify Tbr-2 (green) and Tuj (red, to differentiate the ventricular zone) by indirect immunofluoresence, (Figure 36 ab). There was an observed increase in Ex6DEL cortices. The level of Tbr-2 expression was reduced in Snf2l wildtype and Ex6DEL mice, heterozygous for Foxg1 (Figure 36 bd). The proportion of Tbr2+ cells over DAPI+ (blue) cells in the intermediate zone was calculated, (Figure 36 e). The

increased Tbr2 positive cells in the Ex6DEL Foxg1$^{+/+}$ animals was rescued to wildtype levels in the Ex6DEL Foxg1$^{+/-}$ tissue.

3.7.4.4 Rescue of increased cells in mature Ex6DEL cortices by limiting Foxg1 dosage.

To determine if the hypercellularity observed in the mature Ex6DEL brain could be rescued by limiting *Foxg*1 expression, frozen sections from P7.5 brains were analyzed for cellular and morphological differences with DAPI on a layer by layer basis (Figure 37 a-d). The observed increase in cell number (Figure 17 and Figure 18) within the layers of the Ex6DEL cortices remains consistent (Figure 37 e, blue and black bars), but there was no noticeable disorganization within the cortical lamina. The increased number of cells in Ex6DEL mice was rescued to wildtype levels in Ex6DEL mice heterozygous for *Foxg*1, in all layers except in layers II/III, where the trend was consistent, but not statistically significant (236.5 $\pm$ 27.8 vs. 189.7 $\pm$ 34.1, per 150 μm (width), $p = 0.34$, $n = 3$) (see Figure 37 e). By totalling the number of cells throughout the 150 μm section, the number of cells attributed to the four genotypes is as follows: Snf2l WT/Foxg1$^{+/+}$ have 411.7, Snf2l WT/Foxg1$^{+/-}$ have 391.9 but Ex6DEL/Foxg1$^{+/+}$ with 641.8, Ex6DEL/Foxg1$^{+/-}$ with 471.9. These observations indicate that the principle effect resulting in the increase of cells in the Ex6DEL cortex is though the increase, or continued expression of *Foxg1*, and that by limiting the dosage of *Foxg*1 we can partially rescue the phenotype back towards wildtype levels.

Figure 36 – Ex6DEL embryos have increased Tbr-2 positive progenitor populations in E15.5 cortices, which is rescued in the Foxg1 heterozygotes.

Foxg1 is an important proliferative factor for intermediate progenitor cells, in order to further identify this population of progenitors, E15.5 coronal sections (10 μm) were triple stained for Tbr-2 (green), Tuj (red) and nuclei were counterstained with DAPI (blue). Sample images from Snf2l WT/Foxg1$^{+/+}$ [A], Snf2l WT/Foxg1$^{+/-}$ [B], Ex6DEL/Foxg1$^{+/+}$ [C] and Ex6DEL/Foxg1$^{+/-}$ [D] are shown (yellow scale bar is 120 μm). [E] A graph showing the relative proportion of Tbr-2 positive stained cells (Tbr2+/DAPI) in all four genotypes. 120 μm sections were counted and there is a significant increase in the proportion of Tbr-2 staining in the Ex6DEL/Foxg1$^{+/+}$ tissue that is rescued in the Ex6DEL/Foxg1$^{+/-}$ samples. (* indicates P-values > 0.05, n=3-5 biological replicates) Error bars represent SEM.

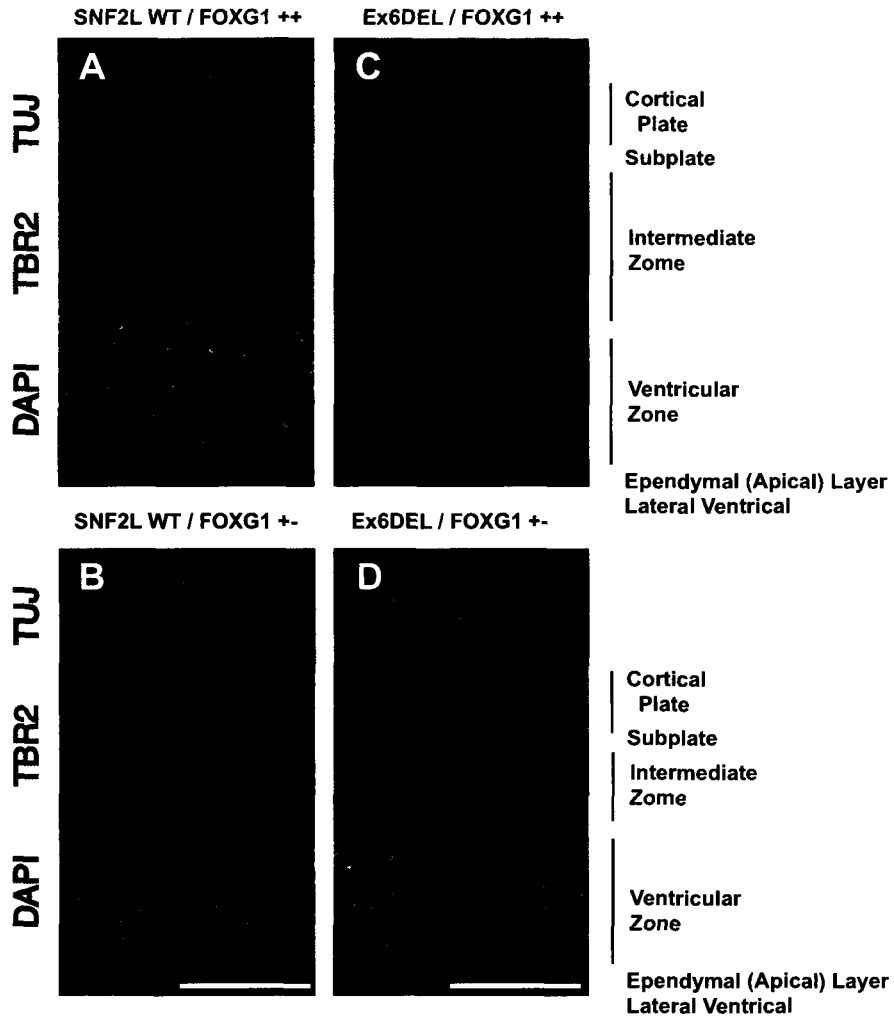
SNF2L WT / FOXG1 ++
Ex6DEL / FOXG1 ++
A
C
TUJ
TBR2
DAPI
Cortical Plate
Subplate
Intermediate Zome
Ventricular Zone
Ependymal (Apical) Layer
Lateral Ventrical
SNF2L WT / FOXG1 +-
Ex6DEL / FOXG1 +-
B
D
TUJ
TBR2
DAPI
Cortical Plate
Subplate
Intermediate Zome
Ventricular Zone
Ependymal (Apical) Layer
Lateral Ventrical

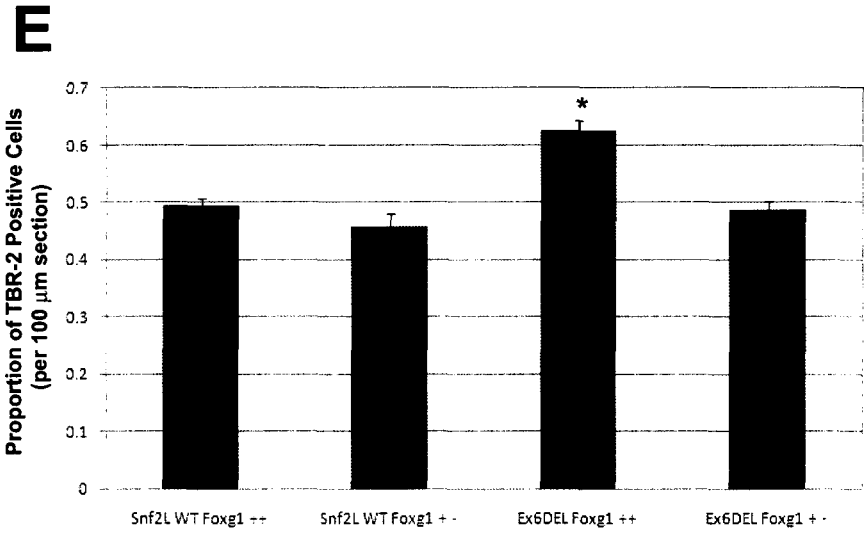
E
Proportion of TBR-2 Positive Cells (per 100 µm section)
0.7
0.6
0.5
0.4
0.3
0.2
0.1
0
*
Snf2L WT Foxg1 ++
Snf2L WT Foxg1 + -
Ex6DEL Foxg1 ++
Ex6DEL Foxg1 + -

Figure 37 – Heterozygousity for *Foxg1* rescues hypercellularity in postnatal Ex6DEL mice.

DAPI stained coronal sections through the lateral cortex (10 μm width) of one-week old (P7.5) postnatal mice show that the previously observed increased cellularity throughout the cortical strata (MZ-VI), marginal zone (MZ) and ventricular zone (VZ), is rescued in Ex6DEL *Foxg1* heterozygotes. Sample images from Snf2l WT/Foxg1$^{+/+}$ (XY++) [A], Snf2l WT/Foxg1$^{+/-}$ (XY+-) [B], Ex6DEL/Foxg1$^{+/+}$ (-Y++), [C] and Ex6DEL/Foxg1$^{+/-}$ (-Y+-) [D] are shown (yellow scale bar is 100 μm). [E] Graph of cell number (DAPI positive) in the P7.5 brain show a statistically significant rescue in all cortical layers except II/III ($p = 0.347$). Due to the difficulty in distinguishing layers II and III they were grouped together (*, P-values < 0.05; $N = 3$) error bars represent SEM.

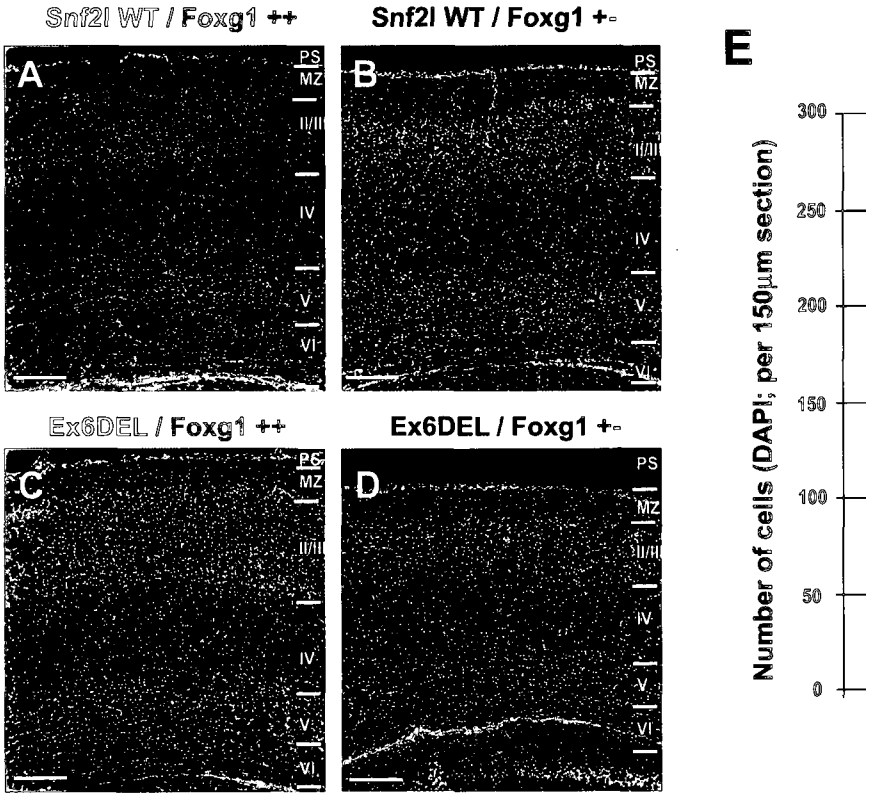
Snf2l WT / Foxg1 ++
Snf2l WT / Foxg1 +-
Ex6DEL / Foxg1 ++
Ex6DEL / Foxg1 +-
A
B
C
D
PS
MZ
II/III
IV
V
VI
E
Number of cells (DAPI; per 150µm section)
300
250
200
150
100
50
0

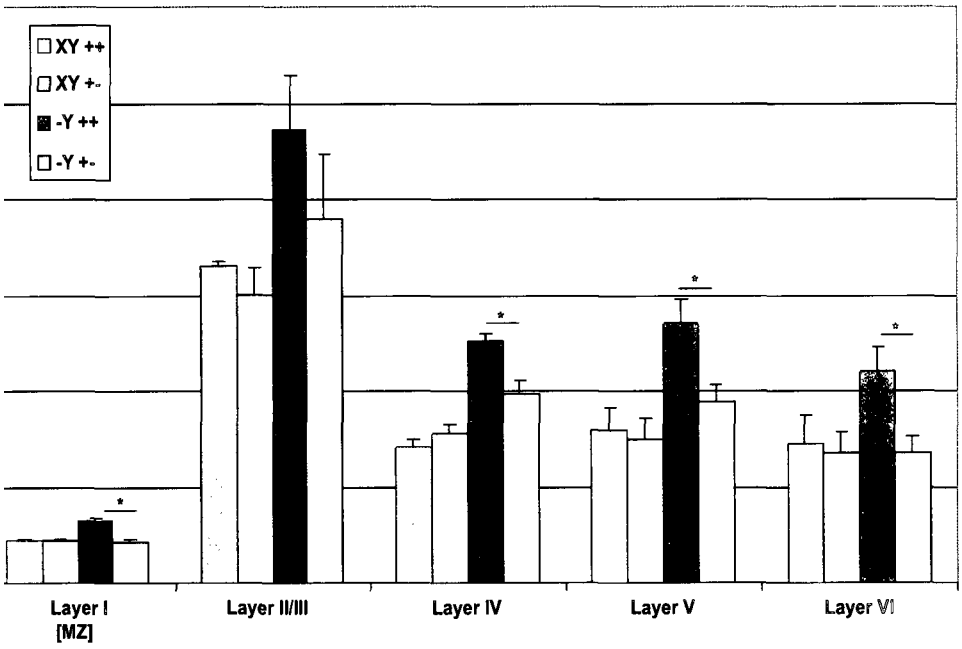
XY ++
XY +-
-Y ++
-Y +-
*
*
*
*
Layer I
[MZ]
Layer II/III
Layer IV
Layer V
Layer VI

4.0 Discussion.

The focus of this project has been to provide a detailed understanding of the functions of Snf2l and Snf2h in the development of the central nervous system. It is important to establish a connection between neurogenic factors, chromatin remodelling and transcriptional regulation during neurogenesis. Most studies of chromatin remodelling associated proteins have focused on their abilities to alter chromatin structure rather than their developmental functions. Our findings suggest that the Snf2l is involved in the regulation of several genes but that the specific regulation of a single gene, *Foxg1*, plays a substantial role in brain development. Stem cell maintenance, progenitor proliferation, and properly-timed differentiation are the key components in regulating brain size, and yet, little is known of the multifaceted functional interactions which govern these processes. Specific defects involving cell fate among progenitor populations are caused by the loss of Snf2l; they result in cell expansion and ultimately increase the size of the brain and other organs. The Ex6DEL mice which exhibit an enhanced level of *Foxg1* display an amplified number of neurons in all layers of the cortical plate, hippocampus, and cerebellum. A partial rescue of this hyperplasia in the cortex was achieved by limiting the dose of *Foxg1*. These findings suggest that Snf2l modulates the chromatin environment that regulates the timely repression of *Foxg1* during the early stages of neuronal differentiation and that Snf2l is a key regulator of brain development.

4.1 SNF2L and SNF2H have complementary roles during development.

In vitro, Snf2l and Snf2h have an active and complementary role in the management of proliferation and differentiation. Previous work from the Picketts' lab has identified

SNF2H as an upregulated factor correlating to metastatic ovarian tumours and drug resistance in cultured cells (DJ Picketts, unpublished data). In our experiments, NIH3T3 cells overexpressing SNF2H displayed an increased growth potential, while the overexpression of a mutant version of the SNF2H protein resulted in a 40% reduction in growth. Furthermore SNF2H overexpression conferred an ability to grow in soft agarose (which was absent in SNF2L overexpressing clones, MA Lazzaro and DJ Picketts, unpublished data). It was also shown that overexpression of SNF2L had the opposite effect and reduced the growth of cells by 20% compared to parental strains (MA Lazzaro and DJ Picketts, unpublished data). In the developing brain, early expression of Snf2H IS Localized predominantly to proliferating progenitors, while Snf2l expression is localized to post-mitotic neurons [175]. Moreover, ectopic expression of SNF2L in N1E115 cells led to the spontaneous induction of a differentiated morphology, suggesting that SNF2L is an early regulator of this process [169]. During a N1E115 cell differentiation time course, I observed that *Snf2l* levels are steadily increased, with no corroborating change in *Snf2h*. In human SH-SY5Y neuroblastoma cells, an increase in *SNF2L* was also observed. These results indicate that the expression of SNF2H is intimately linked to proliferation in many tissues, whereas SNF2L is involved in either cell cycle exit or initiation of differentiation.

4.2 Ablation of Snf2l and macroencephalic brains.

Using a Snf2l-null animal model, the role of Snf2l during neurogenesis was assessed. Snf2l's involvement in the initiation of neurogenesis and in the regulation of the *engrailed* genes, led us to believe that Snf2l was a vital transcriptional regulator of neurodevelopment [169]. Many studies of brain development factors in standard knockout

mice have been precluded by the onset of severe malformation at earlier developmental stages. So a strategy employing a conditionally targeted disruption in the *Snf2l* gene was chosen using the bacteriophage P1 Cre-LoxP excision system. The conditionally inactive *Snf2l* line was then bred onto the ubiquitous expressing Gata-1 Cre line, effectively developing a global Snf2l ATPase-null animal which we termed Ex6DEL (for *Snf2l* exon 6 deleted). Surprisingly, these experiments showed that loss of Snf2l ATPase activity does not result in embryonic lethality, but results in increased organ size, most notably in the brain. There is an approximately 1.4-fold increase (at 11 weeks) in the ratio of brain weight to body weight between male Ex6DEL and wildtype animals and also between female Ex6DEL and their wildtype and heterozygous counterparts. As the heterozygous animals appear normal it suggests that the loss of exon 6 in the *Snf2l* locus does not result in a "gain of function" mutation.

4.3 Misregulation of multiple genes in Ex6DEL brains results in increased cortical cells.

Macroencephaly can be caused by an increase in cell number (hyperplasia) or by increased cell size (hypertrophy), as is observed in the Kv1.1 mutant shaker mouse [295]. A microarray screen of expressed sequences identified 256 misregulated genes with greater than 2-fold alteration in the cortices of Ex6DEL mice (183 decreased and 73 genes increased). Included were the perturbations of several neurogenic and cell cycle related factors. Similar large numbers of misregulated genes have been identified in gene expression experiments for ISWI mutants in yeast and *Drosophila* [171, 296]. These results suggest that the regulation of multiple genes by ISWI is common throughout evolution. A 2.23-fold decrease, was observed for $p21^{Cip1}$ [*Cdkn1a*], a cyclin dependant

kinase [CDK] inhibitor. During development the proper size of the brain is precisely controlled by stimulatory and inhibitory signals and is intimately linked to the cell cycle. All of the Cip/Kip family members (p21, p27 and p57) possess the ability to inhibit CDK complexes [297-299]. Moreover the Ink4 family (p16, p15, p18 and p19) as CDK4/CDK6 specific inhibitors are also involved in regulating CDK complexes and regulating the cell cycle [300-302]. All members of these groups cause G1-arrest and initiate cell cycle exit. A pointed example of this is that $p21^{Cip1}$ is induced in many cell lines undergoing differentiation [303, 304]. Gene expression analysis by qRT-PCR of the total RNA isolated from Ex6DEL cortices confirmed a decrease in the CDK inhibitors, $p16^{Ink4a}$, $p21^{Cip1}$, and $p27^{Kip1}$, with the largest alteration in $p21^{Cip1}$, representing a 5.4-fold decrease (0.184 ± 0.048). There was no change in the expression of *Cyclin*B1 or *Cyclin*D2. Like the Ex6DEL mice, p21 knockouts undergo normal development until challenged with DNA damage, wherein their fibroblasts are defective in G1-arrest [305]. Moreover, postnatal p21 mutants have increased neural stem cells; *in vitro* these stem cells have been shown to undergo only a few extra rounds of self-renewal before quiescence [306]. Interestingly, targeted disruption of $p27^{Kip1}$ (down regulated 2.8-fold in the Ex6DEL mouse), results in increased body size (ranging from 20-40%) and uniformly enlarged brains, with no anatomical abnormality in the brain, other than increased cell number and density [299, 307, 308]. These results are comparable to observations from the Ex6DEL mouse, with the exception of increased body size. Also akin to the Ex6DEL model is the presence of testicular and ovarian hyperplasia (only testicles were analyzed for the Snf2l-null animal). The $p27^{Kip1}$ gene disrupted male mice are fertile, however, unlike Ex6DEL animals, female $p27^{-/-}$ mice are sterile due to impairment in luteal cell differentiation [299, 308]. The misregulation of these CDK inhibitors in the Ex6DEL brain provides an interesting insight

into the function of Snf2l during cell cycle regulation. Many disruptions in the balance of cortical progenitor proliferation and differentiation cycles lead to disorganized lamination, which is often characterized by layer-specific defects. For example, Tlx mutants undergo premature cell cycle exit and have a smaller cortical plate with the superficial layers specifically reduced and the deep, early born layers relatively unaffected [309, 310]. All cortical layers (I-VI) of the Ex6DEL animals demonstrate an increased cell density with no gross anatomical abnormality. This suggests that Snf2l inactivation affects a general process throughout neurodevelopment rather than at a specific regulatory stage. In both the adult and 1 week old Ex6DEL mice the largest increases lie within the Layers II/III (Figure 17c and Figure 18c). This is of particular interest because these superficial layers are the last to be born (E15.5-E17.5) and migrate to their final position just prior to birth. In the E15.5 embryos an increase was observed in the number of cells within the cortical plate (at this point only Layers I and VI, with the migrating cells of Layer V, not yet in position), however, increases in cells within the subventricular zone and the intermediate zone (a transient region of cell migration) suggest that the heightened cellular proliferation may be exacerbated at later developmental stages.

4.4 Hypercellularity in the Ex6DEL cortex is the result of neuroprogenitor expansion.

The neurons of the cortex initially arise from divisions within the ventricular zone. Here a population of multipotent neuroepithelial cells and their neural polarized derivative radial glia make up the germinal epithelium of the developing telencephalon. Pioneering work by electron microscopy in the 1970's recorded the orientations of apical divisions in the mammalian cerebral cortex [311]. There are three commonly accepted modes of

division that these precursors undertake: (1) symmetrical self-renewing, which produces two precursors, (2) asymmetrical, which generate one precursor to repopulate the progenitor pool and another to become a post-mitotic cell (neuron, astrocyte or oligodendrocyte), and (3) symmetrical terminal divisions, in which both daughter cells are postmitotic. Symmetrical terminal divisions occur later in corticogenesis and are thus thought to deplete the precursor pool [279, 280]. As corticogenesis progresses a transient pool of secondary progenitors arises in the subventricular zone. The intermediate progenitors (IPCs) can be expanded by up to 3 rounds of self-renewing divisions but undergo predominantly (90%) symmetrical terminal divisions [67, 68]. These progenitors produce the majority of cortical neurons in the later stages of corticogenesis although cells derived from IPCs are present in all layers [36, 68]. Birthdating experiments using thymidine incorporation intimately linked the inside-first, outside-last formation of cortical layering to the time of cell cycle exit [53, 312]. These results highlighted the importance of timely differentiation and laminar fate. There are many factors that affect this process and disruption of any could cause imbalances in proliferation or differentiation cues. For instance, a mutation that precipitates early differentiation would prevent precursor self-renewal and prematurely deplete the progenitor population. In this case there would be less cellular expansion, and thus a smaller cortical plate particularly in the superficial layers. In contrast, a mutation which induces self-renewal would lead to an excessive population of progenitors and upon differentiation would produce many more neurons and a larger cortical plate. One clear means of progenitor amplification is a shortening of the cell cycle creating a shorter doubling time. Considerable variations in the length of G1, and also S-phase have been attributed to a faster proliferative rate leading to expansion within the progenitor pool and increased size of the developing brain [313, 314]. In our experiments

we did not observe a difference in the proportion of BrdU incorporation between the wildtype controls and the Ex6DEL samples, although the abundance of BrdU positive cells were increased in the Ex6DEL animals. These results indicated that there were no differences in the relative fraction of cells undergoing S-phase. Yet, a 3-fold increase in the proportion of mitotic cells (PH3 positive cells) was visible along the ependymal layer of the ventricular zone suggesting a heightened amount of proliferation. An increase of this nature indicates a disruption in cell cycle kinetics possibly a lengthening of M-phase or decrease in the length of another phase of the cell cycle. In order to address if this effect is a cell autonomous alteration in some aspect of cell cycle kinetics we could investigate the length of S-Phase and the entire cycle length using IdU/BrdU co-labelling as has been described for *Pax6*$^{-/-}$ progenitors [315].

By labelling the S-phase cells at E13.5 with BrdU we were able to track the relative abundance of marked cells in the cortical layers of animals at one week of age (P7.5). There was a 2-fold increase in total numbers of BrdU positive cells throughout the cortical strata of the Ex6DEL animals. The densely stained cells are the derivatives of an S-phase cell that was labelled with BrdU at the time of injection and then this cell promptly exited the cell cycle and migrated out into the cortical lamina. A faintly labelled cell corresponds to an S-phase cell labelled with BrdU that re-entered the proliferative phase and thus subsequently diluted the relative abundance of BrdU. This can be clearly defined as the typical self-renewing symmetric division. A 4-fold increase in the proportion of faintly stained cells amongst the Ex6DEL tissues was concomitant with a 2-fold decrease in the proportion of densely BrdU positive cells suggesting that at the very least 2 times more symmetric self-renewing divisions must have occurred in these animals. To further evaluate this potential increase in self-renewal the number of cells that re-entered the cell

cycle were identified by labelling S-phase cells and allowing them to proceed through one round of division and co-staining with BrdU and Ki67. There was a 3.5-fold increase in double stained BrdU+Ki67+ cells that re-entered the cell cycle.

By PH3 staining we had identified a group of dividing cells along the subplate that were later determined to be IPCs. Staining with the centrioles staining marker γ-Tubulin was used to further identify this population and the dividing cells within the ventricular zone. There was an increase in asymmetric and symmetric orientated divisions in both ventricular zone and the IPC layer. Several factors affect cell cycle re-entry and cell number in the cortex. One such factor is Paired box 6 [Pax6]. Pax6 is a transcription factor, required for production of ventricular zone progenitors, which includes neuroepithilial cells and their derivative radial glia progenitors and is conspicuously absent from intermediate progenitors [68, 316, 317]. Pax6 is fundamental in repression of precocious differentiation and an early depletion of the progenitor pool. $Pax6^{-/-}$ mice present accelerated cortical development, increased expression of neurotrophic markers, a reduction in interkinetic nuclear migration, and display reduced cortex size throughout development [315, 318]. The increased cell numbers of the Ex6DEL cortex and the larger brains suggest the Snf2l is important for cell cycle exit and differentiation. However, the mice did not show the effects of excessive proliferation such as exencephaly. Indeed overexpression of β-catenin leads to larger heads, with exencephalic brains that display undulating folds, which resemble the gyri and sulci of higher mammals [319]. Increased expression of *Hes5* and *Hes1* denoted an increased neuroprogenitor population in the mutant brains at E15.5. Moreover, they observed an upregulation of *Tbr-1* expression, demarking an increase in the production of post-mitotic neuronal cells in the cortical plate of the β-catenin overexpressing mice suggested that the increased brain size was due to the

increased proliferation of neural precursors [319, 320]. However, other animal models such as the transgenic expression of *CyclinD1* give a phenotype that is much more similar to the Ex6DEL mice. Overexpression of *CyclinD1* alone is insufficient to completely block differentiation, and will only force a couple of extra rounds of division [321]. Gene hybridization analysis in E15.5 Ex6DEL cortex revealed an increase in cortical neuroprogenitors, particularly of the *Pax6*-staining population. *CyclinD*1 positive neuroprogenitors were also increased in Ex6DEL tissue. It may be that the loss of Snf2l mainly effects IPC differentiation which results in 1-3 rounds of extra proliferation. Consistent with this proposition we observed increases in neuroprogenitor population but with a concomitant increase in differentiated neurons, as identified by *Tbr1* and *Id2* hybridization. This also suggested that the condition is only transient in nature and can account for why the Ex6DEL brains display a mild macroencephaly and not the more severe exencephaly. In E13.5 Ex6DEL embryos, *Pax6* cortical staining showed no change, and only a nominal increase in *CyclinD*1 was observed, signifying that the increase at neuron production previously identified at E15.5, might involve a process naturally occurring in and around this timepoint. During corticogenesis, E15.5 represents a key switch between the natural balance of proliferation and differentiation, midway through neurogenesis and reflects an increase in terminal symmetric divisions particularly in the IPC population [322]. At E13.5 increases in post mitotic cells labelled with *Id2* and *Tbr1*, and the resulting increase in the postnatal cortical layers I, V, and VI (which represent the early born neuronal layers) suggest that a less explicit increase in neuroprogenitors is also present at earlier stages.

4.5 Identification of *Foxg1*, a genetic target of Snf2l regulation.

Another gene of interest, which was identified with a 7.38-fold upregulation in cortices of Ex6DEL mice by a microarray screen was the ***Forkhead box g1*** [*Foxg1*] gene, previously called ***Brain factor-1*** [*Bf-1*]. The upregulation of this gene was confirmed by qRT-PCR, albeit with a much more modest 1.4-fold increase. Foxg1 is a transcription factor that is critical in forebrain development and is expressed as early as E8.0 [291]. It is particularly important later on in neurogenesis for its function in intermediate progenitor cell maintenance and inducing self-renewal in the developing telencepalon [291, 323]. Foxg1 is limited to the progenitor population it plays a role in maintaining an undifferentiated state (fate conversion), preventing neurogenesis by down regulating the WNTs, and allowing sufficient time for progenitor expansion [323, 324, 325, 326]. The *Foxg1*$^{-/-}$ phenotype is one of reduced or even absent cortical plate formation that is replaced by an ectopic layer of Reelin expressing Cajal-Retzius cells, followed by late embryonic lethality associated with heightened expression of *BMP4* [293, 323]. Moreover, *Foxg1* has been implicated directly in the regulation of neuroprogenitor expansion by suppression of *p21*^{Cip1} and *Mash1*, two genes also identified in the microarray screen of Ex6DEL tissue that are important for differentiation of neurons (Figure 31) [291, 292, 327]. By ChIP-qPCR Snf2l was bound, with a 3.5-fold enrichment, to a region overlapping a portion of the 5'UTR and the first coding exon of the *Foxg1* locus. Results from wildtype mouse cortical extracts suggests that Snf2l normally has a direct role in the regulation of expression of *Foxg1* and implies that in the absence of functional Snf2l, continued expression of *Foxg1* might explain the increased cell number in the Ex6DEL brain. These results suggest that under normal circumstances, Snf2l regulates the repression of this gene upon cell cycle

exit. In yeast, Isw1 and Isw2 cooperate to represses transcription of the B-type cyclin gene *Clb2* during G2/M [328]. Here it is suggested that *Clb2* gene repression by the yeast ISWI proteins was similarly initiated early in the coding region of the gene and that repressive remodelling then spreads along to cover the promoter and regulatory sequences. Further analysis of the Histone modification occurring on the *Foxg1* gene are required to determine if a similar mechanism is invoked by Snf2l.

4.6 Limiting Foxg1 dosage rescues the Ex6DEL cortical phenotype.

Overexpression of *Foxg1* leads to outgrowth of the telencephalon and medulloblastoma, while *Foxg1*$^{-/-}$ mice have severely compromised growth of the telencephalon [327, 329]. Heterozygotes have a subtler phenotype with thinner cortices particularly in the superficial layers (Layer II/III) [252, 291, 330]. It has been proposed that a large proportion of the neurons born to Layer II/III arise from the subventricular zone implying the involvement of intermediate progenitors [36, 281]. A similar thinning of the cortex has also been observed in the *Foxg1* haploinsufficient hippocampus [330]. In Ex6DEL mice haploinsufficient for *Foxg1* there was a comparative decrease in *Foxg1* levels and this decrease fell close to wildtype *Foxg1* levels suggesting that the gene's expression in Ex6DEL *Foxg1*+/- was similar to wildtype animals (*Snf2l*$^{+/+}$, *Foxg1*$^{+/+}$). In the developing cortex reduced *Foxg1* leads to a complete rescue of cell cycle kinetics (identified by PH3 staining) in both the apical layer of the ventricular zone and the ventricular zone, incorporating the subplate region. Moreover, in limiting Foxg1 activity in this manner the number of symmetrically and asymmetrically orientated divisions of the

VZ and the IPC layer identified by γ-Tubulin staining was also rescued to near wildtype levels.

Neuronal progenitor stem cells, which account for only about 1% of all progenitors in the ventricular zone, give rise to neural committed radial glial cells that maintain proliferative status through the expression of Pax6 [249, 315, 317, 318]. Asymmetric divisions of RGC produce the intermediate progenitor population that is divergent from RGCs when Pax6 is attenuated and Tbr2 becomes expressed [331, 332]. In the IPC layer, 90% of divisions are symmetric-terminal and during the final switch from IPC to differentiated neurons, Tbr2 is down regulated and replaced by Tbr1 [36, 281]. To define the differences in radial glial progenitors (in the VZ) from the production of IPC progenitors (in the IPL), the IPCs were further identified by Tbr2-staining. Tbr2 positive cells between Ex6DEL and wildtype controls are particularly enhanced in the intermediate zone, and this proportional increase is also rescued by limiting Foxg1 dosage. As a further confirmation for Foxg1 involvement in the hypercellularity phenotype, DAPI stained nuclei from P7.5 cortical sections were quantified and the number of cells in each layer was equivalent to wildtype levels except Layer II/III, where the results were not significant (Figure 29).

Despite the complexity of the mammalian forebrain, the telencephalon starts off as a simple primordial sheet / layer of cells at the anterior end of the neural plate. Through several discrete phases, this layer is divided into multiple proliferative zones and eventually a modular brain structure (reviewed in [333]). Recently, Foxg1 has been identified as an early mediator of Shh patterning activity and a negative regulator of Wnt activity in the developing Zebrafish telencephalon [333, 334]. This suggests that Foxg1 also regulates proliferation of early telencephalic neuroprogenitors, and affects the size of the progenitor

pool from a much earlier timepoint than E15.5. This could explain why in the ventricular zone the multipotent neuroepithelial and radial glial progenitor cells are increased in the Ex6DEL tissues, and rescued in the *Foxg1* heterozygous dosage experiments. Moreover, a functional link between the polycomb protein Bmi-1 and Foxg1 has been shown to maintain neural stem cell self-renewal in the forebrain *ex vivo* [292]. In these experiments a 1.5-fold increase in *Foxg1* was sufficient to maintain an undifferentiated state, allowing Bmi-1 to induce consecutive rounds of stem cell proliferation. A similar increase in *Foxg1* (1.4-fold by qRT-PCR) was observed in the Ex6DEL cortices, although the levels of *Bmi-1* were not affected (data not shown). It is possible that in the absence of active Snf2l the continued action of proliferation inducing Snf2h complexes encourages consecutive rounds of cell cycle re-entry. This seems to affect both VZ progenitors and the IPCs, as identified by Tbr-2 staining. Perhaps, ultimately, Snf2h is incorporated into the Snf2l complexes (such as CERF and NURF) and functionally replaces the loss of Snf2l, leading to terminal differentiation. Under normal conditions, Snf2l has been isolated in 5% of CHRAC complexes, which are defined as Snf2h-containing, and providing a precedent for functional compensation in our model [178]. Such compensation may also explain why the progenitors do not continue to proliferate throughout neurogenesis (see discussion bellow).

4.7 Loss of the Snf2l-ATPase and potential functional compensation by Snf2h.

Chromatin organization is a highly dynamic process in cells and given the extensive range of cellular functions governed by chromatin remodelling it has been suggested that these proteins are essential for normal development. Indeed, the targeted inactivation of several chromatin remodelling protein complexes in mice has resulted in early embryonic

lethality, including the loss of ATRX, Brg1, Snf5 and Snf2h [186, 194, 195, 335]. Our initial assumption was that the global loss of Snf2l would result in embryonic lethality similar to the Snf2h knockout [186]. Continued survival of the Ex6DEL mice is comparable to the Brm-null mice, which endure as a result of compensation from the closely related Brg1 protein, whose transcripts and proteins are elevated in Brm-null animals [198]. *Brg1* and *Brm* have an overlapping expression pattern, but with functional differences, a situation similar to *Snf2h* and *Snf2l*. *Brm*, like *Snf2l*, is upregulated in growth arrested cells, suggesting a role in differentiation while Brg1, with ubiquitous expression, is vital for proliferation [198, 199, 336, 337]. Moreover, induced overexpression of *Brm* was shown to repress proliferation, in a manner similar to our *in vitro* observations of *Snf2l* expression [200, 336]. There is some controversy over the roles Brg1 and Brm have in the balance of proliferation and differentiation, however it seems likely that these roles are dependent upon composition differences of the BAF complexes, particularly during neural stem cell self-renewal [223]. The absence of functional Snf2l may reflect a miscue or a delay during fate conversion resulting in the continued activities of Snf2h and its respective complexes to force further rounds of cell proliferation. These cells do eventually differentiate; in the absence of an active Snf2l protein perhaps Snf2h is able to compensate as a functional ATPase alternative for the chromatin remodeling complexes in a manner similar to the Brm-Brg1 paradigm [198]. However the level of Snf2h, RNA transcripts and proteins are not augmented in the Ex6DEL cortices when compared to wildtype controls. The relatively mild defect observed in the Ex6DEL brains may be due to a systematic compensatory effect during embryonic development, in place to ensure proper brain formation. There are several built-in redundancies with overlapping roles in embryonic neural precursors, which may limit the effects of loss of Snf2l to a moderate increase in cell

density rather than full blown exencephaly. Perhaps alternative pathways can compensate for the misregulation of *Foxg1*. A clear example is the systemic compensation that is observed when *Cyclind1* or *Cyclind2* is overxpressed, the result is minimal increase in progenitor proliferation, 1-3 extra cycles, but no grand effect in the correct timing of differentiation and no lasting defects [321]. These results signify that even though a key component of the cell cycle machinery is overexpressed there is compensation via the combined effect of other pathway components that ultimately regulate differentiation.

The adult $Brm^{-/-}$ mice are ~15% heavier then littermate controls, a result of the increased cell proliferation, which was demonstrated by an enhanced mitotic index [198]. Also it was observed that early passage $Brm^{-/-}$ mouse embryonic fibroblasts grow significantly faster than $Brm^{+/+}$ cells [198]. Cell proliferation in the Snf2l-Ex6DEL mouse is similarly increased but this seems to be limited to specific organs. There was an increase in the organ weight to body weight ratio for the kidney, testes and most notably the brain. Snf2l expression in the adult mouse is limited to the CNS and the gonads, however for a short period during embryogenesis, Snf2l is expressed ubiquitously [175]. It is possible that during this short period, the proliferation dynamics of many progenitor populations are disturbed, and as such multiple tissues could be affected. Stem cell behaviour and self-renewal are regulated by extrinsic signals which induce chromatin reorganization [338, 339]. In *Drosophila* larvae that contain mutant Iswi, progenitor cells have been shown to have reduced division rates, signifying that ISWI is involved in stem cell proliferation from an early time point [339].

4.8 Future Directions.

This study has provided some insights into the role that the mammalian ISWI proteins have in neuronal development and have identified *Foxg1* as a genetic target of Snf2l. The molecular basis of this delay in differentiation remains to be determined and therefore will be the focus of further studies. In this regard, microarray profiling of gene expression in the Ex6DEL cortex has been very insightful. We have focused on the interaction of Snf2l and *Foxg1,* which is noteworthy, through the downstream interaction of Foxg1 and *p21*, but these experiments have identified several disruptions in the normal regulation of multiple cell cycle regulators and neurotrophic factors suggesting that multiple pathways may be misregulated [291, 292]. Some results such as the up regulation *Sox4* (2.14-fold) and *Sox5* (2.58-fold) are interesting as these factors have been shown to promote proliferation and repress differentiation by enhancing β-catenin activity in various tissues including neurons [340-345]. However, Sox5 has also been implicated in postmitotic regulation of deep layer cortical neuron differentiation [346]. Another promising gene of interest is *Fezf1* (6.25-Fold upregulation) since its repression results in a smaller brain [346]. Moreover, *Fgf15* (2.50-fold upregulation) a prominent growth factor in the developing brain, and *Arid1a* (2.75-fold upregulation) the defining subunit of the SWI/SNF containing BAF complex, important for ES cell pluripotency and self renewal, are also deregulated [347, 348]. Conversely, *Frizzled-related protein-1* (*Frzb*, down 3.14-fold) can normally inhibit proliferation and induce differentiation. To determine if these genes/pathways are indeed targets of *Snf2l* gene regulation or only genetic bystanders of the *Foxg1* misregulation, a detailed analysis is justified. It would also be valuable to determine

which Snf2l complexes, NURF or CERF, regulate *Foxg1*, and/or alternative Snf2l regulated genes. Conversely, these analyses may identify a novel Snf2l complex.

Chromatin immunoprecipitation experiments of the *Foxg1* regulatory region, focused only on a small domain encompassing 2kb proximal of the ATG initiation codon. This region corresponded primarily to the 5'UTR. A more detailed analysis of the highly conserved regions proximal and distal to the *Foxg1* gene must also be undertaken in order to determine if there are other Snf2l regulatory regions. Furthermore, a detailed understanding of the chromatin rearrangements across the *Foxg1* region may also be beneficial in the greater understanding of the role Snf2l plays in this gene's transcriptional regulation. Recent studies have shown that the ISWI chromatin-remodelling factor plays a key role in repression by promoting the assembly of repressive chromatin by modulating the interaction of histone H1 [171, 349]. In *Drosophila*, ISWI has also been shown to alter Histone H4 acetylation through formation of a complex with Sin3A/Rpd3 deacetylase [350]. ChIP may also be used to identify if the acetylation status of H4 residues and the H1 levels in the Foxg1 regulatory region are altered during differentiation.

In order to fully address whether the continued activity of Snf2h may represent a functional compensation in Ex6DEL tissue I would propose determining whether Snf2h could become a constituent of Snf2l characterized complexes. This could be conclusively determined by Co-IP experiments with known Snf2l binding partners, such as BPTF (in NURF complexes) or CECR2 (in CERF complexes). Alternatively, genetically limiting *Snf2h* dosage, in a manner similar to the *Foxg1* haploinsufficiency mouse model may also prove useful in the determination of potential compensation. Recently, the Picketts' lab has acquired the mouse line, heterozygous for Snf2h, from Arthur Skoultchi (Albert Einstein College of Medicine, Bronx NY) and these experiments are being undertaken.

A long term goal of the Picketts' lab has been to study the role of chromatin remodelling in developmental disorders, such as **m**ental **r**etardation [MR]. Initially, through genetic and sequence similarities to the ATPase ATRX, Snf2l was identified as a potential candidate for MR. Snf2l's involvement in neurodevelopment, expression in key components of the developing and adult brain and its overlapping position along the human X chromosome at Xq25 with several mapped MR families drew further notice [169, 175, 180]. However, we have yet to identify Snf2l as a causative gene for any disease [180]. Recently, interest has been generated around expression of, and mutations within, the homeobox transcription factor *En-2* and autism spectrum disorder [ASD]. ASD is a prevalent and heritable neurodevelopmental disorder [351, 352]. The mammalian engrailed proteins produce key neuronal transcription factors involved in mid/hindbrain patterning and neuronal axon guidance [353]. In Drosophila and humans, Snf2l binds to the proximal promoter of *En-2*, and is a known modulator of the gene's transcriptional activity [169, 170, 172]. En-2 knockout mice display the subtle neuropathological changes similar to the human disease and behavioural abnormalities [354, 355]. In humans, multiple autistic disorders (~25%) are affiliated with macroencephaly, including expansions within the cerebral cortex [356, 357]. Recently *Foxg1*-truncating mutations were identified in three patients affected by the congenital variant of Rett syndrome [358, 359]. Taken together, these results suggest that a thorough screening of ASD families with macroencephaly for mutations within the Snf2l locus might be fruitful.

4.9 Conclusions.

It can be challenging to distinguish between the effects of cell fate conversion and cell cycle re-entry. In order to identify specific progenitor populations that are affected one has to check the proportions of one type of neuron from another. We scrutinized the distinct layers and observed increases in all (I-VI, including the embryonic proliferative zones), suggesting the loss of functional Snf2l leads to an increase in cell proliferation throughout neurogenesis. However, in postnatal brain there is a consistently larger increase in the neurons of cortical Layers II/III. A large constituent of the neurons born to Layers II/III are derived from the IPCs, for which Foxg1 is a major regulator. Indeed, we observed an upregulation of *Foxg1*, which was further identified as a Snf2l target gene. Confirmation of Foxg1 involvement was provided through genetically limiting *Foxg1* dosage by breeding the Ex6DEL Snf2l-null allele onto the *Foxg1* haploinsufficient mouse line. In doing so, we reduced the mitotic index at both the ependymal surface of the ventricular zone and within the subventricular zone, which led to a partial rescue of hypercellularity in postnatal brains. Furthermore these results indicated that similar to the overexpression of β-catenin, inactivation of Snf2l influenced the decision to re-enter the cell cycle rather than differentiate. These gain and loss of function studies suggest that Snf2l is a key regulator in the development of the cerebral cortex and is fundamental in the maintenance of the proliferation/differentiation switch.

REFERENCES

1. Kuruvilla, R., H. Ye, and D.D. Ginty, *Spatially and functionally distinct roles of the PI3-K effector pathway during NGF signaling in sympathetic neurons.* Neuron, 2000. **27**(3): p. 499-512.
2. Mager, J. and M.S. Bartolomei, *Strategies for dissecting epigenetic mechanisms in the mouse.* Nat Genet, 2005. **37**(11): p. 1194-200.
3. Tojima, T. and E. Ito, *Signal transduction cascades underlying de novo protein synthesis required for neuronal morphogenesis in differentiating neurons.* Prog Neurobiol, 2004. **72**(3): p. 183-93.
4. Cockell, M. and S.M. Gasser, *Nuclear compartments and gene regulation.* Curr Opin Genet Dev, 1999. **9**(2): p. 199-205.
5. Eissenberg, J.C. and S.C. Elgin, *The HP1 protein family: getting a grip on chromatin.* Curr Opin Genet Dev, 2000. **10**(2): p. 204-10.
6. Peterson, C.L. and I. Herskowitz, *Characterization of the yeast SWI1, SWI2, and SWI3 genes, which encode a global activator of transcription.* Cell, 1992. **68**(3): p. 573-83.
7. Tsui-Pierchala, B.A., J. Milbrandt, and E.M. Johnson, Jr., *NGF utilizes c-Ret via a novel GFL-independent, inter-RTK signaling mechanism to maintain the trophic status of mature sympathetic neurons.* Neuron, 2002. **33**(2): p. 261-73.
8. Kaufman, M., H. and J.B.L. Bard, *The Anatomical Basis of Mouse Development.* 1999, New York: Academic Press.
9. Lavdas, A.A., et al., *The medial ganglionic eminence gives rise to a population of early neurons in the developing cerebral cortex.* J Neurosci, 1999. **19**(18): p. 7881-8.
10. Nakatsu, T., C. Uwabe, and K. Shiota, *Neural tube closure in humans initiates at multiple sites: evidence from human embryos and implications for the pathogenesis of neural tube defects.* Anat Embryol (Berl), 2000. **201**(6): p. 455-66.
11. Jessell, T.M., *Neuronal specification in the spinal cord: inductive signals and transcriptional codes.* Nat Rev Genet, 2000. **1**(1): p. 20-9.
12. Lumsden, A. and R. Krumlauf, *Patterning the vertebrate neuraxis.* Science, 1996. **274**(5290): p. 1109-15.
13. Akin, Z.N. and A.J. Nazarali, *Hox genes and their candidate downstream targets in the developing central nervous system.* Cell Mol Neurobiol, 2005. **25**(3-4): p. 697-741.
14. Scardigli, R., et al., *Direct and concentration-dependent regulation of the proneural gene Neurogenin2 by Pax6.* Development, 2003. **130**(14): p. 3269-81.
15. Mastick, G.S., et al., *Pax-6 functions in boundary formation and axon guidance in the embryonic mouse forebrain.* Development, 1997. **124**(10): p. 1985-97.
16. Stoykova, A., et al., *Pax6 modulates the dorsoventral patterning of the mammalian telencephalon.* J Neurosci, 2000. **20**(21): p. 8042-50.
17. Bishop, K.M., G. Goudreau, and D.D. O'Leary, *Regulation of area identity in the mammalian neocortex by Emx2 and Pax6.* Science, 2000. **288**(5464): p. 344-9.
18. Heng, J.I., et al., *Neurogenin 2 controls cortical neuron migration through regulation of Rnd2.* Nature, 2008. **455**(7209): p. 114-8.

19. Ohnuma, S. and W.A. Harris, *Neurogenesis and the cell cycle.* Neuron, 2003. **40**(2): p. 199-208.
20. Qian, X., et al., *Timing of CNS cell generation: a programmed sequence of neuron and glial cell production from isolated murine cortical stem cells.* Neuron, 2000. **28**(1): p. 69-80.
21. Ferguson, K.L. and R.S. Slack, *Growth factors: can they promote neurogenesis?* Trends Neurosci, 2003. **26**(6): p. 283-5.
22. Kempermann, G., L. Wiskott, and F.H. Gage, *Functional significance of adult neurogenesis.* Curr Opin Neurobiol, 2004. **14**(2): p. 186-91.
23. Bally-Cuif, L. and M. Hammerschmidt, *Induction and patterning of neuronal development, and its connection to cell cycle control.* Curr Opin Neurobiol, 2003. **13**(1): p. 16-25.
24. Hsieh, J. and F.H. Gage, *Epigenetic control of neural stem cell fate.* Curr Opin Genet Dev, 2004. **14**(5): p. 461-9.
25. Seri, B., et al., *Astrocytes give rise to new neurons in the adult mammalian hippocampus.* J Neurosci, 2001. **21**(18): p. 7153-60.
26. Martens, D.J., V. Tropepe, and D. van Der Kooy, *Separate proliferation kinetics of fibroblast growth factor-responsive and epidermal growth factor-responsive neural stem cells within the embryonic forebrain germinal zone.* J Neurosci, 2000. **20**(3): p. 1085-95.
27. Sweatt, J.D., *The neuronal MAP kinase cascade: a biochemical signal integration system subserving synaptic plasticity and memory.* J Neurochem, 2001. **76**(1): p. 1-10.
28. Kempermann, G., et al., *Early determination and long-term persistence of adult-generated new neurons in the hippocampus of mice.* Development, 2003. **130**(2): p. 391-9.
29. Sun, Y., et al., *Neurogenin promotes neurogenesis and inhibits glial differentiation by independent mechanisms.* Cell, 2001. **104**(3): p. 365-76.
30. Baron, W., et al., *Regulation of integrin growth factor interactions in oligodendrocytes by lipid raft microdomains.* Curr Biol, 2003. **13**(2): p. 151-5.
31. Ehrlich, M., et al., *DNA methyltransferase 3B mutations linked to the ICF syndrome cause dysregulation of lymphogenesis genes.* Hum Mol Genet, 2001. **10**(25): p. 2917-31.
32. Nakashima, K., et al., *Synergistic signaling in fetal brain by STAT3-Smad1 complex bridged by p300.* Science, 1999. **284**(5413): p. 479-82.
33. Tanabe, Y. and T.M. Jessell, *Diversity and pattern in the developing spinal cord.* Science, 1996. **274**(5290): p. 1115-23.
34. Takahashi, T., R.S. Nowakowski, and V.S. Caviness, Jr., *The leaving or Q fraction of the murine cerebral proliferative epithelium: a general model of neocortical neuronogenesis.* J Neurosci, 1996. **16**(19): p. 6183-96.
35. Kosodo, Y., et al., *Asymmetric distribution of the apical plasma membrane during neurogenic divisions of mammalian neuroepithelial cells.* Embo J, 2004. **23**(11): p. 2314-24.
36. Noctor, S.C., et al., *Cortical neurons arise in symmetric and asymmetric division zones and migrate through specific phases.* Nat Neurosci, 2004. **7**(2): p. 136-44.

37. Calegari, F. and W.B. Huttner, *An inhibition of cyclin-dependent kinases that lengthens, but does not arrest, neuroepithelial cell cycle induces premature neurogenesis.* J Cell Sci, 2003. **116**(Pt 24): p. 4947-55.
38. Horvitz, H.R. and I. Herskowitz, *Mechanisms of asymmetric cell division: two Bs or not two Bs, that is the question.* Cell, 1992. **68**(2): p. 237-55.
39. Gho, M., Y. Bellaiche, and F. Schweisguth, *Revisiting the Drosophila microchaete lineage: a novel intrinsically asymmetric cell division generates a glial cell.* Development, 1999. **126**(16): p. 3573-84.
40. Knoblich, J.A., *Asymmetric cell division during animal development.* Nat Rev Mol Cell Biol, 2001. **2**(1): p. 11-20.
41. Zhong, W. and W. Chia, *Neurogenesis and asymmetric cell division.* Curr Opin Neurobiol, 2008. **18**(1): p. 4-11.
42. Li, H.S., et al., *Inactivation of Numb and Numblike in embryonic dorsal forebrain impairs neurogenesis and disrupts cortical morphogenesis.* Neuron, 2003. **40**(6): p. 1105-18.
43. Mizutani, K. and T. Saito, *Progenitors resume generating neurons after temporary inhibition of neurogenesis by Notch activation in the mammalian cerebral cortex.* Development, 2005. **132**(6): p. 1295-304.
44. Rhyu, M.S., L.Y. Jan, and Y.N. Jan, *Asymmetric distribution of numb protein during division of the sensory organ precursor cell confers distinct fates to daughter cells.* Cell, 1994. **76**(3): p. 477-91.
45. Iacopetti, P., et al., *Expression of the antiproliferative gene TIS21 at the onset of neurogenesis identifies single neuroepithelial cells that switch from proliferative to neuron-generating division.* Proc Natl Acad Sci U S A, 1999. **96**(8): p. 4639-44.
46. Fishell, G. and A.R. Kriegstein, *Neurons from radial glia: the consequences of asymmetric inheritance.* Curr Opin Neurobiol, 2003. **13**(1): p. 34-41.
47. Wodarz, A. and W.B. Huttner, *Asymmetric cell division during neurogenesis in Drosophila and vertebrates.* Mech Dev, 2003. **120**(11): p. 1297-309.
48. Levitt, P., M.F. Barbe, and K.L. Eagleson, *Patterning and specification of the cerebral cortex.* Annu Rev Neurosci, 1997. **20**: p. 1-24.
49. McConnell, S.K., *Constructing the cerebral cortex: neurogenesis and fate determination.* Neuron, 1995. **15**(4): p. 761-8.
50. Gage, F.H., *Mammalian neural stem cells.* Science, 2000. **287**(5457): p. 1433-8.
51. Smart, I.H., *Proliferative characteristics of the ependymal layer during the early development of the mouse diencephalon, as revealed by recording the number, location, and plane of cleavage of mitotic figures.* J Anat, 1972. **113**(Pt 1): p. 109-29.
52. Jacobson, M. and M.S. Roa, *Developmental Neurobiology. 4 edt.* 2005: Springer.
53. Gupta, A., L.H. Tsai, and A. Wynshaw-Boris, *Life is a journey: a genetic look at neocortical development.* Nat Rev Genet, 2002. **3**(5): p. 342-55.
54. O'Rourke, N.A., et al., *Tangential migration of neurons in the developing cerebral cortex.* Development, 1995. **121**(7): p. 2165-76.
55. Hevner, R.F., et al., *Beyond laminar fate: toward a molecular classification of cortical projection/pyramidal neurons.* Dev Neurosci, 2003. **25**(2-4): p. 139-51.
56. Marin-Padilla, M., *Early prenatal ontogenesis of the cerebral cortex (neocortex) of the cat (Felis domestica). A Golgi study. I. The primordial neocortical organization.* Z Anat Entwicklungsgesch, 1971. **134**(2): p. 117-45.

57. Hevner, R.F., et al., *Cajal-Retzius cells in the mouse: transcription factors, neurotransmitters, and birthdays suggest a pallial origin.* Brain Res Dev Brain Res, 2003. **141**(1-2): p. 39-53.
58. Allendoerfer, K.L. and C.J. Shatz, *The subplate, a transient neocortical structure: its role in the development of connections between thalamus and cortex.* Annu Rev Neurosci, 1994. **17**: p. 185-218.
59. Chenn, A. and S.K. McConnell, *Cleavage orientation and the asymmetric inheritance of Notch1 immunoreactivity in mammalian neurogenesis.* Cell, 1995. **82**(4): p. 631-41.
60. Luskin, M.B., A.L. Pearlman, and J.R. Sanes, *Cell lineage in the cerebral cortex of the mouse studied in vivo and in vitro with a recombinant retrovirus.* Neuron, 1988. **1**(8): p. 635-47.
61. Noctor, S.C., et al., *Neurons derived from radial glial cells establish radial units in neocortex.* Nature, 2001. **409**(6821): p. 714-20.
62. Walsh, C. and C.L. Cepko, *Clonally related cortical cells show several migration patterns.* Science, 1988. **241**(4871): p. 1342-5.
63. Jacobowitz, D. and L. Abott, *Chemoarchitechinic Atlas of the Developing mouse brain.* 1998, USA: CRC Press.
64. McConnell, S.K. and C.E. Kaznowski, *Cell cycle dependence of laminar determination in developing neocortex.* Science, 1991. **254**(5029): p. 282-5.
65. Sauer, M.E. and B.E. Walker, *Radioautographic study of interkinetic nuclear migration in the neural tube.* Proc Soc Exp Biol Med, 1959. **101**(3): p. 557-60.
66. Ishii, Y., S. Nakamura, and N. Osumi, *Demarcation of early mammalian cortical development by differential expression of fringe genes.* Brain Res Dev Brain Res, 2000. **119**(2): p. 307-20.
67. Haubensak, W., et al., *Neurons arise in the basal neuroepithelium of the early mammalian telencephalon: a major site of neurogenesis.* Proc Natl Acad Sci U S A, 2004. **101**(9): p. 3196-201.
68. Pontious, A., et al., *Role of intermediate progenitor cells in cerebral cortex development.* Dev Neurosci, 2008. **30**(1-3): p. 24-32.
69. Blaschke, A.J., K. Staley, and J. Chun, *Widespread programmed cell death in proliferative and postmitotic regions of the fetal cerebral cortex.* Development, 1996. **122**(4): p. 1165-74.
70. Rabinowicz, T., et al., *Human cortex development: estimates of neuronal numbers indicate major loss late during gestation.* J Neuropathol Exp Neurol, 1996. **55**(3): p. 320-8.
71. Berger, S.L. and G. Felsenfeld, *Chromatin goes global.* Mol Cell, 2001. **8**(2): p. 263-8.
72. Rea, S., et al., *Regulation of chromatin structure by site-specific histone H3 methyltransferases.* Nature, 2000. **406**(6796): p. 593-9.
73. Lu, X., et al., *Linker histone H1 is essential for Drosophila development, the establishment of pericentric heterochromatin, and a normal polytene chromosome structure.* Genes Dev, 2009. **23**(4): p. 452-65.
74. Nemeth, A. and G. Langst, *Chromatin higher order structure: opening up chromatin for transcription.* Brief Funct Genomic Proteomic, 2004. **2**(4): p. 334-43.
75. Wolffe, A.P., ed. *Chromatin, Structure and Function, 2nd Edition.* 1995, Academic Press: Toronto, Ontario.

76. Woodcock, C.L. and S. Dimitrov, *Higher-order structure of chromatin and chromosomes.* Curr Opin Genet Dev, 2001. **11**(2): p. 130-5.
77. Tsukiyama, T., et al., *Characterization of the imitation switch subfamily of ATP-dependent chromatin-remodeling factors in Saccharomyces cerevisiae.* Genes Dev, 1999. **13**(6): p. 686-97.
78. Lodish, H., et al., *Molecular Cell Biology.* 4th ed. 2000, New York: Freeman and Company.
79. Ringrose, L. and R. Paro, *Gene regulation. Cycling silence.* Nature, 2001. **412**(6846): p. 493-4.
80. Lyko, F. and R. Paro, *Chromosomal elements conferring epigenetic inheritance.* Bioessays, 1999. **21**(10): p. 824-32.
81. Weiler, K.S. and B.T. Wakimoto, *Heterochromatin and gene expression in Drosophila.* Annu Rev Genet, 1995. **29**: p. 577-605.
82. Lohe, A.R. and A.J. Hilliker, *Return of the H-word (heterochromatin).* Curr Opin Genet Dev, 1995. **5**(6): p. 746-55.
83. Nielsen, A.L., et al., *Heterochromatin formation in mammalian cells: interaction between histones and HP1 proteins.* Mol Cell, 2001. **7**(4): p. 729-39.
84. Lupo, R., et al., *Drosophila chromosome condensation proteins Topoisomerase II and Barren colocalize with Polycomb and maintain Fab-7 PRE silencing.* Mol Cell, 2001. **7**(1): p. 127-36.
85. Henikoff, S., K. Ahmad, and H.S. Malik, *The centromere paradox: stable inheritance with rapidly evolving DNA.* Science, 2001. **293**(5532): p. 1098-102.
86. Lloyd, V.K., D.A. Sinclair, and T.A. Grigliatti, *Genomic imprinting and position-effect variegation in Drosophila melanogaster.* Genetics, 1999. **151**(4): p. 1503-16.
87. Ahmad, K. and S. Henikoff, *Centromeres are specialized replication domains in heterochromatin.* J Cell Biol, 2001. **153**(1): p. 101-10.
88. Elgin, S.C., *Heterochromatin and gene regulation in Drosophila.* Curr Opin Genet Dev, 1996. **6**(2): p. 193-202.
89. Felsenfeld, G., *Chromatin as an essential part of the transcriptional mechanism.* Nature, 1992. **355**(6357): p. 219-24.
90. Wu, C., *Chromatin remodeling and the control of gene expression.* J Biol Chem, 1997. **272**(45): p. 28171-4.
91. Vignali, M., et al., *ATP-dependent chromatin-remodeling complexes.* Mol Cell Biol, 2000. **20**(6): p. 1899-910.
92. Lusser, A. and J.T. Kadonaga, *Chromatin remodeling by ATP-dependent molecular machines.* Bioessays, 2003. **25**(12): p. 1192-200.
93. Carrozza, M.J., et al., *The diverse functions of histone acetyltransferase complexes.* Trends Genet, 2003. **19**(6): p. 321-9.
94. Fischle, W., Y. Wang, and C.D. Allis, *Histone and chromatin cross-talk.* Curr Opin Cell Biol, 2003. **15**(2): p. 172-83.
95. Weinmann, A.S., et al., *Isolating human transcription factor targets by coupling chromatin immunoprecipitation and CpG island microarray analysis.* Genes Dev, 2002. **16**(2): p. 235-44.
96. Stallcup, M.R., *Role of protein methylation in chromatin remodeling and transcriptional regulation.* Oncogene, 2001. **20**(24): p. 3014-20.
97. Bird, A.P. and A.P. Wolffe, *Methylation-induced repression--belts, braces, and chromatin.* Cell, 1999. **99**(5): p. 451-4.

98. Miranda, T.B. and P.A. Jones, *DNA methylation: the nuts and bolts of repression.* J Cell Physiol, 2007. **213**(2): p. 384-90.
99. Reik, W. and W. Dean, *DNA methylation and mammalian epigenetics.* Electrophoresis, 2001. **22**(14): p. 2838-43.
100. Reik, W., W. Dean, and J. Walter, *Epigenetic reprogramming in mammalian development.* Science, 2001. **293**(5532): p. 1089-93.
101. Kiefer, J.C., *Epigenetics in development.* Dev Dyn, 2007. **236**(4): p. 1144-56.
102. Sharma, R.P., et al., *Chromatin, DNA methylation and neuron gene regulation--the purpose of the package.* J Psychiatry Neurosci, 2005. **30**(4): p. 257-63.
103. Feng, Y., et al., *FMRP associates with polyribosomes as an mRNP, and the I304N mutation of severe fragile X syndrome abolishes this association.* Mol Cell, 1997. **1**(1): p. 109-18.
104. Sutcliffe, J.S., et al., *DNA methylation represses FMR-1 transcription in fragile X syndrome.* Hum Mol Genet, 1992. **1**(6): p. 397-400.
105. Amir, R.E. and H.Y. Zoghbi, *Rett syndrome: methyl-CpG-binding protein 2 mutations and phenotype-genotype correlations.* Am J Med Genet, 2000. **97**(2): p. 147-52.
106. Grant, P.A., *A tale of histone modifications.* Genome Biol, 2001. **2**(4): p. REVIEWS0003.
107. Strahl, B.D. and C.D. Allis, *The language of covalent histone modifications.* Nature, 2000. **403**(6765): p. 41-5.
108. Roth, S.Y., J.M. Denu, and C.D. Allis, *Histone acetyltransferases.* Annu Rev Biochem, 2001. **70**: p. 81-120.
109. Kuo, M.H. and C.D. Allis, *Roles of histone acetyltransferases and deacetylases in gene regulation.* Bioessays, 1998. **20**(8): p. 615-26.
110. Narlikar, G.J., H.Y. Fan, and R.E. Kingston, *Cooperation between complexes that regulate chromatin structure and transcription.* Cell, 2002. **108**(4): p. 475-87.
111. Kouzarides, T., *Chromatin modifications and their function.* Cell, 2007. **128**(4): p. 693-705.
112. Clarke, S., *Protein methylation.* Curr. Opin. Cell Biol., 1993. **5**: p. 977-983.
113. Zhang, Y. and D. Reinberg, *Transcription regulation by histone methylation: interplay between differnent modifications of the core histone tails.* Genes Dev, 2001. **15**: p. 2343-2360.
114. Gary, J.D. and S. Clarke, *RNA and protein interactions modulated by protein arginine methylation.* Prog Nucleic Acid Res Mol Biol, 1998. **61**: p. 65-131.
115. Chen, D., et al., *Regulation of transcription by a protein methyltransferase.* Science, 1999. **284**: p. 2174-2177.
116. Aagaard, L., et al., *Functional mammalian homologues of the Drosophila PEV-modifyer Su(var)3-9 encode centromere-associated proteins which complex with the heterochromatin component M31.* Embo J, 1999. **18**(7): p. 1923-1938.
117. Nakayama, J., et al., *Role of histone H3 lysine 9 methylation in epigenetic control of heterochromatin assembly.* Science, 2001. **292**(5514): p. 110-3.
118. Brasher, S.V., et al., *The structure of the mouse HP1 suggest a unique mode of single peptide recognition by the shadow chromodomain dimer.* Embo J, 2000. **19**: p. 1587-1597.
119. Nowak, S.J. and V.G. Corces, *Phosphorylation of histone H3 correlates with transcriptionally active loci.* Genes Dev, 2000. **14**: p. 3003-3013.

120. Lo, W.S., et al., *Phosphorylation of serine 10 in histone H3 is functionally linked in vitro and in vivo to GCN5-mediated acetylation at lysine 14.* Mol Cell, 2000. **5**: p. 917-926.
121. Hendzel, M.J., et al., *Mitossis-specific phosphorylation of histone H3 initiates primarily with pericentromeric heterochormatin during G2 and spreads in an ordered fashion coinisides with mitotic chromosome condensation.* Chromosoma, 1997. **106**: p. 348-360.
122. Wei, Y., et al., *Phosphorylation of histone H3 is required for proper chromosome condensation and segregation.* Cell, 1999. **97**: p. 99-109.
123. Eberharter, A., et al., *Acf1, the largest subunit of CHRAC, regulates ISWI-induced nucleosome remodelling.* Embo J, 2001. **20**(14): p. 3781-8.
124. Ferreira, H., A. Flaus, and T. Owen-Hughes, *Histone modifications influence the action of Snf2 family remodelling enzymes by different mechanisms.* J Mol Biol, 2007. **374**(3): p. 563-79.
125. Chakalova, L., et al., *Developmental regulation of the beta-globin gene locus.* Prog Mol Subcell Biol, 2005. **38**: p. 183-206.
126. Tang, Y., D.P. Liu, and C.C. Liang, *Further understanding of the beta-globin locus regulation at the molecular level: looping or linking models?* Genes Cells, 2002. **7**(9): p. 889-900.
127. Bultman, S.J., T.C. Gebuhr, and T. Magnuson, *A Brg1 mutation that uncouples ATPase activity from chromatin remodeling reveals an essential role for SWI/SNF-related complexes in beta-globin expression and erythroid development.* Genes Dev, 2005. **19**(23): p. 2849-61.
128. Hirschhorn, J.N., et al., *Evidence that SNF2/SWI2 and SNF5 activate transcription in yeast by altering chromatin structure.* Genes Dev, 1992. **6**(12A): p. 2288-98.
129. Durr, H., et al., *Snf2 family ATPases and DExx box helicases: differences and unifying concepts from high-resolution crystal structures.* Nucleic Acids Res, 2006. **34**(15): p. 4160-7.
130. Eberharter, A. and P.B. Becker, *ATP-dependent nucleosome remodelling: factors and functions.* J Cell Sci, 2004. **117**(Pt 17): p. 3707-11.
131. Hassan, A.H., et al., *Function and selectivity of bromodomains in anchoring chromatin-modifying complexes to promoter nucleosomes.* Cell, 2002. **111**(3): p. 369-79.
132. Awad, S. and A.H. Hassan, *The Swi2/Snf2 bromodomain is important for the full binding and remodeling activity of the SWI/SNF complex on H3- and H4-acetylated nucleosomes.* Ann N Y Acad Sci, 2008. **1138**: p. 366-75.
133. Boyer, L.A., et al., *Essential role for the SANT domain in the functioning of multiple chromatin remodeling enzymes.* Mol Cell, 2002. **10**(4): p. 935-42.
134. Boyer, L.A., R.R. Latek, and C.L. Peterson, *The SANT domain: a unique histone-tail-binding module?* Nat Rev Mol Cell Biol, 2004. **5**(2): p. 158-63.
135. Hall, J.A. and P.T. Georgel, *CHD proteins: a diverse family with strong ties.* Biochem Cell Biol, 2007. **85**(4): p. 463-76.
136. Auble, D.T., et al., *Mot1, a global repressor of RNA polymerase II transcription, inhibits TBP binding to DNA by an ATP-dependent mechanism.* Genes Dev, 1994. **8**(16): p. 1920-34.

137. Eisen, J.A., K.S. Sweder, and P.C. Hanawalt, *Evolution of the SNF2 family of proteins: subfamilies with distinct sequences and functions.* Nucleic Acids Res, 1995. **23**(14): p. 2715-23.
138. Pazin, M.J. and J.T. Kadonaga, *SWI2/SNF2 and related proteins: ATP-driven motors that disrupt protein-DNA interactions?* Cell, 1997. **88**(6): p. 737-40.
139. Kingston, R.E. and G.J. Narlikar, *ATP-dependent remodeling and acetylation as regulators of chromatin fluidity.* Genes Dev, 1999. **13**(18): p. 2339-52.
140. Aoyagi, S., et al., *Nucleosome remodeling by the human SWI/SNF complex requires transient global disruption of histone-DNA interactions.* Mol Cell Biol, 2002. **22**(11): p. 3653-62.
141. Aoyagi, S., P.A. Wade, and J.J. Hayes, *Nucleosome sliding induced by the xMi-2 complex does not occur exclusively via a simple twist-diffusion mechanism.* J Biol Chem, 2003. **278**(33): p. 30562-8.
142. Hanai, K., et al., *RSF governs silent chromatin formation via histone H2Av replacement.* PLoS Genet, 2008. **4**(2): p. e1000011.
143. Havas, K., et al., *Generation of superhelical torsion by ATP-dependent chromatin remodeling activities.* Cell, 2000. **103**(7): p. 1133-42.
144. Alberts, B., et al., *Molecular Biology of the Cell.* 2002, New York: Garland Science.
145. Becker, P.B. and W. Horz, *ATP-dependent nucleosome remodeling.* Annu Rev Biochem, 2002. **71**: p. 247-73.
146. Gushchin, D. and A.P. Wollfe, *SWItched-on Mobility.* Curr Biol, 1999. **9**): p. R742-746.
147. Redon, C., et al., *Histone H2A variants H2AX and H2AZ.* Curr Opin Genet Dev, 2002. **12**: p. 162-169.
148. Winston, F. and M. Carlson, *Yeast SNF/SWI transcriptional activators and the SPT/SIN chromatin connection.* Trends Genet, 1992. **8**(11): p. 387-91.
149. Huang, M., et al., *Chromatin-remodelling factor BRG1 selectively activates a subset of interferon-alpha-inducible genes.* Nat Cell Biol, 2002. **4**(10): p. 774-81.
150. Johnson, C.N., N.L. Adkins, and P. Georgel, *Chromatin remodeling complexes: ATP-dependent machines in action.* Biochem Cell Biol, 2005. **83**(4): p. 405-17.
151. Laurent, B.C., I. Treich, and M. Carlson, *The yeast SNF2/SWI2 protein has DNA-stimulated ATPase activity required for transcriptional activation.* Genes Dev, 1993. **7**(4): p. 583-91.
152. Peterson, C.L., A. Dingwall, and M.P. Scott, *Five SWI/SNF gene products are components of a large multisubunit complex required for transcriptional enhancement.* Proc Natl Acad Sci U S A, 1994. **91**(8): p. 2905-8.
153. Laurent, B.C., M.A. Treitel, and M. Carlson, *Functional interdependence of the yeast SNF2, SNF5, and SNF6 proteins in transcriptional activation.* Proc Natl Acad Sci U S A, 1991. **88**(7): p. 2687-91.
154. Tamkun, J.W., et al., *brahma: a regulator of Drosophila homeotic genes structurally related to the yeast transcriptional activator SNF2/SWI2.* Cell, 1992. **68**(3): p. 561-72.
155. Kwon, H., et al., *Nucleosome disruption and enhancement of activator binding by a human SW1/SNF complex.* Nature, 1994. **370**(6489): p. 477-81.
156. Armstrong, J.A., et al., *The Drosophila BRM complex facilitates global transcription by RNA polymerase II.* Embo J, 2002. **21**(19): p. 5245-54.

157. Martens, J.A. and F. Winston, *Recent advances in understanding chromatin remodeling by Swi/Snf complexes.* Curr Opin Genet Dev, 2003. **13**(2): p. 136-42.
158. Dhalluin, C., et al., *Structure and ligand of a histone acetyltransferase bromodomain.* Nature, 1999. **399**(6735): p. 491-6.
159. Winston, F. and C.D. Allis, *The bromodomain: a chromatin-targeting module?* Nat Struct Biol, 1999. **6**(7): p. 601-4.
160. Knoepfler, P.S. and R.N. Eisenman, *Sin meets NuRD and other tails of repression.* Cell, 1999. **99**(5): p. 447-50.
161. Gangaraju, V.K. and B. Bartholomew, *Mechanisms of ATP dependent chromatin remodeling.* Mutat Res, 2007. **618**(1-2): p. 3-17.
162. Brehm, A., et al., *dMi-2 and ISWI chromatin remodelling factors have distinct nucleosome binding and mobilization properties.* Embo J, 2000. **19**(16): p. 4332-41.
163. Ng, H.H., et al., *MBD2 is a transcriptional repressor belonging to the MeCP1 histone deacetylase complex.* Nat Genet, 1999. **23**(1): p. 58-61.
164. Underhill, C., et al., *A novel nuclear receptor corepressor complex, N-CoR, contains components of the mammalian SWI/SNF complex and the corepressor KAP-1.* J Biol Chem, 2000. **275**(51): p. 40463-70.
165. Langst, G. and P.B. Becker, *ISWI induces nucleosome sliding on nicked DNA.* Mol Cell, 2001. **8**(5): p. 1085-92.
166. Tsukiyama, T., et al., *ISWI, a member of the SWI2/SNF2 ATPase family, encodes the 140 kDa subunit of the nucleosome remodeling factor.* Cell, 1995. **83**(6): p. 1021-6.
167. Ito, T., et al., *ACF consists of two subunits, Acf1 and ISWI, that function cooperatively in the ATP-dependent catalysis of chromatin assembly.* Genes Dev, 1999. **13**(12): p. 1529-39.
168. Becker, P.B., T. Tsukiyama, and C. Wu, *Chromatin Assembly extracts from Drosophila embryos.* Method Cell Biol, 1994. **44**: p. 207-223.
169. Barak, O., et al., *Isolation of human NURF: a regulator of Engrailed gene expression.* Embo J, 2003. **22**(22): p. 6089-100.
170. Badenhorst, P., et al., *Biological functions of the ISWI chromatin remodeling complex NURF.* Genes Dev, 2002. **16**(24): p. 3186-98.
171. Corona, D.F., et al., *ISWI regulates higher-order chromatin structure and histone H1 assembly in vivo.* PLoS Biol, 2007. **5**(9): p. e232.
172. Deuring, R., et al., *The ISWI chromatin-remodeling protein is required for gene expression and the maintenance of higher order chromatin structure in vivo.* Mol Cell, 2000. **5**(2): p. 355-65.
173. Stephens, G.E., et al., *Heterochromatin protein 2 interacts with Nap-1 and NURF: a link between heterochromatin-induced gene silencing and the chromatin remodeling machinery in Drosophila.* Biochemistry, 2006. **45**(50): p. 14990-9.
174. Whitehouse, I., et al., *Evidence for DNA translocation by the ISWI chromatin-remodeling enzyme.* Mol Cell Biol, 2003. **23**(6): p. 1935-45.
175. Lazzaro, M.A. and D.J. Picketts, *Cloning and characterization of the murine Imitation Switch (ISWI) genes: differential expression patterns suggest distinct developmental roles for Snf2h and Snf2l.* J Neurochem, 2001. **77**(4): p. 1145-56.
176. Okabe, I., et al., *Cloning of human and bovine homologs of SNF2/SWI2: a global activator of transcription in yeast S. cerevisiae.* Nucleic Acids Res, 1992. **20**(17): p. 4649-55.

177. Aihara, T., et al., *Cloning and mapping of SMARCA5 encoding hSNF2H, a novel human homologue of Drosophila ISWI.* Cytogenet Cell Genet, 1998. **81**(3-4): p. 191-3.
178. Poot, R.A., et al., *HuCHRAC, a human ISWI chromatin remodelling complex contains hACF1 and two novel histone-fold proteins.* Embo J, 2000. **19**(13): p. 3377-87.
179. Barak, O., et al., *A tissue-specific, naturally occurring human SNF2L variant inactivates chromatin remodeling.* J Biol Chem, 2004. **279**(43): p. 45130-8.
180. Lazzaro, M.A., et al., *Characterization of novel isoforms and evaluation of SNF2L/SMARCA1 as a candidate gene for X-linked mental retardation in 12 families linked to Xq25-26.* BMC Med Genet, 2008. **9**: p. 11.
181. Fan, H.Y., et al., *Swapping function of two chromatin remodeling complexes.* Mol Cell, 2005. **17**(6): p. 805-15.
182. Aalfs, J.D., G.J. Narlikar, and R.E. Kingston, *Functional differences between the human ATP-dependent nucleosome remodeling proteins BRG1 and SNF2H.* J Biol Chem, 2001. **276**(36): p. 34270-8.
183. Aalfs, J.D. and R.E. Kingston, *What does 'chromatin remodeling' mean?* Trends Biochem Sci, 2000. **25**(11): p. 548-55.
184. Cote, J., et al., *Stimulation of GAL4 derivative binding to nucleosomal DNA by the yeast SWI/SNF complex.* Science, 1994. **265**(5168): p. 53-60.
185. Varga-Weisz, P., *ATP-dependent chromatin remodeling factors: nucleosome shufflers with many missions.* Oncogene, 2001. **20**(24): p. 3076-85.
186. Stopka, T. and A.I. Skoultchi, *The ISWI ATPase Snf2h is required for early mouse development.* Proc Natl Acad Sci U S A, 2003. **100**(24): p. 14097-102.
187. Dirscherl, S.S., J.J. Henry, and J.E. Krebs, *Neural and eye-specific defects associated with loss of the Imitation Switch (ISWI) chromatin remodeler in Xenopus laevis.* Mech Dev, 2005. **122**(11): p. 1157-70.
188. Pepin, D., et al., *ISWI chromatin remodeling in ovarian somatic and germ cells: revenge of the NURFs.* Trends Endocrinol Metab, 2007. **18**(5): p. 215-24.
189. Banting, G.S., et al., *CECR2, a protein involved in neurulation, forms a novel chromatin remodeling complex with SNF2L.* Hum Mol Genet, 2005. **14**(4): p. 513-24.
190. Norman, K.A. and R.C. O'Reilly, *Modeling hippocampal and neocortical contributions to recognition memory: a complementary-learning-systems approach.* Psychol Rev, 2003. **110**(4): p. 611-46.
191. Treves, A. and E.T. Rolls, *Computational analysis of the role of the hippocampus in memory.* Hippocampus, 1994. **4**(3): p. 374-91.
192. Kaeser, M.D. and B.M. Emerson, *Remodeling plans for cellular specialization: unique styles for every room.* Curr Opin Genet Dev, 2006. **16**(5): p. 508-12.
193. Berube, N.G., et al., *The chromatin-remodeling protein ATRX is critical for neuronal survival during corticogenesis.* J Clin Invest, 2005. **115**(2): p. 258-67.
194. Klochendler-Yeivin, A., et al., *The murine SNF5/INI1 chromatin remodeling factor is essential for embryonic development and tumor suppression.* EMBO Rep, 2000. **1**(6): p. 500-6.
195. Bultman, S., et al., *A Brg1 null mutation in the mouse reveals functional differences among mammalian SWI/SNF complexes.* Mol Cell, 2000. **6**(6): p. 1287-95.

196. Muchardt, C. and M. Yaniv, *The mammalian SWI/SNF complex and the control of cell growth.* Semin Cell Dev Biol, 1999. **10**(2): p. 189-95.
197. Muchardt, C. and M. Yaniv, *When the SWI/SNF complex remodels...the cell cycle.* Oncogene, 2001. **20**(24): p. 3067-75.
198. Reyes, J.C., et al., *Altered control of cellular proliferation in the absence of mammalian brahma (SNF2alpha).* Embo J, 1998. **17**(23): p. 6979-91.
199. Muchardt, C., et al., *ras transformation is associated with decreased expression of the brm/SNF2alpha ATPase from the mammalian SWI-SNF complex.* Embo J, 1998. **17**(1): p. 223-31.
200. Nagl, N.G., Jr., et al., *Distinct mammalian SWI/SNF chromatin remodeling complexes with opposing roles in cell-cycle control.* Embo J, 2007. **26**(3): p. 752-63.
201. Matsumoto, S., et al., *Brg1 is required for murine neural stem cell maintenance and gliogenesis.* Dev Biol, 2006. **289**(2): p. 372-83.
202. Raabe, E.H., et al., *An SNF2 factor involved in mammalian development and cellular proliferation.* Dev Dyn, 2001. **221**(1): p. 92-105.
203. Sun, L.Q., et al., *Growth retardation and premature aging phenotypes in mice with disruption of the SNF2-like gene, PASG.* Genes Dev, 2004. **18**(9): p. 1035-46.
204. Seo, S., G.A. Richardson, and K.L. Kroll, *The SWI/SNF chromatin remodeling protein Brg1 is required for vertebrate neurogenesis and mediates transactivation of Ngn and NeuroD.* Development, 2005. **132**(1): p. 105-15.
205. Cho, K.S., L.I. Elizondo, and C.F. Boerkoel, *Advances in chromatin remodeling and human disease.* Curr Opin Genet Dev, 2004. **14**(3): p. 308-15.
206. Davis, P.K. and R.K. Brackmann, *Chromatin remodeling and cancer.* Cancer Biol Ther, 2003. **2**(1): p. 22-9.
207. Hendricks, K.B., F. Shanahan, and E. Lees, *Role for BRG1 in cell cycle control and tumor suppression.* Mol Cell Biol, 2004. **24**(1): p. 362-76.
208. Wong, A.K., et al., *BRG1, a component of the SWI-SNF complex, is mutated in multiple human tumor cell lines.* Cancer Res, 2000. **60**(21): p. 6171-7.
209. Xue, Y., et al., *The human SWI/SNF-B chromatin-remodeling complex is related to yeast rsc and localizes at kinetochores of mitotic chromosomes.* Proc Natl Acad Sci U S A, 2000. **97**(24): p. 13015-20.
210. Muchardt, C., et al., *The hbrm and BRG-1 proteins, components of the human SNF/SWI complex, are phosphorylated and excluded from the condensed chromosomes during mitosis.* Embo J, 1996. **15**(13): p. 3394-402.
211. Flowers, S., et al., *Antagonistic roles for BRM and BRG1 SWI/SNF complexes in differentiation.* J Biol Chem, 2009.
212. Machida, Y., et al., *Expression of chromatin remodeling factors during neural differentiation.* J Biochem, 2001. **129**(1): p. 43-9.
213. Strobeck, M.W., et al., *Compensation of BRG-1 function by Brm: insight into the role of the core SWI-SNF subunits in retinoblastoma tumor suppressor signaling.* J Biol Chem, 2002. **277**(7): p. 4782-9.
214. Sheu, J.J., et al., *The roles of human sucrose nonfermenting protein 2 homologue in the tumor-promoting functions of Rsf-1.* Cancer Res, 2008. **68**(11): p. 4050-7.
215. Shih Ie, M., et al., *Amplification of a chromatin remodeling gene, Rsf-1/HBXAP, in ovarian carcinoma.* Proc Natl Acad Sci U S A, 2005. **102**(39): p. 14004-9.

216. Mohamed, M.A., et al., *Epigenetic events, remodelling enzymes and their relationship to chromatin organization in prostatic intraepithelial neoplasia and prostatic adenocarcinoma.* BJU Int, 2007. **99**(4): p. 908-15.
217. Mao, T.L., et al., *Expression of Rsf-1, a chromatin-remodeling gene, in ovarian and breast carcinoma.* Hum Pathol, 2006. **37**(9): p. 1169-75.
218. Mulero-Navarro, S. and M. Esteller, *Chromatin remodeling factor CHD5 is silenced by promoter CpG island hypermethylation in human cancer.* Epigenetics, 2008. **3**(4): p. 210-5.
219. Mulero-Navarro, S. and M. Esteller, *Epigenetic biomarkers for human cancer: the time is now.* Crit Rev Oncol Hematol, 2008. **68**(1): p. 1-11.
220. Hermanson, O., K. Jepsen, and M.G. Rosenfeld, *N-CoR controls differentiation of neural stem cells into astrocytes.* Nature, 2002. **419**(6910): p. 934-9.
221. Nowakowski, R.S., *Basic concepts of CNS development.* Child Dev, 1987. **58**(3): p. 568-95.
222. Lein, E.S., et al., *Genome-wide atlas of gene expression in the adult mouse brain.* Nature, 2007. **445**(7124): p. 168-76.
223. Lessard, J., et al., *An essential switch in subunit composition of a chromatin remodeling complex during neural development.* Neuron, 2007. **55**(2): p. 201-15.
224. Ooi, L. and I.C. Wood, *Regulation of gene expression in the nervous system.* Biochem J, 2008. **414**(3): p. 327-41.
225. Jaenisch, R. and R. Young, *Stem cells, the molecular circuitry of pluripotency and nuclear reprogramming.* Cell, 2008. **132**(4): p. 567-82.
226. Bertrand, N., D.S. Castro, and F. Guillemot, *Proneural genes and the specification of neural cell types.* Nat Rev Neurosci, 2002. **3**(7): p. 517-30.
227. Parras, C.M., et al., *Divergent functions of the proneural genes Mash1 and Ngn2 in the specification of neuronal subtype identity.* Genes Dev, 2002. **16**(3): p. 324-38.
228. Jacob, J., et al., *Transcriptional repression coordinates the temporal switch from motor to serotonergic neurogenesis.* Nat Neurosci, 2007. **10**(11): p. 1433-9.
229. Britz, O., et al., *A role for proneural genes in the maturation of cortical progenitor cells.* Cereb Cortex, 2006. **16 Suppl 1**: p. i138-51.
230. Crosio, C., et al., *Chromatin remodeling and neuronal response: multiple signaling pathways induce specific histone H3 modifications and early gene expression in hippocampal neurons.* J Cell Sci, 2003. **116**(Pt 24): p. 4905-14.
231. Seo, S., et al., *Geminin regulates neuronal differentiation by antagonizing Brg1 activity.* Genes Dev, 2005. **19**(14): p. 1723-34.
232. Seo, S. and K.L. Kroll, *Geminin's double life: chromatin connections that regulate transcription at the transition from proliferation to differentiation.* Cell Cycle, 2006. **5**(4): p. 374-9.
233. Yoshida, K., *Geminin organizes the molecular platform to balance cellular proliferation and differentiation.* Front Biosci, 2007. **12**: p. 2984-92.
234. Schoor, M., K. Schuster-Gossler, and A. Gossler, *The Etl-1 gene encodes a nuclear protein differentially expressed during early mouse development.* Dev Dyn, 1993. **197**(3): p. 227-37.
235. Delmas, V., D.G. Stokes, and R.P. Perry, *A mammalian DNA-binding protein that contains a chromodomain and an SNF2/SWI2-like helicase domain.* Proc Natl Acad Sci U S A, 1993. **90**(6): p. 2414-8.

236. Gibbons, R.J., et al., *Mutations in a putative global transcriptional regulator cause X-linked mental retardation with alpha-thalassemia (ATR-X syndrome).* Cell, 1995. **80**(6): p. 837-45.
237. Ballas, N., et al., *REST and its corepressors mediate plasticity of neuronal gene chromatin throughout neurogenesis.* Cell, 2005. **121**(4): p. 645-57.
238. Ballas, N. and G. Mandel, *The many faces of REST oversee epigenetic programming of neuronal genes.* Curr Opin Neurobiol, 2005. **15**(5): p. 500-6.
239. Schoenherr, C.J. and D.J. Anderson, *The neuron-restrictive silencer factor (NRSF): a coordinate repressor of multiple neuron-specific genes.* Science, 1995. **267**(5202): p. 1360-3.
240. Ekici, M., et al., *Transcription of genes encoding synaptic vesicle proteins in human neural stem cells: chromatin accessibility, histone methylation pattern, and the essential role of rest.* J Biol Chem, 2008. **283**(14): p. 9257-68.
241. Schoenherr, C.J., A.J. Paquette, and D.J. Anderson, *Identification of potential target genes for the neuron-restrictive silencer factor.* Proc Natl Acad Sci U S A, 1996. **93**(18): p. 9881-6.
242. Lunyak, V.V., et al., *Corepressor-dependent silencing of chromosomal regions encoding neuronal genes.* Science, 2002. **298**(5599): p. 1747-52.
243. Battaglioli, E., et al., *REST repression of neuronal genes requires components of the hSWI.SNF complex.* J Biol Chem, 2002. **277**(43): p. 41038-45.
244. Johnson, R., et al., *Identification of the REST regulon reveals extensive transposable element-mediated binding site duplication.* Nucleic Acids Res, 2006. **34**(14): p. 3862-77.
245. Obendorf, M., et al., *FoxG1, a member of the forkhead family, is a corepressor of the androgen receptor.* J Steroid Biochem Mol Biol, 2007. **104**(3-5): p. 195-207.
246. Hui, C.C., et al., *Expression of three mouse homologs of the Drosophila segment polarity gene cubitus interruptus, Gli, Gli-2, and Gli-3, in ectoderm- and mesoderm-derived tissues suggests multiple roles during postimplantation development.* Dev Biol, 1994. **162**(2): p. 402-13.
247. Ohtsuka, T., et al., *Hes1 and Hes5 as notch effectors in mammalian neuronal differentiation.* Embo J, 1999. **18**(8): p. 2196-207.
248. Jen, Y., K. Manova, and R. Benezra, *Expression patterns of Id1, Id2, and Id3 are highly related but distinct from that of Id4 during mouse embryogenesis.* Dev Dyn, 1996. **207**(3): p. 235-52.
249. Engelkamp, D., et al., *Role of Pax6 in development of the cerebellar system.* Development, 1999. **126**(16): p. 3585-96.
250. Kolk, S.M., et al., *A unique subpopulation of Tbr1-expressing deep layer neurons in the developing cerebral cortex.* Mol Cell Neurosci, 2006. **32**(1-2): p. 200-14.
251. Tsao, S.W., et al., *Characterization of human ovarian surface epithelial cells immortalized by human papilloma viral oncogenes (HPV-E6E7 ORFs).* Exp Cell Res, 1995. **218**(2): p. 499-507.
252. Hebert, J.M. and S.K. McConnell, *Targeting of cre to the Foxg1 (BF-1) locus mediates loxP recombination in the telencephalon and other developing head structures.* Dev Biol, 2000. **222**(2): p. 296-306.
253. Li, E., T.H. Bestor, and R. Jaenisch, *Targeted mutation of the DNA methyltransferase gene results in embryonic lethality.* Cell, 1992. **69**(6): p. 915-26.

254. Mao, X., Y. Fujiwara, and S.H. Orkin, *Improved reporter strain for monitoring Cre recombinase-mediated DNA excisions in mice.* Proc Natl Acad Sci U S A, 1999. **96**(9): p. 5037-42.
255. Jensen, A.M. and V.A. Wallace, *Expression of Sonic hedgehog and its putative role as a precursor cell mitogen in the developing mouse retina.* Development, 1997. **124**(2): p. 363-71.
256. Sambrook, J., E. Fritsch, F., and T. Maniatis, *Molecular Cloning: A Laboratory Manual, 2nd edt.* 1989, Cold Spring Harbour, NY: Cold Spring Harbour Laboratoy Press.
257. Inoue, H., H. Nojima, and H. Okayama, *High efficiency transformation of Escherichia coli with plasmids.* Gene, 1990. **96**(1): p. 23-8.
258. Chomczynski, P. and N. Sacchi, *Single-step method of RNA isolation by acid guanidinium thiocyanate-phenol-chloroform extraction.* Anal Biochem, 1987. **162**(1): p. 156-9.
259. Yip, D.J. and D.J. Picketts, *Increasing D4Z4 repeat copy number compromises C2C12 myoblast differentiation.* FEBS Lett, 2003. **537**(1-3): p. 133-8.
260. Berube, N.G., C.A. Smeenk, and D.J. Picketts, *Cell cycle-dependent phosphorylation of the ATRX protein correlates with changes in nuclear matrix and chromatin association.* Hum Mol Genet, 2000. **9**(4): p. 539-47.
261. Reyes, J.C., C. Muchardt, and M. Yaniv, *Components of the human SWI/SNF complex are enriched in active chromatin and are associated with the nuclear matrix.* J Cell Biol, 1997. **137**(2): p. 263-74.
262. Zhou, Q.P., et al., *Identification of a direct Dlx homeodomain target in the developing mouse forebrain and retina by optimization of chromatin immunoprecipitation.* Nucleic Acids Res, 2004. **32**(3): p. 884-92.
263. Boutillier, A.L., E. Trinh, and J.P. Loeffler, *Selective E2F-dependent gene transcription is controlled by histone deacetylase activity during neuronal apoptosis.* J Neurochem, 2003. **84**(4): p. 814-28.
264. Cartharius, K., et al., *MatInspector and beyond: promoter analysis based on transcription factor binding sites.* Bioinformatics, 2005. **21**(13): p. 2933-42.
265. Rozen, S. and H. Skaletsky, *Primer3 on the WWW for general users and for biologist programmers.* Methods Mol Biol, 2000. **132**: p. 365-86.
266. Altschul, S.F., et al., *Gapped BLAST and PSI-BLAST: a new generation of protein database search programs.* Nucleic Acids Res, 1997. **25**(17): p. 3389-402.
267. He, D.C., J.A. Nickerson, and S. Penman, *Core filaments of the nuclear matrix.* J Cell Biol, 1990. **110**(3): p. 569-80.
268. Han, J., et al., *A MAP kinase targeted by endotoxin and hyperosmolarity in mammalian cells.* Science, 1994. **265**(5173): p. 808-11.
269. Mendelson, E. and M. Bustin, *Monoclonal antibodies against distinct determinants of histone H5 bind to chromatin.* Biochemistry, 1984. **23**(15): p. 3459-66.
270. Kwek, S.S., et al., *Functional analysis and intracellular localization of p53 modified by SUMO-1.* Oncogene, 2001. **20**(20): p. 2587-99.
271. Hirose, M., et al., *Molecular dissection of the Rho-associated protein kinase (p160ROCK)-regulated neurite remodeling in neuroblastoma N1E-115 cells.* J Cell Biol, 1998. **141**(7): p. 1625-36.

272. Greene, J.J. and C.I. Brophy, *Induction of protein disulfide isomerase during proliferation arrest and differentiation of SH5Y neuroblastoma cells.* Cell Mol Biol (Noisy-le-grand), 1995. **41**(4): p. 473-80.
273. Land, H., L.F. Parada, and R.A. Weinberg, *Tumorigenic conversion of primary embryo fibroblasts requires at least two cooperating oncogenes.* Nature, 1983. **304**(5927): p. 596-602.
274. Williams, R.W., *Mapping genes that modulate mouse brain development: a quantitative genetic approach.* Results Probl Cell Differ, 2000. **30**: p. 21-49.
275. Caviness, V.S., Jr., *Architectonic map of neocortex of the normal mouse.* J Comp Neurol, 1975. **164**(2): p. 247-63.
276. Takahashi, E., et al., *Neuron-specific expression of reporter gene in transgenic mice carrying the 5'-upstream region of mouse P/Q-type Ca2+ channel alpha 1A subunit gene fused to E. coli lacZ reporter gene.* Brain Res, 1999. **850**(1-2): p. 47-54.
277. Poucet, B., et al., *Spatial navigation and hippocampal place cell firing: the problem of goal encoding.* Rev Neurosci, 2004. **15**(2): p. 89-107.
278. Gilbert, P.E. and A.M. Brushfield, *The role of the CA3 hippocampal subregion in spatial memory: A process oriented behavioral assessment.* Prog Neuropsychopharmacol Biol Psychiatry, 2009.
279. Caviness, V.S., Jr., T. Takahashi, and R.S. Nowakowski, *Numbers, time and neocortical neuronogenesis: a general developmental and evolutionary model.* Trends Neurosci, 1995. **18**(9): p. 379-83.
280. Rakic, P., *Radial versus tangential migration of neuronal clones in the developing cerebral cortex.* Proc Natl Acad Sci U S A, 1995. **92**(25): p. 11323-7.
281. Englund, C., et al., *Pax6, Tbr2, and Tbr1 are expressed sequentially by radial glia, intermediate progenitor cells, and postmitotic neurons in developing neocortex.* J Neurosci, 2005. **25**(1): p. 247-51.
282. Dwyer, N.D. and D.D. O'Leary, *Tbr1 conducts the orchestration of early cortical development.* Neuron, 2001. **29**(2): p. 309-11.
283. Havrda, M.C., et al., *Id2 is required for specification of dopaminergic neurons during adult olfactory neurogenesis.* J Neurosci, 2008. **28**(52): p. 14074-86.
284. Donovan, S.L. and M.A. Dyer, *Regulation of proliferation during central nervous system development.* Semin Cell Dev Biol, 2005. **16**(3): p. 407-21.
285. Rakic, P., *Radial unit hypothesis of neocortical expansion.* Novartis Found Symp, 2000. **228**: p. 30-42; discussion 42-52.
286. Kuan, C.Y., R.A. Flavell, and P. Rakic, *Programmed cell death in mouse brain development.* Results Probl Cell Differ, 2000. **30**: p. 145-62.
287. Kuan, C.Y., et al., *Mechanisms of programmed cell death in the developing brain.* Trends Neurosci, 2000. **23**(7): p. 291-7.
288. Ferguson, K.L., et al., *Telencephalon-specific Rb knockouts reveal enhanced neurogenesis, survival and abnormal cortical development.* Embo J, 2002. **21**(13): p. 3337-46.
289. Scholzen, T. and J. Gerdes, *The Ki-67 protein: from the known and the unknown.* J Cell Physiol, 2000. **182**(3): p. 311-22.
290. Verdugo, R.A. and J.F. Medrano, *Comparison of gene coverage of mouse oligonucleotide microarray platforms.* BMC Genomics, 2006. **7**: p. 58.

291. Siegenthaler, J.A., B.A. Tremper-Wells, and M.W. Miller, *Foxg1 haploinsufficiency reduces the population of cortical intermediate progenitor cells: effect of increased p21 expression.* Cereb Cortex, 2008. **18**(8): p. 1865-75.
292. Fasano, C.A., et al., *Bmi-1 cooperates with Foxg1 to maintain neural stem cell self-renewal in the forebrain.* Genes Dev, 2009. **23**(5): p. 561-74.
293. Dou, C.L., S. Li, and E. Lai, *Dual role of brain factor-1 in regulating growth and patterning of the cerebral hemispheres.* Cereb Cortex, 1999. **9**(6): p. 543-50.
294. Huttner, W.B. and Y. Kosodo, *Symmetric versus asymmetric cell division during neurogenesis in the developing vertebrate central nervous system.* Curr Opin Cell Biol, 2005. **17**(6): p. 648-57.
295. Petersson, S., et al., *Truncation of the Shaker-like voltage-gated potassium channel, Kv1.1, causes megencephaly.* Eur J Neurosci, 2003. **18**(12): p. 3231-40.
296. Whitehouse, I., et al., *Chromatin remodelling at promoters suppresses antisense transcription.* Nature, 2007. **450**(7172): p. 1031-5.
297. Harper, J.W., et al., *The p21 Cdk-interacting protein Cip1 is a potent inhibitor of G1 cyclin-dependent kinases.* Cell, 1993. **75**(4): p. 805-16.
298. Lee, M.H., I. Reynisdottir, and J. Massague, *Cloning of p57KIP2, a cyclin-dependent kinase inhibitor with unique domain structure and tissue distribution.* Genes Dev, 1995. **9**(6): p. 639-49.
299. Nakayama, K., et al., *Mice lacking p27(Kip1) display increased body size, multiple organ hyperplasia, retinal dysplasia, and pituitary tumors.* Cell, 1996. **85**(5): p. 707-20.
300. Serrano, M., G.J. Hannon, and D. Beach, *A new regulatory motif in cell-cycle control causing specific inhibition of cyclin D/CDK4.* Nature, 1993. **366**(6456): p. 704-7.
301. Hannon, G.J. and D. Beach, *p15INK4B is a potential effector of TGF-beta-induced cell cycle arrest.* Nature, 1994. **371**(6494): p. 257-61.
302. Hirai, H., et al., *Novel INK4 proteins, p19 and p18, are specific inhibitors of the cyclin D-dependent kinases CDK4 and CDK6.* Mol Cell Biol, 1995. **15**(5): p. 2672-81.
303. Jiang, H., et al., *Induction of differentiation in human promyelocytic HL-60 leukemia cells activates p21, WAF1/CIP1, expression in the absence of p53.* Oncogene, 1994. **9**(11): p. 3397-406.
304. Steinman, R.A., et al., *Induction of p21 (WAF-1/CIP1) during differentiation.* Oncogene, 1994. **9**(11): p. 3389-96.
305. Deng, C., et al., *Mice lacking p21CIP1/WAF1 undergo normal development, but are defective in G1 checkpoint control.* Cell, 1995. **82**(4): p. 675-84.
306. Kippin, T.E., D.J. Martens, and D. van der Kooy, *p21 loss compromises the relative quiescence of forebrain stem cell proliferation leading to exhaustion of their proliferation capacity.* Genes Dev, 2005. **19**(6): p. 756-67.
307. Fero, M.L., et al., *A syndrome of multiorgan hyperplasia with features of gigantism, tumorigenesis, and female sterility in p27(Kip1)-deficient mice.* Cell, 1996. **85**(5): p. 733-44.
308. Kiyokawa, H., et al., *Enhanced growth of mice lacking the cyclin-dependent kinase inhibitor function of p27(Kip1).* Cell, 1996. **85**(5): p. 721-32.
309. Roy, K., et al., *The Tlx gene regulates the timing of neurogenesis in the cortex.* J Neurosci, 2004. **24**(38): p. 8333-45.

310. Li, W., et al., *Nuclear receptor TLX regulates cell cycle progression in neural stem cells of the developing brain.* Mol Endocrinol, 2008. **22**(1): p. 56-64.
311. Smart, I.H., *Proliferative characteristics of the ependymal layer during the early development of the mouse neocortex: a pilot study based on recording the number, location and plane of cleavage of mitotic figures.* J Anat, 1973. **116**(Pt 1): p. 67-91.
312. McConnell, S.K., *The determination of neuronal fate in the cerebral cortex.* Trends Neurosci, 1989. **12**(9): p. 342-9.
313. Falk, S., et al., *Brain area-specific effect of TGF-beta signaling on Wnt-dependent neural stem cell expansion.* Cell Stem Cell, 2008. **2**(5): p. 472-83.
314. Ko, L., A. Koestner, and W. Wechsler, *Characterization of cell cycle and biological parameters of transplantable glioma cell lines and clones.* Acta Neuropathol, 1980. **51**(2): p. 107-11.
315. Quinn, J.C., et al., *Pax6 controls cerebral cortical cell number by regulating exit from the cell cycle and specifies cortical cell identity by a cell autonomous mechanism.* Dev Biol, 2007. **302**(1): p. 50-65.
316. Kriegstein, A.R. and M. Gotz, *Radial glia diversity: a matter of cell fate.* Glia, 2003. **43**(1): p. 37-43.
317. Gotz, M., A. Stoykova, and P. Gruss, *Pax6 controls radial glia differentiation in the cerebral cortex.* Neuron, 1998. **21**(5): p. 1031-44.
318. Estivill-Torrus, G., et al., *Pax6 is required to regulate the cell cycle and the rate of progression from symmetrical to asymmetrical division in mammalian cortical progenitors.* Development, 2002. **129**(2): p. 455-66.
319. Chenn, A. and C.A. Walsh, *Regulation of cerebral cortical size by control of cell cycle exit in neural precursors.* Science, 2002. **297**(5580): p. 365-9.
320. Chenn, A. and C.A. Walsh, *Increased neuronal production, enlarged forebrains and cytoarchitectural distortions in beta-catenin overexpressing transgenic mice.* Cereb Cortex, 2003. **13**(6): p. 599-606.
321. Lobjois, V., et al., *Forcing neural progenitor cells to cycle is insufficient to alter cell-fate decision and timing of neuronal differentiation in the spinal cord.* Neural Dev, 2008. **3**: p. 4.
322. Takahashi, T., et al., *Sequence of neuron origin and neocortical laminar fate: relation to cell cycle of origin in the developing murine cerebral wall.* J Neurosci, 1999. **19**(23): p. 10357-71.
323. Muzio, L. and A. Mallamaci, *Foxg1 confines Cajal-Retzius neuronogenesis and hippocampal morphogenesis to the dorsomedial pallium.* J Neurosci, 2005. **25**(17): p. 4435-41.
324. Tao, W. and E. Lai, *Telencephalon-restricted expression of BF-1, a new member of the HNF-3/fork head gene family, in the developing rat brain.* Neuron, 1992. **8**(5): p. 957-66.
325. Bourguignon, C., J. Li, and N. Papalopulu, *XBF-1, a winged helix transcription factor with dual activity, has a role in positioning neurogenesis in Xenopus competent ectoderm.* Development, 1998. **125**(24): p. 4889-900.
326. Hanashima, C., et al., *Brain factor-1 controls the proliferation and differentiation of neocortical progenitor cells through independent mechanisms.* J Neurosci, 2002. **22**(15): p. 6526-36.
327. Adesina, A.M., et al., *FOXG1 dysregulation is a frequent event in medulloblastoma.* J Neurooncol, 2007. **85**(2): p. 111-22.

328. Sherriff, J.A., N.A. Kent, and J. Mellor, *The Isw2 chromatin-remodeling ATPase cooperates with the Fkh2 transcription factor to repress transcription of the B-type cyclin gene CLB2.* Mol Cell Biol, 2007. **27**(8): p. 2848-60.
329. Ahlgren, S., P. Vogt, and M. Bronner-Fraser, *Excess FoxG1 causes overgrowth of the neural tube.* J Neurobiol, 2003. **57**(3): p. 337-49.
330. Shen, L., et al., *FoxG1 haploinsufficiency results in impaired neurogenesis in the postnatal hippocampus and contextual memory deficits.* Hippocampus, 2006. **16**(10): p. 875-90.
331. Sessa, A., et al., *Tbr2 directs conversion of radial glia into basal precursors and guides neuronal amplification by indirect neurogenesis in the developing neocortex.* Neuron, 2008. **60**(1): p. 56-69.
332. Cappello, S., et al., *The Rho-GTPase cdc42 regulates neural progenitor fate at the apical surface.* Nat Neurosci, 2006. **9**(9): p. 1099-107.
333. Hebert, J.M. and G. Fishell, *The genetics of early telencephalon patterning: some assembly required.* Nat Rev Neurosci, 2008. **9**(9): p. 678-85.
334. Danesin, C., et al., *Integration of telencephalic Wnt and hedgehog signaling center activities by Foxg1.* Dev Cell, 2009. **16**(4): p. 576-87.
335. Garrick, D., et al., *Loss of Atrx affects trophoblast development and the pattern of X-inactivation in extraembryonic tissues.* PLoS Genet, 2006. **2**(4): p. e58.
336. Itoh, T., K. Miyake, and S. Iijima, *Differentiation-specific expression of chromatin remodeling factor BRM.* Biochem Biophys Res Commun, 2008. **366**(3): p. 827-33.
337. Inayoshi, Y., et al., *Mammalian chromatin remodeling complex SWI/SNF is essential for enhanced expression of the albumin gene during liver development.* J Biochem, 2006. **139**(2): p. 177-88.
338. Xi, R., D. Kirilly, and T. Xie, *Molecular mechanisms controlling germline and somatic stem cells: similarities and differences.* Curr Opin Genet Dev, 2005. **15**(4): p. 381-7.
339. Xi, R. and T. Xie, *Stem cell self-renewal controlled by chromatin remodeling factors.* Science, 2005. **310**(5753): p. 1487-9.
340. Cheung, M., et al., *Roles of Sox4 in central nervous system development.* Brain Res Mol Brain Res, 2000. **79**(1-2): p. 180-91.
341. Huang, D.Y., et al., *Transcription factor SOX-5 enhances nasopharyngeal carcinoma progression by down-regulating SPARC gene expression.* J Pathol, 2008. **214**(4): p. 445-55.
342. Smits, P., et al., *Sox5 and Sox6 are needed to develop and maintain source, columnar, and hypertrophic chondrocytes in the cartilage growth plate.* J Cell Biol, 2004. **164**(5): p. 747-58.
343. Pevny, L.H., et al., *A role for SOX1 in neural determination.* Development, 1998. **125**(10): p. 1967-78.
344. Hoser, M., et al., *Prolonged glial expression of Sox4 in the CNS leads to architectural cerebellar defects and ataxia.* J Neurosci, 2007. **27**(20): p. 5495-505.
345. Sinner, D., et al., *Sox17 and Sox4 differentially regulate beta-catenin/T-cell factor activity and proliferation of colon carcinoma cells.* Mol Cell Biol, 2007. **27**(22): p. 7802-15.
346. Kwan, K.Y., et al., *SOX5 postmitotically regulates migration, postmigratory differentiation, and projections of subplate and deep-layer neocortical neurons.* Proc Natl Acad Sci U S A, 2008. **105**(41): p. 16021-6.

347. Borello, U., et al., *FGF15 promotes neurogenesis and opposes FGF8 function during neocortical development.* Neural Dev, 2008. **3**: p. 17.
348. Gao, X., et al., *ES cell pluripotency and germ-layer formation require the SWI/SNF chromatin remodeling component BAF250a.* Proc Natl Acad Sci U S A, 2008. **105**(18): p. 6656-61.
349. Siriaco, G., et al., *Drosophila ISWI Regulates the Association of Histone H1 With Interphase Chromosomes in vivo.* Genetics, 2009.
350. Burgio, G., et al., *Genetic identification of a network of factors that functionally interact with the nucleosome remodeling ATPase ISWI.* PLoS Genet, 2008. **4**(6): p. e1000089.
351. Brune, C.W., et al., *Heterogeneous association between engrailed-2 and autism in the CPEA network.* Am J Med Genet B Neuropsychiatr Genet, 2008. **147B**(2): p. 187-93.
352. Gharani, N., et al., *Association of the homeobox transcription factor, ENGRAILED 2, 3, with autism spectrum disorder.* Mol Psychiatry, 2004. **9**(5): p. 474-84.
353. Morgan, R., *Engrailed: complexity and economy of a multi-functional transcription factor.* FEBS Lett, 2006. **580**(11): p. 2531-3.
354. Kuemerle, B., et al., *The mouse Engrailed genes: a window into autism.* Behav Brain Res, 2007. **176**(1): p. 121-32.
355. Cheh, M.A., et al., *En2 knockout mice display neurobehavioral and neurochemical alterations relevant to autism spectrum disorder.* Brain Res, 2006. **1116**(1): p. 166-76.
356. Mosconi, M.W., et al., *Longitudinal study of amygdala volume and joint attention in 2- to 4-year-old children with autism.* Arch Gen Psychiatry, 2009. **66**(5): p. 509-16.
357. White, S., H. O'Reilly, and U. Frith, *Big heads, small details and autism.* Neuropsychologia, 2009. **47**(5): p. 1274-81.
358. Ariani, F., et al., *FOXG1 is responsible for the congenital variant of Rett syndrome.* Am J Hum Genet, 2008. **83**(1): p. 89-93.
359. Mencarelli, M.A., et al., *14q12 Microdeletion syndrome and congenital variant of Rett syndrome.* Eur J Med Genet, 2009. **52**(2-3): p. 148-52.
360. Spruill, L.S., et al., *Selective translation of mRNAs in the left ventricular myocardium of the mouse in response to acute pressure overload.* J Mol Cell Cardiol, 2008. **44**(1): p. 69-75.

Appendix:

Appendix I: Oligonucleotide Sequences.

Genotyping Primers

B-actin (positive control);
Forward 5'ctgaaccctaaggccaaccgt 3' Reverse 5'ccgtcaggcagctcatagctcttc 3'

Fabp1 (positive control);
Forward 5'tggacaggactggacctctgctttcctaga 3'
Reverse 5'tagagctttgccacatcacaggtcattcag 3'

Sry (sex specification);
Forward 5'ttgtctagagagcatggagggccatgtcaaa 3'
Reverse 5'ccactcctctgtgacactttaggcctccga 3'

Snf2L (Mulitplex, Floxed Exon 6 Genotyping);
2L-Forward 5'tagacagctatgagcctcttg 3' 2L-Reverse 5'taaagtcttcccaagaccctg 3'
Cre-Forward 5'tgctctgtccgtttgccg 3' Cre-Reverse 5'actgtgtccagaccaggc 3'
Neo-Forward 5'gatcggccattgaacaagat 3' Neo-Reverse 5'ccaccatgatattcggcaag 3'

Snf2L (Multiplex, Ex6DEL Genotyping);
1-Forward 5'ccatgtggggtccaggaatg 3' Reverse 5'gtatggacaagtgtgtgaagcc 3'
2-Forward 5'cctgggctggaaccatgatc 3'

Snf2H (Muliplex, deleted Snf2H);
Forward 5'gatttctgatagggttagaagc 3' 1-Reverse 5'tgtaaggcaagggagaactg 3'
2-Reverse 5'cctcctatcccctacatattaccctagcc 3'

Cre-recombinase (used to identify Foxg1 Heterozygous);
Cre-Forward 5'tgctctgtccgtttgccg 3' Cre-Reverse 5'actgtgtccagaccaggc 3'

Sequencing Primers

Snf2H (*Snf2h* coding sequence);
Forward 5' gaccgggcaaatagattcg 3' Reverse 5' tccaagaaccagatcctacc 3'
Forward 5' gtgctgagatgaaactcag 3' Reverse 5' gcaagatggacaaaatgagg 3'
Forward 5' gaacaaggttcacgagtac 3' Reverse 5' caacggatagtaagttctg 3'
Forward 5' cgaggaccaaagccttcaac 3 Reverse 5' cctttgcattttgctgagg 3'
Forward 5' gatcgttttctgatttgtatg 3' Reverse 5' aggtaggatctggttcttgg 3'
Forward 5' cacgtttatttgaattactgg 3'
Forward 5' ttcagcagatgactttgattcc 3'
Forward 5' acgaaggaggaatggacgcaaaacc 3'

Snf2L (*Snf2L* coding sequence):

Forward 5'ccggaattcatggacccagaatatgaagag 3'	Reverse 5'caaccaattcagtcctcgaatctg 3'
Forward 5'cggagacaaggatgccagagc 3'	Reverse 5' ttctaggctttaggatttc 3'
Forward 5'gcttgctcctaactggaac 3'	Reverse 5' gtggctccatgccgtatc 3'
Forward 5' ctggtccaccttataccac 3'	Reverse 5' gtaagaggttcagctccatc 3'
Forward 5' gtacttagcataaagatg 3'	Reverse 5' atggagccttgtatcttg 3'
Forward 5' caagctatggatcgagcac 3'	Reverse 5' ttctaggctttaggatttc 3'
Forward 5' gagactgagttgacagatgaag 3'	
Forward 5' ataacctgcatgaactgtgggc 3'	

Semi-quantitative RT-PCR Primers

Snf2l (mouse cDNA);

Forward 5'cctctcaacatgaaactggc 3'	Reverse 5'tcacgcaaacatcccactct 3'

Snf2h (mouse cDNA);

Forward 5'cctgtgagcttcatctataac 3'	Reverse 5'gcgaggattgaattggctc 3'

Bactin (positive control);

Forward 5'ctgaaccctaaggccaaccgt 3'	Reverse 5'ccgtcaggcagctcatagctcttc 3'

Gapdh (positive control);

Forward 5'gcccgcaccaaccatgcc 3'	Reverse 5'ccgggctggggccccagg 3'

Engrailed 1 (known target of Nurf);

Forward 5'catgccaaactgcttacgac 3'	Reverse 5' gcagacacacaaggaaacac 3'

Engrailed 2 (known target of Nurf);

Forward 5'gttctttgctgaggtctgag 3'	Reverse 5' ggaagatgattccaactcgc 3'

Quantitative "Realtime" PCR Primers

18s (loading control);

Forward 5'cggctaccacatccaagg 3'	Reverse 5'ctggaattaccgcggct 3'

p21;

Forward 5'gtccaatcctggtgagtcc 3'	Reverse 5'gttttcggccctgagatgt 3'

p16ink4a;

Forward 5'aagcgaactcgaggagagc 3'	Reverse 5'gtacgaccgaaagagttcg 3'

p27;

Forward 5`cctgactcgtcagacaattcc 3' Reverse 5'tgttctgttggccctttg 3'

p57;
Forward 5`cagatgcccagcaagttctc 3' Reverse 5'ctctccaaacgtggctcct 3'

p107 (rbl1);
Forward 5'aaactgacatcacaggccag 3' Reverse 5'gggtggtgactgcctct 3'

Akt3;
Forward 5'agaggcaagaggaggaggagg 3' Reverse 5'ccattgccttctctcgaac 3'

Bmi1;
Forward 5' tgtccaggttcacaaaacca 3' Reverse 5'cgggtgagctgcataaaat 3'

Brd4;
Forward 5'gcctttcagcagcacctcacttc 3' Reverse 5'gctcctgcttctgtttgtcc 3'

Cam2ka;
Forward 5'tctgagagcaccaacaccac 3' Reverse 5'ccattgcttatggcttcgat 3'

Cbx3;
Forward 5'gagatgctgctgacaaacca 3' Reverse 5'gctcctcgtagaaggcaatg 3'

Caspase 3;
Forward 5'gggcctgttgaactgaaaaa 3' Reverse 5'ccgtcctttgaatttctcca 3'

Cdk2;
Forward 5`aaatgcacctagtgtgtaccc 3' Reverse 5`gggtgtggggcagaca 3'

CyclinB2;
Forward 5'ctagctcccaaggatcgtcc 3' Reverse 5'gttctccctgtcctcgttatctat 3'

CyclinD1;
Forward 5`cggatgagaacaagcagacc 3' Reverse 5`gagggtgggtggaaatga 3'

CyclinD2;
Forward 5`tcccgcagtgttcctatttc 3' Reverse 5`ggtaattcatggccagagga 3'

Dct;
Forward 5'agcagacggaacactggact 3' Reverse 5'gcatctgtggaagggtgtt 3'

Dkk2;
Forward 5'accagagtggacaggtggtc 3' Reverse 5'tcactgtctcgggtgcatag 3'

Fgf15;

Forward 5`aagaacagctccaggaccaga 3' Reverse 5`tccatgctgtcactctccag 3'

Foxg1;
Forward 5'ctactccctcaacccctgct 3' Reverse 5'cagacagtcccccagacagt 3'

Frzb;
Forward 5'caagggacaccgtcaatctt 3' Reverse 5'cgatccttccacttctcagc 3'

Gapdh (loading control);
Forward 5'tgaaaggggtcgttgatgg 3' Reverse 5'aaaatggtgaaggtcggtgt 3'

Gli1;
Forward 5'cactacctggcctcacacct 3' Reverse 5'gtactcggttcggcttctcc 3'

Gli2;
Forward 5' aatggggataatgaggccag 3' Reverse 5'gtcttgatggctttgatatgt 3'

Gli3;
Forward 5'agcaaccaggagcctgaagtc 3' Reverse 5'gtcttgagtaggcttttgtgc 3'

Hes1;
Forward 5`aaagacggcctctgagcaca 3' Reverse 5`tcatggcgttgatctgggtca 3'

Hes5;
Forward 5`aagagcctgcaccaggacta 3' Reverse 5`cgctggaagtggtaaagca 3'

Hox3a;
Forward 5'cacctggaactggagaccat 3' Reverse 5'accgtagatcgctgagctgt 3'

Irx6;
Forward 5'aggctgagtgagtgacctggaaga 3' Reverse 5'gattgtggggcctcagtaaa 3'

Jairid7a;
Forward 5'gccacacttgaggccataat 3' Reverse 5'ctccaggagtgtgctgtcaa 3'

Mab112;
Forward 5'aaggaagtggaggtgcaaaga 3' Reverse 5'gtagccagacgctgtgatga 3'

Mash1;
Forward 5'catctcccccaactactcca 3' Reverse 5'caaagtccattcccaggaga 3'

NeuroD1;
Forward 5'gaacacgcggcagacaagaaaga 3' Reverse 5'ctcccccgtttctcagagagt 3'

Nrgn;
Forward 5'ccaagccagacgacgatatt 3' Reverse 5'aaacgttcagctctggccta 3'

Numb;
Forward 5'cggggaaagaaagcagtgaag 3' Reverse 5'agtggtgccatcacgacata 3'

Patched1;
Forward 5`ggtacctgtaaaggggtaaagttttcggatcc 3'
Reverse 5`atttgcctcattgctgatgcatgtggtacc 3'

Pax6;
Forward 5' gtgctggacaatgaaaacgtat 3' Reverse 5' ggctattttgcttacaacttctgg 3'

Poufl;
Forward 5'ctgtcaggaagccaaacaca 3' Reverse 5'ctcatccagacttggggtgt 3'

Postn;
Forward 5'agtgctctgaggccatcact 3' Reverse 5'aggtcggtaaagtggtttg 3'

Ptprs;
Forward 5'gaggccaagtcagagaccag 3' Reverse 5'cggaacgcatactccgtatt 3'

Reelin;
Forward 5'gaggaatctgtgaccctgga 3' Reverse 5'gtggctcttttgcctgagac 3'

Shh;
Forward 5`gcaccccaaaaagctgac 3' Reverse 5`aatcgttcggagtttcttgtg 3'

Snf2l (mouse cDNA);
Forward 5'cctctcaacatgaaactggc 3' Reverse 5'tcacgcaaacatcccactct 3'

Snf2h (mouse cDNA);
Forward 5'cctgtgagcttcatctataac 3' Reverse 5'gcgaggattgaattggctc 3'

Sp8;
Forward 5'tcgggagaaactgagcatagc 3' Reverse 5'actggaacccactacgttgc 3'

Spry2;
Forward 5'acatcgctggaagaagagga 3' Reverse 5'ctgggtaagggcatctcttg 3'

Realtime Chromatin Immunoprecipitation Primers

Cdc2 Promoter (positive control for p107 ChIP);
Forward 5' agtcagttggcgcccgccct 3' Reverse 5'cacaccgcagttccggactg 3'

FoxG1 proxomal region Primer sets;

Rxn1-Forward 5'aatgctggcatgggtagagt 3' Reverse 5'cagtagggcgaaatcagct 3'
Rxn2-Forward 5'gccgcaggaagctgtaagta 3' Reverse 5'ctagccgtcgaccaatcg 3'

Rxn3-Forward 5'ggctagccagacgctcct 3' Reverse 5'gcatgtagcaaaagctgcaa 3'
Rxn4-Forward 5'acaattttcaagccgccata 3' Reverse 5'tcatttcgatgtaaaatttgctg 3'
Rxn5-Forward 5'atacccacgtttggcacttt 3' Reverse 5'tcgtagtcggtctagcgtga 3'
Rxn6-Forward 5'tcacgctagaccgactacga 3' Reverse 5'tttgtccccaaatatccttcc 3'
Rxn7-Forward 5'tggaaggatatttggggaca 3' Reverse 5'cacaaatcctcactggctca 3'
Rxn8-Forward 5'gatctgtgtgctccgcacta 3' Reverse 5'cactccacctcctcttcagc 3'
Rxn9-Forward 5'gagctgattcgccctacg 3' Reverse 5'caggccggtacttacttacgctt 3'

Gapdh Promoter (nonspecific promter control);
Forward 5'aagccaaactagcagctagg 3' Reverse 5'gggctagtctatcattgcag 3'

Mutagenic Primers
Snf2H (for the generation of non-functional ATPase);
Forward 5'ggaaaagagaagcttctaAcacagggatttacc 3'
Reverse 5'ggtaaatccctgtgTtagaagcttctcttttcc 3'

Appendix II: The Snf2l gene targeting strategy, in vitro and in vivo analysis.

[A] A schematic diagram of the *mSfn2l* gene demonstrating the 24 exons; exons that generate the catalytic helicase domains (blue) and the SANT domains (green) are shown, exon 6, which was chosen for excision, is highlighted (yellow). The *Neomycin resistance* gene (*Neo*, blue) was introduced for selection. [B] *mSnf2l* genomic sequence (wt) with the targeting vector and homologous recombinant (hr). Location of the LoxP sites (green triangles); *Sac1* (s) and *HindIII* (H) restriction endonuclease sites are shown. [C] Southern blot analysis of wildtype ES cells and recombinant ES clone #105 DNA (probe location (red) and predicted band sizes are shown in [B]). [D] Two males chimeras were generated by blastocyst injection (top panel) with 80% and 20% transfer efficiency/ the first litters generated by these chimeras crossed onto the CD-1 strain are shown (bottom panel). [E] Sample genotyping PCR analysis for positive floxed mice.

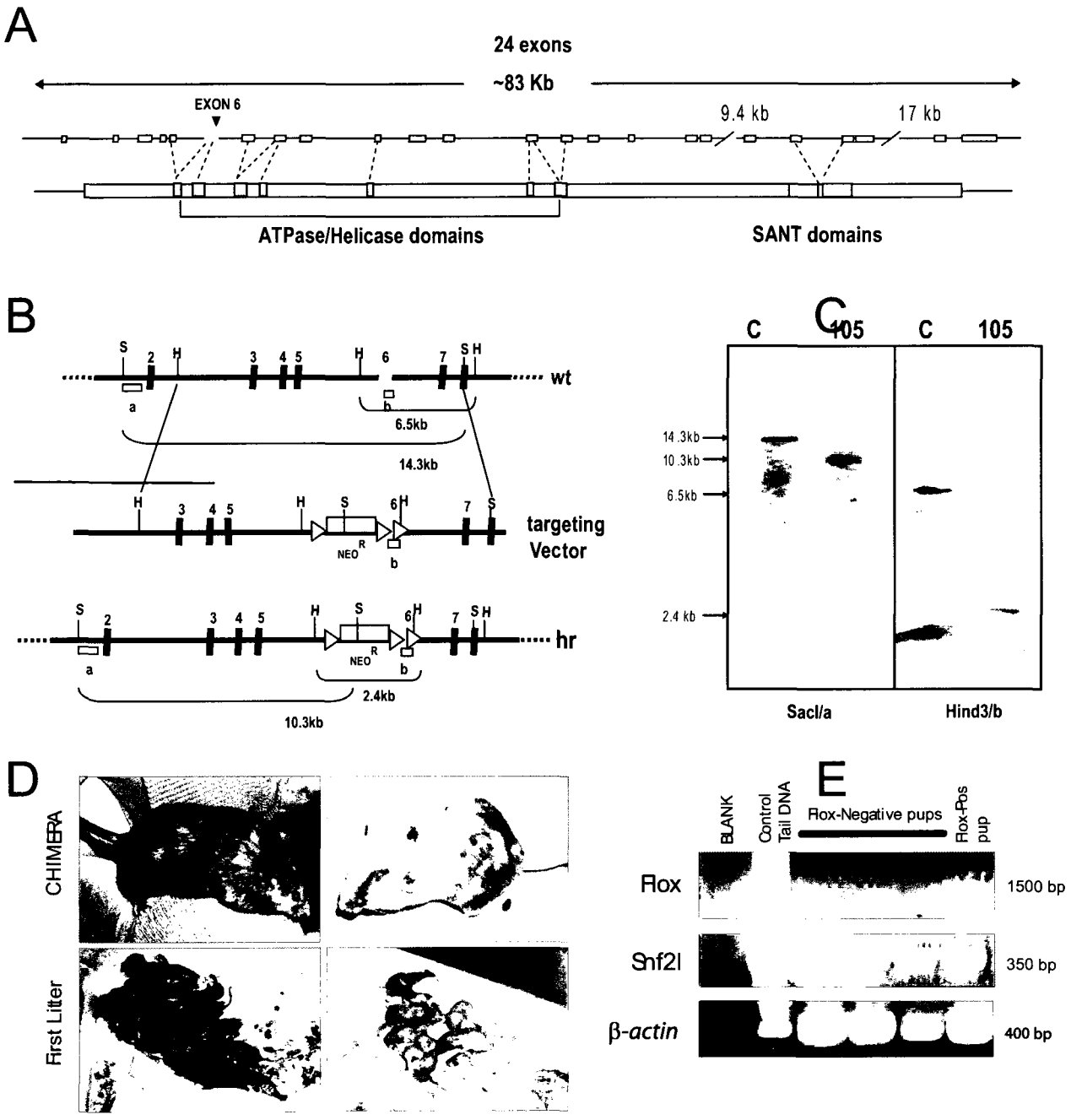
A
24 exons
~83 Kb
EXON 6
9.4 kb
17 kb
ATPase/Helicase domains
SANT domains
B
wt
6.5kb
14.3kb
targeting
Vector
NEO
hr
2.4kb
10.3kb
C
C
105
C
105
14.3kb
10.3kb
6.5kb
2.4 kb
SacI/a
Hind3/b
D
CHIMERA
First Litter
E
BLANK
Control
Tail DNA
Rox-Negative pups
Rox-Pos
pup
Rox
Snf2l
β-actin
1500 bp
350 bp
400 bp

Appendix III: Polysome fractionation by layered continuous sucrose gradient of cell lysates shows expression of Snf2l $^{\pm}$ exon 13 by RT-PCR.

Both of the *SNF2L* exon 13 splice variants are translated. In order to determine if there was a disproportionate selection of active or inactive SNF2L transcripts (+/- exon 13) a polysome fractionation was performed. It has been shown previously that the amount of transcript that is incorporated into polysomes is an accurate indicator for relative level of translation [360]. In order to determine if these messages are translated a polysome fractionation for RNA from three cell lines the hepatic HEPG2, kidney 293-T and neuronal SH-SY5Y was performed. An A_{254} profile (top panel) of polysomes obtained from cultured HEPG2 cell lysates fractionated by density ultracentrifugation over a 10 mL continuous layered sucrose gradient. Cells were treated with CHX at 100 μg/mL (37°C, 3 min) and lysed. RNA (HEPG2, HEK 293-T, SH-SY5Y) extracted from pooled fractions A (Cell Debris including small molecules and fragmented ribosomes), B-C (monosomes) and D-H (polysomes) was then analysed by RT-PCR for *Snf2l* +/- exon 13. The Total RNA lane represents non-fractionated input cell lysate PCR products were separated by TBE-PAGE electrophoresis on a 0.8% gel and visualized by ethidium bromide staining. Results indicate that both splice variants of the human *Snf2l* gene are highly expressed in polysome fractions.

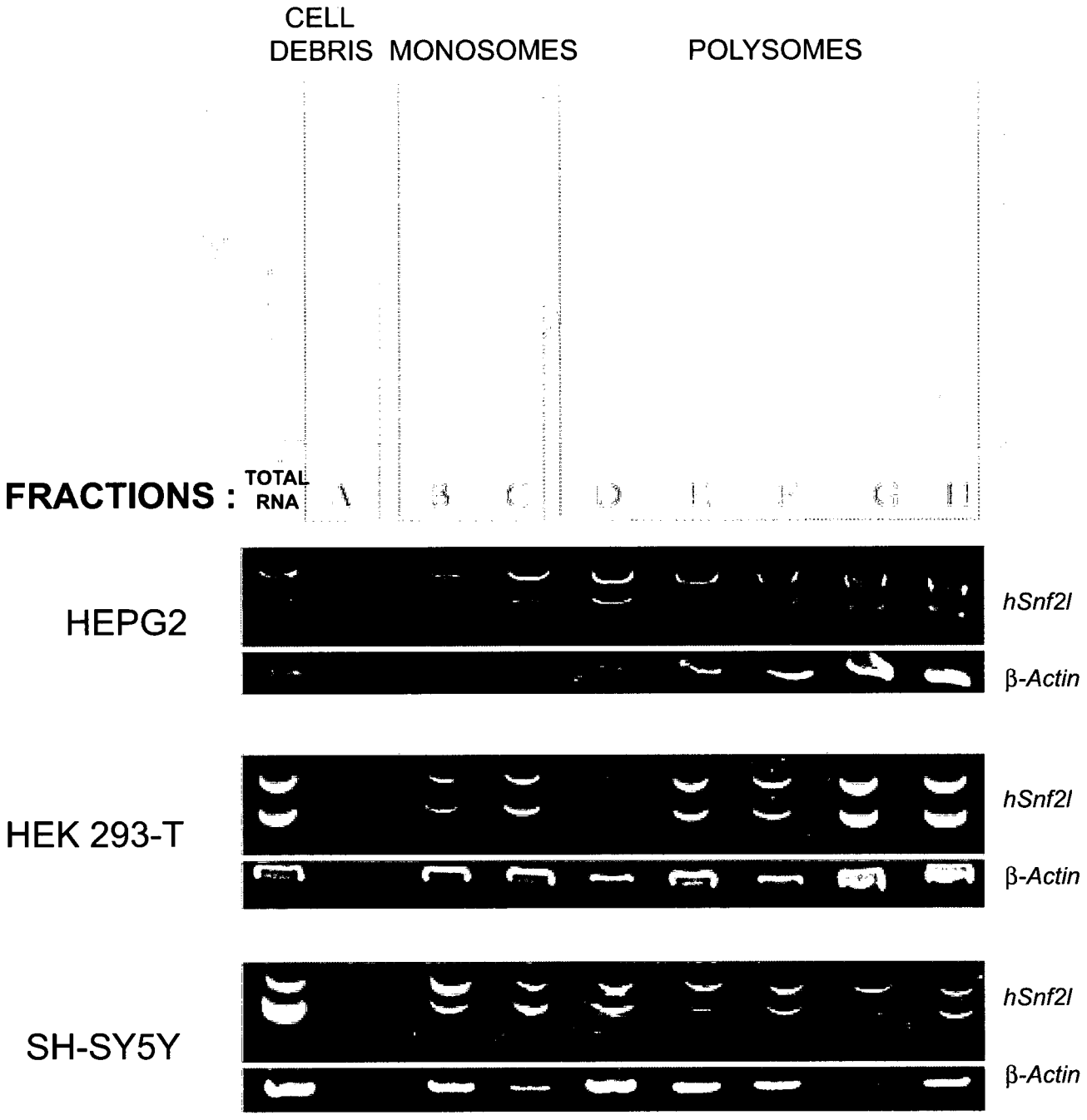
CELL
DEBRIS
MONOSOMES
POLYSOMES
FRACTIONS :
TOTAL RNA
A
B
C
D
E
F
G
H
HEPG2
hSnf2l
β-Actin
HEK 293-T
hSnf2l
β-Actin
SH-SY5Y
hSnf2l
β-Actin

Appendix IV: Raw data for Wildtype and Ex6DEL organ weight to body weight ratios (11 weeks).

I performed dissections on mice at 11 weeks old, and analyzed the organ weight to body weight ratio to compare Wildtype and Ex6DEL animals. The following table includes the raw data for weight of each animal and the weights of the brain, kidneys, heart and testes. Animals were anaesthetized and weight on a table top scale. All dissected organs were weighted using a table top analytical scale. Values for student's T-test statistical analysis are included.

		AGE				AVE of 2				AVE of 2		
	ID	(weeks)	Genptype	BODY g	Brain g	B/B	Kidney g	K/B	Heart g	H/B	Testes g	T/B
Males												
WT	380	11	WT	29.9	0.45	**0.0151**	n/a	n/a	n/a	n/a	n/a	n/a
n=23	381	11	WT	31.5	0.43	**0.0137**	n/a	n/a	n/a	n/a	n/a	n/a
	391	11	WT	29.8	0.4533	**0.0152**	n/a	n/a	n/a	n/a	n/a	n/a
	3468	11	WT	29.44	0.4885	**0.0166**	n/a	n/a	n/a	n/a	n/a	n/a
	589	11	WT	35.9	0.53	**0.0148**	n/a	n/a	n/a	n/a	n/a	n/a
	588	11	WT	31.9	0.43	**0.0135**	n/a	n/a	n/a	n/a	n/a	n/a
	386	11	WT	35.3	0.4	**0.0113**	n/a	n/a	n/a	n/a	n/a	n/a
	389	11	WT	37	0.41	**0.0111**	n/a	n/a	n/a	n/a	n/a	n/a
	390	11	WT	38.75	0.49	**0.0126**	n/a	n/a	n/a	n/a	n/a	n/a
	383	11	WT	57.02	0.48	**0.0084**	n/a	n/a	n/a	n/a	n/a	n/a
	385	11	WT	51.02	0.52	**0.0102**	n/a	n/a	n/a	n/a	n/a	n/a
	589	11	WT	33.9	0.53	**0.0156**	0.3301	**0.0097**	0.3242	**0.0096**	0.1771	**0.00522**
	3468	11	WT	29.44	0.4488	**0.0152**	0.2881	**0.0098**	0.1824	**0.0062**	0.1163	**0.00395**
	4466	11	WT	36.12	0.4545	**0.0126**	0.3226	**0.0089**	0.2364	**0.0065**	0.1698	**0.0047**
	4489	11	WT	36.26	0.4177	**0.0115**	0.2541	**0.007**	0.1743	**0.0048**	0.1218	**0.00336**
	4494	11	WT	33.84	0.4519	**0.0134**	0.2698	**0.008**	0.2426	**0.0072**	0.1297	**0.00383**
	4496	11	WT	33.85	0.4612	**0.0136**	0.2199	**0.0065**	0.1856	**0.0055**	0.153	**0.00452**
	4498	11	WT	37.95	0.461	**0.0121**	0.2935	**0.0077**	0.2353	**0.0062**	0.1533	**0.00404**
	4499	11	WT	37.48	0.4552	**0.0121**	0.2695	**0.0072**	0.16	**0.0043**	0.139	**0.00371**
	4500	11	WT	39.94	0.4383	**0.011**	0.2926	**0.0073**	0.2195	**0.0055**	0.1721	**0.00431**
	4504	11	WT	36.64	0.4322	**0.0118**	0.2685	**0.0073**	0.2103	**0.0057**	0.1456	**0.00397**
	4501	11	WT	46.08	0.474	**0.0103**	0.3829	**0.0083**	0.3099	**0.0067**	0.1601	**0.00347**
	4490	11	WT	38.66	0.4407	**0.0114**	0.25685	**0.0066**	0.176	**0.0046**	0.1389	**0.00359**
			AVE	36.856087	0.45858	**0.0127**	0.28737	**0.0079**	0.22138	**0.0061**	0.148	**0.00406**
			STDEV	6.7514724	0.03526	0.002	0.04246	0.0011	0.05244	0.0014	0.0198	0.00055
			SEM	1.4077793	0.00735	0.0004	0.00885	0.0002	0.01093	0.0003	0.0041	0.00011
Males												
Ex6DEL	585	11	Ex6DEL	32.3	0.6706	**0.0208**	0.4199	**0.013**	0.409	**0.0127**	0.1777	**0.0055**
n=14	587	11	Ex6DEL	29.4	0.6097	**0.0207**	0.3698	**0.0126**	0.3676	**0.0125**	0.1393	**0.00474**
	588	11	Ex6DEL	33	0.6501	**0.0197**	0.3955	**0.012**	0.3671	**0.0111**	0.1858	**0.00563**
	387	11	Ex6DEL	35.2	0.74	**0.021**	0.3206	**0.0091**	0.3402	**0.0097**	0.1655	**0.0047**
	4464	11	Ex6DEL	33.68	0.49	**0.0145**	0.2743	**0.0081**	0.1897	**0.0056**	0.1672	**0.00496**
	4465	11	Ex6DEL	32.78	0.4942	**0.0151**	0.2651	**0.0081**	0.2421	**0.0074**	0.1413	**0.00431**
	4491	11	Ex6DEL	26.7	0.4435	**0.0166**	0.174	**0.0065**	0.161	**0.006**	0.1274	**0.00477**
	4492	11	Ex6DEL	33.28	0.4798	**0.0144**	0.21525	**0.0065**	0.1849	**0.0056**	0.131	**0.00393**
	4493	11	Ex6DEL	33.62	0.483	**0.0144**	0.2963	**0.0088**	0.2259	**0.0067**	0.1552	**0.00462**
	4495	11	Ex6DEL	34.8	0.4996	**0.0144**	0.2452	**0.007**	0.2579	**0.0074**	0.1422	**0.00409**
	4497	11	Ex6DEL	32.29	0.445	**0.0138**	0.2646	**0.0082**	0.2397	**0.0074**	0.13	**0.00402**
	4502	11	Ex6DEL	32.79	0.5146	**0.0157**	0.3431	**0.0105**	0.2331	**0.0071**	0.169	**0.00515**
	4503	11	Ex6DEL	32.48	0.5126	**0.0158**	0.31065	**0.0096**	0.2672	**0.0082**	0.1486	**0.00458**
	4505	11	Ex6DEL	32.8	0.5506	**0.0168**	0.3386	**0.0103**	0.2564	**0.0078**	0.1567	**0.00478**
			AVE	32.508571	0.54166	**0.0167**	0.30235	**0.0093**	0.26727	**0.0082**	0.1526	**0.0047**
			STDEV	2.1424496	0.0907	0.0027	0.06872	0.0021	0.07545	0.0024	0.0185	0.00051
			SEM	0.5725937	0.02424	0.0007	0.01836	0.0006	0.02017	0.0006	0.0049	0.00014

STATS:

	BODY g	Brain g	**B/B**	Kidney g	**K/B**	Heart g	**H/B**	Testes g	**T/B**
tTEST	0.0258305	0.00035	1E-05	0.51899	0.0472	0.08942	0.0105	0.5478	0.00496
RESULT	**DIFF**	**DIFF**	**DIFF**	SAME	**DIFF**	SAME	SAME	SAME	**DIFF**

Appendix V: SNF2H levels are increased in drug resistant cancer lines and malignant human ovarian tumour samples.

The C13 and A2780 parental cell lines are susceptible (Sus.) to the chemotherapeutic drug Cisplatin; however over time with constant treatment of Cisplatin in culture, resistant (Res.) cells can be selective. [A] Western analysis of the two human ovarian cancer cell lines shows a down regulation of SNF2L (top panel) in cancer cell lines (except for A2780 Resistant cells) compared to primary human derived Ovarian Surface epithelial (hOSE) cells. Increased SNF2H levels are observed in Cisplatin resistant cells for both lines. [B] SNF2H levels are increase in malignant human ovarian cancers (grade 1 and 3) but not in low malignant potential tumours (L). These result highlight a correlation of SNF2H expression with aggressive and drug resistance in human Ovarian cancer.

A

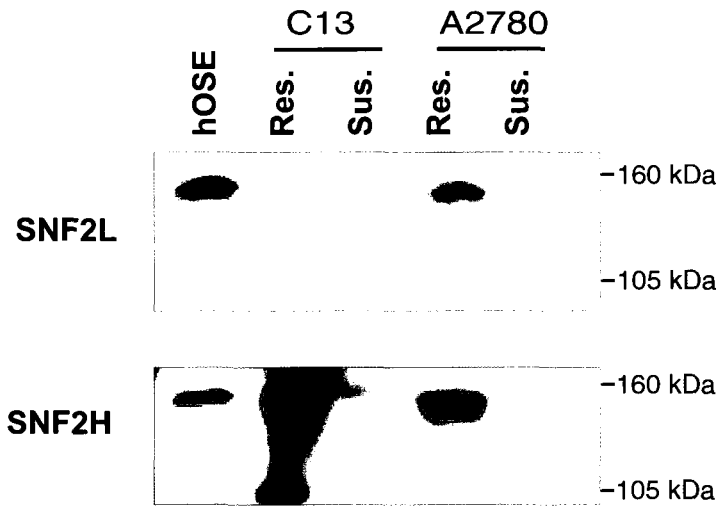
C13
A2780
hOSE
Res.
Sus.
Res.
Sus.
SNF2L
160 kDa
105 kDa
SNF2H
160 kDa
105 kDa

B

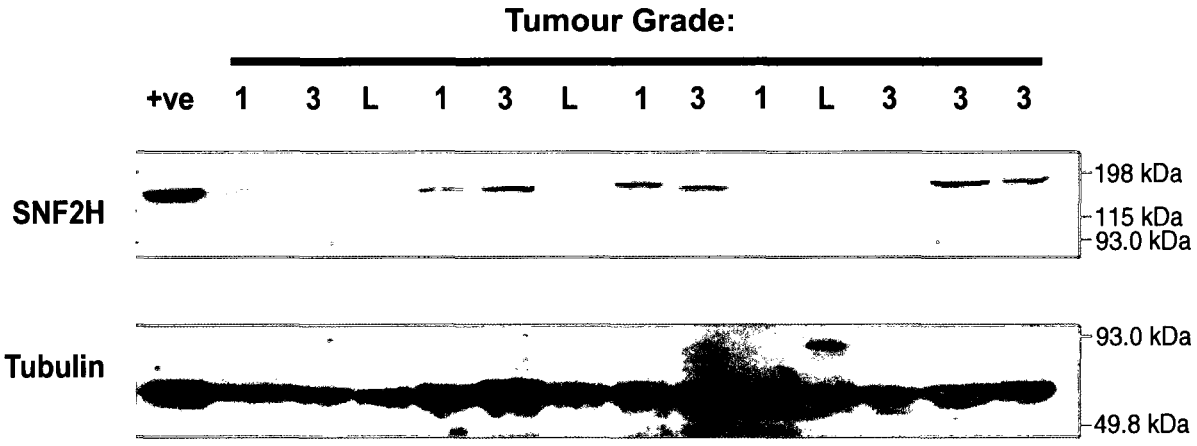
Tumour Grade:
+ve
1
3
L
1
3
L
1
3
1
L
3
3
3
SNF2H
198 kDa
115 kDa
93.0 kDa
Tubulin
93.0 kDa
49.8 kDa

Appendix VI: Summary of Microarray expression analysis from E15.5 cortex (WT vs. ex6DEL mice; n=4).

We performed a global gene expression analysis using cortical RNA from E15.5 wildtype and Ex6DEL animals on the MEEBO array. Results demonstrated altered expression (≥2-fold) of 256 genes (183 decreased and 73 increased, included are the perturbation of several cell cycle regulatory factors and many neurogenic transcription factors. avA; average signal intensity (Log^2), avM; average fold change (Log^2), Fold up/down; fold change absolute values

UP-REGULATED GENES

Accession	Symbol	avM	avA	fold up
NM_008241	Foxg1	2.88	12.71	7.38
XM_133029	FezF1	2.64	8.23	6.25
NM_011218	Ptprs	2.44	8.75	5.44
NM_013866	Zfp385	2.34	8.27	5.07
	Lonrf3	2.13	7.67	4.39
NM_029365	Med25	2.09	9.43	4.26
NM_175542	Rttn	1.94	8.32	3.84
NM_021399	Bcl11b	1.94	12.61	3.83
	Bcl11b	1.88	11.82	3.69
NM_177193	Islr2	1.80	14.26	3.49
	LOC215866	1.79	9.75	3.46
AK088219	Bcl11b	1.79	9.35	3.45
NM_013915	Zfp238	1.77	11.67	3.40
NM_007624	Cbx3	1.76	10.22	3.38
NM_018741	Igfbpl1	1.73	12.18	3.31
NM_009217	Sstr2	1.64	10.22	3.12
NM_144811	Cbx7	1.62	7.24	3.08
NM_010024	Dct	1.61	9.38	3.05
NM_022029	Nrgn	1.59	9.37	3.02
NM_175355	E330013P04Rik	1.56	7.66	2.94
NM_019835	B4galt5	1.50	8.21	2.82
NM_172900	Siglec10	1.49	8.13	2.81
XM_148399	Kalrn	1.48	8.70	2.79
NM_033566	Arid1a	1.46	8.71	2.75
NM_199143	Znrf2	1.46	11.62	2.74
NM_026886	1500001A10Rik	1.46	8.30	2.74
NM_008553	Ascl1	1.42	10.15	2.68
NM_021344	Tesc	1.41	8.36	2.66
XM_194983	Phf21b	1.41	12.24	2.65
NM_008078	Gad2	1.38	8.35	2.61
NM_008983	Ptprk	1.38	8.69	2.60
NM_011444	Sox5	1.37	9.91	2.58
NM_024435	Nts	1.36	10.15	2.56
NM_183252	2610017I09Rik	1.35	12.83	2.54
NM_178638	Tmem108	1.34	10.00	2.54
NM_008881	Plxna1	1.34	8.63	2.54
NM_008003	Fgf15	1.32	9.26	2.50
NM_173867	Rcc2	1.27	10.78	2.42
	9030417H13Rik	1.27	7.27	2.42
NM_008804	Pde9a	1.24	10.09	2.36
NM_138595	Gldc	1.24	8.79	2.36
NM_199143	Znrf2	1.23	10.04	2.34
NM_031404	Actl6	1.22	10.74	2.33
NM_173426	1700012H17Rik	1.20	10.74	2.29
	B230375D24Rik	1.20	10.01	2.29

UP-REGULATED GENES (cont'd)

Accession	Symbol	avM	avA	fold up
NM_134141	Ciapin1	1.20	10.25	2.29
NM_153587	Rps6ka5	1.19	9.24	2.29
NM_008487	Arhgef2	1.19	9.15	2.28
NM_010127	Pou6f1	1.18	11.72	2.26
NM_172430	Sphkap	1.17	9.32	2.25
NM_011261	Reln	1.16	11.62	2.24
NM_024435	Nts	1.16	8.92	2.24
NM_010500	Ier5	1.16	13.15	2.24
NM_008709	Nmyc1	1.15	12.38	2.22
NM_175229	Srrm2	1.13	9.38	2.19
NM_134071	Ankrd32	1.11	10.62	2.16
NM_145393	Ythdf2	1.11	8.76	2.16
NM_009238	Sox4	1.10	14.74	2.14
M36778	G0B-alpha	1.10	8.96	2.14
	Nin	1.09	8.76	2.14
NM_029850	Bcl7a	1.08	13.00	2.12
	E230008J23Rik	1.08	7.46	2.11
NM_008702	Nlk	1.07	9.42	2.10
NM_009281	Zfp143	1.06	9.18	2.08
NM_010124	Eif4ebp2	1.06	8.78	2.08
	Rabgap11	1.06	11.78	2.08
XM_131857	2610109H07Rik	1.04	10.42	2.05
NM_172681	D930015E06Rik	1.02	12.08	2.03
NM_145839	Rasgef1b	1.02	11.88	2.03
NM_011141	Pou3f1	1.02	11.20	2.03
NM_008595	Mfng	1.01	11.88	2.02
NM_011889	Sept3	1.01	11.39	2.01
NM_008043	Frat1	1.00	8.86	2.00

DOWN-REGULATED GENES

Accession	Symbol	avM	avA	fold change	fold down
NM_015784	Postn	-5.352	10.17	0.02	40.83
NM_008963	Ptgds	-4.419	12.29	0.05	21.39
XM_135854	1100001E04Rik	-3.584	10.05	0.08	11.99
NM_145633	Ankrd27	-3.340	8.31	0.10	10.12
NM_026323	1600023A02Rik	-3.028	7.73	0.12	8.16
NM_008047	Fstl1	-2.820	11.81	0.14	7.06
NM_028266	Col16a1	-2.724	10.90	0.15	6.60
NM_009378	Thbd	-2.712	9.04	0.15	6.55
NM_026473	2310057H16Rik	-2.610	11.36	0.16	6.10
NM_145978	Pdlim2	-2.387	8.15	0.19	5.23
NM_019949	Ube2l6	-2.299	8.83	0.20	4.92
NM_008343	Igfbp3	-2.259	10.15	0.21	4.79
NM_001001					
491	Tpm4	-2.251	12.87	0.21	4.76
NM_024263	1200013A08Rik	-2.224	9.84	0.21	4.67
NM_007998	Fech	-2.173	9.35	0.22	4.51
NM_011782	Adamts5	-2.138	8.65	0.23	4.40
NM_009131	Scgf	-2.108	8.84	0.23	4.31
NM_023116	Cacnb2	-2.049	10.25	0.24	4.14
NM_027402	Fndc5	-2.018	9.79	0.25	4.05
NM_007689	Chad	-2.008	7.39	0.25	4.02
	Gcap4	-1.986	8.17	0.25	3.96
NM_011122	Plod1	-1.970	10.33	0.26	3.92
NM_027078	1700023M03Rik	-1.958	9.34	0.26	3.88
NM_172570	Trim47	-1.957	9.12	0.26	3.88
NM_025522	Dhrs7	-1.918	8.28	0.26	3.78
NM_008655	Gadd45b	-1.894	8.45	0.27	3.72
NM_010473	Hrc	-1.893	10.76	0.27	3.71
NM_144799	Lmcd1	-1.883	8.78	0.27	3.69
NM_008409	Itm2a	-1.843	11.78	0.28	3.59
NM_021474	Efemp2	-1.833	11.58	0.28	3.56
NM_178593	BC025872	-1.806	8.44	0.29	3.50
NM_177152	Lrig3	-1.772	8.59	0.29	3.41
NM_008512	Lrp1	-1.768	9.18	0.29	3.41
NM_010518	Igfbp5	-1.766	13.12	0.29	3.40
	4930533K18Rik	-1.759	9.80	0.30	3.38
NM_025371	Acy1	-1.756	9.82	0.30	3.38
	AW123240	-1.751	9.29	0.30	3.37
NM_009109	Ryr1	-1.748	9.53	0.30	3.36
NM_177470	Acaa2	-1.739	9.87	0.30	3.34
NM_028331	C1qtnf6	-1.735	9.33	0.30	3.33
AK083573	Fbln1	-1.733	10.77	0.30	3.32

DOWN-REGULATED GENES (cont'd)

Accession	Symbol	avM	avA	fold change	fold down
NM_172508	Sart2	-1.719	9.35	0.30	3.29
NM_175641	Ltbp4	-1.716	9.54	0.30	3.29
NM_007653	Cd63	-1.696	13.35	0.31	3.24
NM_020564	Sult5a1	-1.688	7.31	0.31	3.22
NM_022024	Gmfg	-1.686	7.91	0.31	3.22
XM_486216	D930036J05	-1.677	9.12	0.31	3.20
NM_010283	Ggta1	-1.677	8.72	0.31	3.20
NM_019696	Cpxm1	-1.675	9.39	0.31	3.19
NM_010831	Snf1lk	-1.675	8.24	0.31	3.19
NM_153081	Slc16a11	-1.672	13.95	0.31	3.19
NM_011839	Mab21l2	-1.672	11.37	0.31	3.19
NM_009735	B2m	-1.638	9.84	0.32	3.11
NM_080728	Myh7	-1.635	11.28	0.32	3.11
NM_009801	Car2	-1.620	8.79	0.33	3.07
NM_010336	Edg2	-1.620	10.54	0.33	3.07
NM_029044	4930449E07Rik	-1.616	12.33	0.33	3.06
NM_008309	Htr1d	-1.609	8.88	0.33	3.05
NM_011356	Frzb	-1.605	9.04	0.33	3.04
NM_028733	Pacsin3	-1.589	9.85	0.33	3.01
NM_013870	Smtn	-1.580	8.13	0.33	2.99
AK031718	Mest	-1.573	8.75	0.34	2.98
NM_009949	Cpt2	-1.571	10.16	0.34	2.97
NM_007656	Kai1	-1.569	9.96	0.34	2.97
NM_010397	H2-T22	-1.560	9.38	0.34	2.95
NM_025294	Gtlf3b	-1.554	8.99	0.34	2.94
NM_138594	D6Wsu163e	-1.546	10.54	0.34	2.92
NM_023061	Mcam	-1.538	11.45	0.34	2.90
XM_358428	Dio3as	-1.537	8.16	0.34	2.90
NM_008691	Nef3	-1.518	12.51	0.35	2.86
NM_175214	Kif27	-1.517	9.80	0.35	2.86
NM_177657	D630003M21	-1.517	8.00	0.35	2.86
NM_013732	Cart	-1.515	8.90	0.35	2.86
NM_011576	Tfpi	-1.507	8.48	0.35	2.84
	2810482I07Rik	-1.497	9.87	0.35	2.82
NM_007594	Calu	-1.496	9.65	0.35	2.82
	2300006M17Rik	-1.494	9.91	0.35	2.82
NM_007631	Ccnd1	-1.488	8.19	0.36	2.80
NM_207246	Rasgrp3	-1.468	7.36	0.36	2.77
NM_026959	Stx18	-1.468	11.32	0.36	2.77
NM_144945	Lgi2	-1.463	8.27	0.36	2.76
NM_013599	Mmp9	-1.462	10.09	0.36	2.75

DOWN-REGULATED GENES (cont'd)

Accession	Symbol	avM	avA	fold change	fold down
NM_145475	Cerk	-1.457	12.02	0.36	2.75
AY267348	App	-1.438	8.30	0.37	2.71
	2310014D11Rik	-1.437	10.36	0.37	2.71
XM_489200	9530064J02	-1.432	8.52	0.37	2.70
NM_008048	Igfbp7	-1.430	11.73	0.37	2.69
NM_019521	Gas6	-1.425	10.21	0.37	2.68
NM_009813	Casq1	-1.421	8.44	0.37	2.68
NM_027153	Pir	-1.417	9.47	0.37	2.67
XM_155643	4921513O20Rik	-1.405	7.84	0.38	2.65
NM_015814	Dkk3	-1.396	10.99	0.38	2.63
XM_488964	E130013N09Rik	-1.396	13.43	0.38	2.63
NM_013590	Lzp-s	-1.396	8.43	0.38	2.63
NM_029659	1700011C14Rik	-1.395	10.26	0.38	2.63
NM_174870	Slc26a1	-1.393	9.59	0.38	2.63
XM_484355	2310047A01Rik	-1.392	11.04	0.38	2.62
NM_008034	Folr1	-1.387	7.82	0.38	2.62
NM_026447	2810423O19Rik	-1.382	9.76	0.38	2.61
NM_009287	Stim1	-1.374	8.68	0.39	2.59
NM_007631	Ccnd1	-1.367	8.58	0.39	2.58
NM_011223	Pxn	-1.367	7.89	0.39	2.58
	E030037F02	-1.366	8.69	0.39	2.58
NM_009372	Tgif	-1.365	8.58	0.39	2.58
NM_029813	2210418O10Rik	-1.365	9.24	0.39	2.58
	2810427A07Rik	-1.355	8.42	0.39	2.56
NM_011957	Creb3l1	-1.354	9.71	0.39	2.56
NM_008596	Mg29	-1.348	8.65	0.39	2.55
NM_026883	1500011H22Rik	-1.337	11.87	0.40	2.53
NM_008141	Gnat2	-1.335	11.97	0.40	2.52
NM_008483	Lamb2	-1.330	10.42	0.40	2.51
NM_011639	Trip6	-1.327	9.56	0.40	2.51
NM_010549	Il11ra1	-1.324	9.48	0.40	2.50
NM_009755	Bmp1	-1.322	8.50	0.40	2.50
XM_111398	Gm22	-1.321	9.24	0.40	2.50
NM_010452	Hoxa3	-1.314	11.80	0.40	2.49
NM_134125	Trip10	-1.311	10.22	0.40	2.48
AF259073	TRAV4D-2	-1.305	13.47	0.40	2.47
NM_016791	Nfatc1	-1.296	8.31	0.41	2.46
	Ctla2b	-1.293	8.35	0.41	2.45
NM_023910	0610009M14Rik	-1.291	10.27	0.41	2.45
NM_032418	Dm15	-1.279	9.04	0.41	2.43
BC055908	Cald1	-1.278	8.75	0.41	2.43

DOWN-REGULATED GENES (cont'd)

Accession	Symbol	avM	avA	fold change	fold down
NM_011838	Lynx1	-1.275	8.83	0.41	2.42
NM_007594	Calu	-1.269	8.96	0.41	2.41
NM_015744	Enpp2	-1.266	10.83	0.42	2.41
NM_010745	Ly86	-1.260	8.31	0.42	2.40
NM_009106	Rtkn	-1.252	9.71	0.42	2.38
NM_177732	Slc35d1	-1.249	8.29	0.42	2.38
NM_028173	Tram1	-1.249	8.54	0.42	2.38
	1500041O16Rik	-1.243	11.35	0.42	2.37
NM_172779	6330505F04Rik	-1.238	10.27	0.42	2.36
NM_009323	Tbx15	-1.236	9.41	0.42	2.36
NM_021292	Evc	-1.211	8.60	0.43	2.32
NM_007594	Calu	-1.205	12.40	0.43	2.31
NM_138602	Praf2	-1.198	14.77	0.44	2.29
NM_183022	Accn4	-1.195	9.72	0.44	2.29
NM_144827	Tisp78	-1.195	8.75	0.44	2.29
NM_019417	Pdlim4	-1.183	11.62	0.44	2.27
NM_011890	Sgcb	-1.173	9.18	0.44	2.26
NM_178017	Hmgb2l1	-1.169	8.10	0.44	2.25
NM_007669	Cdkn1a	-1.159	12.12	0.45	2.23
	1700096P03Rik	-1.159	8.73	0.45	2.23
NM_028283	Uaca	-1.158	10.94	0.45	2.23
NM_026680	0610012C01Rik	-1.156	12.93	0.45	2.23
NM_011430	Sncg	-1.151	13.45	0.45	2.22
NM_010444	Nr4a1	-1.148	8.35	0.45	2.22
NM_080288	Elmo1	-1.138	11.37	0.45	2.20
NM_001001					
491	Tpm4	-1.134	10.49	0.46	2.19
NM_007647	Entpd5	-1.130	9.93	0.46	2.19
NM_028787	Slc35f5	-1.123	9.48	0.46	2.18
NM_011609	Tnfrsf1a	-1.123	9.75	0.46	2.18
NM_172630	Mppe1	-1.121	8.27	0.46	2.17
NM_026353	4930570C03Rik	-1.119	9.15	0.46	2.17
	E430002D04Rik	-1.101	11.68	0.47	2.15
NM_019552	Abcb10	-1.095	10.63	0.47	2.14
NM_007382	Acadm	-1.091	9.36	0.47	2.13
NM_013556	Hprt	-1.089	10.47	0.47	2.13
NM_024269	Arl2bp	-1.082	8.29	0.47	2.12
NM_009831	Ccng1	-1.069	8.94	0.48	2.10
XM_486200	4931431C02Rik	-1.066	10.11	0.48	2.09
NM_153065	Ddx27	-1.065	11.16	0.48	2.09
NM_008546	Mfap2	-1.063	13.33	0.48	2.09

DOWN-REGULATED GENES (cont'd)

Accession	Symbol	avM	avA	fold change	fold down
NM_008160	Gpx1	-1.062	13.10	0.48	2.09
NM_153157	Olfm3	-1.060	8.21	0.48	2.09
NM_177263	Zhx3	-1.058	12.11	0.48	2.08
NM_009448	Tuba6	-1.052	11.68	0.48	2.07
NM_144534	1110001E17Rik	-1.051	10.50	0.48	2.07
NM_198629	LOC328644	-1.048	9.82	0.48	2.07
NM_181988	Rerg	-1.044	8.31	0.48	2.06
NM_198649	D930036B08Rik	-1.042	9.98	0.49	2.06
NM_011773	Slc30a3	-1.030	9.71	0.49	2.04
NM_172476	Tmc7	-1.030	8.80	0.49	2.04
NM_007438	Aldoa	-1.028	13.89	0.49	2.04
NM_144859	Pja2	-1.028	10.93	0.49	2.04
NM_012011	Eif2s3y	-1.026	12.04	0.49	2.04
NM_144882	2810022L02Rik	-1.025	11.29	0.49	2.03
NM_021406	Trem1	-1.020	10.14	0.49	2.03
	4930520K10Rik	-1.016	10.25	0.49	2.02
NM_030695	Lrba	-1.015	9.81	0.49	2.02
NM_011975	Rpl27a	-1.014	11.52	0.50	2.02
NM_178846	C77032	-1.013	8.84	0.50	2.02
NM_177470	Acaa2	-1.004	9.68	0.50	2.01

Appendix VII: Contribution from Collaborators.

Alan Mears: Assistant Professor, Department of Ophthalmology, University of Ottawa. Dr Mears and his lab members were performed the MEEBO Microarray and bioinformatics analysis on E15.5 cortical derived from Ex6DEL mice in Appendix VI (pp165).

Maribeth A. Lazzaro: Dr Lazzaro, a past postdoctoral fellow in the Picketts' lab performed the Western blot analysis on tumours and drug resistant ovarian cancer cell lines (Appendix IV pp163)). She also initiated growth pattern analysis of 293-T cells over expressing *Snf2h* and *Snf2l*.

Adriana De Maria: Dr De Maria, a past postdoctoral fellow in the Picketts' lab generated the floxed Snf2l exon 6 targeting construct and performed J1ES cell transfection and positive clone selection. I have adapted her original data in Appendix II (pp161).

Jossee Couloumbe a postdoctoral fellow in the laboratory of Michael Rudnicki, Professor, Department of Medicine and Cellular and Molecular Medicine, University of Ottawa, performed blastocyst injections and developed the Snf2l-floxed exon 6 Chimera, and was instrumental in developing the Snf2l floxed exon 6 mouse colonies.

Damiano Conte: Dr Conte, a past postdoctoral fellow in the Picketts' Lab performed the Southern blot hybridization, used in Figure 3.3.1, part B.

Brian McNeill, PhD candidate in the laboratory of **Dr Valerie Wallace**, Associate Professor, Department of Biochemistry, Microbiology and Immunology, University of Ottawa, had been very helpful in providing instruction of the analysis and initiating qRT-PCR experiments, and had provided aliquots and sequences for several primer pairs for analysis.

curriculum vitae

Darren John Yip (M.Sc.)

SUMMARY OF SKILLS

- 10 years of academic research laboratory related experience
- Strong technical expertise in multiple molecular biological and biochemical laboratory techniques using *in vivo, ex vivo* and *in vitro* models including: Immunohistochemistry, *in situ* hybridization, microscopy, Protein, DNA and RNA techniques (Southern blot, Western Blot, PCR, RT-PCR, quantitative realtime RT-PCR, Chromatin Immunoprecipitation, multiple cloning techniques), animal breeding, colony management and dissection.
- Strong communication and interpersonal skills (teaching, presentations, leadership, mentorship)
- Proficiency with Microsoft Office and Adobe programs, adeptness with statistical computer programs including Prism, Slidewrite and Sigmaplot, and practical knowledge of various analytical sequence programs.
- An excellent and dynamic team player with a particular interest in teaching and mentorship
- Displays initiative and has the ability to work independently.

EDUCATION

Ph.D. Candidate (Sept 2003-present, *anticipated completion spring 2009*),
University of Ottawa, Department of Biochemistry, Microbiology and Immunology (specialization in Human and Molecular Genetics) under the supervision of Dr David Picketts

- Thesis Title: *The chromatin remodelling protein SNF2L mediates cell number in the developing brain.*
- OGSST Scholar (2004-2008).
- Undergraduate teaching experience.
- Maintained A+ average
- Area of expertise: embryonic neurodevelopment, development and characterization of murine transgenic models, chromatin remodelling and regulation and the regulation of proliferation and differentiation (*in vivo, ex vivo* and *in vitro* models)

Masters of Science (Sept 1999-2002)
University of Ottawa, Department of Biochemistry, Microbiology and Immunology (specialization in Human and Molecular Genetics) under the supervision of Dr. David Picketts

- Thesis Title: *Examining the repressive nature of D4Z4 repeats and their role in the pathogenesisof Facioscapulohumeral Muscular Dystrophy*
- Maintained A+ average
- Areas of expertise: *in vitro* models of muscle differentiation, cloning and the development of expression vectors

Bachelors of Science (Honours in Biology/Biotechnology) (Sept 1995-May 1999)
University of Ottawa, Department of Biology

- Graduated with honours (*cum laude*)
- Research project involving the transgenic expression of a cold-temperature inducible promoter in agriculturally important crops [under the supervision of Dr. Jas Singh, Research Scientist, Agriculture and Agri-Food Canada, Ottawa, Ontario]
- Areas of study: molecular biology, genetics, physiology, zoology, chemistry, biochemistry

GRANTS and HONOURS / AWARDS

- Government of Ontario - Graduate Scholarship in Science and Technology, four years of external funding [$15 000 per annum] 2004 -2008
- First Prize: Microbiology and Immunology, Ph.D. departmental seminar competition 2006
- First Prize: Trainee Seminar Competition, 6th Annual OHRI Research Day 2006
- First Prize: Ph.D. Student Poster Competition, 5th Annual OHRI Research Day 2005
- First Prize: Ph.D. Student Poster Competition, 4th Annual OHRI Research Day 2004

PUBLICATIONS

Articles

Yip DJ, Picketts DJ. Increasing D4Z4 repeat copy number compromises C2C12 myoblast differentiation. 2003. *FEBS Lett.* **537**: 133-8.

Yip DJ, De Maria AC, Coulombe J, Rudnicki M, and Picketts DJ *Foxg1, a target of* SNF2L controls neuoprogenitor proliferation in the developing brain. (*In preparation*)

Yip DJ, Pepin D, Lazzaro MA, Vanderhyden B, Picketts DJ. Aberrant expression of the mammalian ISWI protein, Snf2H a contributing factor to ovarian cancer. (*In preparation*)

Abstracts

Yip DJ, De Maria AC, Coulombe J, Rudnicki M, and Picketts DJ. SNF2L-Mediated Control of Cell Number in the Developing Brain. *17th Biennial Meeting of the international Society for Developmental Neuroscience*. Asilomar, California (June 1-4, 2008)

Yip DJ, Rennick S, De Maria A, Coulombe J, Rudnicki M and Picketts DJ. SNF2l-Mediated control of cell number in the developing brain. *Chromatin; Structure and Function.* Punta Cana, Dominican Republic (December 5-8, 2006)

Yip DJ, De Maria AC, Coulombe J, Rudnicki M, and Picketts DJ. SNF2L-Mediated Control of Cell Number in the Developing Brain. *16th Biennial Meeting of the International Society for Developmental Neuroscience*. Banff, Alberta (August 24-28, 2006)

Yip DJ, De Maria AC, Lazzaro MA, Lavigne P, Vallee D and Picketts DJ. Molecular characterization of the mammalian ISWI gene SNF2L, and its assessment as an X-linked Mental Retardation (XLMR) candidate gene. 54th Annual meeting of *The American Society of Human Genetics*. Toronto, Ontario. (October 26-30, 2004)

Yip DJ, Dawson KM, Lazzaro MA, Vanderhyden BC and Picketts DJ. Aberrant expression of the mammalian ISIW protein, SNF2H: A potential contributing factor to ovarian cancer. (2004) *Canadian Conference on Ovarian Cancer Research*. Ottawa, Ontario. (May 16-18, 2004)

EMPLOYMENT HISTORY

Teaching Assistant (Demonstrator/Lab Monitor) – Sept - Dec 2008, Sept - Dec 2007
University of Ottawa, Faculty of Science, Department of Biochemistry, 3rd year Molecular Biology Laboratory Course

- Was responsible for teaching sessions, leading discussions and providing student mentorship
- Provided guidance with calculations, problem solving and demonstrated proper lab techniques
- Evaluation of students and marked written reports, oral presentations and in-lab proficiency and was responsible for providing feedback in a timely and constructive fashion.

Teaching Assistant (Proctor/Marker) – Jan - May 2008
University of Ottawa, Faculty of Science, Department of Biochemistry, 3rd year Molecular Genetics Class

- Was responsible for exam proctoring and exam marking
- Scheduled and provided open sessions for student post-exam review and discussion.

Laboratory Technician – Jan - Sept 2002
Ottawa Hospital Research Institute, Regenerative Medicine Program [Laboratory of Dr. David Picketts]

- Initiated the development of transgenic mouse lines and was responsible for cloning, characterization and colony maintenance
- Was responsible for experimental design, implementation, data interpretation and data presentation.
- Performed extensive *in vitro* experimentation
- General laboratory duties included, laboratory maintenance, creating a chemical and reagent inventories, made solutions and buffers, kept the lab spaces clean and in order

Research Technician – May - Sept 1999
Agriculture and Argi-Food Canada, Eastern Cereal and Oilseed Research Center [Laboratory of Dr. Linda Harris]

- Studied the early expression of *Fusarium* mycotoxins response genes in corn.
- Maintained experimental crops and was responsible for preparation of and inoculation with *Fusarium* mycotoxin, and the harvest of experimental tissue
- Lab duties included plant tissue preparation, total RNA extraction, Northern blot transfer, preparation of cDNAs, and reverse transcriptase PCR.